Chemical Processing of Phosphorus Inclusions within Iron Meteorites and Related Investigations

Barry Herschy

200469017

Submitted in accordance with the requirements for the degree of

Doctor of Philosophy

The University of Leeds

School of Chemistry

September 2013

The candidate confirms that the work submitted is his own, except where the work which has formed part of jointly-authored publications has been included. The contribution of the candidate and the other authors to this work has been explicitly indicated below. The candidate confirms that appropriate credit has been given in the thesis where reference has been made to the work of others.

This copy has been supplied on the understanding that it is copyright material and that no quotation from the thesis may be published without proper acknowledgment.

Publications

"Hydrothermal modification of the Sikhote-Alin iron meteorite under low pH geothermal environments. A plausibly prebiotic route to activated phosphorus on the early Earth"

David E. Bryant, David Greenfield, Richard D. Walshaw, Benjamin R. G. Johnson, Barry Herschy, Caroline Smith, Matthew A. Pasek, Richard Telford, Ian Scowen, Tasnim Munshi, Howell G. M. Edwards, Claire R. Cousins, Ian A. Crawford, Terence P. Kee.

Part of Chapter 4 is based on this publication. B. Herschy planned (along with T. P. Kee) and conducted all experiment work reported relating to the fieldwork expedition to Kverkfjöll, Iceland. The experiments conducted and reported explored corrosion of Sikhote Alin meteorite samples in natural hydrothermal fluids and dehydration of calcium phosphite under natural geological conditions. Dehydration of phosphite produced by corrosion of sample SA1 with pyrophosphite, identified as a product of this experiment by ^{31}P NMR, reported in this article. All NMR analysis and some IFM analysis (Samples SA2 and SA4) reported on the Iceland samples were conducted by B. Herschy. The remaining IFM analysis was conducted by D. Greenfield. Experimental details and analytical procedures for the work were written for inclusion in the supplementary material. Appropriate credit is given in the Thesis.

"Glaciovolcanic hydrothermal environments in Iceland and implications for their detection on Mars"

Claire R. Cousins, Ian A. Crawford, J.L. Carrivick, M. Gunn, J. Harris, Terence P. Kee, Magnus T. Karlsson, Laura Carmody, Charles Cockell, Barry Herschy, K.H. Joy.

Parts of Chapters 3 and 4 are based on this publication. B. Herschy and T. P. Kee were both part of the field team which went to Kverkfjöll, Iceland. Site information collected by B. Herschy and detailed in Chapter 3 was used in this publication including locations, pH and temperature data. Water chemistry analysis was conducted on fluids from the sample sites detailed in Chapter 3 and the analysis data for those samples are reported in Chapter 4. The water chemistry analysis was conducted by C. R. Cousins and was

included in this paper to give an over-arching view of the geochemistry taking place at this site. Appropriate credit is given in the Thesis.

"Phosphate Activation via Reduced Oxidation State Phosphorus (P). Mild Routes to Condensed-P Energy Currency Molecules"

Terence P Kee, David E Bryant, Barry Herschy, Katie E. R. Marriott, Nichola E. Cosgrove, Matthew A. Pasek, Zackary D. Atlas, Claire R. Cousins

Part of Chapter 4 is based on this publication. B. Herschy planned (along with T. P. Kee) and conducted all experiment work reported relating to the fieldwork expedition to Kverkfjöll, Iceland. The experiments conducted and reported explored corrosion of iron phosphide samples in natural hydrothermal fluids. Dehydration of phosphite found after corrosion of sample A5 is also reported in this article with pyrophosphite identified by NMR from these experiments. All NMR analysis reported on the Iceland samples were conducted by B. Herschy. Experimental details and analytical procedures for the work were written for inclusion in the supplementary material. Appropriate credit is given in the Thesis.

Acknowledgments

Firstly I would like to extend my heart-felt thanks to Dr. Terence P. Kee for the opportunity to undertake this research project. Terry, it has been a great pleasure to work with you and I thank you for all the help, support, advice and guidance over the course of my PhD. You have always been there with words of encouragement and support through what has been the toughest period of my life. You gave me the belief that I could do this even through my darkest hours and kept me on track. I would never have got to this point without your kind words and ever available ear. I would also like to thank the EPSRC for funding my research as without this, my PhD would not have been possible.

My thanks also to Dr. David Bryant and Dr. Ian Gorrell, throughout my PhD you have both taught me so much and really helped me to reach this point with the support, guidance and inspiration to pursue my ideas while also keeping me grounded. You have both spent countless hours talking me through my thought processes and listening to me trying to reason my findings and without this I would never have got this far.

Dr Katie Marriott, you have been there for me throughout this PhD process offering guidance, support, advice and the occasional pint (or two or three) to get me through. Your friendship is one of the best things to come out of my time here at Leeds and I was so proud to watch you obtain your PhD in such magnificent style.

I would also like to thank Dr. Nichola Cosgrove and Dr. Gerhard Zieboll for putting up with me, cups of tea, occasional beers and cake, all of which added to what have been the most fantastic experiences of my life.

I also must thank Dr. Patrick McGowan, Dr. Charlotte Willans and their respective groups for listening to my talks, offering advice and support through my time as a PhD student.

I must thank David Ashley, Tanya Marinko-Covell, Ian Blakeley, Dave Fogarty and Simon Barrett from the University of Leeds for their assistance and instruction in the various analytical techniques which have been undertaken during my work. Thanks also to Dr. Ian Scowen, Dr. Tas Munshi, Darren Whitaker and other staff members from the University of Bradford for use of various pieces of equipment, direction and instruction in usage and their help and support throughout my PhD. A special thank you to Tas for her faith in allowing me to re-enter the University system, her guidance throughout my undergraduate days and for pushing me towards undertaking the PhD in the first place. I am here because of your faith and I will be eternally grateful.

My thanks also to Dr. David Greenfield from Sheffield Hallam University for use of the IFM

and SEM/EDX equipment and attempt to help me understand the dynamics of corrosion. Thanks to Prof. Matthew Pasek from the University of South Florida for undertaking ICP/MS and ion chromatography and offering experimental advice in my early days. It has been a pleasure working with you Matt and hope we can do so again one day.

I thank Dr. Claire Cousins and Prof. Ian Crawford for allowing me the opportunity to go to Iceland, which proved a pivotal point in my life and also a major chunk of my thesis. I must also personally thank Claire for assistance with the ICP-AES analysis, instruction on geological sampling and analysis contained in this thesis and her sterling choice of field assistant for the Iceland trip. I also take this opportunity to thank Magnus Karlsson, Viljálmur (Villy) Kjartansson and members of the Icelandic Glaciological society for their assistance in planning and logistical support for the trip to Kverkfjöll and the opportunity to visit the site of the Grimsvötn eruption in May 2011.

To Laura, you have been a real star through all of this and made my life just about bearable. Thank you so much for all you have done, the hours of phone calls, the advice and lengthy discussions about mineralogy and geochemistry. I am grateful for you for sticking by me through all of this and for not saying "I told you so!" every time I opened my mouth to moan about something else I should have done and leaving everything to the last minute. Your love has kept me going, kept me strong and kept me sane through the final stages. You changed my world, my outlook on life and I owe you everything. Here's to a happy, stress free future together.

Finally I must thank my whole family for their love, faith and support. This has been one of the toughest times I can remember but you have all been there for me. Mum, Dad, Nicola, without your help, support and encouragement, none of this would have been possible. I am sorry for all the moaning phone calls, stress and anxiety I have caused you through this. I hope you think it is now worth all the pain.

This is for you Nanna, I dedicate this thesis to you. Your words sparked all of this. You inspired me to go back, to finish what I started nearly 20 years ago. I finally made it and my only wish is that you were still here to share this moment with me. I hope I made you proud. xxx

Abstract

'How did life on Earth originate?' is a question that, as yet, scientists have been unable to answer. From simple building blocks, under certain conditions, a series of chemical reactions occurred leading to the formation of a living cell.

Meteorites have long been considered a source of prebiotic chemicals which could have assisted in the origin of life on Earth. Iron meteorites are known to contain the mineral Schreibersite [$(FeNi)_3P$], a good source of reduced oxidation state phosphorus (P) on the prebiotic Earth. Meteorites would be exposed, post-impact, to moisture from the atmosphere and oceans which could instigate a series of chemical reactions, giving rise to chemical precursors required for production of life.

Current investigations are looking at the conditions to which Earth impacting meteorites would be exposed. Hydrothermal reactions of siderophilic P minerals such as Schreibersite were undertaken to identify and quantify any reduced P species produced and investigate reactions which could be utilised *en route* to life.

Chapter 2 outlines the laboratory work conducted for the identification and quantification of reduced oxidation state phosphorus species (phosphine and phosphite). It investigates potential prebiotic chemistry of observed species including formation of condensed phosphorus species (pyrophosphite and isohypophosphate). Effects of temperature, pH and different metals (including magnesium [Mg], calcium [Ca] and iron [Fe]) on formation of condensed phosphorus species were investigated.

Chapter 3 describes the fieldwork conducted at the Hveraldur hydrothermal field on the Kverkfjöll sub-glacial volcano. It describes the site, conditions and sampling methods.

Chapter 4 covers the analysis of the experiments undertaken during the fieldwork in Iceland. It looks at products observed from corrosion of schreibersite, present in samples of Sikhote Alin meteorite and iron phosphide in natural hydrothermal fluids and repeats prebiotic chemistry attempted in Chapter 2.

Glossary

ablation the removal of material from the surface of an object by vaporization, chipping, or other erosive processes.

anomeric from anomeric centre. A stereocentre created from the intramolecular formation of an acetal (or ketal) of a sugar hydroxyl group and an aldehyde (or ketone) group. The two stereoisomers formed from the two possible stereochemistries at the anomeric centre are called anomers. They are diastereoisomers of one another.

accretion the growth of a massive object by gravitationally attracting more matter, typically gaseous matter in an accretion disk.

amphiphilic a molecule having a polar, water-soluble group attached to a nonpolar, water-insoluble hydrocarbon chain

anion an ion with more electrons than protons, giving it a negative charge.

Archean the second geological era dated between 4.0 billion years and 2.5 billion years ago.

asthenosphere is a highly viscous region of the upper mantle.

bilayer a double layer of closely packed atoms or molecules.

bona fide real or genuine.

cation an ion with fewer electrons than protons, giving it a positive charge.

chert a sedimentary rock composed mainly of micro-crystalline silica.

de novo a Latin expression meaning "from the beginning".

dibasic having two hydrogen ions to donate.

divalent having two binding sites.

en route a French expression meaning "on or along the way".

et al. an abbreviation of a Latin phrase *et alia* meaning "and others".

fumarole s an opening in a planet's crust, often in the neighbourhood of volcanoes, which emits steam and gases such as carbon dioxide, sulphur dioxide, hydrogen chloride, and hydrogen sulphide

Hadean the first geological era dated between 4.6 billion years and 4.0 billion years ago.

hydrophilic capable of interacting with water through hydrogen bonding.

hydrophobic repelling water.

komatiite	a type of ultramafic mantle-derived volcanic rock. Komatiites have low silicon, potassium and aluminium, and high to extremely high magnesium content.
macrocycle	a cyclic molecule with three or more potential donor atoms that can coordinate to a metal centre
monobasic	Having only one hydrogen ion to donate.
nebula	an interstellar cloud of dust, hydrogen, helium and other ionised gases.
paramagnetic	attracted by an external applied magnetic field.
phospholipid	a class of lipids that are the major component of all cell membranes. They ususally contain a phosphate group, a diglyceride and a simple organic molecule such as choline.
planetesimal	a solid object thought to exist in protoplanetary disks and in debris disks.
Proterazoic	the third geological era dated between 2.5 billion years and 541 million years ago, just before the proliferation of complex life.
purine	a heterocyclic aromatic organic compound. It consists of a pyrimidine ring fused to an imidazole ring.
pyrimidine	an aromatic heterocyclic organic compound similar to pyridine.
semi-permeable	allowing passage of certain, especially small, molecules or ions but acting as a barrier to others.
siderophilic	a Latin word meaning "iron loving".
tephra	fragments of volcanic material produced during an eruption i.e. ash and pumice.
trivalent	having three binding sites.
vesicle	a small compartment within a cell.

Abbreviations

pH	a measure of the acidity or basicity of an aqueous solution
HEPES	a zwitterionic organic chemical buffering agent; 2-[4-(2-hydroxyethyl)piperazin-1-yl]ethanesulfonic acid
A	adenine
ADP	adenosine diphosphate
AMP	adenosine monophosphate
ATP	adenosine triphosphate
AU	Astronomical Unit, distance from Sun to Earth
AES	Atomic Emission Spectroscopy
amu	atomic mass unit
BIF	banded iron formation
wt.	by weight
CCD	charge coupled detector
cTMP	cyclic trimetaphosphate
C	cytosine
Conc.	concentrated or concentration
DNA	deoxyribonucleic acid
D	deuterium
d	doublet
dd	doublet of doublets
EDX	Electron Dispersive X-ray
ESI	electrospray ionisation
ΔG_{hyd}	Gibbs free energy of hydration
Ga	Gigayear, $\times 10^9$ years
Gly	glycine
g	gram
G	guanine
Hz	Hertz
ICP	Inductively Coupled Plasma
IFM	Infinite Focus Microscopy
IDPs	interstellar dust particles
IC	Ion Chromatography
J	Joule
K	Kelvin

kg	kilogram
km	kilometre
LHB	late heavy bombardment
MS	Mass Spectrometry
MHz	Megahertz
m	meter
μg	microgram
μM	micromolar
μmol	micromole
mm	millimetre
mM	millimolar
mmol	millimoles
mW	milliwatt
M	Molar
nm	nanometre
NAD+	nicotinamide adenine dinucleotide
NASA	National Aeronautics and Space Agency
NMR	Nuclear Magnetic Resonance
OFN	Oxygen Free Nitrogen
ppm	part per million
PEP	phosphoenol pyruvate
pXRD	powder X-ray diffraction
PPi$_{(V)}$	pyrophosphate
PPi$_{(III)}$	pyrophosphite
NADH	reduced NAD+
RNA	ribonucleic acid
SEM	Scanning Electron Microscopy
s	singlet
SMOW	standard mean ocean water
STP	standard temperature and pressure (25C and 1 atm)
T	thymine
t	triplet
TPP	tripolyphosphate
AA'XX'	type of spin coupling
UV/Vis	ultraviolet and visible light
UGA	Universal Gas Analyser

UCL	University College London
USF	University of South Florida
U	uracil
W	Watt
WHO	World Health Organisation

Contents

List of Figures

List of Spectra

List of Tables

Chapter 1

Introduction

'How did life on Earth originate?' remains one of the biggest questions facing the scientific community today. Though great progress has been made in determining how and when the universe was formed and also in working back through the branches of the tree of life toward its origin, this single point in our history remains a mystery. We still need to answer at what point in the history of the planet did life commence? How and where did it start? Did it start more than once? At what point and how did the chemistry become biology? To answer these questions we must consider the molecular inventory which would have been available for participation in prebiotic chemistry, how these reagents could have come together, the series of chemical reactions required for life to start and the geological conditions under which such reactions would have taken place.

There has been much experimental investigation into the synthesis of organic compounds relevant to contemporary biochemistry from simple inorganic precursors using a variety of energy sources under prebiotic conditions.[1] One of the most seminal of these was conducted in 1953 when Stanley Miller and Harold Urey[2] conducted an experiment in which an atmosphere of methane [CH_4], ammonia [NH_3], hydrogen [H_2] and water [H_2O] was sparked to simulate lightning discharge. Results from this experiment indicated that under prebiotic atmospheric conditions and lightning discharge as a source of energy, it was possible to produce organic compounds from simple inorganic starting materials. From this experiment Miller and Urey identified at least five amino acids (glycine, α- and β-alanine, aspartic acid and α-amino-η-butyric acid, though a later analysis in 2008 using more sophisticated technology confirmed the production of twenty-two.[3] A similar atmospheric experiment was conducted and published by Rabinowitz $et\ al.$ (1969) using an atmosphere of CH_4, NH_3, H_2, H_2O and a gaseous form of phosphorus known as phosphine [PH_3], which produced many organophosphate compounds such as o-phosphoethanolamine and aminoethanephosphonic acid, also phosphorus free compounds like glycine, alanine, aspartic and glutamic acids and ethanolamine.[4,5]

While these experiments prove it possible to produce organic compounds in this manner, the actual constitution of the early Earth atmosphere is still under debate. These experiments rely on a highly reduced atmosphere but there is no geological evidence available to support this theory. Due to high levels of incident UV radiation, the presence of ammonia in the atmosphere would be minimal due to photolysis but also the geological record is

much more supportive of a weakly reducing atmosphere and was thought to have consisted of mainly CO_2, N_2 and H_2O, with trace amounts of H_2, H_2S, NH_3 and SO_2 supplied by volcanic degassing. Attempts to repeat the Miller-Urey experiment under weakly reducing conditions resulted in very low yields of organic compounds[6] though findings of Cleaves *et al.* (2007) showed an increase in organic yields of several orders of magnitude by addition of oxidation inhibitors, such as ferrous iron [Fe^{2+}], prior to hydrolysis.[7,8] There has been a great deal of speculation as to the actual composition of the primitive atmosphere which is discussed later in this chapter.

Though creating structurally complex organic molecules from inorganic precursors is possible, this in itself would not be enough to start life on Earth. Both structural and functional complexity are needed.[9] For example, all known living organisms on Earth require activated phosphorus compounds such as adenosine triphosphate (ATP), phosphoenolpyruvate (PEP) and creatine phosphate to provide energy to drive biochemical processes but despite its importance in biological systems, the mechanisms by which phosphorus has become incorporated into primitive biochemistry are unknown. Understanding how such phosphorus-driven biology emerged is a central problem in origins research and the one that lies at the heart of the work reported herein.

1.1 Role of phosphorus in current biology

Phosphorus (P) is one of the elements considered key to life. It is present in all living things, making up approximately 1% of human body weight (approximately 780 g in the average 75 kg body).[10] It has a wide and varied chemistry and this is crucial to the biochemistry of all life on this planet.[11] It is known to participate in almost every biological function including cell structure, information transfer, replication and metabolism. Phosphorus is obtained from the environment principally in the form of orthophosphates and their derivatives[12] and is considered to be a limiting factor to life as it is currently believed that replication cannot happen without its presence. Life will only grow where there is available P in the system and will stop once it is all consumed,[12] until further addition allows growth to start again. This is seen in algal blooms where organisms will rapidly reproduce to use up available P.[13]

In 2011, a paper published by Wolfe-Simon *et al.* claimed to have identified a bacterium (GFAJ-1) which could use arsenic to grow instead of phosphorus.[14] The paper claimed that the bacterium would grow slowly using arsenic when phosphorus was not available. This was widely publicised by NASA but was strongly challenged by the scientific community. It was unsure if the bacterium were actually using arsenic in replacement of phosphorus for replication and growth or if some other source of phosphorus was becoming available allowing the slow growth such as contamination of the growth medium or the arsenic which was used to feed the bacteria.[15] In 2012, Erb *et al.* and Reaves *et al.* separately published papers describing attempts to repeat the work published by Wolfe-Simon. The studies were conducted independently and without the others knowledge and both showed that, while GFAJ-1 was arsenic resistant and would grow in the presence of arsenic, there was no uptake of arsenic into its DNA.[16,17] These studies showed without question, that while

life may grow in the presence of arsenic, phosphorus was still required to facilitate growth.
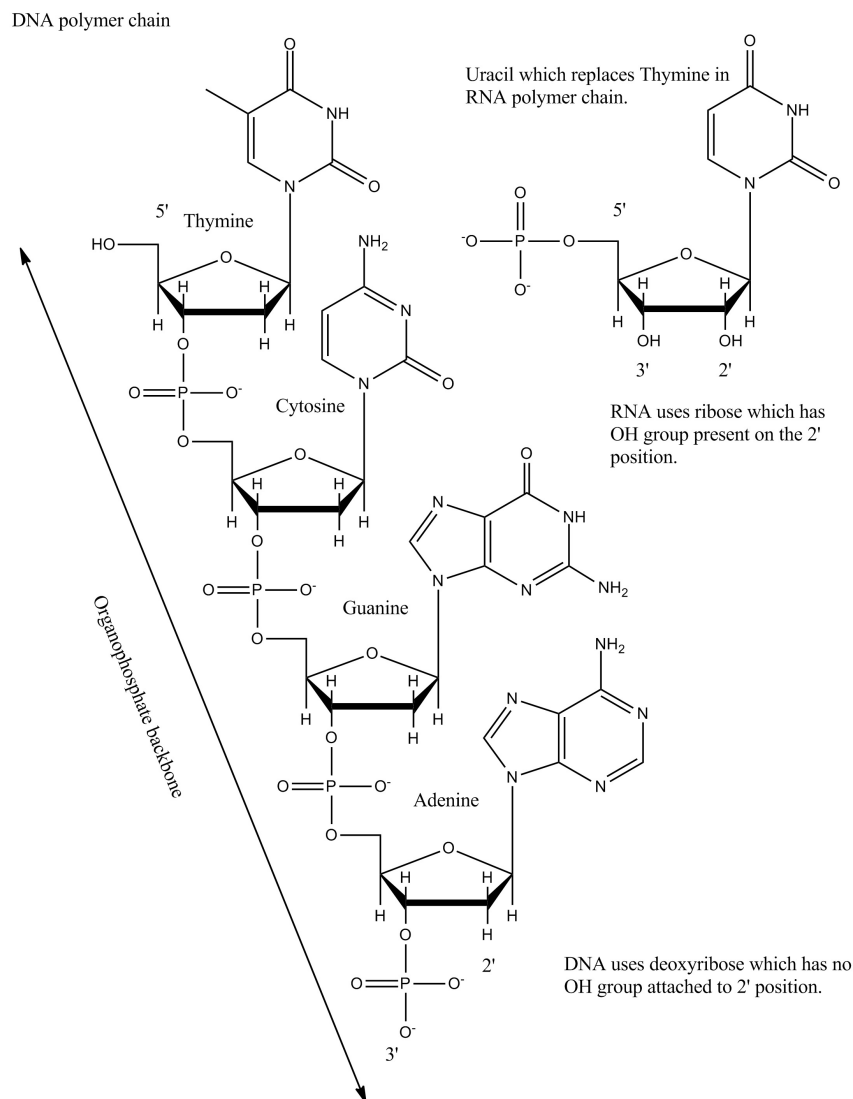
Figure 1.1: Diagram showing DNA polymer chain construction and relevant nucleobases. Uracil is used as a replacement nucleobase for thymine in RNA which uses the same organophosphate chain structure but has an additional hydroxyl group on the 2' position on the ribose sugar.

The importance of phosphorus to life becomes apparent when you start to look in detail at the essential areas in which it has become involved in contemporary biology. Phosphate diesters make up the backbone of DNA (deoxyribonucleic acid) and RNA (ribonucleic acid) polymers (Figure 1.1). These consist of an organophosphate diester covalently attached to the 5' and 3' positions on a ribose (for RNA) or deoxyribose (for DNA) sugar ring to which either a purine (adenine and guanine) or pyrimidine (thymine or cytosine) base is connected to the anomeric 1' position. DNA strands are hydrogen bonded to each other by complimentary (Watson-Crick) base-pairing (A to T and G to C) and form a double helix structure that provides the genetic code to create all the items the cell will need to function and reproduce. RNA is of similar construction to DNA. RNA employs a different base, uracil (U) in place of thymine (T) in its secondary structure and, amongst its many functions, acts as reader to the genetic code used to transcribe DNA information in to the primary sequences of proteins. The trivalent nature of the orthophosphate group is what makes it an ideal linkage in DNA and RNA. It allows connection of the nucleoside monomers in a tape-like structure while remaining negatively charged and is therefore

stabilised against hydrolysis and also secured against loss from the cell as the charge prevents travel through the cell walls.[18,19]
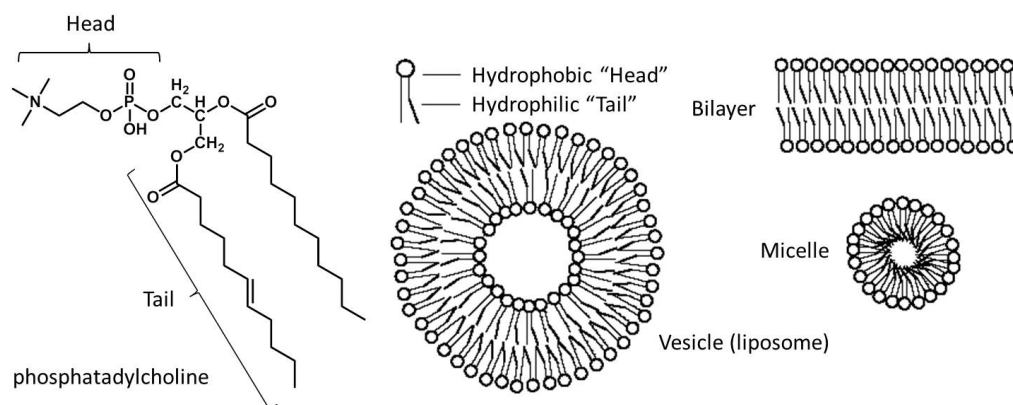
Figure 1.2: Diagram showing the construction of phospholipid structures. Dependent on size of the "head" group, length of the "tail" group, concentration, temperature, pH and ionic strength of the solvent, either bilayers (small head, long tail) or micelles (large head, short tail) will be formed. Phosphatadylcholine is an example of a common phospholipid used in the construction of cell membranes. (Image adapted from online course literature from www.winona.edu and used under kind permission of Dr. Steven P. Berg, Professor Emeritus, Biology Department, Winona State University, Winona, Minnesota, USA)

Molecular DNA and RNA are contained within cell structures, the walls of these cells themselves contain P and are constructed from phospholipid bilayers[11] (Figure 1.2). The cell walls are formed due to hydrophobic and hydrophilic effects on the phospholipid molecule, i.e. phosphatidylcholine (Figure 1.2). These structures occur due to the interaction of the hydrophobic "tails" of the phospholipids with water. As the hydrophobic groups attempt to minimise their contact with water, structures are formed in which only the hydrophilic phosphorus "head" groups are exposed to the water. Dependent on size of the "head" group, length of the "tail" group, concentration, temperature, pH and ionic strength of the solvent, either bilayers (small head, long tail) or micelles (large head, short tail) will be formed. Cells are formed from vesicles which are made from phospholipids in a bilayer configuration. Once a bilayer is formed, if the concentration of phospholipid is increased, the bilayer will start to fold to minimise Gibbs Free Energy (ΔG) forming vesicle structures. The phospholipid bilayer forms a semi-permeable membrane allowing access to nutrients and sources of energy while keeping in the contents of the cell but also allowing waste products to be excreted.

Other phosphorus compounds are also used in living organisms for example most co-enzymes are phosphoric or pyrophosphoric acids (Figure 1.3). Co-enzymes are essential in biochemistry as they assist in the function of enzyme processes. For example, co-enzyme-A is involved in the synthesis and oxidation of fatty acids while co-enzyme-B is utilised in redox reactions by methanogens. Many processes in metabolism are oxidative in nature and thus require a reducing agent to accept electrons and protons. Nicotinamide adenine dinucleotide (NAD^+) is a major co-enzyme involved in redox processes in biochemistry. Enzymes transfer protons and electrons to NAD^+ to form the reduced NADH which can transfer the protons and electrons to other redox reactions. The reduction of NAD^+ to NADH is a process often involved in catabolism assisting in the production of adenosine triphosphate (ATP) which is an essential energy transfer molecule in biochemistry by oxidative phosphorylation.[20]
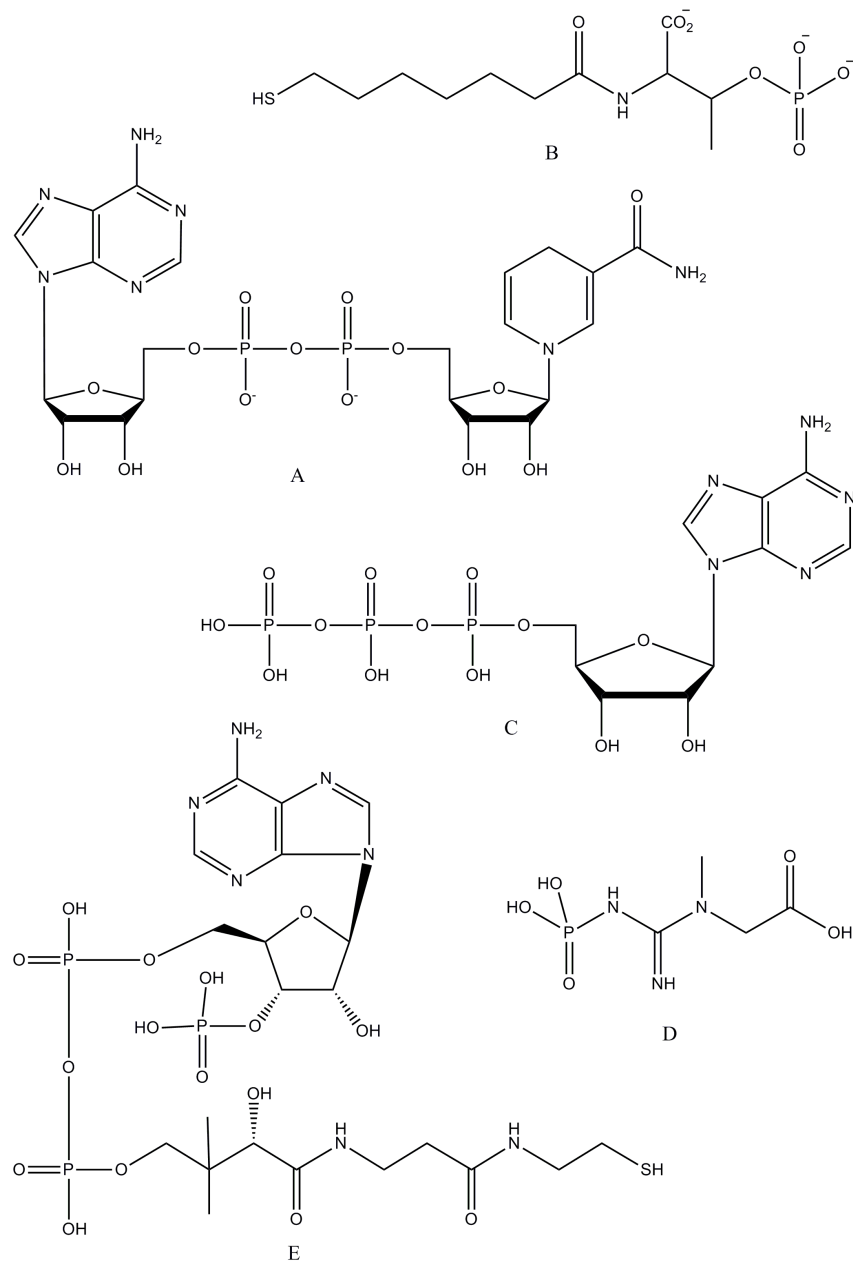
Figure 1.3: Examples of co-enzymes and phosphorus containing energy molecules used in current biochemistry. The molecules shown are: A) Nicotinamide adenine dinucleotide (shown in the reduced form NADH) which is involved in the citric acid cycle and oxidative phosphorylation reactions in living cells. B) Co-enzyme B which is used by methanogens in redox reactions. C) Adenosine triphosphate (ATP) is a major energy currency molecule. D) Creatine phosphate or phosphocreatine is used in the regeneration of ATP from ADP. E) Co-enzyme A which is involved in the synthesis and oxidation of fatty acids.

Adenosine triphosphate is the principle biochemical energy transfer mechanism involve phosphates and is often referred to as a unit of energy currency in in intracellular energy transfer.[21] ATP contains three linked phosphate groups and is produced enzymatically from adenosine monophosphate (AMP) and adenosine diphosphate (ADP) *via* either photophosphorylation in photosynthesis, substrate-level phosphorylation (direct phosphate transfer) or oxidative phosphorylation in cellular respiration. During metabolic processes, ATP is converted back into its molecular precursors (ADP + phosphate or AMP + pyrophosphate) releasing energy ($\Delta G_{Hyd}(ATP)$ = -30 to -50 kJ mol) but can then be recycled back to ATP with an input of energy from redox reactions using simple and complex sugars (carbohydrates) or lipids as an energy source.

The structures of molecular DNA, RNA and other biochemical phosphorus species highlighted above (Figure 1.1) are very complex and would be unlikely to have been constructed *de novo*. Specific favourable conditions (acidic, alkaline or high temperature) would be required; the reactants introduced in the correct sequence and in the ideal concentrations to create such molecules and therefore the ability to create each of the individual components alone would not be enough. Phosphorus has become central to all life on our planet but from a chemical point of view poses several problems when trying to recreate the origins of life. The major issue in biochemistry is the availability of sufficiently chemically active, water-soluble phosphorus to drive some of the key chemical processes *en-route* to life.

1.2   Why did nature choose phosphorus?

Phosphorus is ubiquitous to life on Earth. It is the 18th most abundant element in the cosmos, the 11th most abundant on the Earth and makes up *ca.* 1% of composition by weight of the human body.[10] It has become an integral element in current biochemistry but why did nature choose to use this element in particular? The answer to his question is in the specific chemical properties that phosphorus possesses which make it very suited and almost unique. Current biochemistry uses phosphorus mainly as phosphates and almost exclusively in the fully oxidised P^{5+} state. Phosphate is soluble in deionised water which is the solvent used in nearly all known metabolic reactions. Many organic compounds are phosphorylated when they enter a cell to increase solubility in water. The increase in solubility is due to the addition of a charged functional group to the molecule. The charged group also acts to help the cell retain the molecules as ionically charged species are unable to cross the amphiphilic membrane. This would have been an important feature in early life as it allows for concentration of useful molecules within cells. Losing these to the outside world would be a major issue and a barrier to the sustainability and development of life.

As previously stated, a major property of phosphate containing compounds is the ability to store and release energy. Many phosphorus bio-molecules are thermodynamically unstable and will release energy during degradation and hydrolysis, examples of these molecules can be seen in Table 1.1.[22] Though many phosphorus bio-molecules are thermodynamically unstable they are kinetically stable due to the resistance of the negatively charged phosphate group to hydrolysis. These molecules can be further stabilised by the presence of divalent

Name	Class	$\Delta\,G^0_{HYD}$ (kJ/mol)
Phosphoenol pyruvate	Reactive P compound	-61.9
1, 3-bisphosphoglycerate	Reactive P compound	-49.3
phosphocreatine	Reactive P compound	-43.0
ADP	Condensed phosphate	-32.8
ATP	Condensed phosphate	-30.5
ATP $\rightarrow$ AMP + pyrophosphate [a]	**Condensed phosphate**	**-45.6**
AMP	Stable P compound	-14.2
Pyrophosphate	Condensed phosphate	-19.2
Glucose 1-phosphate	Stable P compound	-20.9
Fructose 1-phosphate	Stable P compound	-15.9
Glucose 6-phosphate	Stable P compound	-13.8
Glycerol 1-phosphate	Stable P compound	-9.2
Acetyl Co-A [b]	**Thioester**	**-31.4**
Acetic anhydride [c]	**Acid anhydride**	**-91.1**

Table 1.1: Standard free energy of hydrolysis for assorted compounds. Data from Nelson and Cox (2005)[22] and references therein. Table reproduced from Pasek and Kee (2011).[23] With the exception of those species marked in bold, all reactions consist of loss of a PO_3 group. [a] This reaction is the loss of a pyrophosphate group from ATP. [b] Acetyl Co-A has a S-C linkage which is hydrolysed to form SH and HO-C. [c] The Hydrolysis of acetic anhydride forms two acetate groups and is shown to indicate the potential energy available from hydrolysis of anhydride linkages.

cations such as Mg^{2+} which reduce available space for water, preventing hydrolysis.

1.3   The "phosphate problem"

The "phosphate problem", is one hurdle life would have to overcome to utilise phosphorus as nature does in living organisms today. On Earth today, the majority of P exists in the form of orthophosphate minerals [PO_4^{3-}] in the fully oxidised form (P^{5+}). There are over 200 known crystalline phosphates on Earth, belonging mainly to one group known as apatites which are used primarily for industrial production of fertilizers.[24] On a pre-biotic Earth, the main P mineral would probably not have been apatite [$Ca_{10}(PO_4)_6X_2$ where X= F, OH, Cl] which is a biologically precipitated P mineral[25] but whitlockite [$Ca_9(MgFe^{2+})(PO_4)_6PO_3OH$] which is the P mineral which is thermodynamically and kinetically favoured under abiotic conditions.[26] The case for whitlockite being the favoured prebiotic phosphate mineral is strengthened when it is noted to be found in Martian and lunar meteorites and also in chondritic meteorites.[27]

There are three problems with phosphate minerals which can pose an issue for inclusion in origin of life reactions. The first issue is the solubility in water. Pasek and Lauretta (2005) state that in the presence of divalent cations (specifically Mg^{2+} and Ca^{2+}) commonly found in seawater[28] the concentration will typically be lower than 1 μM (neutral pH at Standard Temperature and Pressure, STP) and above this the phosphate will precipitate out.[29] Even under acidic conditions as the early oceans were believed to be the solubility is still very low typically 10 μM (pH 5 at STP).[24] When this figure is compared to the P content of the human body of between 250 and 750 ppm,[30,31] it suggests that a more reactive and water-soluble form of phosphorus must presumably have been present on the

early Earth to allow such concentrations to be utilised.

The second issue with phosphate is its reactivity. Phosphate is thermodynamically stable, it is phosphorus at its lowest energy form as can be seen on a Frost diagram (Figure 1.4). It has no need to partake in reactions to become more stable and therefore needs to be activated to participate in chemical reactions. Current biochemistry relies on activated, reactive forms of P such as condensed phosphates (ATP or pyrophosphate) or phosphorylated organics (P-C bond containing molecules such as phosphocreatine or acyl-phosphate) and uses enzymes to create and control these processes. These enzymes will have developed over time and would not have been available to assist during the formation of life. Therefore, there must have been a more active form of P available for origins of life reactions.

The third issue is that due to the reactivity and solubility issues, the geological recycling of phosphorus is very slow meaning that the availability of P would be a major limiting factor for the origin of life on earth. It has been reported that geological processes can produce small amounts of reduced or activated phosphorus. Yamagata (1999) found trace amounts of pyrophosphate and trimetaphosphate in fluids around hydrothermal vents[32] while Pech *et al.* (2009) found trace amounts of phosphite in hydrothermal fluids in Hot Creek Gorge near Mammoth Lakes, California.[33] Current redox conditions on Earth favour the locking of P in the thermodynamically stable P^{5+} form which means that reduced P is not stable for long periods of time.[29, 34] On an early Earth the environment would be less oxidising allowing for greater stability and longevity for reduced P species making them ideal candidates for inclusion in origins of life reactions.

1.3.1 Reduced oxidation state phosphorus (ROSP)- Solution to the phosphate problem

With phosphorus having a central and irreplaceable role in current biochemistry, nature must have found a way to overcome the solubility, reactivity and recycling issues discussed earlier. One plausible explanation is the use of reduced oxidation state phosphorus species[35] in early biochemistry until nature was able to develop enzymes to incorporate phosphate.

In 1955, Addison Gulick first suggested that reduced species of phosphorus may have been required for inclusion in origins of life reactions.[36] Gulick suggested alternatives to phosphate (P^{5+}) which were more reactive and also more soluble in water. The alternatives suggested such as phosphite (P^{3+}, also referred to as H-phosphonate), hypophosphite (P^{1+}, H-phosphinate), hypophosphate (P^{4+}) and phosphine (P^{3-}) are between $\times 10^3$ and $\times 10^6$ times more soluble in water in the presence of divalent cations than phosphate.[30] Gulick stated that, if there was a source of these reduced phosphorus compounds on an early Earth, then there would be much more reactive P around for inclusion in reactions than if there was just phosphate on its own.[36] Gulick was not able to name a source of reduced P on an early Earth and therefore his idea was generally dismissed, particularly by Miller and Urey (1959)[37] as it was assumed that phosphate would have been the only available P supply for inclusion in reactions.

The discovery of phosphonic acid [H_3PO_3], the acid form of phosphite, in the Murchison meteorite[38] opened the gates for Miller's assumption to be challenged. The question was
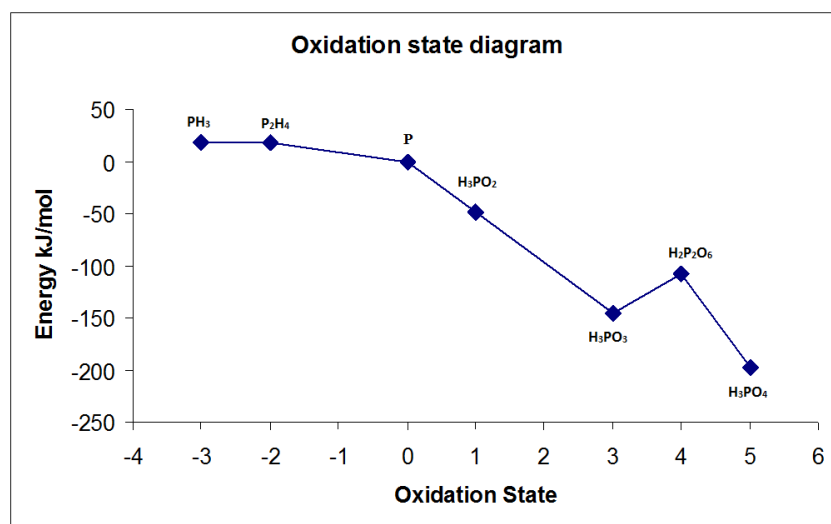
Figure 1.4: Oxidation state diagram for phosphorus under acidic conditions indicating the relative stability of each oxidation state. Adapted from Greenwood and Earnshaw, Chemistry of the Elements (1993)[11]

asked 'could meteorites have been an abundant source of reduced P to an early Earth, especially through the late heavy bombardment (LHB)?' The Murchison meteorite was an observed fall of a type II carbonaceous chondrite (CM2) in 1969 just outside the town of Murchison, Victoria in Australia.[39] The meteorite was recovered from an area covering 13 km^2 with a total recovered mass of 4.5 kg. As the fragments were recovered quickly, Murchison was not subjected to weathering and biological contamination as in normal meteorite finds of this type, giving great significance to the identification of phosphonic acid within its chemical library. Murchison was found to contain a large number of organic compounds such as amino acids, sugars, carboxylic acids and additionally contained organophosphonates [see Kvenvolden *et al.*(1970),[40] Oro *et al.* (1971),[41] Ponnamperuma (1972),[42] Cooper *et al.* (1992)[38] and Schmitt-Kopplin *et al.* (2010)[43] as examples]. The latter are organo-phosphorus species containing reduced oxidation state phosphorus (contain P-C bonds rather than P-O-C bonds seen normally in organophosphates). The source of these organic species was alluded to by de Graaf *et al.* (1995) as a direct result of photolysis reactions of phosphite and organic compounds present[44] while Gorrell *et al.* (2006) claimed the formation of such species could be the result of gas-phase reactions.[45]

The presence of reduced phosphorus on the Murchison meteorite opened research to the idea of meteorites as a viable potential source of reduced, active phosphorus on the early Earth. As stated earlier in this chapter, whitlockite [$Ca_9(MgFe)(PO_4)_6PO_3OH$], considered to be a prebiotic phosphate mineral, is commonly found in Martian, Lunar and chondritic meteoritic falls on Earth.[27] Research has shown that it may have been possible to reduce this phosphate mineral to phosphite (P^{3+}) or even phosphide (P^0) by shock impacting during a high-speed collision with the Earth surface.[46] During the impact meteorites are exposed to extreme surface temperatures and forces which would cause partial vaporisation during impact (ablation). The meteoritic material and any metal vapours present would create a reducing environment which may be capable of phosphate reduction.[46,47] It may also be possible to reduce phosphate rocks present at the impact site, again due to the high energy/high temperature nature of meteoritic impacts.
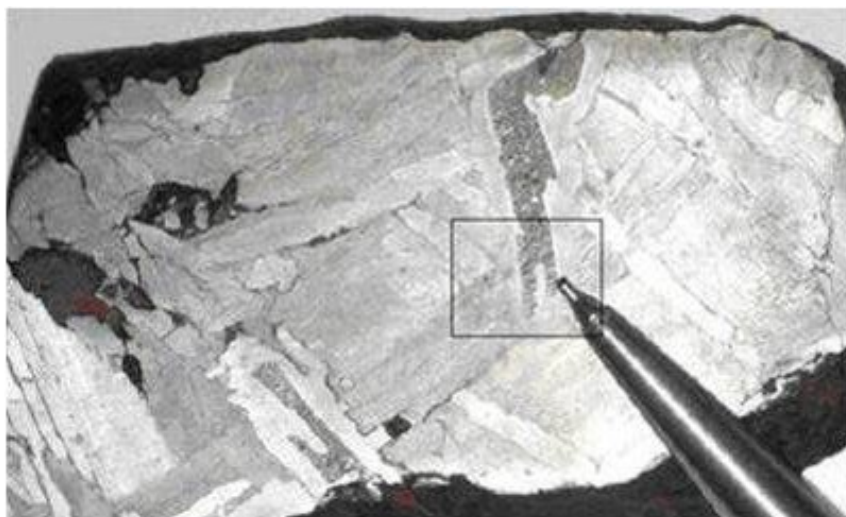
Figure 1.5: Photograph of sample of the Seymchan meteorite showing an inclusion of the mineral schreibersite. Schreibersite inclusions [FeNi$_3$P] are often found in iron meteorites and are generally iron poor and nickel rich compared to the main body of the meteorite. (Credit: T. P. Kee, University of Leeds)

Another potential source of reduced phosphorus is from the mineral schreibersite (Figure 1.5, (FeNi)$_3$P) which is an iron/nickel phosphide found commonly in iron meteorites such as the Seymchan, Canyon Diablo and Sikhote Alin meteorites. Schreibersite is an iron/nickel phosphide mineral which is commonly found in iron meteorites (up to about 0.5% wt).[28,48] It is a very brittle mineral and is formed by differentiation during cooling after accretion of materials produced by supernovae. Schreibersite forms small inclusions within the iron meteorite matrix, which itself consists of two iron/nickel alloys, Kamacite (90:10 to 95:5 composition Fe:Ni) and taenite (80:20 to 35:65 composition Fe:Ni) which form in an interlaced pattern of long crystals known as a Widmanstätten pattern. The composition of schreibersite has been shown to be three metal atoms to one phosphorus which form in a tri-capped trigonal biprism (space group $/\bar{4}$), with Fe:Ni ratios of 1.65:1.35 to 1.8:1.2 reported in the literature.[49–51] Phosphorus contained in schreibersite is already in a reduced [P^0] form upon delivery to Earth, with just extraction from the meteorite required for potential use in prebiotic chemical reactions.

1.4 Sources of ROSP

Phosphites [HPO$_3^{2-}$], hypophosphites [H$_2$PO$_2^-$], phosphides such as iron phosphide [Fe$_3$P] and phosphine [PH$_3$] are reduced oxidation state forms of P which are more chemically reactive under milder conditions than P locked in orthophosphates (Figure 1.6). Identification of sources of these reduced phosphorus species on the prebiotic Earth is required and this has been the subject of much research. Volcanism was proposed by Yamagata *et al.* (1991) as a potential source of reduced and condensed P species.[52] In simulation experiments Yamagata was able to identify pyrophosphate, tripolyphosphate, tetrapolyphosphate and small amounts of cyclic trimetaphosphate (cTMP) along with other unidentified condensed polyphosphates by ^{31}P NMR analysis (Figure 1.7). While pyrophosphate is thought to have been an early energy molecule for life it is relatively insoluble in water and is quickly precipitated from water by the presence of divalent cations.[53] Tripolyphosphate

and tetrapolyphosphate are only produced in small amounts and also have low solubility in the presence of divalent cations and are mainly used as corrosion inhibitors and detergent additives. The species of interest was cTMP as this is an activated condensed P species and is capable of coupling amino acids and also phosphorylating organics. The issue was that in simulations only small amounts were made and it was not possible to identify this species from actual volcanic samples which could be considered a blow for its prebiotic provenance as a molecule of interest.
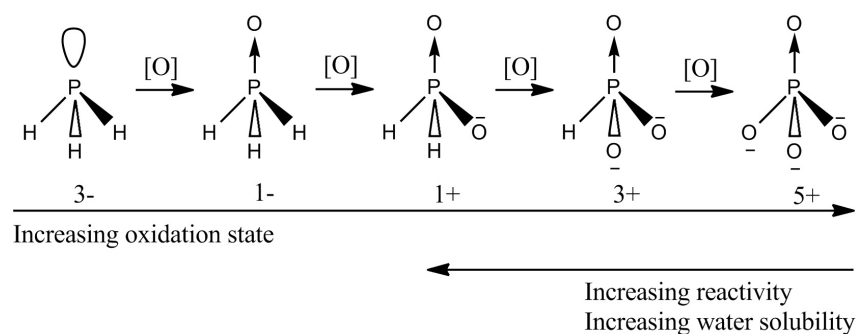
Figure 1.6: Diagram showing the different oxidation state of phosphorus species. Starting with phosphine (P^{3-}) going through to hypophosphite (P^{1+}), phosphite (P^{3+}) and finally phosphate (P^{5+}). The P^{1-} species is phosphine oxide (PH_3O) which is a highly reactive and unstable intermediate *en-route* to hypophosphite which can tautomerise to phosphinous acid (PH_2OH). This species has been detected by mass spectrometry as a direct reaction product between oxygen and phosphine.[54] The diagram also shows that with decreasing oxidation state that both reactivity and water solubility increases. The exception to this general rule is phosphine which is very highly reactive but only slightly soluble in water (0.22 mL of gas dissolve in 1 mL of water[5])
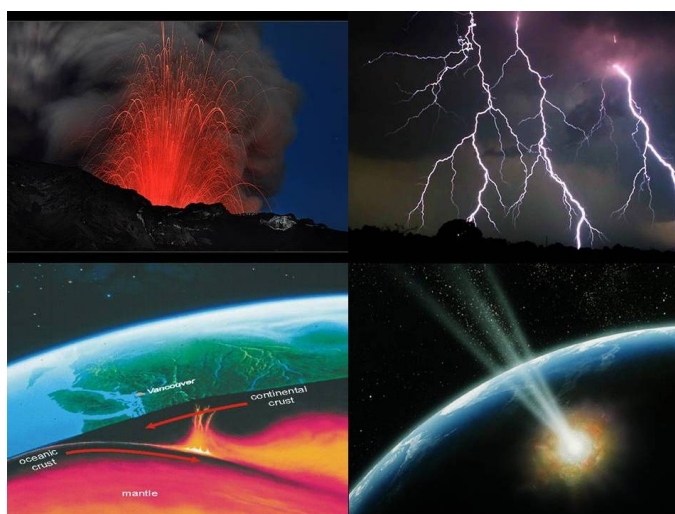
Figure 1.7: Image showing potential sources of reduced and activated phosphorus species. Clockwise from top left are: Volcanism - Shown by Yamagata *et al.* (1991) to produce activated phosphorus species such as pyrophosphate, tripolyphosphate and cyclic trimetaphosphate.[52] Lightning - Investigated by Pasek and Block and shown to be able to reduce phosphate to phosphite.[55] Meteorites - The discovery of phosphonic acid on the Muchison meteorite[38] introduced meteorites as a source of reduced oxidation state phosphorus. Meteorites are also known to contain schreibersite [$(FeNi)_3P$], an iron/nickel phosphide which is also a reduced oxidation state phosphorus source.[28,56] Mantle subduction - This method was proposed by Glindemann *et al.* (1998) with reduced phosphorus species produced as part of crustal recycling through the mantle.[57] One issue with this process is it is very slow and it is also believed that plate tectonics began after life had already started.[58]

Mantle subduction was proposed by Glindemann *et al.* (1998) as a source of reduced P species, mainly phosphides (Figure 1.7).[57] It was proposed that plate tectonics would carry apatite into the mantle and that in the presence of iron metal and other reducing material

at temperatures in excess of 1200°C the apatite will be reduced to form iron phosphides. A major issue with this method however is it is a very slow process[12,29]. Industrial production of calcium phosphide [Ca_3P_2] involves reduction of phosphate by heating apatite $Ca_3(PO_4)_2$ to 1200°C in the presence of carbon,[11] elemental phosphorus [P_4] is manufactured today by heating apatite, silica and coke to 1500°C[11] and metal phosphides such as the fumigant aluminium phosphide [AlP] are prepared by passing gaseous phosphorus over heated aluminium metal. Phosphine is a known product of hydrolysis of metal phosphides such as calcium, aluminium and zinc phosphide which are used commercially as insecticides, rodenticides and fumigants (World Health Organisation, Environmental Health Criteria 73: Phosphine and selected metal phosphides and references herein[59]). Glindemann also proposed that phosphine gas [PH_3, P^{3-}] is part of the global phosphorus cycle (Glindemann *et al.* (2003) and references herein[60]) and can be produced abiotically by corrosion of phosphorus-rich iron[57] but also by tectonic pressure[61]and lightning.[62]

Lightning is a major source of energy and can contain up to $\times 10^9$ J per strike,[63] heating the air around the bolt up to $\times 10^5$ K almost instantaneously.[64] Bolts are estimated to strike the surface at a rate of *ca.* 44 events every second (Figure 1.7).[65] Due to the temperature and energy provided by each strike, lightning is capable of altering the chemistry and morphology of the ground material flowing through areas of high moisture content or conductive material such as plant roots, rapidly heating them to over 2500 K causing the formation of glassy units of melted ground material which is known as a fulgarite.[55] Pasek and Block (2009) also looked at the reduction of phosphate by lightning by analysis of fulgarites produced by lightning strikes. During analysis of ten fulgarites they found phosphorus present as phosphate, pyrophosphate, phosphite and hypophosphite and that between 21 and 68% of available phosphorus was reduced during a lightning strike estimating that between 2,000 and 3,000 kg per year of reduced P was produced by this method.[55] Based on these findings, lighting could be considered a good source of reduced phosphorus though maybe not the only available source.

As stated previously, reduced P-oxyacids and organophosphonates were identified in the chemical inventory of the Murchison meteorite[38] which led to the thought that meteorites could have been an abundant source of reduced P on the early Earth (Figure 1.7). The Murchison meteorite is a type CM2 chondrite. Such materials only make up a small amount of falls recorded on Earth (*ca.* 4% recorded falls), with all types chondrites making up around 86% of all falls to Earth.[48] Iron meteorites were also established as a good source of reduced phosphorus by Pasek and Lauretta (2005) and also Bryant and Kee (2006). They are known to contain the mineral Schreibersite [$(FeNi)_3P$], an iron/nickel phosphide which when corroded in water released phosphite, hypophosphate and hypophosphite amongst other condensed and reduced P species (see Figure 1.8 and Figure 1.9 for examples).[28,56] It has been estimated that between 5×10^{19} and 5×10^{21} kg of phosphide minerals were delivered to the Earth during the late heavy bombardment period making these iron meteorites a significant source of reduced P on the early Earth.[29] Pasek and Lauretta (2005) produced a variety of reduced and condensed phosphorus species including phosphite and pyrophosphite (see Figure 1.8) by aqueous processing at 20°C both under anaerobic and aerobic conditions.[28] This research also showed that processing under anaerobic conditions produced the same species just at a reduced rate.[28]

Bryant and Kee (2006) conducted processing under interstellar-like conditions (N_2 atmosphere, 77 K exposed to UV radiation at 254 nm at *ca.* 500 mW and 185 nm at *ca.* 40 mW for 3 hours) producing both phosphite and hypophosphite (see Figure 1.9).[56] The reactions were shown to proceed by photo-oxidation of P by water involving generation of phosphite radicals and also H· and HO· radicals which then react to form the species observed.[56,66] It was also shown that at the schreibersite/matrix interface there was potential for cathodic reactions as electrons passed from the matrix to the phosphide during corrosion as the inclusion is observed to be more noble than the iron matrix.[67]
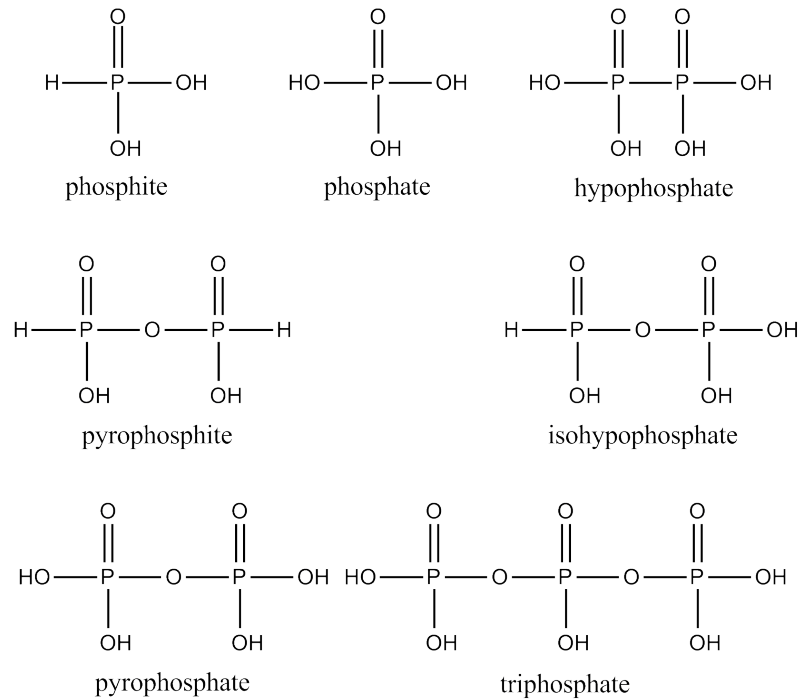
Figure 1.8: Diagram of the phosphorus species reported by Pasek and Lauretta (2005) from schreibersite containing meteorites by aqueous processing at 20℃ both under anaerobic and aerobic conditions.[28]

Figure 1.9: Diagram of the phosphorus species reported by Bryant and Kee (2006) by processing under interstellar-like conditions (N_2 atmosphere, 77 K exposed to UV radiation at 254 nm at *ca.* 500 mW and 185 nm at *ca.* 40 mW for 3 hours)

In 2009, Pech *et al.* reported the presence of geothermally produced phosphite in hydrothermal fluids from Hot Creek Gorge, near Mammoth Lakes in California (Figure 1.10).

They reported detection of 0.06 ± 0.02 μM of phosphite in a pristine geothermal pool initially using suppressed conductivity ion chromatography and confirmed by ion chromatography/mass spectrometry[33] giving credence to the possibility that phosphite and other reduced oxidation state phosphorus species were present on an early Earth. It could be construed that if reduced P can be found in current environmental conditions, which are highly oxidising in nature, that with the early Earth being less oxidising it is possible that there would be greater amounts of reduced, reactive P around on an early Earth to participate in origins of life reactions. Mulkidjanian et $al.$ (2012) gave credence to this theory stating that volcanic hydro-geothermal systems such as those seen in Kamchatka, Russia may have the ability to reduce phosphate to phosphite while also allowing for the concentration of P and other required molecules and ions required for the origins of the first cells, particularly K^+, Na^+, Zn^{2+} and Mn^{2+}.[68] Mulkidjanian et $al.$ claim that geothermal pools, by vapour deposition were able to produce the correct K^+/Na^+ ratio seen in current cell biology while also having high Zn^{2+} and Mn^{2+} and P concentrations and the fluids in these pools are analogous to the content of current cells.[68] This theory was met with wide criticism though Mulkidjanian and co-authors attempted to clarify and strengthen their position with the publication of a follow up article addressing the major questions raised regarding the theory (see Mulkidjanian et $al.$ 2012a and references therein).

Figure 1.10: Photograph of a hot pool in Hot Creek gorge, Mono County, California which is a highly geothermally active area. It was in such a pool where Pech et $al.$ (2009) identified phosphite in the hydrothermal fluids using ion chromatography.[33] Credit: Photo from University of California, Santa Cruz. (http://emerald.ucsc.edu)

It seems plausible that phosphite and reduced oxidation state phosphorus species would have been present on an early Earth though the species and quantities have yet to be fully established. It would seem appropriate to further investigate the sources of P on an early Earth and to try to establish the species and quantities present, and also the conditions and environment they would be exposed to. To do this we first must look for answers to these questions: 'How was the Earth was formed?', 'How was the atmosphere on Earth was formed and what was its composition?', 'How did the oceans come into being?', 'How soon after accretion was there liquid water on the surface?', 'What was the pH?', 'What was the temperature, the salinity and the composition?'. Only with all of these conditions

established will we truly understand the molecular and chemical inventory which would be available for origins of life reactions. The major issue is that there is no geological record of these conditions to draw on so it is an area of great speculation and argument.

1.5   Formation of the Earth

The Earth was formed around 4.5 billion years ago, accreting from grains and small planetesimals which had formed in the nebula surrounding a very young star. The grains and planetesimals are the same composition as chondritic meteorites which are believed to have formed from the same nebula material around the same time as the Earth.[69] Once the heavier elements, molecules and grains are collected from the nebula to form the planetary mass, the lighter elements and gases are collected to form the early atmosphere. The primary atmosphere would have been composed mainly of H_2 with other simple hydrides [H_2O, CH_4, and NH_3] which are seen in the gas and ice giants of Jupiter, Saturn, Uranus and Neptune.[70–72] There would be degassing into the atmosphere caused by impacting material to the surface removing volatile gases from the solid Earth.[73–78] Recent theoretical studies on the subject of impact degassing have shown that this method of degassing would have been responsible for an atmosphere of highly reduced gases.[79–81]

Studies have modelled the out-gassing of volatiles from impacts using chondritic material as an analogue for the early Earth.[79] Articles by Zahnle (2010) and Schaefer and Fegley (2007 and 2010) refer to unpublished work by Bukvic (1979) which showed that the major out-gassing products were CH_4 and H_2 at high temperatures and N_2 at lower temperatures while Schaefer and Fegley (2007)[79] found the major components of degassing chondritic material to 1225 K (melting point for Fe-Ni sulphides) were CH_4, H_2, H_2O, N_2 and NH_3. The conclusion of these studies was that the primary atmosphere was rich in reduced gases like those claimed by Urey (1952)[82] and similar in composition to those used in the world-famous Miller-Urey experiment in 1953.[2] The primary atmosphere would start to escape by diffusion once the nebula material was used up, though for a planet the size of Earth, escape by this method would be difficult.[83,84] A major impact, such as the Moon forming impact however would have caused the loss of the primary atmosphere in a matter of hours[85] though the primary atmosphere would have had some effect on the redox state of the planet prior to its loss.[69] While this study gives credence to the atmosphere used in the Miller-Urey experiment, it does not give consideration to the high levels of incident UV radiation which would photolyse ammonia to trace levels or that the moon-forming impact would have obliterated any organics formed during the time of the primary atmosphere.

The Moon is broadly accepted to have been formed by a collision between the early Earth and a planet roughly the size of Mars and took place between 30 and 100 million years after the formation of the solar system (Figure 1.11).[86–89] The impact would have liquified the planet and led to significant loss of the primary atmosphere though Genda and Abe (2003, 2005) state that much of the water present in the atmosphere would have remained.[90,91] Immediately after the impact, the atmosphere would be filled with water vapour and other volatile gases but also hot vaporised silicate which would have rained out over *ca.* 1000 years.[85] After loss of silicate from the atmosphere, the rate of cooling of the Earth would

Figure 1.11: Artistic impression of the collision of Thea with the proto-Earth which is believed to have formed the Moon. The impact liquefied the planet, caused loss of the primary atmosphere and loss of nearly all volatiles present on the Earth from accretion. Credit: Fahad Sulehria, www.novacelestia.com

be controlled by clouds of water vapour in the atmosphere.[91] This would have limited heat loss from the atmosphere leading to a temperature rise close to a runaway greenhouse threshold.[92] The molten rock surface of the planet was between 1800 K and 2000 K and would have allowed for great heat exchange with the atmosphere (140 W/m^2),[92] rivalling solar radiation in terms of energy input.[69] During this time, differentiation of the mantle would have occurred with heavy metals moving towards the core making the mantle metal-free.[93] The mantle would have then started to solidify from the bottom up due to the pressure effects on the melting point of silicate, taking between 2 million[69] to 20 million years[92] to reach the planet surface. The heat flow from the planet would then have reduced considerably (to *ca.* 0.5 W/m^2)[92] which would be unable to sustain the runaway greenhouse atmosphere. This would result in the condensation of water vapour from the atmosphere, removing water soluble volatiles from the atmosphere and creating a hot, salty ocean.[69]

The amount of CO_2 in the atmosphere, though much greater than today's levels (*ca.* 10-200 bars),[69,92,94,95] was not enough to cause a runaway greenhouse effect but was enough to keep the temperature of the atmosphere around 500 K.[96,97] With liquid water on the surface and the basalt crust, the CO_2 atmosphere would be unsustainable.[82] CO_2 would be removed from the atmosphere as carbonates[97] by reaction with MgO and CaO (formed by interaction with basalt and water). Sleep (2010) claims that with vigorous hydrothermal circulation and rapid mantle turnover, around 100 bars of CO_2 could have been removed from the atmosphere in less than 10 million years.[92] Without the CO_2 dominant atmosphere the surface temperature of the Earth would fall from *ca.* 500 K to around 220 K which would lead to freezing of the oceans, though a mixture of heat from the mantle and salt content would prevent them from freezing completely.[69] The impacts of meteorites and asteroids would trigger impact "summers" causing melting of the ice allowing for control of CO_2 levels in the atmosphere. The secondary Earth atmosphere would slowly

develop due to degassing of the mantle and volcanism resulting in an atmosphere composed mostly of H_2O, CO_2 and N_2 with small amounts of CO and H_2.[98–101]

1.6   Late Heavy Bombardment (LHB)

Due to the impact degassing of the early Earth and then subsequent loss of the primary atmosphere during and after the Moon forming impact, The Earth was depleted in volatiles (C, N, O and S) compared to chondritic meteorites (believed to have formed from the same nebula material as the Earth) and their known solar abundances.[102] The Earth would then require a source of these volatile materials but also metals which were removed from the crust and mantle during differentiation of the mantle post Moon-forming impact.[103–106] A method of replenishment of volatiles would be required to reintroduce elements lost from the atmosphere during the Moon impact and mantle/core differentiation. A postulated source of this essential volatile material was the late heavy bombardment period (LHB).

The LHB is said to have occurred post Moon-forming impact between 4.1 and 3.8 billion years ago[107] as a result of perturbation of the main asteroid belt by the migration in orbital positions of two of the outer planets, Saturn and Jupiter.[108–110] It is proposed that, after accretion from the nebula, Saturn and Jupiter's orbits were closer together but also that Saturn was orbiting inside Jupiter. At a critical point *ca.* 4.1 billion years ago their mean mass resonance caused a migration of Jupiter's orbit inward towards the sun and that Saturn moved out taking up the current positions after *ca.* 100 million years of instability.[108] This caused gravitational distortion of all the planets' orbits, and caused a major perturbation of the main asteroid belt sending material inwards towards the inner planets and also outwards towards the Kuiper belt and the Oort cloud. The migration theory was successfully modelled in the Nice model,[108,110] which showed that the rapid giant planet orbit migration would cause orbit destabilisation of asteroids and planetesimals in the main asteroid belt which then in turn caused a "sudden massive delivery of material towards the inner planets"[108] and that this inward traveling material was responsible for the LHB.[111,112]

The Earth and inner planets have always been subject to meteoritic and cometary influx but this one period in Earth's history is thought to have brought the majority of volatile elements and compounds to the early Earth.[66,121] There is very little evidence on Earth today of this cataclysmic impact period in the geological record, due to the recycling of the rock record by plate tectonics over the last 4 billion years. There is, however, evidence of the LHB on our own Moon which still bears the impact crater scars today. With no plate tectonics the Moon has become a major source of geological information regarding the events of the early solar system.[122] The dating of the LHB period was possible by radiogenic dating of Moon rocks collected by NASA during the Apollo missions. The distribution of impact craters on the moon and radiogenic dating of Lunar rocks and meteorites lead to the conclusion of a period of heavy impact between 4.1 and 3.9 billion years ago, and if the Moon was subjected to such impacts it can be extrapolated that the other inner planets, including the Earth, were subject to the same intensity and period of bombardment.[123]
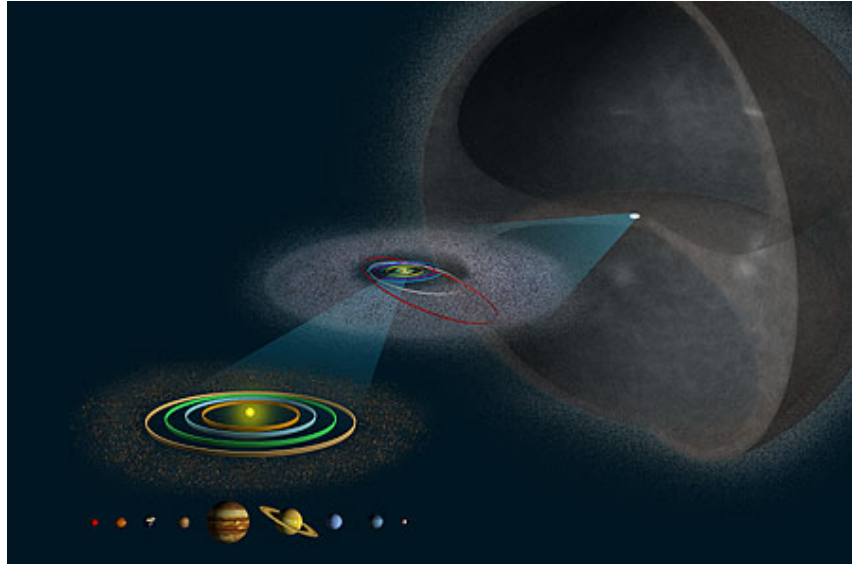
Figure 1.12: Illustration showing the current composition of the solar system. The Oort cloud is made up of dust, ices of water, methane, ethane, carbon monoxide and hydrogen cyanide[113] which envelopes the entire solar system, is believed to be a near-perfect example of the composition of the initial solar nebula, and is situated between 2000 and 50,000 AU.[114] The Kuiper belt is situated on the outer edge of the solar system outside Neptune between 30 to 55 AU.[115] Kuiper belt objects are composed of ices such as methane, ammonia and water, a composition similar to that of comets.[116] The main asteroid belt is situated between Mars and Jupiter between 2.0 and 3.5 AU.[117] The asteroid belt is composed of carbonaceous (*ca.* 75% of visible asteroids), S-type which are silicate-rich (*ca.* 15% of visible asteroids) and M-type which are metal-rich (*ca.* 10% of visible asteroids).[117]

1.7   Meteorites

The composition of meteorites is highly varied and can be split, based on their chemical, petrological and isotopic characteristics, into classifications. These classifications may be then further split dependent on their composition into Clans and Groups.[124] Meteorites are either referred to as Falls or Finds depending on whether the fall was observed or it was found without a known connection to an observed fall and are given names based on the location of the find. The three main classifications of meteorites are stoney, stoney irons and iron meteorites though they are more aptly described as chondrites (undifferentiated) and achondrites (differentiated, covers stony irons and iron meteorites).[124] A flow diagram of meteorite classification can be seen in Figure 1.14.

Chondrites are characterised by the content of small spheres, or chondrules, of *ca.* 1mm diameter and account for *ca.* 88% of all meteorite impacts on Earth.[48,125] They are composed mainly of silicates, sulphides and metals which themselves separate into five categories, carbonaceous (CC), ordinary (OC), enstatite (EC), Rumurutiite (RC) and Kakangari (KC) classifications.[124,126]

Carbonaceous chondrites are *ca.* 4% of recorded falls for this classification.[48,125] They contain high percentages of water (between 3% and 22% by wt[127]) and are composed mainly of silicates, oxides and sulphides. These meteorites have also been shown to contain significant amounts of organic materials including amino acids, carboxylic acids and hydrocarbons.[38] Ordinary chondrites account for *ca.* 82% of recorded chondritic falls and are composed mainly of silicates and are further classified by their iron and other metals content, while the enstatites account for only *ca.* 2% of falls and are composed mainly of
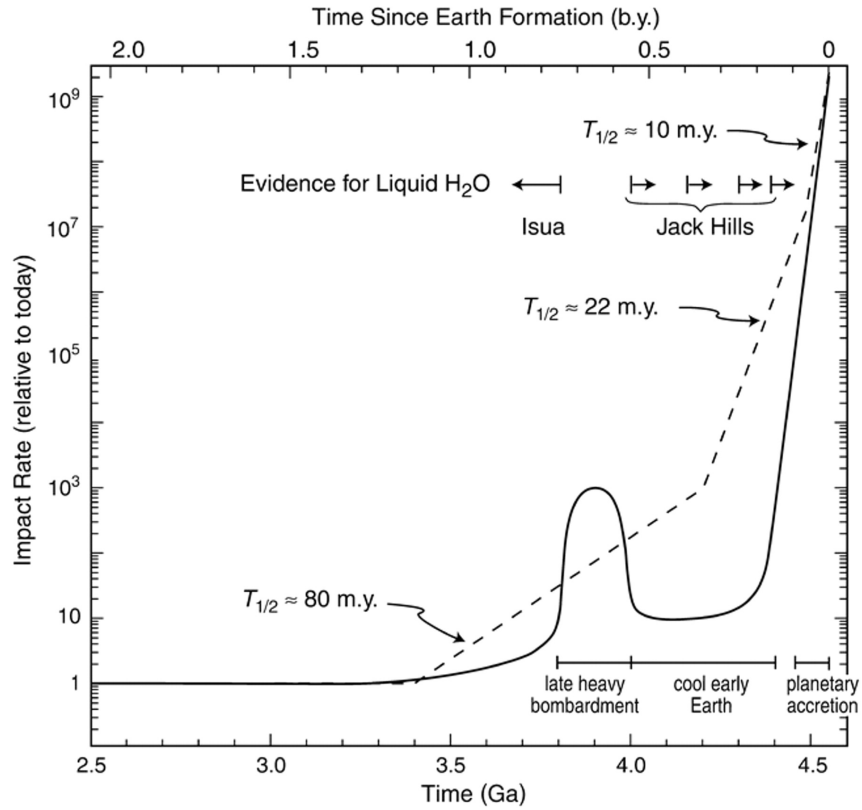
Figure 1.13: Graph showing the estimated impact rate of meteorites during the first 2 billion years after accretion. Dashed lines indicate the exponential decay hypothesis proposed by Hartmann *et al.* (2000).[118] The approximate half-life for periods of exponential decline in flux are given. The solid line indicates rates of impact for the cool early Earth hypothesis suggesting impact rates dropped rapidly by 4.4 billion years with a spike in impacts occurring between 4.1 and 3.8 billion years which signify the Late Hevy Bombardment (LHB). There is evidence of liquid water on the Earth's surface from high -δ^{18}O ratios present in Jack Hills zircons indicating water may have been present on the surface as early as 4.4 billion years ago.[119,120] This evidence would support the cool early Earth hypothesis. Image taken from Valley *et al.* (2002).[119]
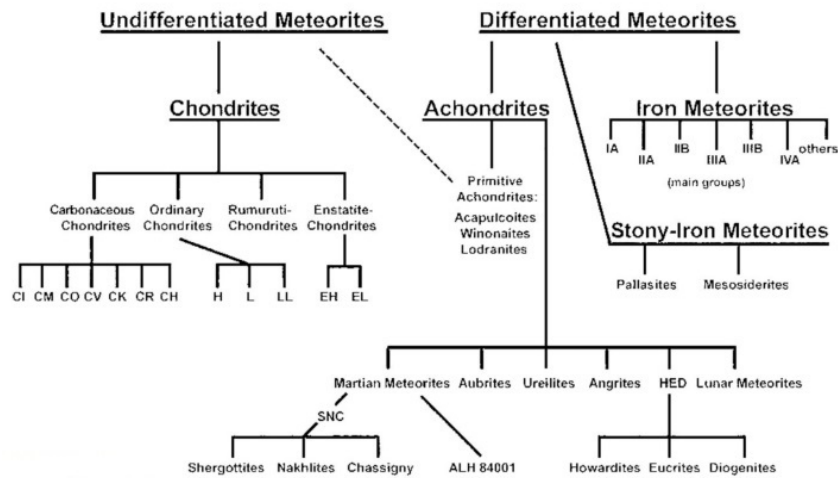
Figure 1.14: Flow chart showing the various classifications if meteorites. The meteorites are split into Classifications, Clans and Groups based on their chemical, petrological and isotopic composition. Credit: Dr. Dante Lauretta, University of Arizona, USA.

the mineral enstatite [$MgSiO_3$]. Rumurutiite chondrites are extremely rare with only one documented fall. These meteorites are identified by their low iron/nickel content which is mostly fully oxidised or present as sulphides.[124] Rumurutiites are also enriched in ^{17}O compared to ordinary chondrites. Kakangari chondrites are also rare with three recorded falls. They are highly reduced and have a large metal composition (typically between 6-10% volume).[124]

Chondrite meteorites are highly chemically reduced as they contain very little iron oxide and mainly iron and other metal sulphide minerals.[127] Chondrites are thought to be analogous to the composition of the crust of the early Earth as they are thought to have accreted from the same stellar nebula materials[37] around the same time period.

Achondrites account for *ca.* 8% of Earth impacts[48,125] and are principally of the same mineral composition as chondrites but do not contain any chondrules. Their mineral composition is thought to be similar to basalt and they have been subjected to differentiation and recrystallisation during melting. Due to this process they therefore have a mineral composition which is indicative of igneous processes on Earth.[127] Achondrites can be split into nine categories which include Acapulcoite, Lodranite, Winonaite, Howardite-Eucrite-Diogenite (HED), Angrite, Aubrite, Ureilite, Brachinite, Lunar and SNC meteorite classifications.[124]

Stony irons are also iron/nickel alloys but contain non-metallic mineral matter. This type of meteorite fall is extremely rare and these only account for *ca.* 1% of meteoritic Earth impacts.[48,125] Stony irons can be split into subcategories, pallasites and mesosiderite groups. Pallasites are composed mainly of olivine crystals (up to *ca.* 1 cm in size) in an iron/nickel matrix with minor quantities of the minerals schreibersite [$(FeNi)_3P$] and troilite [FeS] but also phosphate minerals (whitlockite [$Ca_9(MgFe)(PO_4)_6PO_3OH$], stanfieldite [$Ca_7Ca_2Mg_9(PO_4)_{12}$], farringtonite [$Mg_3(PO_4)_2$] and merrillite [$Ca_9NaMg(PO_4)_7$]).[128,129] Pallasite falls are considered very rare with only 61 known falls to date and are thought to originate from impact shattering of asteroids which have undergone differentiation. Mesosiderites are found to contain almost equal amounts of silicate and iron/nickel alloys with the silicates containing olivine [$(MgFe^{2+})_2SiO_4$], pyroxenes and calcium rich feldspars.[127] Again mesosiderites are extremely rare with only 167 recorded known falls to date.

Iron meteorites account for *ca.* 5% of Earth impacts but are *ca.* 88% of the total mass of meteoritic finds[48,125] due to their resilience to atmospheric entry and weathering but also as they are easily distinguishable from terrestrial rocks and minerals. Iron meteorites are considered analogous to the Earth's core and are known to originate from the cores of planetesimals formed during accretion.[130] Irons are composed of iron/nickel alloys such as kamacite (90:10 iron/nickel ratio) and taenite (up to 65% nickel content) and are known to contain smaller inclusions of phosphide (schreibersite, Figure 1.5), carbide (Cohenite, $(FeNiCo)_3C$) and sulphide (Troilite, FeS). Iron meteorites can be split into three subcategories and 20 groups dependent on chemical composition (Ni/[Ga, Ge and Ir] ratios) and whether the meteorites are considered magmatic or non-magmatic (primitive irons) in origin.[130]

During this research project, samples of the Sikhote Alin meteorite were sourced from

the Natural History Museum, London for use in some experiments. This meteorite was chosen for experimentation due to its large fall size, the common occurrence of schreibersite inclusions in the matrix and has been used previously for experimentation within the Kee group so could be compared to previous work.

The Sikhote Alin meteorite is an example of a type IIAB octahedrite iron meteorite, an observed fall in the Sikhote Alin mountains in eastern Siberia, Russia in 1947. The Sikhote Alin meteorite is known to be made up of 93% iron, 5.9% nickel with the remaining composition consisting of cobalt, phosphorus and sulphur with trace amounts of germanium and iridium.[131] The mineral composition of the Sikhote Alin meteorite is known to include kamacite, taenite, plessite (a mixture of kamacite and taenite), schreibersite $[(FeNi)_3P]$, troilite [FeS] and chromite $[Fe(CrAlFe)_2O_4]$ with an estimated *ca.* 70 tons of meteorite surviving through to Earth impact.[131]

Pasek and Lauretta (2005) estimated the annual flux of meteorites with a mass greater than 20 g through the late heavy bombardment period to be around 159×10^6 km^2 per year with an estimated mass of phosphorus delivered at $\times 10^9$ kg per year[28] making meteorites, particularly iron meteorites a significant source of reduced phosphorus on the early Earth.

In 2004, Orgel outlined three major restrictions important in the consideration of requirements for prebiotic evolution:[132]

1. The starting materials must be present in adequate amounts at the site of synthesis.

2. Reactions must occur in water or in the absence of solvent.

3. The yield of the products must be significant.

Based on the criteria stated by Orgel, Pasek stipulated that meteoritic P, in all cases, fit the criteria. Iron meteorites deliver huge quantities of highly reactive reduced P to a single location where weathering will allow release of this reactive P into the environment and make it available for inclusion in prebiotic reactions.[28] One issue with the meteoritic and planetary core sources of phosphide is that they are localised sources of P and thus limited to specific locations. It may be possible that some of the mineral may find its way into the atmosphere attached to an aerosol though the amount will be very small.[62] A range of metal phosphides are known to react with mineral acids to produce PH_3[5,59] which is an unusual, volatile form of reduced P which would allow the atmospheric distribution of P over a far wider area than that of an exposed and weathering meteorite, but has yet to be seen as a significant player in a global early Earth P-cycle.

1.8 Hadean atmosphere

As stated earlier in this chapter, the Hadean (the first geological era from 4.6 billion years ago to 4.0 billion years ago) atmosphere has been an area of some debate. There are two main alternatives for the composition for the early Earth atmosphere, a primary atmosphere of volatile gases captured from the solar nebula as the Earth accreted and a secondary atmosphere which degassed from the accretion material. Harold Urey (1952)

was much in favour of the primary atmosphere theory and postulated a highly reduced atmosphere predominantly containing H_2 and NH_3 with H_2O and also CH_4[82] which is observed in the gas and ice giants of Jupiter, Saturn, Uranus and Neptune.[70–72] Stanley Miller, a student of Harold Urey used these gaseous components in the now seminal spark discharge experiment (known colloquially as the Miller Urey experiment) to make amino acids and other useful organic molecules which could be used in the origin of life reactions.[2] As stated earlier, it is believed that the primary atmosphere was lost during the Moon forming impact very early in Earth's history[90, 91] and that the secondary atmosphere would have been a more suitable starting place for atmospheric chemistry though it would be foolish to discount the effects of the primary atmosphere entirely.

The secondary early Earth atmosphere is now generally accepted to be a mixture of mainly carbon dioxide [CO_2] with small amounts of hydrogen [H_2], methane [CH_4], nitrogen [N_2], carbon monoxide [CO], hydrogen sulphide [H_2S], phosphine [PH_3] and ammonia [NH_3] (though NH_3 would be unstable in the atmosphere due to high levels incident UV radiation so only present in trace amounts) produced mainly by volcanic venting and degassing of the crust and mantle.[98–101] The Atmosphere would contain a large amount of CO_2 (literature claims levels between 10 bars[94] and 200 bars[92] though this upper region may be extreme and very short lived) and other volatile gases which were not completely soluble in water.[69, 92] The amount of CO_2 in the atmosphere though much greater than today's levels, was not enough to cause a runaway greenhouse effect but was enough to keep the temperature of the atmosphere around 500 K.[96, 97]

There are three different opinions for the emergence of oxygen in the atmosphere,[133] these are (i) the evolution of oxygenic photosynthesis over several hundred million years which reached a tipping point around 2.4 billion years ago culminating in the Great Oxidation event[134] , (ii) a major "explosion" event which caused an immediate environmental change at the time of the Great Oxidation Event[135] and (iii) that biogenic oxygen production began very early in Earth's history leading to a highly oxygenated Archean (the second geological era dating from 4.0 billion years to 2.5 billion years ago) atmosphere.[136] The accepted view is that free oxygen was only produced and available in the atmosphere after the evolution of oxygenic photosynthetic life *ca.* 2.7 billion years ago.[134, 137] Oxygenic photosynthesis evolved over several hundred million years, leading to what is deemed "The Great Oxidation Event", 2.4 billion years ago after the proliferation of oxygen producing cyano-bacteria.[138] The view of late oxygenation of the atmosphere seems to be supported by analysis of chondritic meteorites as analogues of early Earth. These meteorites are thought to have been formed from the same materials and at around the same time period as the Earth formed (around 4.6 billion years ago)[37] and are generally observed to be reducing in nature.[79]

1.9   Hadean ocean

The question 'When and how water was delivered to the early Earth?' is still a fundamental question yet to be answered. Knowledge of when and how the oceans formed is limited and there is no completely accepted hypothesis for how the oceans formed. There have

been several postulated methods of water delivery including that the collection of nearly all Earths water took place during accretion[139–141] or a continuous delivery hypothesis in which water is continuously delivered to Earth by IDPs (interstellar dust particles) and comets and meteorites which implies ever expanding oceans.[142,143] The accepted theory is that water has been present on the Earth since the beginning but exactly how the water was delivered and when has widely debated.[139,140,144–146]

Rubey (1951) looked at the possibility that water was a product of weathering of the continental crust. The crust is known to contain hydrated minerals and hence contains a lot of water, but it was found that there was insufficient water (to produce the oceans) present in the silicate rocks by using a simple mass balance. It was shown that only 10% of the Earth's water could be delivered by this method even if all the water was released from the continental crust.[147,148] Rubey then proposed that water and other volatiles were products of degassing by the Earth at the moment of its formation as observation of volcanic emissions show the main components are H_2O and CO_2, and also sulphates and nitrogen which correspond to the composition of the atmosphere, oceans and ocean sediments.[147] He stated that volcanic degassing explained the formation of the atmosphere and oceans. This hypothesis relies on the understanding that all volatiles trapped by the Earth come from the original nebula material and this was supported by observations of noble gas isotopic composition.[149] An issue with this theory is the proximity of the Earth to the sun, which would imply high condensation temperatures preventing the inclusion of volatiles in the accretion model, suggesting an alternative source of water was required.[150] Morbidelli *et al.* (2000) later claimed that water was carried by planetesimals and comets which formed in the outer asteroid belt (Trojan-class asteroids) which were accreted by Earth in its final stages of formation.[140] It has been postulated that *ca.* 1.8×10^{20} kg of cometary material was delivered to Earth during the late heavy bombardment which still only accounts for *ca.* 6% of current ocean mass.[140] Both of these theories have been challenged and other theories postulated include water carried by comets[145] or chondritic micrometeorites.[151,152]

The origin of water on Earth has been investigated using isotopic ratios of deuterium (D) and hydrogen (H). The D/H ratio increases as you move out through the solar system due to the progressive enrichment of deuterium[141,150,155,159] so this could be used as an indicator of the source of water. Using models of the solar nebula, Drouart *et al.* showed only planetesimals and asteroids which formed in the region of Jupiter and Saturn contain water with the correct D/H ratio.[159] Hydrous carbonaceous chondrites contain water and contain up to 22 g of water per 100 g of rock.[158] This material originates from the asteroid belt located between Mars and Jupiter around 2 AU from the Sun. This region is a major source of meteoritic material which currently arrives on Earth and is dominated by carbonaceous chondrites. Around 40,000 tons of hydrous carbonaceous chondrites are delivered to Earth per year as Antarctic micrometeorites.[151,152] These meteorites are considered rare and only constitute *ca.* 4% of current falls on Earth.[160]

The debate about the origins of water on the Earth is not the only debate about the oceans. The other main topics of argument surrounding this controversial subject are is the chemical composition, pH and temperature of the oceans on the early Earth. The

Reservoirs	Mass (kg) or Concentration (wt%) of H_2O	D/H ($\times10^{-6}$)	δ D (% SMOW)	Refs
Whole Earth	$2.2 - 6.7 \times 10^{21}$	149 - 153	-40 to -20	1
Primitive Earth	-	128 - 136	-180 to +130	1, 2
Mantle	$5 - 50 \times 10^{20}$	143 - 149	-80 to -40	3
Oceans	1.4×10^{21}	155.7	0	3
Organic matter	1.36×10^{18}	135 - 145	-130 to -70	3
Metamorphic rocks	3.6×10^{19}	140 - 146	-100 to -60	3
Sedimentary rocks	2.32×10^{20}	143 - 145	-80 to -70	3
Protosolar nebula	-	21 ± 5	-865	4
Carbonaceous chondrites [a]	6 - 22	128 - 181	-180 to +160	5, 6, 7, 8
Antarctic micrometeorites [a]	2 - 4	120 - 200	-229 to +285	9, 10
Comets [a]	58 - 65	298 - 324	+900 to +1080	3, 4, 8

Table 1.2: Concentration of water and D/H ratios in terrestrial and extraterrestrial reservoirs. [a] H_2O concentration in wt%. References: [1] Dauphas et al., 2000;[139] [2] Déloule et al. 1991;[153] [3] Lécuyer et al. 1998;[154] [4] Robert 2001;[155] [5] Boato 1954;[156] [6] Robert and Epstein 1982;[157] [7] Kerridge 1985;[158] [8] Morbidelli et al. 2000;[140] [9] Engrand et al. 1999;[151] [10] Maurette et al. 2000.[152]

pH of the oceans is generally accepted to be acidic due to the high CO_2 content of the Hadean atmosphere. Sleep *et al.* (2001) predicted a CO_2 level of between 40-210 bars[97] with the pH of the ocean controlled by by an equilibrium dissolution of CO_2 and carbonic acid and based on the partial pressure of CO_2 in the atmosphere. Sleep *et al.* completed initial calculations for this range of CO_2 pressures with an estimated ocean temperature of between 200℃ and 230℃ and obtained a pH range of between 4.8 and 6.5 which seems to support the idea of an acidic ocean.[97] An alternative proposal for an alkaline early ocean with a pH range between 9.0 and 10.5 by Kempe and Degens (1985) involved reactions of atmospheric CO_2 with sodium-rich crustal rocks to produce an ocean saturated in sodium carbonate.[161]

This proposal was dismissed by Sleep *et al.* (2001) based on an issue of thermodynamic and mass balance. Sleep *et al.* stated that at temperatures of between 20℃ and 200℃, CO_2 pressures of between 3 kbar and 6 Gbar would be required to drive the reactions required while only 40-210 bar would be possible.[97] Atmospheric levels of CO_2 were proposed by Walker (1985), Kasting and Ackerman (1986) and Kasting (1987) at between 10 to 20 bars based on the fact that a decreased solar luminosity would require a high concentration of greenhouse gases in the atmosphere to prevent freezing.[96, 162, 163] This level of CO_2 would produce a pH of between 5.6 and 6.1 at temperatures between 70℃ and 100℃ based on thermodynamic calculations.[164] It is believed that the Earth oceans were acidic until around 2 billion years ago and become slowly more alkaline until the current level of pH 8.2 was reached.[150]

The temperature of the Hadean ocean is another subject of debate. Sleep *et al.* (2001) proposed an initial ocean temperature of between 200℃ and 230℃ based on a high atmospheric CO_2 pressure (between 40 bar and 210 bar).[97] Based on this modelling, the temperature of the oceans is directly linked to the pressure of CO_2 in the atmosphere with temperature decreasing in line with decreasing CO_2 levels due to a weakening greenhouse effect.[94, 163, 165, 166] One method of measuring the temperature of the ocean involves using oxygen isotope ratios ($^{18}O/^{16}$ expressed as $\delta^{18}O$) measured in cherts (sedimentary rocks composed mainly of micro-crystalline silica).[167] It is observed that $\delta^{18}O_{\text{WATER-ROCK}}$ in cherts decreases as ocean temperature increases[168] with a recorded $\delta^{18}O$ for early Archean cherts suggesting an ocean which was 50℃ hotter than todays mean.[150]

This method has been disputed due to the questionable source of Archean cherts which could be a result of hydrothermal fluid precipitation rather than a general ambient oceanic precipitation.[169–171] Another method which can be used is the homogenisation temperature of seawater inclusions in iron oxide (ironstone pods) deposits.[172] Using this method, de Ronde *et al.* (1997) calculated the surface temperature of the Archean ocean at 39℃ from inclusions in 3.2 billion year ironstone from Barberton greenstone belt, South Africa.[172]

The salinity of the oceans would be a result of oceanic hydrothermal vents and weathering of the continental crust with hydrothermal vents being the dominant factor during the Hadean and Archean.[173] It is suggested that mid-ocean ridges were 10 times longer than on the Earth presently and the production of oceanic crust was up to 3 times higher.[174] The salinity of the oceans is assumed to be dominated by halite [NaCl], as it is in the modern day ocean, which would be produced by water-rock interactions at mid-ocean ridges.[97] De

Ions	Cl^-	Br^-	I^-	SO_4^{2-}	Na^+	K^+	Mg^{2+}	Ca^{2+}	Sr^{2+}
Archean	920	2.25	0.037	2.3	789	18.9	50.9	232	4.52
Modern	556	0.86	0.0005	28.7	477	10.1	54.2	10.5	0.09
$\Delta_{\text{Mod/Arch}}$	0.604	0.382	0.014	12.478	0.605	0.534	1.065	0.045	0.020

Table 1.3: Ion concentrations of the main dissolved species in Archean and modern day seawater (mmol/L). Data taken from de Ronde *et al.* (1997).[172]

Ronde *et al.* (1997) found fluid inclusions in 3.2 billion year old ironstone pods from South Africa showing fluids containing a mainly NaCl and $CaCl_2$ composition[172] while Foriel *et al.* (2003) found fluid inclusions containing NaCl and $CaCl_2$ in a 3.5 billion year old intrapillow quartz from the North Pole Dome, Western Australia.[175] De Ronde *et al.* (1997) published a full list of ion concentrations in the Archean ocean fluids with a comparison to modern ocean levels (see Table 1.3), showing that levels of sodium and chlorine in the modern ocean are *ca.* 60% of the levels in the Archean ocean while the ratio of Na^+ to Cl^- is the same (Na/Cl = 0.858). The concentration of Ca^{2+}, Sr^{2+} and K^+ are much lower in the modern ocean than in the Archean (4.5%, 2% and 53% respectively) while the concentration of Mg^{2+} is roughly the same in the modern ocean as in the Archean.[172] Based on these trends it would be fair to extrapolate that the Hadean ocean would have been enriched in halides, low in sulphate and have a higher salinity than today's oceans.

It appears that the Hadean ocean would be warm (70-100℃),[164] of higher salinity than today (almost 2 times more saline based on figures published by de Ronde *et al.*),[172] the pH would be acidic due to dissolved CO_2 from the atmosphere (pH 5.6 to pH 6.1)[164] and also anaerobic due to the lack of molecular oxygen in the atmosphere.[134] This view appears to be supported by the formation of banded iron formations (BIF) at the start of the Proterozoic era (geological era between 2.5 billion to 541 million years ago which precedes the proliferation of complex life). BIF's are rocks composed of a succession of deposited bands of cherts, siderite [$FeCO_3$] and hematite [Fe_2O_3].[176,177] It is believed that these formations occurred due to the increase of dissolved iron (as Fe^{2+}) in seawater during the Hadean and Archean periods.[101] Iron present in the Fe^{2+} form would only be soluble in seawater under anaerobic and acidic conditions (pH range 0 to 6) as under aerobic or alkaline conditions the iron will be oxidised to Fe^{3+} and then precipitated as iron hydroxide [$Fe(OH)_3$] and other oxy-hydroxides(goethite, [$\alpha FeO(OH)$] and akagenite, [$\beta FeO(OH)$] dependent on conditions). Precipitation of BIF at the start of the Proterozoic seems strong evidence supporting the shift from an acidic, anaerobic ocean to an oxygenated, alkaline ocean.[150]

1.10 Volcanism on the early Earth

After the formation of the crust on the early Earth the heat loss from the core and mantle was greatly reduced (from 140 W/m^2 to *ca.* 0.5 W/m^2).[92] The mantle is heated by heat transfer from the core but also by decay from radioactive elements in the mantle[178] and with heat loss restricted by the formation of the crust, a mechanism for mantle cooling was required to prevent planetary overheating. The initial release for this energy was volcanism. As mentioned earlier in this chapter, volcanic degassing of the mantle was a

contributor to the early earth atmosphere but also brought materials to the surface for inclusion in chemical reactions.

Volcanism on the early Earth is believed to have started very soon after the formation of the crust and based on isotopic evidence in the Jack Hills zircons (δ^{18}O), was already active in the Earth 4.4 billion years ago.[119,120] Meteoritic impacts of *ca.* 10 km size, believed to have occurred on average every 100,000 years, would punch great holes in the crust allowing massive eruptions of basaltic and komatiitic lavas onto the surface of the planet[179] causing huge interactions of water with hot mafic rocks. Though volcanism would have been an initial source of heat loss, this in itself would not have been sufficient to prevent mantle overheating and thus around 3 billion years ago plate tectonics were developed.[58] It is also thought that the Earth may have developed a kind of plate tectonics in the Hadean period[179] which a larger number of smaller plates which had 10 times more mid-ocean ridge, producing 3 times more new oceanic crust.[174] The Earth was the only planet to develop plate tectonics in the solar system allowing heat regulation, recycling of material and preventing major explosive volcanism as seen on Venus[180] and Mars[181] but also preventing major resurfacing events like those predicted to have occurred on Venus 300 to 500 million years ago.[180]

During the period after formation of the crust and the advent of plate tectonics the surface of the Earth would have been highly volcanically active. The lava extruded from these volcanoes would be of higher temperature than today's lavas (over 2000 K) known as Komatiite lavas. These Komatiite lavas contained olivine, pyroxene, anorthite and chromite and, when exposed to water would begin a process known as serpentinisation, a process seen today in alkaline hydrothermal vents.[182] These hydrothermal systems would have exerted pH and geochemical control over the oceans with water/basaltic interactions producing hot (*ca.* 400℃), acidic (*ca.* pH 1) hydrothermal systems and water/komatiite interactions producing colder (70-100℃), alkaline (pH 9-11) hydrothermal systems.[179] These volcanic hydrothermal vents and mid-ocean ridge systems would have assisted in preventing the freezing of the oceans, while liquid water would also be abundant around volcanic systems and highly active geothermal areas. Muds would have been formed by hydrothermal alteration of basaltic and komatiitic rocks in and around hydrothermal systems.[179] According to Nisbet *et al.* (2007) these muds would have been "dominantly palagonitic" (an alteration product formed by the interaction of water with basalt) and rich in smectites such as nontronite and saponite.[179] This leads to the belief that where there is an area of high volcanic activity there would be hydrothermal/geothermally active areas. These areas have been considered to be ideal hatcheries for the origin of life on Earth with sources of material, energy and water all in close proximity.

Although after the development of plate tectonics as we know them today the Earth would have become less volcanically active, there would still be areas of the Earth which were highly volcanically active and it is these regions which have become the subject of investigations to establish the origin of life. Yellowstone National Park, USA; Kamchatka, Russia and Iceland are such areas of high volcanic and geothermal activity on the Earth today and it is these areas that are considered to be early Earth analogue sites and it is around such sites that the work contained in this thesis is based.

1.11   Early Earth analogue sites

The early Earth is thought to have been highly volcanically active due to high mantle temperatures and mantle degassing. As volcanism would be prolific on the surface it can be assumed that these sites would also be hydrothermally and geothermally active making such sites on Earth today good analogue sites to the early Earth. Areas such as Yellowstone National Park, Wyoming, USA; Lassen National Park, California, USA; Kamchatka, Russia and the country of Iceland therefore would be considered sites suitable for observation and investigation into the conditions available to drive prebiotic chemistry.

Due to its proximity, Iceland was chosen as a destination for an expedition to conduct experiments under natural geological conditions which could be considered as analogous to those present on the early Earth. The idea was to conduct a series of prebiotic experiments in these conditions to attempt to confirm prebiotic plausibility for such reactions on the early Earth. The site chosen for the expedition was the Kverkfjöll sub-glacial volcano and surrounding geothermal fields situated on the northern edge of the Vatnajökull glacier. This site was chosen due to the facts that it is highly geothermally active, and that it is remote, which would mean it would be pristine.

Previous work in this region of the Vatnajökull was carried out by the Icelandic Glaciological Society to assess the area for hydrothermal and geothermal tapping for use in producing electricity.[183,184] This work found that Kverkfjöll was a highly geothermally active area but was deemed too remote and too costly for viable geothermal harnessing for power.

Iceland is an island in the North Atlantic Ocean which is 550 miles North-West of Scotland on the southern edge of the Arctic Circle. It sits on top of the Mid-Atlantic ridge, the divergence point of the North American and Eurasian tectonic plates. Though Iceland is technically nearer North America, due to its proximity to Greenland, than mainland Europe, it is generally considered to be part of Europe due to cultural similarities with the Scandinavian countries (Norway, Finland, Denmark and Sweden).

As Iceland is situated on the edge of the Arctic Circle it has extended daylight hours during the summer months and extended hours of darkness during the winter. It sits at the northern edge of the Gulf Stream, a swift current of warm water which flows up from the southern tip of Florida roughly between the United Kingdom and Iceland. This has a moderating effect on the Icelandic climate. Compared to other land masses on the same latitude it encounters higher than average temperatures resulting in relatively mild winters and damp, cool summers though there is some climate variation between different areas of the island. Due to the flow of the Gulf Stream around the Icelandic coast, the island usually remains free of ice incursion during the winter months despite its proximity to the Arctic Circle.

Almost half of Iceland's land area is made up of mountainous lava desert which is of recent volcanic origin and approximately 11% of Iceland is covered by glaciers, the three largest of which are Vatnajökull, Langjökull and Hofsjökull glaciers. The Vatnajökull glacier is the largest in Europe, covering an area of 8,100 km^2 and is situated on the eastern and northern regions of the Icelandic rift zone and also on top of the Icelandic hot spot. The Icelandic hotspot is caused by an asthenospheric mantle upwelling due to
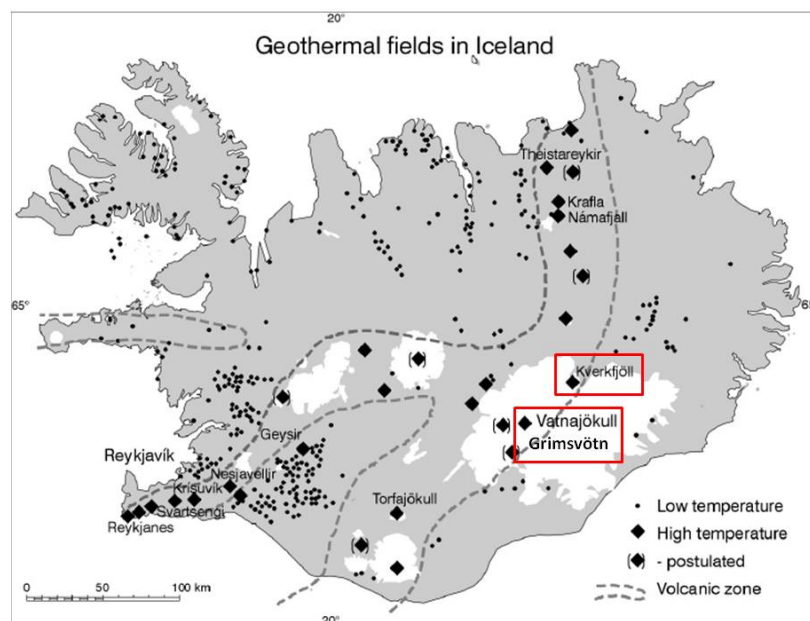
Figure 1.15: Geothermal fields in Iceland and the location of Kverkfjöll and Grimsvötn subglacial volcanoes. Map courtesy of Ármandsson *et al.* (2000) from a paper which surveyed the Kverkfjöll subglacial volcano area[183]

convective currents causing plate divergence. The upwelling mantle occurs as a plume-like phenomenon which causes the overlying crust to bulge and eventually separate due to gravity - known as ridge push. Due to the rift, which runs from the South-West to the North-East across the island, Iceland is extensively volcanic and highly geothermally active (Figure 1.15). The Vatnajökull glacier sits on top of several active volcanic centres which include the recently erupted Grimsvjötn and the Kverkfjöll sub-glacial volcanoes.

The Kverkfjöll sub-glacial volcano lies on the on the north-eastern edge of the Vatnajökull glacier on the Eastern edge of the Icelandic volcanic zone and on the edge of the Mid-Atlantic rift (Figure 1.16). Kverkfjöll is a stratovolcano which is common in subduction/rift zones. Stratovolcanoes are normally tall, conical in shape and are formed by layered deposits of lava and tephra (fragments of volcanic material ejected during an eruption i.e. pumice and ash) from periodic eruptions. The lava that usually flows from stratovolcanoes is known as felsic as it contains high to intermediate levels of silica which makes it viscous. This cools rapidly after eruption and thus does not travel far leading to the classic cone shape formation. The Kverkfjöll volcano system consists of two sub-glacial volcanic calderas which are elliptical in shape and approximately 8 km x 5 km in size (Figure 1.17).

1.12 Aims of thesis

'How was phosphorus included in life?' is a major question which needs to be answered to fully understand how life could have begun on the early Earth. The issues of solubility, reactivity and availability of active phosphorus species would have severely limited the origin of life on Earth. As discussed earlier, there is now significant evidence which suggests that there were large amounts of reactive, reduced oxidation state phosphorus present on the early Earth from various sources and it is this theory which is the subject of this research.
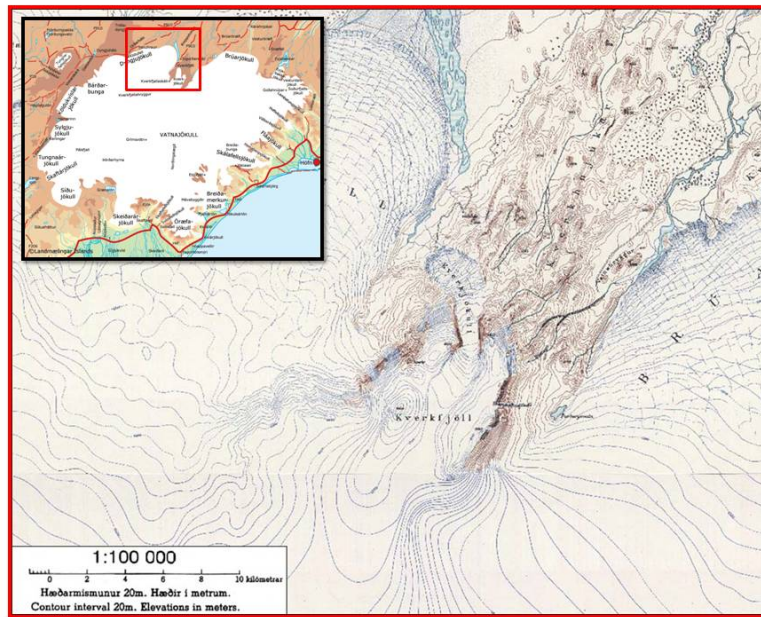
Figure 1.16: Topographic map of Kverkfjöll (1:100000 m scale)with inset map of the Vatnajökull glacier showing the position of area covered. (Map and inset picture from www.skimountaineer.com)
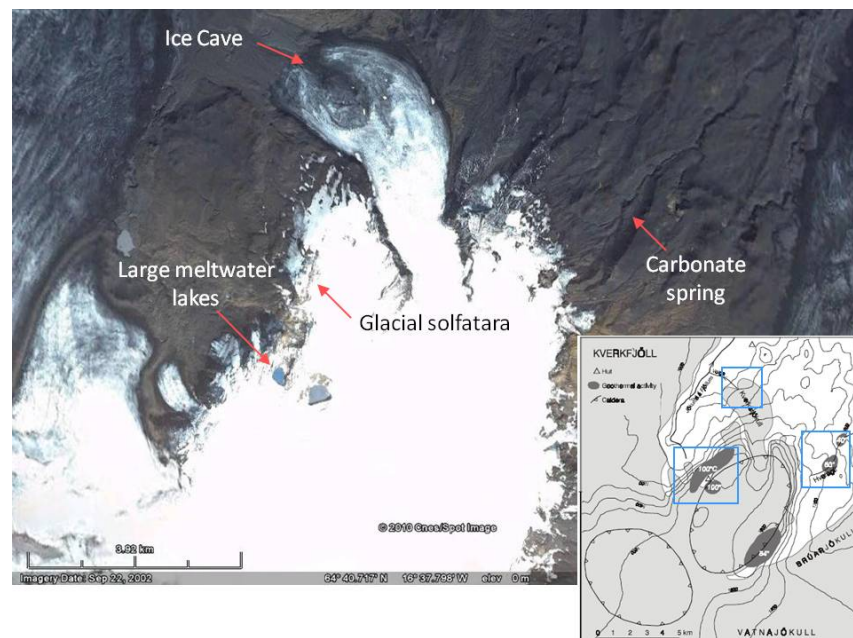
Figure 1.17: Google Earth image and topographic map of Kverkfjöll volcanic region. The Google Earth image was provided by Dr. Claire Cousins to show the areas of interest for the planned fieldwork. The topographical map reproduced from an article by Ólafsson (2000)[184] shows the two subglacial volcanic calderas and the geothermal fields associated with the Northern caldera.

The research reported within this thesis investigates the potential of iron meteorites as an abundant source of reduced oxidation state phosphorus, tries to identify and quantify the species obtained by weathering and corrosion pre- and post-impact, and looks at how these species can be further manipulated to form molecules of interest to the development of biochemistry. The initial aim of the project was to explore two main areas 1). Simulating plasma interactions with iron meteorites pre-impact and 2). Hydrothermal processing of iron meteorites under putative prebiotic conditions with the view to identifying and quantifying the reduced phosphorus species produced which may have been utilised in the emergence of life on Earth.

Specific objectives of this research were:

1. To investigate the production of reduced oxidation state phosphorus species and identify products obtained by hydrothermal processing of iron meteorites. The aim was to confirm and quantify all volatile and non-volatile hydrolysis products produced during acidic hydrothermal processing of meteorites and meteorite analogues. Such a scenario may simulate exposure of iron meteoritic components, post impact to hot acidic lakes, oceans or volcanic fumaroles of which there are several contemporary examples (i.e. Bumpass Hell in the Lasson National Park, California). Previous research by Pasek and Lauretta (2005) and Bryant and Kee (2006) has shown that aqueous corrosion of schreibersite $[(FeNi)_3P]$ can produce significant amounts of reduced, condensed phosphorus species, although only non-volatile species have been observed.[28, 56] Glindemann et $al.$ (1998) have postulated that a volatile species of phosphorus, phosphine $[PH_3]$, could be produced by acidic corrosion of phosphorus rich iron.[57] Phosphine gas emission by acidic corrosion of meteorites would be a useful source of mobile, reduced phosphorus on the early Earth but only if significant amounts could be produced.

2. To undertake the direct observation and quantification of phosphine gas. The observation of phosphine was the primary objective of this early research, to try to establish whether phosphine could be a prevalent prebiotic atmospheric component and a good source of reduced phosphorus for inclusion in origin of life reactions. One challenge faced was to design and build an experimental set-up which will allow the safe identification of (i) volatile PH_3 gas and (ii) non-volatile P-oxyacids liberated by acid hydrolysis of iron phosphide under acidic hydrothermal conditions. Once identified, attempts would be made to quantify the species observed in an attempt to extrapolate the levels of reduced oxidation state phosphorus available for origins of life reactions.

3. To investigate the effects of pH and temperature on corrosion rates of meteorites and meteorite analogues. Depending on the area of meteoritic fall, the meteorite could be exposed to a wide variety of pH and temperature conditions. The focus of this research was mainly around acidic corrosion due to the high amounts of CO_2 in the atmosphere. The pH expected would be between pH 5 – pH 6 in ocean or lake environments from dissolved CO_2 but in hydrothermal/geothermal volcanic environments the pH could be much lower (down to pH 1 is possible). The temperature again

could vary greatly from just above freezing up to boiling with early ocean temperatures postulated at around 75℃ while in hydrothermal/geothermal environments the temperature could be boiling.

4. To repeat the chemistry undertaken and other selected prebiotic chemistry reactions under natural hydrothermal/geothermal conditions. The plan was to partake in a field trip to the Kverkfjöll region of Iceland, which is known to be an area of high volcanic activity and has numerous sites that are hydrothermally and geothermally active. An experiment package would be designed to fully utilise the conditions available and attempt to undertake numerous prebiotic chemistry experiments under natural geological conditions. It was also planned to perform acidic hydrothermal corrosion experiments on meteorites and meteorite analogues under natural geological conditions. This was to investigate the differences, if any, between laboratory based simulated corrosion experiments and corrosion in a natural geological environment. Differences would be sought in the corrosion rate, and in the products obtained. With volcanic regions believed to be prevalent on the early Earth, investigation of these areas should allow identification of potential prebiotic conditions present in these sites on the early Earth.

5. To simulate the corrosion of a schreibersite containing iron meteorite under conditions comparable to a putative early Earth environment. The aim was to conduct corrosion of a meteorite containing inclusions of schreibersite $[(FeNi)_3P]$ under an anaerobic atmosphere in natural hydrothermal fluids under simulated geological conditions. This was to attempt to confirm the viability of iron meteorites as a source of reduced oxidation state phosphorus on an early Earth.

Chapter 2

Production of reduced oxidation state and condensed phosphorus species by simulated processing of meteorites and meteorite analogues

2.1 Introduction

As discussed in Chapter 1, most salts of orthophosphate [PO_4^{3-}] are relatively insoluble in water and are relatively unreactive due to their thermodynamic stability.[11,28] Therefore, it can be assumed that the only way phosphorus could be assimilated and utilised in origins of life reactions is to make it more soluble and/or more reactive. In contemporary biochemistry phosphate is activated and utilised by enzymes and co-enzymes but these complex molecules would not be available for use in prebiotic chemistry. The issues of phosphorus activation and solubility would have to be addressed to allow essential prebiotic reactions to occur and life to evolve.

Back in 1955 and again in 1957, Addison Gulick stated that nature may have utilised reduced oxidation state phosphorus species in origins of life reactions.[30,36] The one thing on which Gulick did not elaborate was the source of prebiotically available reduced oxidation state phosphorus and it was for this reason it was mainly dismissed by the scientific community (see Miller and Urey 1959 as one famous example[37]). The main reduced oxidation state species of interest for prebiotic chemistry are phosphite [HPO_3^{2-}] (+3 oxidation state), hypophosphite [$H_2PO_2^-$] (+1 oxidation state) and phosphine [PH_3] (-3 oxidation state).

As the oxidation state of phosphorus decreases, the reactivity of the P-species increases (see Figure 2.1), making low oxidation state phosphorus species excellent candidates for inclusion in origins of life reactions should one be able to provide reasoned provenance for their availability. The discovery of phosphonic acids [P^{3+}] in the chemical library of the Murchison meteorite[38] reignited the idea of reduced oxidation state phosphorus and its potential for use in prebiotic chemistry.

Natural sources of reduced oxidation state phosphorus, as stated in Chapter 1 include
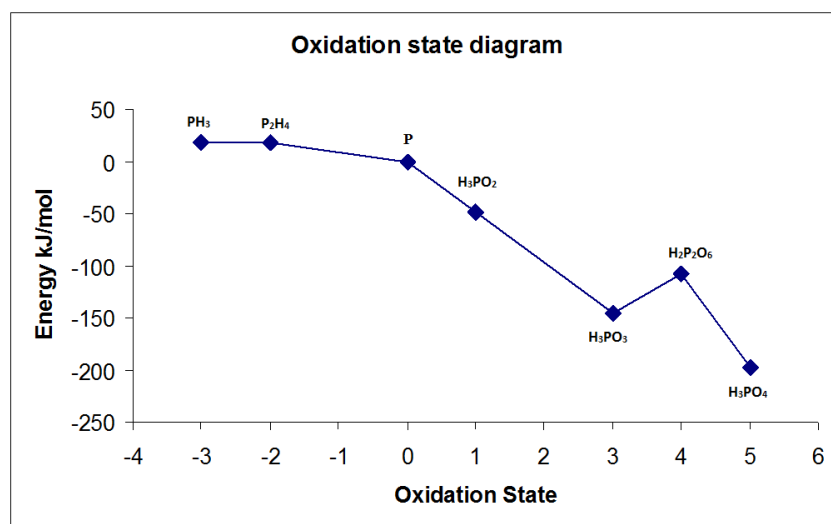
Figure 2.1: Oxidation state diagram for phosphorus under acidic conditions indicating the relative stability of each oxidation state. Adapted from Greenwood and Earnshaw, Chemistry of the Elements (1993)[11]

volcanism,[52] mantle subduction[57] and fulgurites from lightning strikes[55] but it is meteorites which are mainly considered to have been the major source of reduced P on the early Earth. Based on flux calculations, an estimated 10^9 kg per year may have been delivered to Earth as phosphides through the period of the late heavy bombardment (LHB)[28] making it a significant source of phosphorus which could be utilised in origins of life reactions.

Meteorites, particularly stony irons and iron meteorites are known to contain significant proportions of iron/nickel phosphides (such as schreibersite, $[(FeNi)_3P]$, P^0 oxidation state, *ca.* 0.5% wt in iron meteorites such as the Sikhote-Alin meteorite)[126] and hence can be considered as a good source of reduced oxidation state phosphorus. Pasek and Lauretta (2005) showed that a variety of reduced oxidation state and activated phosphorus species could be produced by aqueous corrosion of schreibersite at room temperature (20°C) including significant quantities of phosphite $[P^{3+}]$[28] while Byrant and Kee (2006) showed that, under putative interstellar conditions (77 K, exposed to high UV radiation), it was possible to produce hypophosphite $[P^{1+}]$.[56] The issue is extracting the phosphorus species from the meteorite. Are the reactive P species delivered on the meteorite or a product of chemical processing after arrival on Earth?

This chapter will investigate the production of reduced oxidation state phosphorus species from iron phosphide $[Fe_3P]$ as an analogue to meteoritic schreibersite, which provides an affordable, available, standardised and sacrificial source of iron phosphide mineral. It was planned to use *bona fide* meteorite samples for comparison at a later date to confirm experimental findings. The investigation of reduced oxidation state phosphorus production centred on hydrothermal processing under putative early Earth conditions with the aim of producing reduced and/or activated P species post-impact on Earth.

2.2 Hydrothermal processing

A meteorite impacting the early Earth would then be subjected to weathering, post-impact, by the elements, which would allow release of the full chemical inventory of the meteorite

into the environment. The conditions prevalent on Earth during the Hadean era are a source of much speculation and due to a lack of geological record are unfortunately likely to remain unknown. There is a discussion of potential and generally accepted atmospheric and environmental conditions including atmospheric composition, temperature, ocean temperature, ocean pH and salinity in Chapter 1 but a quick summary of generally accepted conditions is presented here.

The atmosphere contained little or no molecular oxygen. There was a high CO_2 concentration (between 10 bars[94] and 210 bars[69,97]) with the remaining atmosphere consisting of small amounts of hydrogen [H_2], methane [CH_4], nitrogen [N_2] and ammonia [NH_3], carbon monoxide [CO], hydrogen sulphide [H_2S] and phosphine [PH_3] produced mainly by volcanic venting and degassing of the crust and mantle.[98–101] The surface temperature of the Earth was estimated to be 500 K due to the effects of the high CO_2 atmosphere.[69] The oceans were acidic (pH 5.6 to 6.1),[164] hot (between 70℃ and 230℃)[97,150,164,168] and a salinity which was almost twice the levels of the current ocean[172] (though this is still hotly contested as it is also postulated that there was twice as much liquid water in the oceans on the Hadean Earth[119,185]). The High CO_2 atmosphere would not be sustained due to the presence of liquid water and basalt minerals on the surface of the Earth.[82] The CO_2 would slowly be removed from the atmosphere by dissolution in water where it would react with calcium oxide and magnesium oxide present within basaltic minerals to produce carbonates.[97] Volcanism on the early Earth would provide localised areas of high hydrothermal and geothermal activity which would contain very hot Water (*ca.* 100℃) and strongly acidic (*ca.* pH 1).[179]

2.2.1   Identification of hydrothermal corrosion products

Iron phosphide [Fe_3P] and schreibersite [$(FeNi)_3P$] contain phosphorus in the P^0 oxidation state. Hydrothermal processing of these minerals should allow for release of phosphorus but the species of P released needs to be identified and quantified to determine potential concentrations available on a prebiotic Earth. As previously stated, Bryant and Kee found it possible to produce hypophosphite [$H_2PO_2^-$] by corrosion in the presence of water with incident UV light in a low temperature, space-like environment[56] while Pasek and Lauretta (2005) identified a number of species including phosphite [HPO_3^{2-}] liberated by corrosion in water at room temperature in aerobic and anaerobic conditions.[28] Both show the possibility of producing reduced oxidation state phosphorus by oxidation of the P^0 present in Fe_3P or schreibersite to P^{1+} and P^{3+} using water. There is however, also the possibility of the production of phosphine [PH_3], a highly reactive and highly reduced species (P^{3-}) of phosphorus when corrosion is carried out in acidic fluids. This was identified during acidic corrosion of steel by Tanaka (1996)[186] and Glindemann (1998)[57] who estimated that 0.01% of available phosphorus would be converted to phosphine during acidic corrosion of steel.[57]

It has also been shown experimentally and commercially that phosphine can be produced by hydrolysis of certain metal phosphides (aluminium phosphide [AlP], used in fumigation tablets and calcium phosphide [Ca_3P_2], which is a common laboratory source of phosphine though is known to produce a large quantity of higher phosphines such as diphosphine which is highly inflammable and explosive in oxygen[11,59]). Subsequent oxidation of phos-

phine could produce phosphinic and phosphonic acid before full oxidation would lock the phosphorus back in the unreactive and low soluble orthophosphate form.

To establish the species of P present on a prebiotic Earth, experiments were carried out under plausible prebiotic conditions. The primary goal was to design an experimental set-up with the capability to observe and if possible, quantify the production of phosphine gas produced by acidic, anaerobic, hydrothermal corrosion of iron phosphide. Initial conditions decided upon for the hydrothermal experimental work included an inert, anaerobic atmosphere (either argon or nitrogen) and acidic conditions (sulphuric acid, H_2SO_4, 1 M) *ca.* pH 5 adjusted with sodium hydroxide to approximate conditions which may have been present on early Earth. Ideally, the first choice of acid would have been carbonic acid but this was deemed too difficult to control pH effectively. Sulphuric acid was chosen as it was readily available in the lab and deemed appropriate due to the presence of SO_2 in the atmosphere from volcanic degassing though HCl was considered as an alternative. As the experimental method called for destructive treatment of meteorite it was decided to use iron phosphide which was cheaper and in plentiful supply.

2.2.1.1 Attempts to observe phosphine production using silver nitrate

Iron phosphide [Fe_3P] (1.265 g, 6.4 mmol) was placed in a side-arm Schlenk under N_2 in a glove box and connected to the bubbler system shown in Figure 2.2. The bubbler system contained deionised water (40 mL) in bubbler 1, silver nitrate solution (5% solution, 40 mL) in bubbler 2 and standard bleach in bubbler 3 (40 mL). Bubbler 2 was wrapped in aluminium foil to prevent reaction of the silver nitrate with light. A second sample was also wrapped in aluminium foil as a control sample for comparison after the completion of the experiment. Degassed sulphuric acid [H_2SO_4] (*ca.* pH 4.6, 5 ml) was added to the reaction vessel *via* a positive pressure transfer method.

Silver nitrate [$AgNO_3$] was chosen as a good indicator for the detection and confirmation of phosphine gas generation. Phosphine gas is an excellent reducing agent and therefore should cause the reduction of silver ions [Ag^+] to silver metal and this would serve as visible indicator of phosphine production.

Equations for the occurring half reactions are shown below:

$$PH_3 + 2\,H_2O \rightarrow H_3PO_2 + 4\,e^- + 4\,H^+ \tag{2.1}$$

$$Ag^+ + e^- \rightarrow Ag^0 \downarrow \tag{2.2}$$
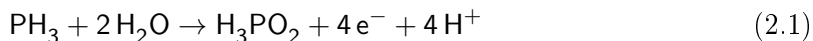
Combining the two half equation gives:

$$PH_3 + 4\,Ag^+ + 2\,H_2O \rightarrow H_3PO_2 + 4\,Ag^0 \downarrow + 4\,H^+ \tag{2.3}$$
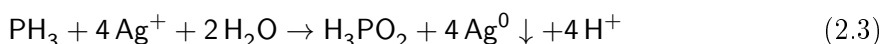
Deionised water served to remove other reducing acidic gases from the gas flow such as hydrogen sulphide [H_2S] which could give a false positive result. The pH of the deionised
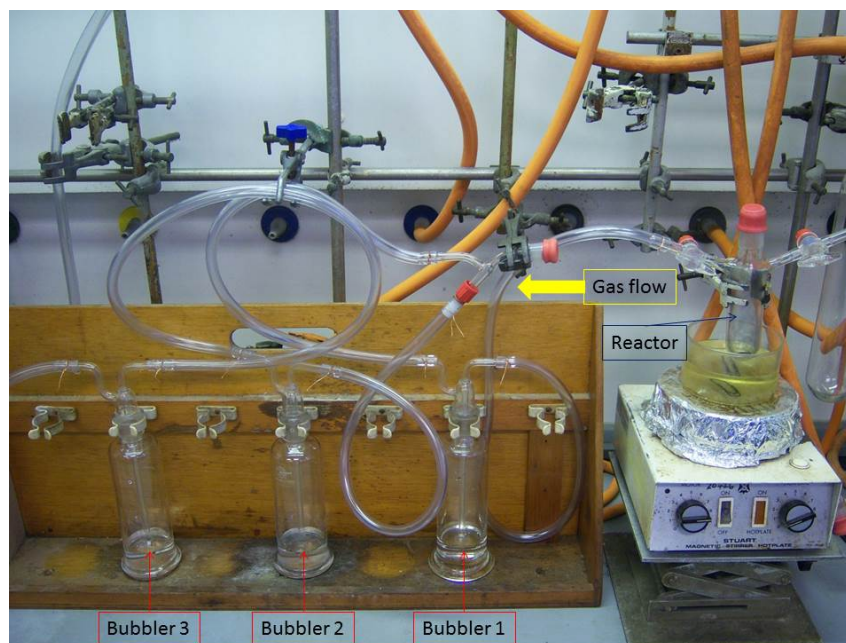
Figure 2.2: Photograph of the initial hydrothermal experiment apparatus which has a 2-arm schlenk tube (reactor vessel) containing Fe$_3$P sealed under N$_2$ connected to an argon cylinder to provide a gas flow. The argon was passed through the system for 15 minutes at 1 bubble per second before the degassed pH 5 sulphuric acid was injected into the reactor using a cannula using a positive pressure method. The reactor vessel was heated to 90 ℃ for *ca.* 120 hours.

water in bubbler 1 was taken before and after the experimental run. The starting pH of the water was measured at pH 6.4; the end reading after the experimental run was pH 7.1 thus indicating no acidic gas transfer from the reactor to bubbler 1. The increase in pH is due to the water in bubbler 1 being degassed by the argon flow thus removing dissolved carbon dioxide from the water which makes it slightly acidic.

Visual inspection of the silver nitrate trap after 120 hours showed some silver metal deposit which was not observed in the control sample indicating a reduction reaction taking place in bubbler 2 which was not present in the control sample. Knowing that PH$_3$ is a highly reducing gas, this was thought to be reducing the Ag$^+$ ions to silver metal, though other sources of reduction such as hydrogen and hydrogen sulphide which are also reducing gases could not be ruled out.

An attempt to duplicate and confirm the result obtained in the initial experiment was made. Two experiments were to be conducted at the same time using a second experimental setup which mirrored the first experimental setup. The original experiment was repeated as above and the second experiment set up using iron metal filings rather than iron phosphide was used to prove that phosphine, not hydrogen or hydrogen sulphide was responsible for the produced silver metal in the initial experiment. As phosphine could only be produced by the hydrolysis of iron phosphide, if silver metal was only found in the iron phosphide reaction set-up, then this would confirm that phosphine, and not hydrogen or hydrogen sulphide, was responsible for the reduction of silver ions.

These experiments were run under the same conditions at the same time for approximately 120 hours but no silver metal was observed in either silver nitrate bubbler. Thus, either no phosphine was produced in the initial experiment, or there was some form of contamination in the initial experiment (which caused the production of silver metal) that was not present

in the repeat experiment. It would seem most reasonable to conclude that contamination by a reducing agent, such as H_2S or H_2 in the initial experiment was the explanation.

2.2.1.2   Attempts to observe phosphine production using sodium hypochlorite

Based on a review of phosphine by Fluck in 1973,[5] sodium hypochlorite [NaOCl] was chosen as a phosphine trap as it allows rapid oxidation of phosphine to phosphinic acid which will then further oxidise through to orthophosphate. The presence of orthophosphate in bubbler 2 could then be confirmed by ^{31}P NMR. Again, deionised water was used in bubbler 1 to prevent possible phosphorus transfer from the reaction vessel to bubbler 2, thus giving a false positive result. It also served to remove acidic gases (i.e. H_2S) from the gas stream.

Iron phosphide [Fe_3P] (1.288 g, 6.5 mmol) was placed in a side-arm Schlenk under N_2 in a glove box and connected to the bubbler system shown in Figure 2.2. The bubbler system contained deionised water (40 mL), sodium hypochlorite [NaOCl] (4% available chlorine, 40 mL) and a final bubbler containing standard bleach (40 mL) as a safety measure. The system was allowed to equilibrate under an argon flow of approximately 1 bubble per second for 15 minutes. Degassed sulphuric acid [H_2SO_4] (pH 4.6, 5 ml) was added to the reaction vessel *via* positive pressure method and the system given a further 15 minutes to equilibrate with the argon flow sparging the acid to prevent re-gassing of the acid.
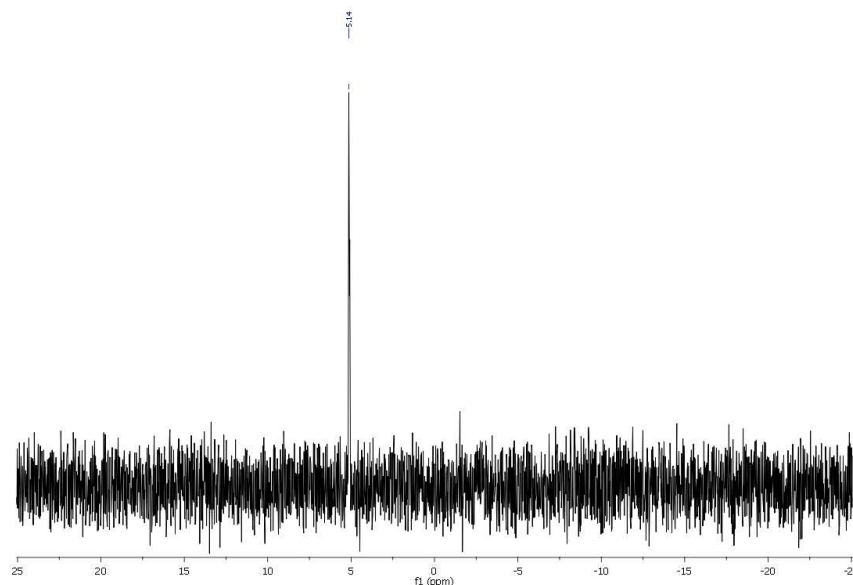
Spectrum 2.1: ^{31}P NMR spectrum (D_2O, 300 K, 202.46 MHz) of the contents of bubbler 2 (*ca. 32,000 scans*) showing a singlet peak at $\delta 5.1$ due to the presence of phosphate in the bleach thus indicating phosphorus transfer from the reaction vessel by the gas flow. NMR spectrum obtained by Mr Simon Barrett, NMR Technician.

The ^{31}P {^1H} NMR spectra for both the sample (Spectrum 2.1) and for the bleach blank (Spectrum 2.2) were inconclusive as a phosphorus signal was observed in both. Initial thoughts were that phosphate may have been present in the bleach due to the water used to prepare it or that the glassware used to prepare the bleach blank for NMR was contaminated with phosphate. A further sample of the bleach used in the phosphine trap was submitted for ^{31}P {^1H} NMR to check if phosphate was present in the bleach or
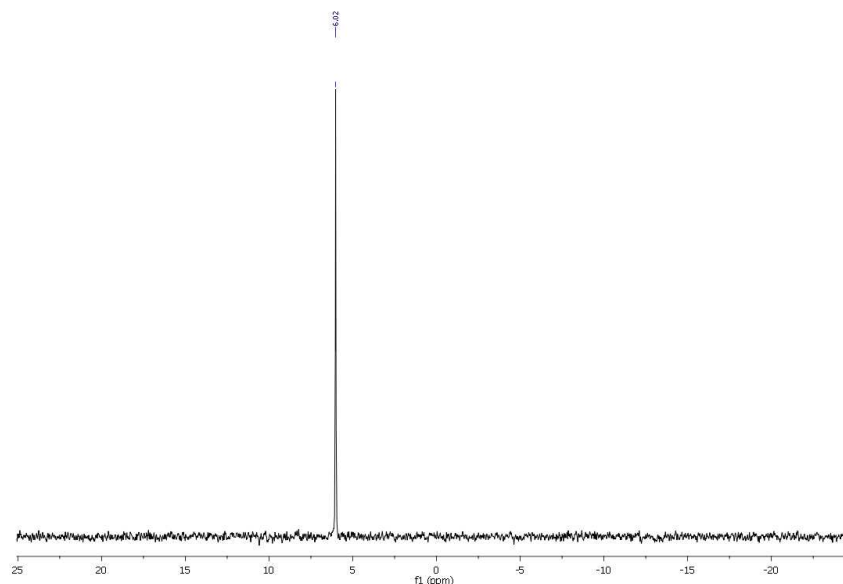
Spectrum 2.2: ^{31}P NMR spectrum (D$_2$O, 300 K, 202.46 MHz) of the stock bleach solution used in bubbler 2 (*ca. 32,000 scans*) showing a singlet peak at δ6.0 indicating the presence of phosphate in the bleach. The cause of the phosphate contamination in the bleach was not known but due to this an alternative trapping fluid was needed. NMR spectrum obtained by Mr Simon Barrett, NMR Technician.

whether it was just contamination from glassware used for preparation of the sample. The glassware used for preparation of the blank was cleaned thoroughly using 2M sulphuric acid, washed with deionised water and dried with acetone. The spectra again confirmed the presence of phosphate in the bleach though it is plausible that some contamination of the original glassware was possible.

Several issues had been identified with the experimental conditions and set-up which needed to be addressed to allow more successful observation of phosphine gas production. These issues were the cleanliness of glassware used in the experiments, the volumes of the traps used for phosphine capture and the trapping agent used for capture of the phosphine gas produced. The cleanliness of the glassware was the first issue to be considered and a strict acid washing protocol was established to limit phosphate contamination of all glassware used in the experiments. This involved a normal washing process using soap and hot water then soaking overnight in sulphuric acid [H$_2$SO$_4$] (1M), rinsing with deionised water and acetone then drying in an oven for an hour.

After consideration of glassware contamination, an alternative source of bleach was sought that could be confirmed as being phosphate free. Calcium hypochlorite [Ca(OCl)$_2$] seemed a logical choice as it is supplied in powder form meaning it can be made to a required concentration using deionised water meaning it should be free of phosphate. A ^{31}P $\{^{1}$H$\}$ NMR taken of the Ca(OCl)$_2$ bleach solution confirmed this to be free of phosphate and therefore suitable for use in future hydrothermal experiments.

The experimental set-up was also addressed. Initially a system of bubbler jars was used but this meant that a volume of *ca.* 40 mL was required to cover the bottom of the bubbler tubes and also the system was connected together using plastic tubing (*ca.* 2 meters) meaning there was a large amount of "dead" space in the system. Redesigning the whole system lead to the custom manufacture of a fully glass bubbler system (see Figure 2.3)
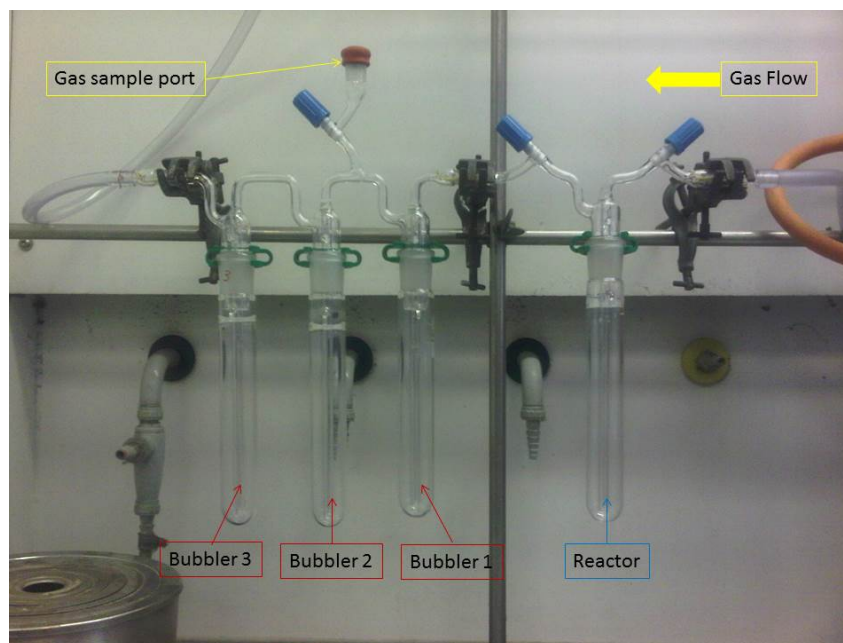
Figure 2.3: Photograph of the new experimental set-up. The bubbler layout is similar to the original experimental system using B24 test tubes and a customised glass bubbler train with quick-fit ground glass joints. The redesigned experimental set-up had less "dead" space and the volumes required in the bubblers were much less than in the previous system (reduced from 40 mL to 5 mL). Credit Barry Herschy

which was connected together with quick-fit joints using test tubes rather than bubbler jars. This meant that each bubbler only required 5 mL fluid to cover the bottom of the bubbler tubes and there was a smaller amount of "dead" space within the system.

2.2.1.3 Attempts to observe phosphine production using calcium hypochlorite

Iron phosphide [Fe_3P] (2.25 g, 11.3 mmol) was placed into the reactor from a glove box under N_2 and degassed sulphuric acid [H_2SO_4] (2M, 5 mL) was added by syringe. The reaction vessel was connected the new altered experimental set-up (see Figure 2.3) in the same bubbler configuration as used in previous experiments with deionised water (5 mL) in bubbler 1, calcium hypochlorite [$Ca(OCl)_2$] (1 mmol, 5 mL) in bubbler 2 and standard bleach [$NaOCl$] (4% available chlorine, 5 mL) in bubbler 3. N_2 gas was then bubbled through the system for 15 minutes and the reactor then heated rapidly to 90℃ in an oil bath for 72 hours then allowed to cool.

In previous experiments dilute sulphuric acid [H_2SO_4] (adjusted to pH 4.6) was used for the hydrothermal treatment of iron phosphide [Fe_3P]. In this experiment the pH of the acid was altered to *ca.* pH 1 to increase the rate of reaction. After allowing to cool to room temperature, the reactor taps were closed and the contents of bubbler 2 were transferred to a 10 mL NMR tube with a D_2O insert and submitted for ^{31}P NMR analysis. The ^{31}P NMR spectrum (Spectrum 2.3) for the sample gave a singlet at $\delta 3.0$ which was identified as phosphate [PO_4^-] and a triplet at $\delta 7.7$ which would indicate hypophosphite [$H_2PO_2^-$]. The sample was resubmitted for ^{31}P {^1H} NMR which confirmed the presence of hypophosphite as the triplet resolved to a singlet at $\delta 7.7$.

Due to the weak concentration of the sample, an overnight run of the ^{31}P NMR was required (*ca.* 33,000 scans) to obtain a defined spectrum. A further ^{31}P NMR (*ca.* 33,000
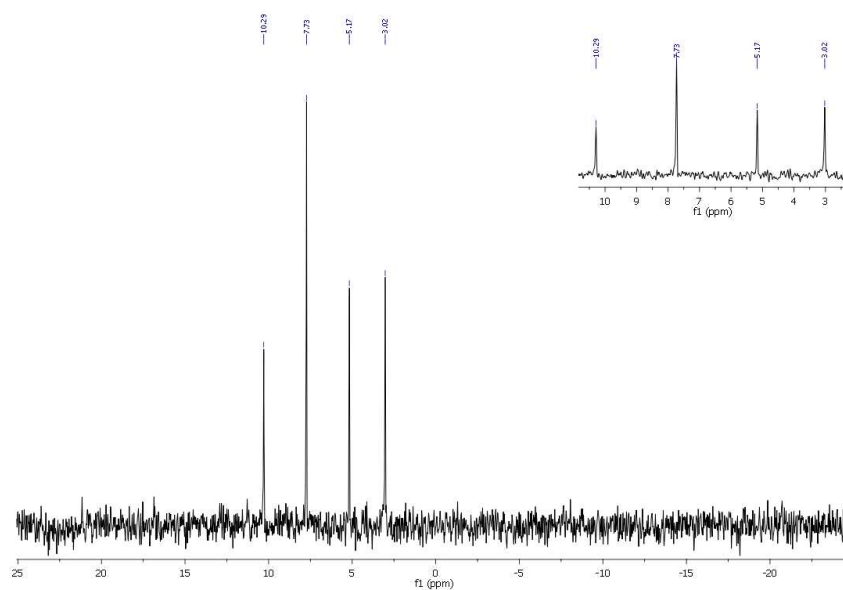
Spectrum 2.3: ^{31}P NMR spectrum (D$_2$O, 300 K, 202.46 MHz) of the contents of bubbler 2 show a singlet peak at δ3.0 indicative of phosphate [PO$_4^{3-}$] and also a triplet of peaks at δ7.7 ($^1J_{\text{P-H}}$= 516 Hz) which indicates the presence of hypophosphite [H$_2$PO$_2^-$] in the bleach sample. As hypophosphite is the first stable oxidation product of phosphine gas, this would indicate that phosphine gas was indeed produced during hydrothermal corrosion. NMR spectrum obtained by Mr Simon Barrett, NMR Technician.
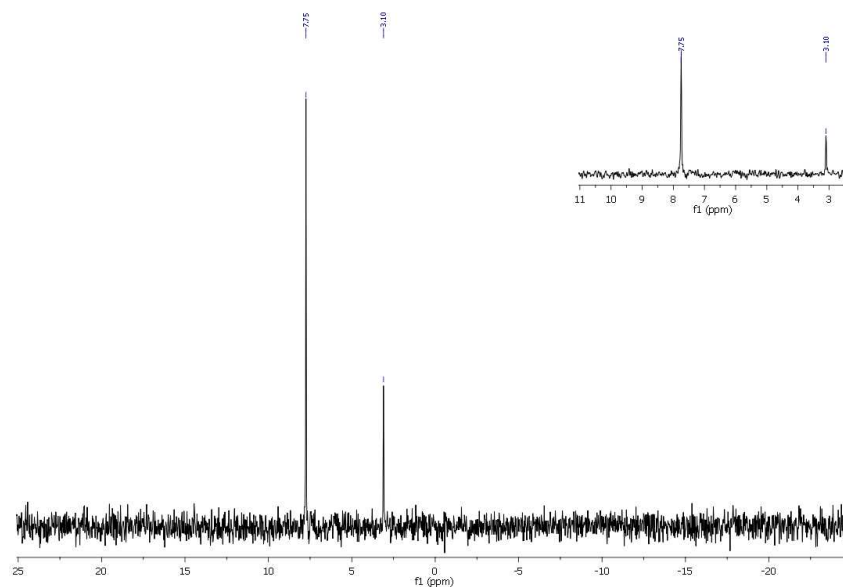
Spectrum 2.4: ^{31}P {^{1}H} NMR spectrum (D$_2$O, 300 K, 202.46 MHz) of the contents of bubbler 2 show a singlet peak at δ3.0 indicative of phosphate [PO$_4^{3-}$] and also the triplet of peaks at δ7.7 has now resolved to a strong singlet again at δ7.7 which confirms that hypophosphite [H$_2$PO$_2^-$] is present in the bleach sample. NMR spectrum obtained by Mr Simon Barrett, NMR Technician.

scans) was submitted of stock calcium hypochlorite solution to confirm no phosphorus was present in the solution, and to rule out contamination. This spectrum, as in the previous ^{31}P NMR for calcium hypochlorite solution showed no phosphorus peaks and was thus assumed to be phosphorus free. With no signs of contamination in the stock solution and phosphinic acid known to be the first oxidation product of phosphine gas,[11] it was a reasonable conclusion that phosphine gas was produced during this experiment.

Several attempts to repeat this result were attempted using iron phosphide (*ca.* 1.5 g) without success. The initial problem was the traps kept drying out before the 72 hours completed which meant that the experiments had to be abandoned without reaching completion. This problem was rectified by slowing the flow of N_2 through the experiment. The second issue was that after 72 hours, no phosphorus signal was observable in the ^{31}P NMR spectra. Unsure as to what was causing this new issue, it was decided to try for an exact repeat of the first successful experiment.

A further repeat of this experiment was performed using iron phosphide (2.25 g) under the same conditions in an attempt to confirm that it was indeed PH_3 transfer from the reaction vessel to the bleach trap and not contamination. The experiment was heated at 90℃ in an oil bath for a period of 72 hours as before then allowed to cool to room temperature. The reactor vessel taps were closed and the contents of bubbler 2 transferred to a 10 mL NMR tube and submitted for both ^{31}P and ^{31}P {^{1}H} NMR as in the previous attempt. The repeat experiment produced a ^{31}P NMR (Spectrum 2.5) spectrum with a triplet at δ7.8 confirming the presence of hypophosphite [$H_2PO_2^-$] and therefore the production of phosphine gas.
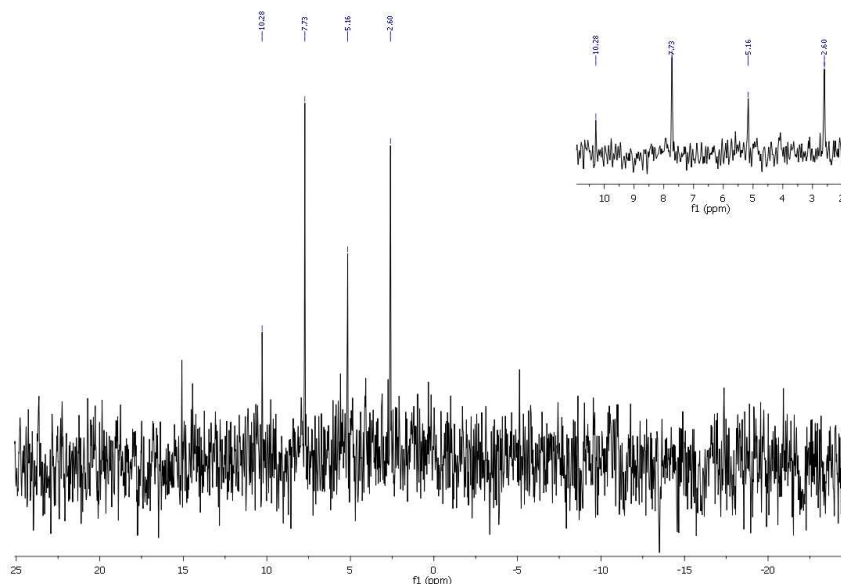
Spectrum 2.5: ^{31}P NMR spectrum (D$_2$O, 300 K, 202.46 MHz) of the contents of bubbler 2 (*ca. 8,000 scans*) show a singlet peak at δ2.6 indicative of phosphate [PO_4^{3-}] and also a triplet of peaks at δ7.7 ($^1J_{P\text{-}H} =$ 518 Hz) indicating the presence of hypophosphite [$H_2PO_2^-$] in the bleach sample. NMR spectrum obtained by Mr Simon Barrett, NMR Technician.

Evaluation of the two successful experiments against the experiments which failed was conducted. The heating times was the same, the same acid batch was used in all experiments and the gas flow through was similar. One major difference was that in the two successful reactions, the reactor vessel dried out almost completely while in the failed experiments,
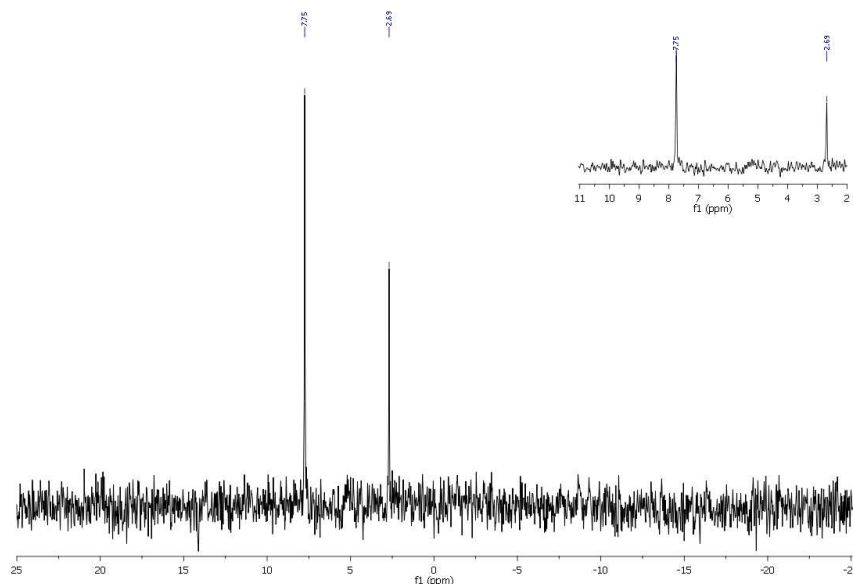
Spectrum 2.6: ^{31}P $\{^1\text{H}\}$ NMR spectrum (D$_2$O, 300 K, 202.46 MHz) of the contents of bubbler 2 (*ca. 8,000 scans*) show a singlet peak at $\delta 2.7$ indicative of phosphate [PO$_4^{3-}$] and also the triplet of peaks at $\delta 7.7$ has now resolved to a strong singlet at $\delta 7.8$ which confirms the indication that hypophosphite [H$_2$PO$_2^-$] is present in the bleach sample. NMR spectrum obtained by Mr Simon Barrett, NMR Technician.

the reaction vessel only slightly reduced in volume meaning no solid iron phosphide was exposed above the top of the acid. Considering this information means that either PH$_3$ is dissolving in the acid and is only released by the drying out of the reaction vessel or that phosphine is only produced when the surface of the iron phosphide is directly exposed to the atmosphere. Further consideration of these findings led to the conclusion that PH$_3$ is dissolving in the acid as protonated PH$_4^+$ ions and is then released into the atmosphere upon evaporation of the acid. To investigate this theory, an experiment was conducted to look at the evolution of phosphine over the running time of the experiment. The Ca(OCl)$_2$ bleach was to be changed every 24 hours and the amount of dissolved P in the bleach measured using phosphomolybdate colorimetry. This method and results are discussed further in Section 2.2.3.

2.2.1.4 Attempts to directly observe phosphine production using a Universal Gas Analyser (UGA)

Previous methods discussed in this chapter have concentrated on the indirect observation of phosphine gas by trapping or reaction of the phosphine with a suitable oxidising agent. Direct observation of phosphine is difficult due to the highly toxic nature of the gas which poses a high safety risk. One method of direct analysis which is low risk is the use of a Universal Gas Analyser to observe gas flow through the reaction system. Direct observation of phosphine gas would be unequivocal proof of production and along with the indirect observation methods, confirm without question the success of these experiments.

The Universal Gas Analyser (UGA) is a quadrupole mass spectrometer which can be used to analyse and observe gas flows for composition. It is possible to select specific mass channels to observe and this allows real-time observation of gas flow systems. A quadrupole mass spectrometer works by drawing a small amount of the gas flow into the ionisation

chamber. The gas molecules are ionised by electron impact (EI) removing electrons from the gas molecules giving them a positive charge. The gas ions are then accelerated into the quadrupole chamber by accelerator and repulsion plates. The different mass:charge ratios (m/Z) are separated by four parallel metal rods which run the length of the quadrupole chamber. The opposing rod pairs are connected electrically and a RF voltage applied to each pair of rods alternately with a super-imposed DC current applied. As the ion stream passes down the center axis of the rods, only ions of the correct mass:charge ratio pass through to the detector. Ions of incorrect mass:charge ratio undergo unstable trajectory and collide with the rods so not reaching the detector. The UGA has the benefit of being able to observe isotopic exchange so substitution of deuterated sulphuric acid $[D_2SO_4]$ to produce deuterated phosphine $[PD_3]$ ($M_r = 37$) could also be tested to fully confirm the production of phosphine in the system. The UGA was used to observe both of the attempted silver nitrate reduction experiments and also the sodium hypochlorite experiment so full details of the experimental contents and conditions are described in Sections 2.2.1.1 and 2.2.1.2 above.

The initial experiments observed were the attempt to capture phosphine with silver nitrate. Before the first attempt was undertaken, the detector was run without heating for a period to observe the residual effects of ambient laboratory conditions on the traces produced for each mass channel by the UGA. More pronounced changes were visible in the mass channels showing the lowest concentration (which would be expected), but there is evidence from comparing the UGA mass channel traces to the temperature profile for the UGA that the ambient temperature in the laboratory also affects the traces produced.

During the heating cycle of the experiment, an increase was noted in the 2 amu and 34 amu channels. The observed increase in the 2 amu channel was sufficiently large to confirm an increase in partial pressure of hydrogen in the system during heating. This was not the case with the 34 amu channel. Although it showed an increase, it was only small and within the realms of increase due to changes in ambient conditions. The result was therefore inconclusive as to whether phosphine was observed. The repeat of the silver nitrate experiment gave similar results but again there were no conclusive results for the production of phosphine.

The third experiment observed the attempt to capture phosphine with sodium hypochlorite. The graphical data produced by the UGA were again inconclusive due to the residual effect on the traces from the change in ambient conditions in the laboratory from day to night. Further consideration about how best to use the UGA for direct observation of phosphine is required as the current methods of monitoring the gas flow are proving inconclusive.

One issue identified when using the UGA to analyse for phosphine was that it was taking a small sample of a flowing gas system. This meant that detection of phosphine would require a reasonable amount of phosphine present in the flow to allow detection. Based on predictions of phosphine production from steel by Glindemann,[57] the amount of available phosphorus converted to phosphine is around 0.01% meaning that from a 1.5 g (7 mmols) sample, 23.8 μg (0.7 μmol) of phosphine would be produced if the full sample was reacted with the sulphuric acid. The evolution of phosphine is too slow and not in sufficient volume

to be successfully detected by the UGA in a flow system so a method of concentration must be found to directly observe phosphine production.

2.2.2 Production and observation of phosphite

The contents of two reaction vessels used previously for successful generation of phosphine were filtered and washed with 10 mL deionised water. The solid was dried in a vacuum desiccator while the dissolved iron was removed from the washings using sodium sulphide [Na_2S] (1 M, *ca.* 1 mL) and sodium hydroxide [NaOH] (1 M, 2 mL) generating a precipitate which was removed by gravity filtration. The pH of the washings was altered to pH 4 using HCl and then they were reduced to dryness on a rotary evaporator. The residues were dissolved in minimal D_2O (*ca.* 2 mL) and *ca.* 1 mL of the sample was transferred to a clean 5 mm NMR tube which was submitted for ^{31}P NMR analysis.

Iron removal was required on samples prepared containing iron due to the interference effects of iron on NMR spectroscopy. Three main methods of iron removal were investigated and used during this work. The first involved treatment of the sample with sodium sulphide solution (Na_2S, 1 M) which formed a green/black precipitate which was removed by centrifuge of the sample for 1 minute to compact the precipitate then gravity filtration. This treatment was abandoned due to the strong sulphur smell. The second was treatment of the sample with potassium ferricyanide ($K_3[Fe(CN)_6]$, 0.01M) which forms a deep royal blue precipitate. The sample was then centrifuged as previous then gravity filtered. This method worked for only low concentrations of iron so was unhelpful in removal of iron from corrosion experiments. The third and most common method used involved treatment of the sample with sodium hydroxide (NaOH, either 1 M or 2M) using dropwise addition until *ca.* pH 12 was obtained. A bottle green precipitate is formed which is removed as previously using a centrifuge and gravity filtration. This method required minimal addition and was effective in most cases. A further method using EDTA (ethylenediaminetetraacetic acid) as a complexing agent for ferrous iron was suggested by Prof. Pasek during personal email correspondence but not used in this study.

Removal of dissolved iron [Fe^{2+}] from the washings was required as it is paramagnetic (due to having unpaired electrons in the *d*-orbitals) and thus has its own inherent magnetic field when a magnetic field is applied. This additional magnetic field causes interference with the applied magnetic field within the instrument, preventing proper nuclear alignment, and also interfering with the relaxation time of the nucleus being observed by NMR, causing peak broadening. The greater the amount of paramagnetic material present, the greater the interference, which can lead to the observation of no peaks in the NMR spectrum.

The first sample attempted for analysis contained a very high concentration of dissolved iron and required several treatments of sodium sulphide and sodium hydroxide to obtain a good quality spectrum. It was assumed, as the concentration of iron was high, that the concentration of phosphorus would also be high and that therefore a shorter run time would be required to obtain a defined spectrum. The sample was run for 8192 scans on a 500 MHz NMR spectrometer. The ^{31}P NMR spectrum for the first reactor sample (2.7) gave a strong doublet at $\delta 4.0$ indicating the presence of phosphite [HPO_3^{2-}] and a singlet at
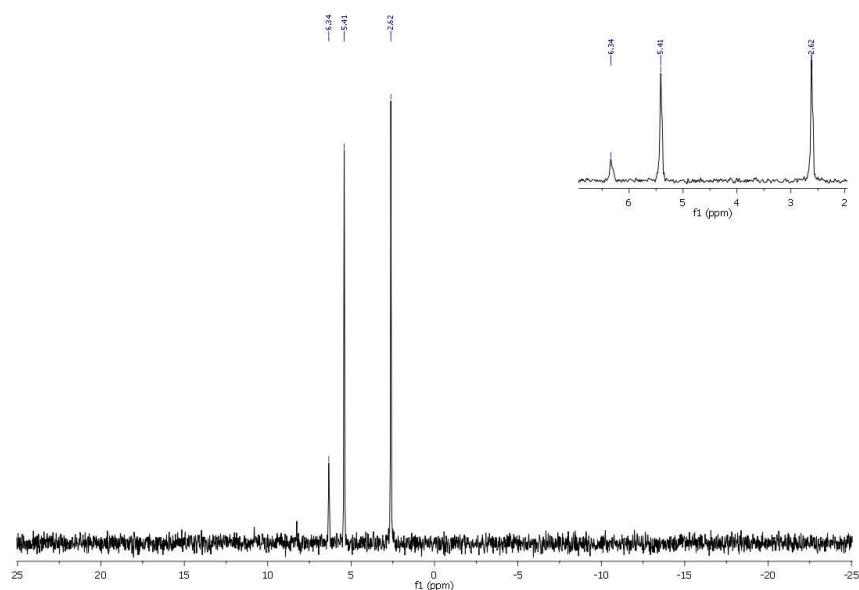
Spectrum 2.7: ^{31}P NMR spectrum (D$_2$O, 300 K, 202.46 MHz) of the washings from the first reactor vessel which shows a strong doublet at δ4.0 ($^1J_{\text{P-H}}$= 566 Hz) indicating phosphite [HPO$_3^{2-}$] and a singlet peak at δ6.3 which is indicative of phosphate [PO$_4^{3-}$]. NMR spectrum obtained by Mr Simon Barrett, NMR Technician.
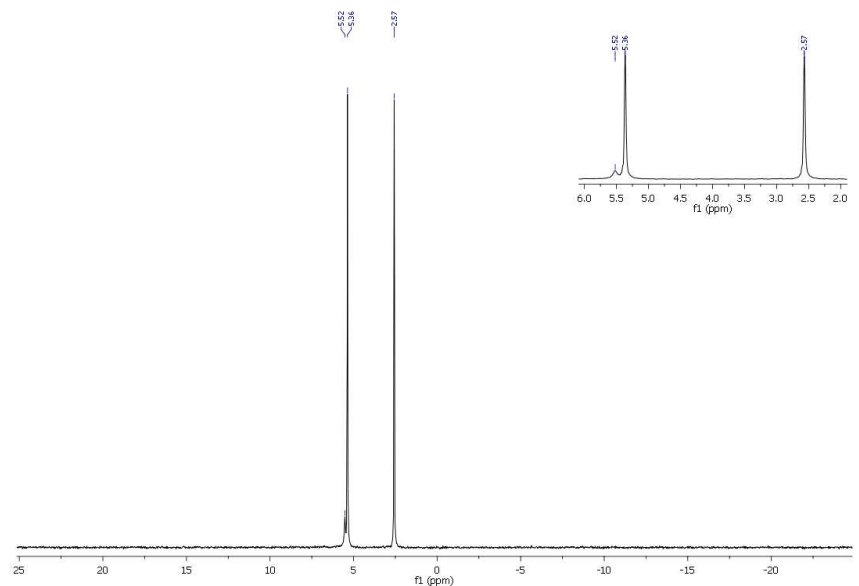
Spectrum 2.8: ^{31}P NMR spectrum (D$_2$O, 300 K, 202.46 MHz) of the washings from the second reactor vessel which again shows a strong doublet at δ4.0 ($^1J_{\text{P-H}}$= 565 Hz) confirming phosphite [HPO$_3^{2-}$] production as the main corrosion product from acidic corrosion of Fe$_3$P and a small singlet peak at δ6.3 which is indicative of phosphate [PO$_4^{3-}$]. NMR spectrum obtained by Mr Simon Barrett, NMR Technician.

$\delta 6.3$ which was phosphate [PO_4^{3-}]. The ^{31}P NMR spectrum for the second reactor sample (2.8) was again analysed on the 500 MHz NMR spectrometer using 8196 scans and gave the same strong doublet at $\delta 4.0$ confirming the production of phosphite [HPO_3^{2-}] and a small singlet at $\delta 6.3$ indicating phosphate [PO_4^{3-}]. The NMR analysis of the reaction vessels showed that the major product of acidic corrosion of Fe_3P is phosphite but it does not give true quantitative data but semi-quantitative data for the amounts of each corrosion product produced. An accurate method of quantitative analysis was required to show how much of each product was produced and after some literature research, the method chosen was phosphomolybdate colorimetry as it was inexpensive and required little equipment.

2.2.3 Quantification of phosphine and phosphite production using phosphomolybdate colorimetry

Colorimetry is a technique used to determine the concentration of a coloured compound in a solution by measuring the absorption of light through the sample which is proportional to its concentration (The Beer-Lambert Law).[187] The use of colorimetric analysis as a tool for quantification requires the production of a calibration curve from the absorption data of a set of standard solutions of the analyte covering the required concentration range (a minimum of six data points is required to produce and accurate calibration curve to calculate concentration).[188,189] A calibration curve must be a straight line through the origin which can then be used to extrapolate the concentration of an unknown sample providing it falls within the linear range.
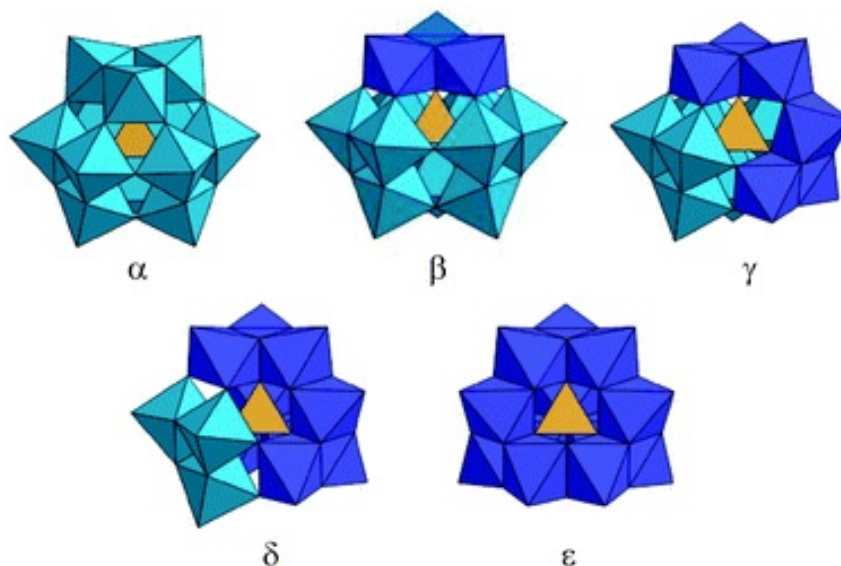
Figure 2.4: Image showing the difference between the different isomers of a Keggin structure. The original Keggin structure of 12-phosphotungstic acid ($H_3[P(W_3O_{10})_4].nH_2O$) was elucidated in 1934 using X-ray diffraction by J.F. Keggin.[190] There are a total of 5 isomers with the original structure designated α- and the remaining isomers (β-, γ-, δ- and ϵ-) identified by the rotational orientations of the molybdate (Mo_3O_{10}) units.[191]

The phosphomolybdate colorimetric technique works due to the reaction of orthophosphate with potassium antimonyl tartrate and ammonium molybdate in an acidic medium to form an antimony-phosphomolybdate complex.[189] This phosphomolybic acid is a hetropoly acid which has an α-Keggin structure (see Figure 2.4). The reduction of this phosphomolybdate

complex in the presence of ascorbic acid causes a change in the electronic structure which leads to a change in physical structure to the β- isomer (Figure 2.4), producing a deep blue colour which is proportional to the concentration of orthophosphate present in the sample. Based on the literature used, the linear range of detection using this method is between 0.15-1.3 ppm (0.15-1.3 mg/L).[188]

Nine different concentrations were used to produce the calibration curve ($R^2 = 0.996$, see Figure 6.4) of concentrations of phosphorus between 0.125 ppm and 1.5 ppm as this covered in detail the estimated concentration region of the sample. The series of standards were prepared from a stock solution of potassium phosphate monobasic [KH_2PO_4] (0.2195 g in 250 mL, 200 ppm phosphorus) prepared in appropriate volumetric glassware.

All standards and samples were digested using the persulphate digestion method stipulated in 4500-P, Standard Methods for the Examination of Water and Wastewater produced by the American Public Health Association[188] (also cited in Methods of Phosphorus Analysis for Soils, Sediments, Residuals and Waters[189]) and were subject to colorimetric analysis using the molybdenum blue/ascorbic acid method also stipulated in this publication. After digestion and cooling, each sample was treated with 8 mL of the development fluid which was prepared from a mixture of sulphuric acid, potassium antimonyl tartrate, ammonium molybdate and ascorbic acid. The samples were then allowed to develop for 20 minutes before reading the maximum absorption at 880 nm on a Heλios γ fixed wavelength UV/Vis spectrometer. The absorption data obtained for the calibration curve are shown in Table 6.9.
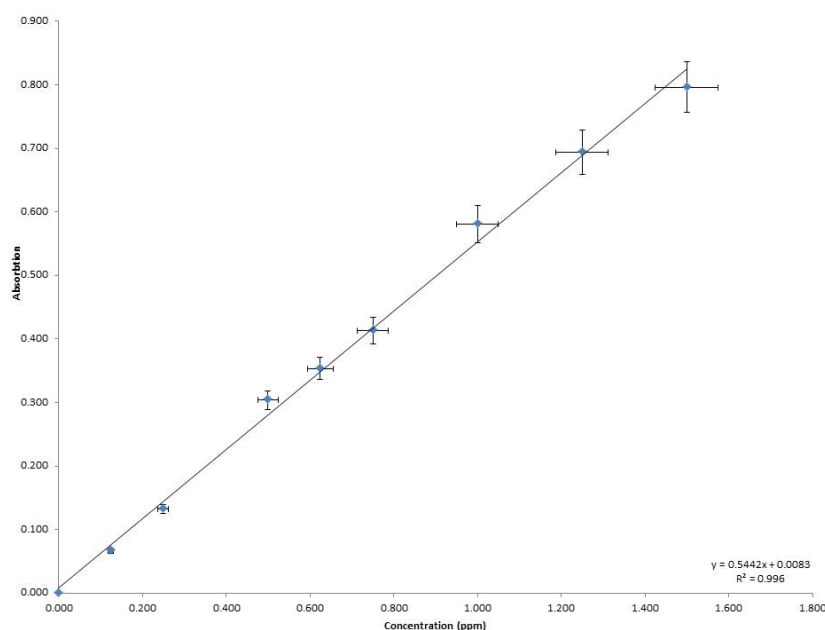
Figure 2.5: Calibration curve graph of the data shown in Table 6.9 which shows a straight line fit for the data with an R^2 value of 0.996

Once the calibration curve had been plotted it was possible to use the curve to calculate a concentration for a given absorption. According to the Beer-Lambert law, absorption (a) is proportional to the concentration (c) of the solution multiplied by path-length (l):

$$a \propto c \times l \tag{2.4}$$

48

The absorption for a known concentration can therefore be calculated from the calibration curve in which the slope of the graph gives the absorption coefficient (ε) of the sample meaning that:

$$a = \varepsilon cl \tag{2.5}$$

So for the calibration curve obtained in this experiment:

$$a = 0.5442c + 0.0083 \tag{2.6}$$

This equation can then be rearranged in terms of "c" to allow calculation of the concentration for a known absorption reading giving:

$$c = \frac{(a - 0.0083)}{0.5442} \tag{2.7}$$

Using this formula, the concentration of P in the samples for the bleach trap and reaction vessels could be calculated from the data shown in Table 2.1. The calculated concentration of P was then corrected for the dilution required to keep the absorption within the linear scale range to give the true concentration of each sample. The concentrations of P in the bleach trap samples were calculated to be 7.5 ppm and 7.1 ppm respectively while the reaction vessel concentrations were calculated to be 6778 ppm and 6282 respectively.

Based on these concentrations, the percentage of total available P for each sample for each experiment was calculated. The average percentage conversion for phosphine production was calculated to be *ca.* 0.01% confirming the figure estimated by Glindemann (1998)[57] and for the average percentage for conversion to phosphite a figure of *ca.* 10% was calculated. The deionised water was also checked via this method to make sure that there was a negligible background. Two different water samples were checked, one was freshly produced deionised water while the other was held in a sealed bottle for 5 days at ambient temperature. As seen in Table 2.1 the results show that fresh deionised water has a negligible background (0.007 ppm) while water which is 5 days old had a significantly higher background (0.134 ppm) which could no longer be considered negligible. This result highlighted the need for a strict analytical procedure while conducting phosphomolybdate analysis as the use of water which was not fresh could seriously impact on the quality of the results obtained.

As discussed earlier in Section 2.2.1.3, there was an issue with some experiments not producing detectable levels of phosphine gas. Comparative analysis of the successful and unsuccessful experiments showed that phosphine was only produced when a larger amount of Fe_3P was used (when *ca.* 2.25 g of Fe_3P used rather than *ca.* 1 g) and the reactor vessel dried out slowly during the 72 hour run time. It seemed that the drying process was linked to the evolution of phosphine gas from the system. After initial consideration it was thought that the acidic solution was protonating the phosphine to form a phosphonium ion $[PH_4^+]$, which was remaining dissolved in the acidic fluids, but was then driven off as the acid evaporated. It was decided to check this by conducting an experiment in which the

Source	Abs.	P (ppm)	Conc.	Dil.	Total P (ppm)
Bubbler (1)	0.214	0.378		20	7.6
Reactor (1)	0.828	1.506		4500	6778
Bubbler(2)	0.201	0.354		20	7.0
Reactor (2)	0.768	1.396		4500	6282
Blank (fresh)	0.012	0.007		1	0.007
blank (5 days)	0.081	0.134		1	0.134

Table 2.1: Table of data for the phosphorus concentration of bubbler 2 and the reaction vessel from two separate runs of the hydrothermal corrosion experiment. This shows that between 7 and 7.5 ppm phosphine was produced over a period of 72 hours while over 6000 ppm of phosphite was produced during the same period in the reaction vessel. The background phosphorus content of the water is also shown which shows trace amounts of phosphate (0.007 ppm) in the fresh deionised water while after 5 days this has risen to significant background levels (0.134 ppm.

evolution of phosphine could be measured over time. This was accomplished by changing the bleach in bubbler 2 every 24 hours then measuring the concentration of phosphorus present in each sample by phosphomolybdate colorimetry.

The samples were subject to the same preparation as stated previously and analysed using the same method and equipment. The results shown in Table 2.2 were very surprising as they showed that the majority of phosphine gas was actually produced in the first 24 hours (whereas if the phosphine was liberated as the acid evaporated, then the reverse would be expected). In explanation, it is suggested, as only a small amount of phosphine is generated (0.01% of available phosphorus is quoted by Glindemann *et al.* (1998)[57]), that the phosphine levels produced by the smaller amount of starting material, were below detection limits for the analytical methods. It is also suggested that the rate of corrosion, through time, is inhibited by the corrosion products so smaller and smaller amounts of phosphine are generated over time. Further investigation of this phenomenon would be required to fully establish the reasons for these observations.

Sample	Abs. 1	Abs. 2	Abs. 3	Avg.	Conc. (ppm)	Dil.	Conc. (ppm)
1	0.140	0.141	0.141	0.141	0.244	20	4.88
2	0.018	0.019	0.018	0.018	0.018	20	0.36
3	0.029	0.029	0.029	0.029	0.038	20	0.76
4	0.012	0.012	0.013	0.012	0.007	20	0.14

Table 2.2: Table showing the colorimetric analysis data for the evolution of phosphine over the runtime of the hydrothermal corrosion experiment. It is seen that the majority of phosphine is evolved within the first 24 hours ot the experiment.

2.3   Production of reactive phosphorus species

The production of reduced oxidation state phosphorus species under putative prebiotic conditions is one way to resolve the issue of solubility in the development of early biochemistry but nature and biology require reactive phosphorus species to function correctly. As discussed in Chapter 1, contemporary biochemistry uses activated and condensed phosphates

for a multitude of purposes including containment (phospholipids in cell membranes) and energy transfer (phosphocreatine, pyrophosphate and ATP) while phosphate diesters are used as scaffolding forming the backbone of DNA and RNA. As stated, life currently uses enzymes and co-enzymes, which themselves contain phosphates and condensed phosphates to facilitate the activation and formation of these phosphate species. Without enzymes to facilitate the formation of these activated and condensed species there must have been prebiotic precursors of these essential molecules which were easily formed under geological conditions and available in useful concentration for utilisation in early biochemistry.

The use of phosphorus in energy transfer molecules was of particular interest as it seemed central to almost all metabolic processes within current biology. The hydrolysis of phosphorus anhydride bonds (P-O-P linkages as seen in ATP, ADP and pyrophosphate) releases a lot of energy, which when coupled to reactions which are normally thermodynamically unfavourable, can make the overall reaction favourable.[192] The energy released by hydrolysis (ΔG_{Hyd}) is dependent on pH, ion concentration and ionic strength of the containing medium, with the energy released by ATP under physiological conditions reported between -30 and -50 kJ mol.[193] With condensed phosphates having such a central role in current metabolism it has been concluded that such molecules or prebiotic equivalents would have been required to establish early metabolic processes.[19] ATP is used as an energy currency but is also capable of phosphorylation which activates organic molecules, increasing solubility and preventing their loss through cell walls. Some bacteria have been reported to use pyrophosphate for this purpose rather than ATP[194] which gives credence to the possibility that current metabolism was developed over time and that it evolved from simpler prebiotic precursors to the enzyme mediated systems we know today.

Potential early metabolic currencies include molecules such as pyrophosphate ($PPi_{(V)}$), tripolyphosphate (TPP) and cyclotrimetaphosphate (cTMP) which were reported as potential components of volcanic gases by Yamagata (1991 and 1999) and therefore could be considered prebiotically plausible polyphosphate precursors of ATP.[32,52] Yamagata showed under experimental conditions that it was possible to produce small amounts of all three molecules, but he was unable to detect cTMP from volcanic gases during field observations.[32,52] Laboratory studies have shown that cTMP is an excellent phosphorylating agent and it has also been shown experimentally to aid in the coupling of amino acids.[195] However, the lack of clear evidence for its volcanic provenance casts doubts on its importance.

Herrick Baltscheffsky has long declared that pyrophosphate could be an ancestor of ATP and has conducted extensive research into this area (see Baltscheffsky *et al.* (1966),[196] Baltscheffsky (1996)[197] and Holm & Baltscheffsky (2011)[198] as examples). Pyrophosphate has been shown to be accessible industrially by heating of phosphate salts to over 200℃ causing a condensation reaction and has also been proposed to form in alkaline hydrothermal vent systems in the presence of Brucite [$Mg(OH)_2$].[199] However, pyrophosphate has very low solubility in the presence of divalent cations and high pH (>pH 8) and is also low in kinetic reactivity without enzymes present to catalyse the reaction.[200] There are very few naturally occurring pyrophosphate minerals known in the geological record with Canaphite [$Na_2Ca(P_2O_7) \cdot 4\,H_2O$], Arnhemite [$(NaK)_4Mg_2(P_2O_7)_2 \cdot 5\,H_2O$] and Wooldridgeite [$Na_2CaCu_2^{2+}(P_2O_7)_2 \cdot 10\,H_2O$] being the most widely studied examples

(information from the mindat database – www.mindat.org). As stated in Chapter 1, reduced oxidation state phosphorus species such as phosphite can overcome the solubility and reactivity issues of phosphate. Can the same be said for reduced condensed phosphorus species? The remainder of this chapter will look at the production of condensed phosphite species, the conditions required for formation for such chemicals and some of the reactions possible with these condensed reduced phosphorus species.

2.3.0.1 Formation of sodium pyrophosphite [$Na_2H_2P_2O_5$]

Sodium phosphite was prepared using very much the same method as specified by Amat (1888a) though by mixing 1:1 molar equivalents of phosphonic acid and sodium hydroxide in deionised water instead of using sodium carbonate for neutralisation.[201] The sodium phosphite was collected by dehydrating the solution using a rotary evaporator until a white gum was obtained, then dried overnight to a white solid in a 50℃ oven. The formation of sodium pyrophosphite involved heating the finely ground white solid in a tube furnace at 160℃ for 72 hours under flowing N_2 gas. The conversion of phosphite to pyrophosphite can be measured by ^{1}H or ^{31}P NMR analysis by integration of the peak areas giving a percentage conversion of available phosphite.

Examples of ^{1}H and ^{31}P NMR spectra can be seen in 2.9 and 2.10. Sodium pyrophosphite is easily identifiable in both ^{1}H and ^{31}P NMR spectra as an observed AA'XX' spin system (protons which are chemically equivalent but magnetically different) resulting in what could be identified as a doublet of triplets. The ^{1}H NMR spectrum (2.9) shows the pyrophosphite AA'XX' spin system at δ6.9 with phosphite showing as a doublet at δ6.7 while the ^{31}P NMR spectrum (2.10) shows the pyrophosphite AA'XX' spin system at δ-5.0 with phosphite showing as a doublet at δ2.9. The areas under the peaks were calculated by integration using Mestrenova NMR processing software and the percentage conversion calculated as a percentage of available phosphorus. Full NMR data are shown in Table 6.16.

As stated, the production of pyrophosphite at 160℃ is well documented (see Grant *et al.* (1964),[202] Mesmer and Carroll (1966)[203] and Godber (1999)[?] as examples) but demonstrating the production of pyrophosphiteat lower temperatures would lend to making this molecule more prebiotically plausible. Unpublished work conducted by the Kee group showed that if sodium phosphite was dissolved in SMOW and dehydrated, and the residues heated to *ca.* 90℃, formation of pyrophosphite was observed with good conversion (typically >60% after 72 hours). Hence, it seemed important to investigate what within the SMOW was causing the effect observed. It was decided to attempt to make different metal phosphites using the metal ions present in SMOW and to evaluate their abilities to aid in the conversion of phosphite to pyrophosphite. The metal ions identified for trial were calcium [Ca^{2+}] and magnesium [Mg^{2+}] because, apart from sodium, they are the main component ions in SMOW (potassium [K^+] and strontium [Sr^{2+}] are also present but were not investigated in this study).
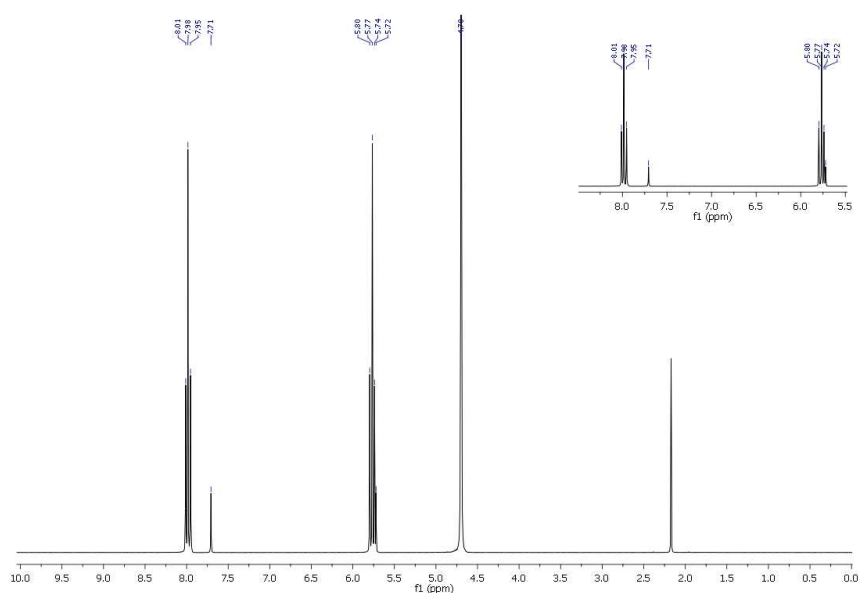
Spectrum 2.9: ^{1}H NMR spectrum (D$_2$O, 300.13 K, 300 MHz) of sodium phosphite dry heated on a sand bath to *ca.* 160℃ under a flow of N$_2$ showing phosphite (δ 6.7, d, $^1J_{\text{P-H}}$= 597 Hz) and also pyrophosphite present (δ6.9, AA'XX', $^1J_{\text{P-H}}$= 663 Hz, $^2J_{\text{P-P}}$= 9 Hz, $^3J_{\text{P-H}}$= 9 Hz.). Other peaks present in the spectrum are water (δ4.7) present as an impurity in the D$_2$O and acetone (δ2.2) which is present as a residue from cleaning of the NMR tubes prior to use.
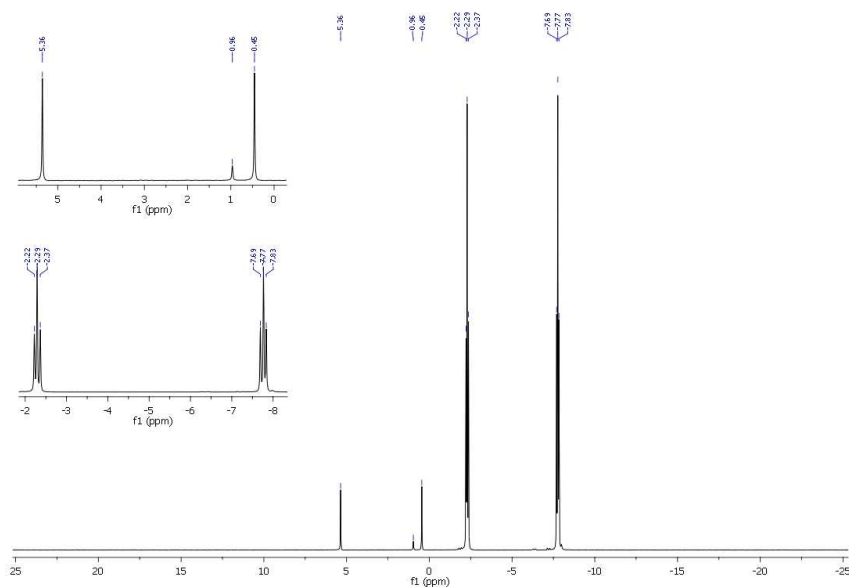
Spectrum 2.10: ^{31}P NMR spectrum (D$_2$O, 300 K, 121.49 MHz) of the same heated sodium phosphite sample shown in Spectrum 2.9 showing the presence of pyrophosphite (δ-5.0, AA'XX', $^1J_{\text{P-H}}$= 666 Hz, $^2J_{\text{P-P}}$= 10 Hz, $^3J_{\text{P-H}}$= 9 Hz) and also phosphite (δ2.9, d, $^1J_{\text{P-H}}$= 596 Hz). There is also a small peak at δ1.0 which shows the presence of orthophosphate and also hints of peaks between δ0.0 and 8.0 which indicate that some isohypophosphate may also have been formed.

2.3.0.2 Attempted formation of magnesium pyrophosphite [MgH$_2$P$_2$O$_5$]

To attempt formation of magnesium pyrophosphite it was first necessary to prepare the monobasic salt of magnesium phosphite [Mg(H$_2$PO$_3$)$_2$]. The preparation of monobasic magnesium phosphite was attempted *via* three different methods which are detailed below.

The first method was adapted from a method of preparation of zinc phosphite published by Ortiz-Avila *et al.* (1989).[204] Magnesium chloride hexahydrate [MgCl$_2 \cdot 6$ H$_2$O] and phosphonic acid [H$_3$PO$_3$] were mixed in deionised water in a 1:2 molar ratio and stirred for 6 hours then left to crystallise. There was no crystal formation after 2 months and despite attempts to induce crystallisation, no crystals were obtained.

The second method involved reaction of magnesium oxide [MgO] with phosphonic acid [H$_3$PO$_3$], dissolved in deionised water in a 1:2 molar ratio, stirred for 6 hours under a N$_2$ atmosphere then left to crystallise. After 3 days a white micro-crystalline precipitate had formed which was collected by vacuum filtration and analysed by ^{31}P NMR spectroscopy. ^{31}P NMR spectra (Spectrum 2.11, full NMR information is shown in Table 6.20) showed the presence of phosphite (δ2.6, d). A portion of the precipitate (*ca.* 1.0 g) was heated on a sand bath to *ca.* 90°C under flowing N$_2$ for 72 hours in an attempt to produce pyrophosphite. It was found by ^{31}P NMR analysis (Spectrum 2.12) that heating the precipitate did produce pyrophosphite (δ6.8, AA'XX').
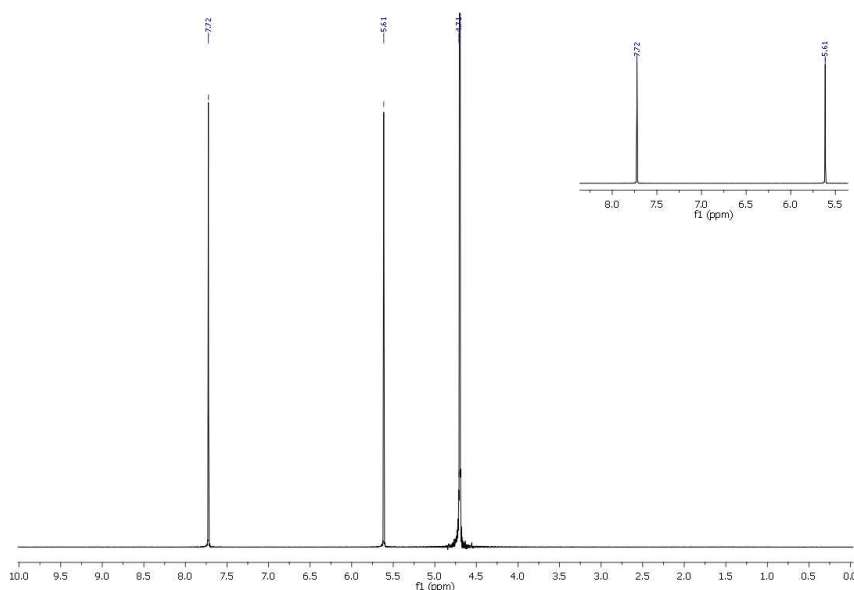
Spectrum 2.11: ^{1}H NMR spectrum (D$_2$O, 300 K, 300.13 MHz) of magnesium phosphite precipitate prepared from magnesium oxide and phosphonic acid. The spectrum shows the presence of phosphite (δ2.6, d, $^1J_{\text{P-H}}$= 627 Hz) in the precipitate.

To confirm the solid obtained was Mg(H$_2$PO$_3$)$_2$ it was decided to analyse the precipitate with powder x-ray diffraction (pXRD). The spectrum was obtained on a Bruker D8 diffractometer and was compared to pXRD spectra of the starting material [MgO] from the Daresbury crystallographic database. Unfortunately the spectrum for the precipitate was almost identical to that of the starting material so it can only be assumed that the precipitate was magnesium oxide coated in residues of phosphonic acid. This might indicate however, that, providing a divalent metal ion was available, the conversion of phosphonic acid to pyrophosphite would be possible without the need for the monobasic metal salt
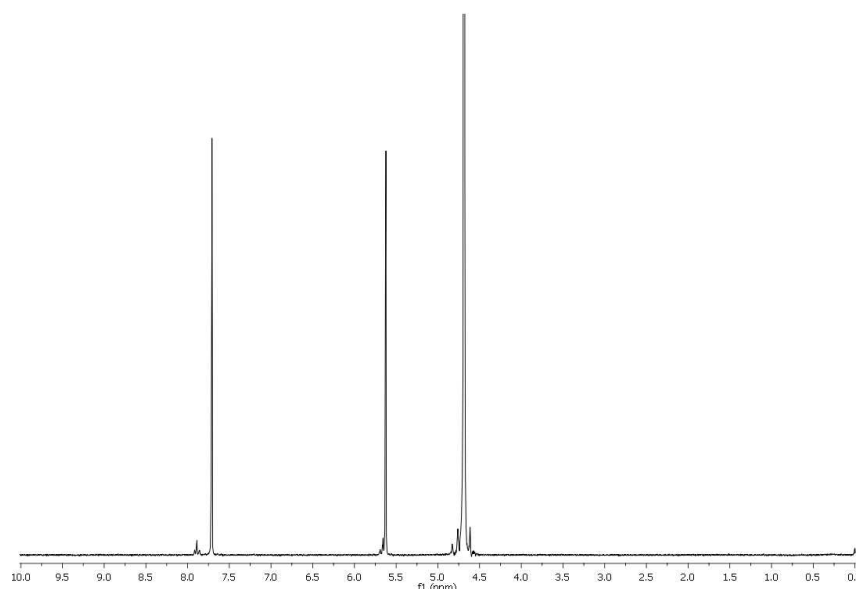
Spectrum 2.12: ^{1}H NMR spectrum (D$_2$O, 300 K, 300.13 MHz) of magnesium phosphite precipitate dry heated on a sand bath to 90℃ for 72 hours under flowing N$_2$. The spectrum shows the presence of phosphite (δ2.6, d, $^1J_{\text{P-H}}$= 627 Hz) and pyrophosphite (δ6.8, AA'XX', $^1J_{\text{P-H}}$= 669 Hz, $^2J_{\text{P-P}}$= 9 Hz, $^3J_{\text{P-H}}$= 9 Hz) in the dry heated sample indicating formation of the monobasic magnesium phosphite salt.

being formed.

The third method for production of Mg(H$_2$PO$_3$)$_2$ was *via* an acid/metal reaction method. Magnesium turnings were added slowly to a solution of phosphonic acid [H$_3$PO$_3$] (1 M) in a 1:2 molar ratio, filtered to remove any unreacted material then left to crystallise. Within 48 hours a large mat of lozenge shaped crystals were obtained which were collected by vacuum filtration. A small portion of crystals were dissolved in D$_2$O and analysed by ^{31}P NMR spectroscopy (Spectrum 2.13) showing clearly the presence of phosphite (δ2.9, d).
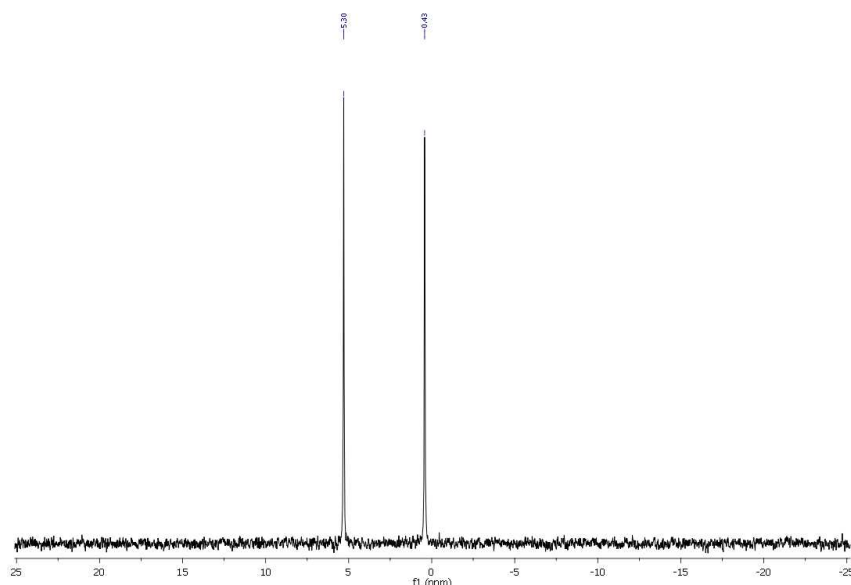
Spectrum 2.13: ^{31}P NMR spectrum (D$_2$O, 300 K, 121.49 MHz) of the acid/metal prepared magnesium phosphite crystals. The presence of phosphite (δ2.9, d, $^1J_{\text{P-H}}$= 592 Hz) is clearly seen. Full NMR data shown in Table 6.22

Single crystal X-ray diffraction was undertaken for characterisation by Dr. David Bryant, a senior member of the Kee group who found after refining the structure of the crystal that a

dibasic magnesium phosphite [MgHPO$_3$] was obtained. This was confirmed by comparison to the unit cell data obtained for MgHPO$_3$ from the Daresbury crystallographic database [triclinic, space group Pi, with a = 7.007(1), b = 8.100(1), c = 6.773(1) Å, α = 84.92(1), β = 96.72(2) and γ = 112.00(1)°; V = 354.1 Å^3, Z = 2; ϱ_x = 2.261 g/cm^3 and ϱ_{ob} = 2.21(1) g^3/cm^3].[205]

Dry heating of the ground crystals at 90℃ under flowing N$_2$ did not produce pyrophosphite. The ^{31}P NMR analysis (Spectrum 2.14) shows no trace of pyrophosphite only phosphite (δ2.6, d, $^1J_{\text{P-H}}$= 627 Hz). It is thought that this was due to the inability of dibasic salts to undergo condensation reactions as reported by Grant et $al.$ (1964)[202] though it was found by NMR analysis (Spectrum 2.15) that if the crystals were dissolved in water and the pH adjusted to $ca.$ pH 4, reduced to dryness then dry heated to $ca.$ 90℃ that this would then facilitate the formation of pyrophosphite.
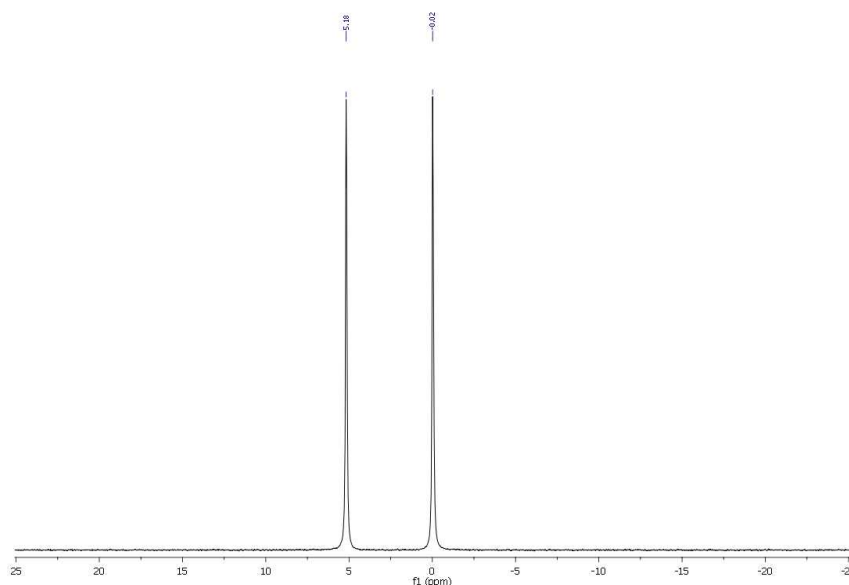
Spectrum 2.14: ^{31}P NMR spectrum (D$_2$O, 300 K, 121.49 MHz) of the magnesium phosphite crystals which dry heated on a sand bath to 90℃ under flowing N$_2$ for 72 hours. It is clearly seen that there is no formation of pyrophosphite from this sample with only phosphite (δ2.6, d, $^1J_{\text{P-H}}$= 627 Hz) visible in the spectrum. Full NMR data shown in Table 6.22

Identification of pH as an issue for conversion of phosphite to pyrophosphite was significant. It was thought that the pH was a factor due to the relevant pK_a2 for phosphite ($ca.$ 7.2). Further investigation of this pH dependence was undertaken with a series of dry heating reactions set up covering a range from pH4 to pH 10. The samples were dry heated to 85℃ in a vacuum oven for 72 hours and the samples analysed by ^{31}P NMR. The results in Table 2.3 showed that at pH 4 the conversion to pyrophosphite was highest ($ca.$ 22% conversion) and that even up to pH 7 ($ca.$ 4% conversion) there was still observed conversion to pyrophosphite but above pH 7 there was no observed conversion. This would confirm that, as the pH approaches the pK_a2 value, the formation of the dibasic metal salt will inhibit the condensation reaction and thus prevent the formation of pyrophosphite.
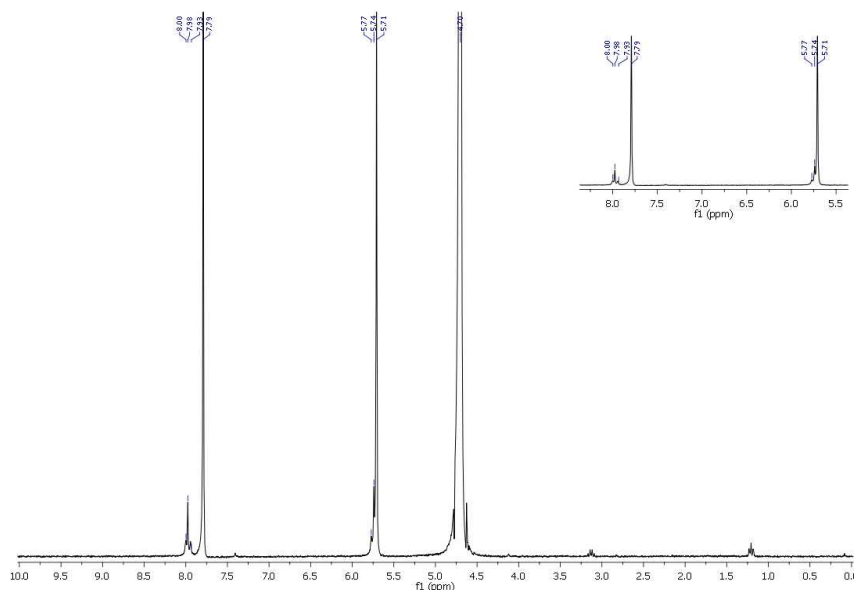
Spectrum 2.15: ^{1}H NMR spectrum (D$_2$O, 300 K, 300.13 MHz) of the pH4 adjusted magnesium phosphite crystals which were dry heated in a vacuum oven to 85℃ for 72 hours. The spectrum shows the formation of pyrophosphite (δ6.9, AA'XX', $^1J_{\text{P-H}}$= 672 Hz, $^2J_{\text{P-P}}$= 15 Hz, $^3J_{\text{P-H}}$= 6 Hz) and also phosphite (δ6.8, d, $^1J_{\text{P-H}}$= 624 Hz) and water (δ4.7, s). Full NMR data shown in Table 6.22

Compound:	Pyrophosphite [H$_2$P$_2$O$_5^{2-}$]	Phosphite [HPO$_3^{2-}$]
Conditions:	90℃, 72 hours, N$_2$ flow	
	31P NMR (D$_2$O, 300 K, 121.49 Hz)	
Analysis	Composition (%)	
pH 4	22	78
pH 5	18	82
pH 6	4	96
pH 7	3	97
pH 8	0	100
pH 9	0	100
pH 10	0	100

Table 2.3: Table showing percentage conversion of Mg$_2$HPO$_3$ under different pH conditions. The data shows that the phosphite salts need to be dry heated under acidic conditions to afford conversion of phosphite to pyrophosphite.

2.3.0.3   Attempted formation of calcium pyrophosphite [CaH₂P₂O₅]

As with the attempted formation of magnesium pyrophosphite, it was first required to prepare the monobasic calcium phosphite salt $[Ca(H_2PO_3)_2 \cdot H_2O]$. The preparation of monobasic calcium phosphite was attempted by two different methods. The first method was adapted from the preparation of zinc phosphite published by Ortiz-Avila *et al.* (1989)[204] and was essentially the same as that used for the preparation of magnesium phosphite monobasic. Calcium chloride $[CaCl_2]$ and phosphonic acid $[H_3PO_3]$ were mixed in deionised water in a 1:2 molar ratio and stirred for 6 hours then left to crystallise. As for the attempt to form magnesium phosphite by this method, there was no crystal formation after 2 months and despite repeated attempts to induce crystallisation, no crystals were obtained.
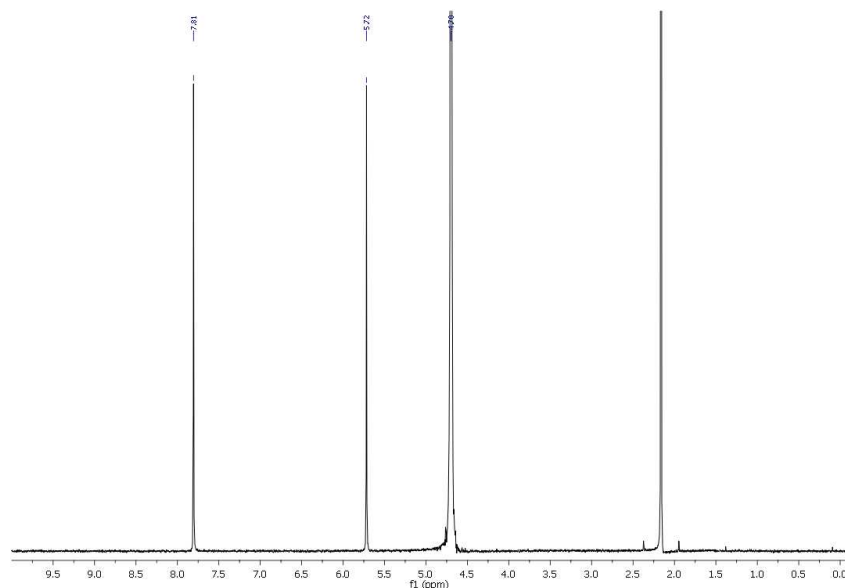
Spectrum 2.16: ^{1}H NMR spectrum (D₂O, 300 K, 300.13 MHz) of calcium phosphite prepared by mixing calcium carbonate with phosphonic acid in deionised water. The presence of phosphite ($\delta 6.8$, d, $^1J_{\text{P-H}}$= 627 Hz) is clearly visible. Other visible peaks in the spectrum are water ($\delta 4.7$) and acetone ($\delta 2.2$).

The second method was published by Larbot *et al.* (1984) for the preparation of monobasic calcium phosphite monohydrate $[Ca(H_2PO_3)_2 \cdot H_2O]$.[206] Calcium carbonate $[CaCO_3]$ and phosphonic acid $[H_3PO_3]$ were mixed in deionised water in a 1:2 molar ratio, stirring until there was no further effervescence. The solution was gravity filtered to remove any unreacted material, placed in a 60°C oven for 4 hours to drive off any dissolved CO_2, then allowed to cool at room temperature to allow crystallisation. After *ca.* 3 days a white micro-crystalline precipitate was formed which was collected by vacuum filtration and analysed by ^{1}H NMR spectroscopy. The ^{1}H NMR spectrum (2.16, full NMR information is shown in Table 6.25) showed the presence of phosphite ($\delta 6.8$, d).

The precipitate was also analysed by powder X-ray diffraction (pXRD) and the presence of calcium phosphite confirmed by pattern matching from the crystallographic database service, Daresbury. The filtered solution was left for further crystallisation which after a further 2 weeks resulted in a large crop of thick, rod-like crystals which were collected by vacuum filtration, washed with chilled ethanol and dried under vacuum. Single crystal X-ray diffraction was again undertaken for characterisation by Dr. David Bryant who found after refining the structure of the crystal that the monobasic calcium phosphite
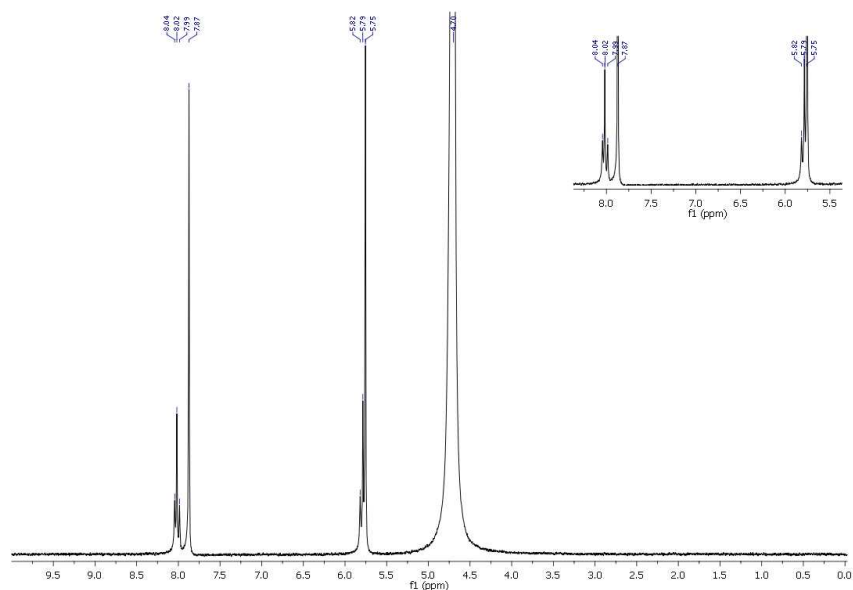
Spectrum 2.17: ^{1}H NMR spectrum (D_2O, 300 K, 300.13 MHz) of calcium phosphite dry heated on a sand bath to 90℃ under flowing N_2. The presence of phosphite (δ6.8, d, $^1J_{P-H}$= 627 Hz) is clearly visible and also pyrophosphate (δ6.9, AA'XX', $^1J_{P-H}$= 669 Hz, $^2J_{P-P}$= 9 Hz, $^3J_{P-H}$= 6 Hz). The other visible peak in the spectrum is water (δ4.7).
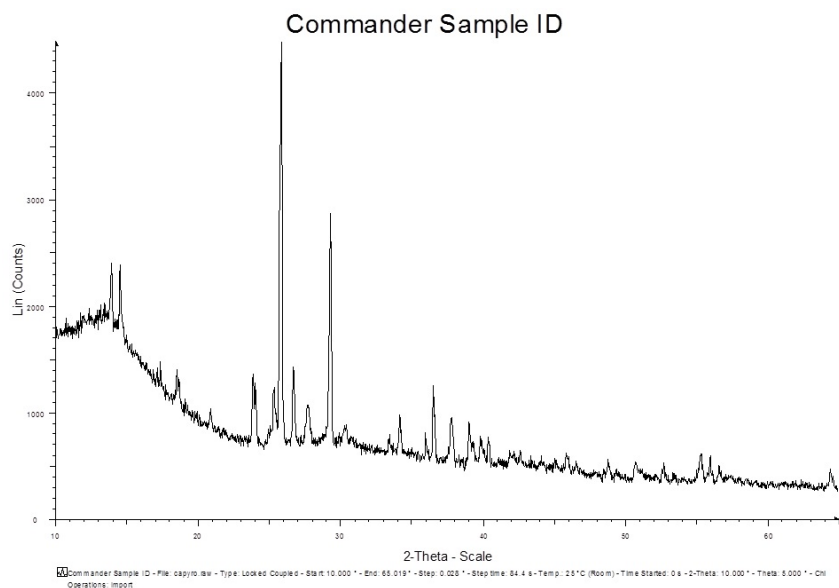
Spectrum 2.18: Spectrum of calcium phosphite analysed by powder X-ray diffraction. The diffraction pattern was obtained on a Bruker D8 diffractometer and the identification of calcium phosphite was confirmed by pattern matching from the crystallographic database service, Daresbury.

monohydrate $[Ca(H_2PO_3)_2 \cdot H_2O]$ unit cell was obtained as per the literature [triclinic, space group Pi, with a = 7.007(1), b = 8.100(1), c = 6.773(1) Å, α = 84.92(1), β = 96.72(2) and γ = 112.00(1)°; V = 354.1 Å^3, Z = 2; ϱ_x = 2.261 g/cm^3 and ϱ_{ob} = 2.21(1) g^3/cm^3].[206]

A portion of the crystals was ground in a mortar and pestle and dry heated at *ca.* 90℃ on a sand bath under flowing N_2 for 72 hours. A portion of the sample (0.5 g) was dissolved in D_2O and submitted for ^{1}H NMR analysis. The formation of pyrophosphite (δ6.9, AA'XX') was observed in the NMR spectrum (Spectrum 2.17) with no further manipulation indicating and confirming the production of the acidic calcium phosphite salt $[Ca(H_2PO_3)_2 \cdot H_2O]$.

2.3.1 Attempted formation of pyrophosphite in the presence of iron

In the previous sections, it has been shown that the presence of bivalent metal ions has aided in the formation of pyrophosphite via a condensation reaction. The bivalent metals seem to have lowered the energy required to facilitate the condensation of phosphite to form pyrophosphite at lower temperatures than with the monovalent sodium ions. This effect is thought to be due to the close proximity of the two phosphite ions when bound to the divalent metal allowing for easier condensation. One metal which would be present in solution due to corrosion of iron meteorites would be iron in the form of ferrous ions $[Fe^{2+}]$. With ferrous ions being present in the corrosion fluids, it was decided to investigate the effects of ferrous iron on the formation of pyrophosphite as with previous metal ions.

It was decided initially to try production of pyrophosphite directly from the dry heating of corrosion products from the simulated hydrothermal treatment of Fe_3P and analysing the samples by ^{31}P NMR spectroscopy. As previously, Fe_3P was heated at 90℃ in H_2SO_4 for 7 days. The solution was then filtered and the pH adjusted to *ca.* pH 4 using sodium carbonate solution (1 M). The solution was then reduced to dryness on a rotary evaporator and the residue collected and ground in a mortar and pestle before dry heating on a sand bath at 160℃ for 72 hours. No iron removal was undertaken for this experiment. The flask was removed from the heat and allowed to cool before dissolving the residues in deionised water and again treating with sodium carbonate until pH 8.5 was obtained. The solution was gravity filtered to remove iron precipitates and again reduced to dryness on a rotary evaporator. A portion of the residues (0.5 g) was dissolved in D_2O and submitted for ^{31}P and ^{31}P $\{^1H\}$ NMR spectroscopy.

The presence of hypophosphite $[H_2PO_2^-]$ was identified in the ^{31}P NMR spectrum (Spectrum 2.19, δ 7.9, t, $^1J_{P\text{-}H}$ = 516 Hz. Full NMR data are presented in Table 6.29) as a triplet at 7.9 ppm and was confirmed in the ^{31}P $\{^1H\}$ NMR spectrum (Spectrum 2.20, δ 7.9, s) as the triplet at 7.9 ppm has collapsed to a singlet at 7.9 ppm. This was a very interesting result as it showed that the iron was apparently reducing the phosphite to hypophosphite, and not aiding in the condensation as with the other metals in the previous dry heating experiments. A further set of experiments was conducted using iron metal powder and iron (II) chloride to see if it was Fe^{2+} or Fe metal which was responsible for the reduction.

Two experiments were set up. In one, sodium phosphite solution (5 mmol) was mixed with iron metal powder (15 mmol) and in the other, sodium phosphite solution (5 mmol) was
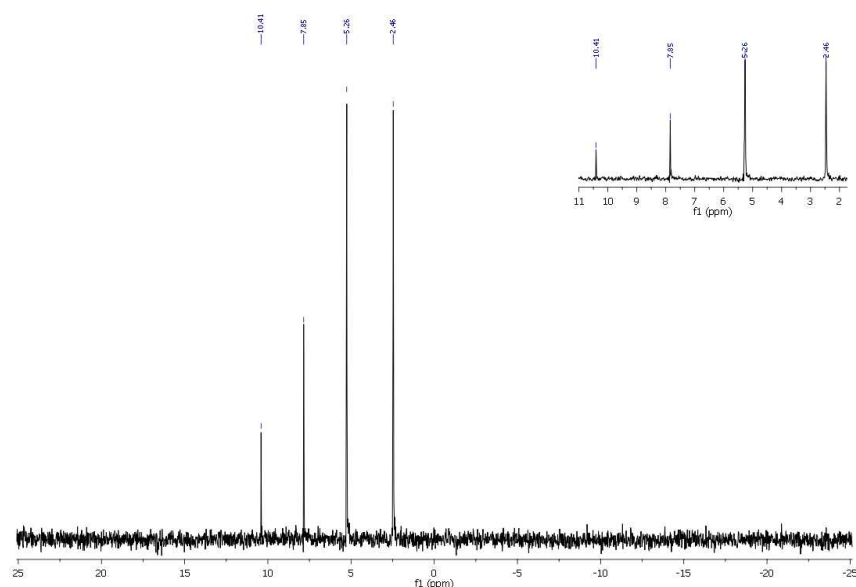
Spectrum 2.19: ^{31}P NMR spectrum (D$_2$O, 300 K, 202.46 MHz) of the post heated Fe$_3$P residues showing a doublet at 3.9 ppm indicating the presence of phosphite (δ 3.9, d, $^1J_{\text{P-H}}$= 567 Hz) but also a triplet at 7.9 ppm which would indicate the presence of hypophosphite (δ 7.9, t, $^1J_{\text{P-H}}$= 516 Hz). This result indicates that reduction of phosphite is occurring while dry heating in the presence of iron.
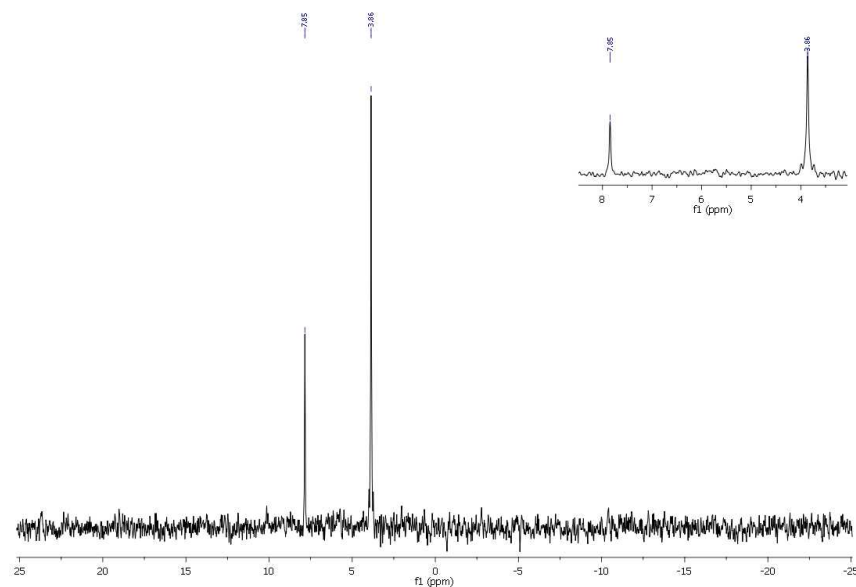
Spectrum 2.20: ^{31}P $\{^1$H$\}$ NMR spectrum (D$_2$O, 300 K, 202.46 MHz) of the post heated Fe$_3$P residues showing the doublet at 3.9 ppm has collapsed to a singlet at 3.9 ppm confirming the presence of phosphite. The triplet at 7.9 ppm has also collapsed to a singlet at 7.9 ppm which also confirms the presence of hypophosphite in the sample. This result indicates that dry heating phosphite in the presence of iron will reduce phosphite to hypophosphite rather than aid in the condensation to pyrophosphite as expected.

mixed with iron (II) chloride (15 mmol). Both were pH adjusted to *ca.* pH 4 and then reduced to dryness on a rotary evaporator. The residues were collected and dry heated on a sand bath to 160℃ under flowing N_2 for 72 hours. The samples were allowed to cool to room temperature, dissolved in deionised water, treated with sodium carbonate solution to remove dissolved iron, and filtered. The samples were both then reduced to dryness on a rotary evaporator and the residues dissolved in D_2O then submitted for ^1H NMR analysis.
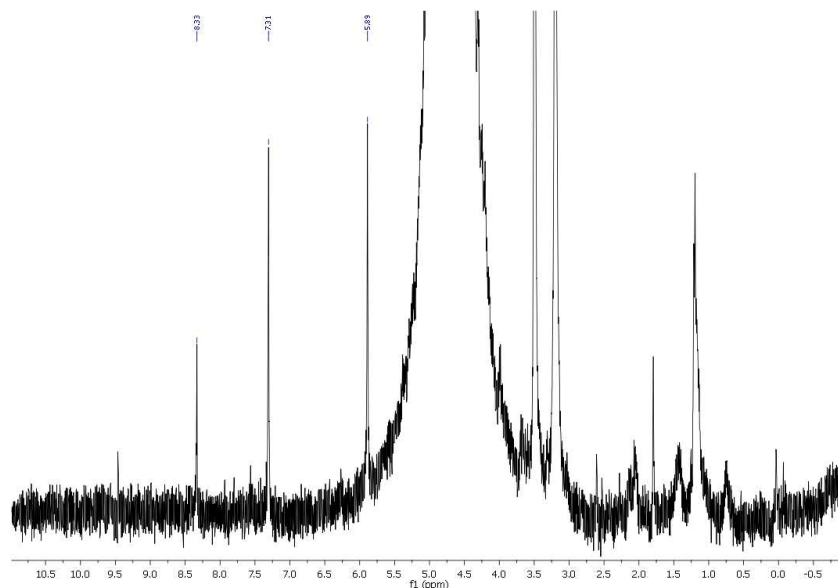
Spectrum 2.21: ^1H NMR spectrum (D_2O, 300 K, 400.13 MHz) of sodium phosphite dry heated in the presence of iron powder. The sample was heated on a sand bath to 160℃ under flowing N_2 for 72 hours. The spectrum is quite broad and messy due to some iron contamination and the concentration of phosphite in the sample being very small compared to the water peak (4.7 ppm) the spectrum has been magnified greatly. It is possible however to see the presence of phosphite as a doublet of peaks at 6.6 ppm. Full NMR data are shown in Table 6.30.

The ^1H NMR spectrum (Spectrum 2.21) of the reaction with iron metal powder showed only the presence of phosphite (δ6.6, d, $^1J_{P-H}= 568$ Hz) while the NMR spectrum of the reaction containing ferrous ion (Spectrum 2.22) showed again phosphite (δ6.7, d, $^1J_{P-H}= 567$ Hz) but also the presence of hypophosphite (δ7.0, d, $^1J_{P-H}= 516$ Hz). This showed that it was the oxidation of Fe^{2+} ions which was responsible for the reduction of phosphite to hypophosphite and not the oxidation of iron metal. This result also suggested that schreibersite containing iron meteorites were capable of producing highly reduced P species given the right conditions but it also raised further questions. If it is possible to reduce phosphite by heating in the presence of ferrous ions, would it be possible to reduce phosphate under the same conditions? and what effects do ferric ions have on the above processes? These became the subject of further investigation.

2.3.1.1 Investigation of phosphate reduction using ferrous iron

The reduction of phosphate was attempted by mixing dibasic sodium phosphate with iron (II) chloride in deionised water. The pH was adjusted to *ca.* pH 4 using sodium hydroxide (1 M) then the mixture was reduced to dryness on a rotary evaporator. The residues were collected and dry heated over a sand bath to 160℃ under flowing N_2 for 7 days. The sample was allowed to cool to room temperature as before. The residue was dissolved in
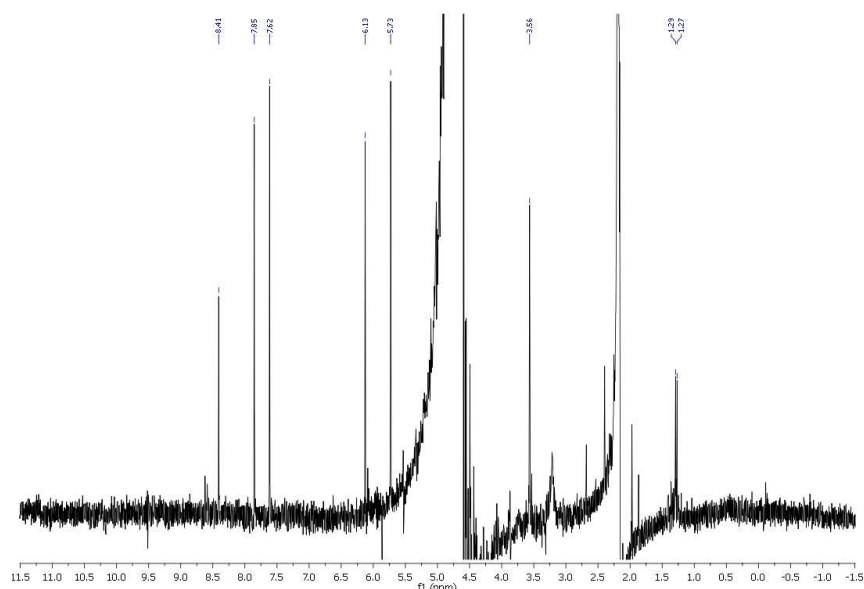
Spectrum 2.22: ^{1}H NMR spectrum (D$_2$O, 300 K, 300.13 MHz) of sodium phosphite dry heated in the presence of iron (II) chloride. The sample was heated on a sand bath to 160℃ under flowing N$_2$ for 72 hours. The spectrum is quite broad and messy due to the factors stipulated in 2.21 but it is possible to see the presence of hypophosphite as a doublet of peaks at 7.0 ppm and phosphite as a doublet of peaks at 6.6 ppm. Full NMR data are shown in Table 6.30.

deionised water, treated with sodium hydroxide to remove any dissolved iron, then filtered and reduced to dryness again on a rotary evaporator. A portion of the residues (0.5 g) was dissolved in D$_2$O and submitted for ^{31}P NMR analysis.

The ^{31}P NMR spectrum (Spectrum 2.23) showed the presence of phosphate (δ1.7, s) and the presence of pyrophosphate (δ-7.5, s) but also a doublet indicating the presence of phosphite in the sample (δ3.0, d). This experiment was repeated to confirm this result and a blank of the phosphate was also run to confirm there was no contamination prior to heating. With the blank sample clear of phosphite and with the same results obtained from the dry heating of the sample it proves the possibility for the reduction of phosphate at moderate temperatures to phosphite in the presence of ferrous iron and thus the possibility of greatly increased levels of reduced oxidation state phosphorus on the early Earth.

Given the prevalence of ferrous iron in basalts and other mineral rocks it would be possible to reduce phosphate present in the environment to produce small amounts of phosphite by heating to *ca.* 160℃ in anaerobic conditions. This would add credence to the findings of Pech *et al.* (2009) who reported detecting small amounts of phosphite dissolved in the waters at Hot Creek Gorge, California by HPLC/Ion Chromatography[33] and also to a proposal for this reductive mechanism by Mulkidjanian *et al.* (2012).[68]

2.3.1.2 Investigation of the effects of ferrous and ferric iron on the production of reduced phosphorus species

As discussed previously in this chapter, it has been shown to be possible to reduce both phosphate and phosphite using ferric iron at temperatures *ca.* 160℃. It was decided to investigate the effects of ferrous and ferric iron at lower temperatures using calcium phosphite hydrate [Ca(H$_2$PO$_3$)$_2$ · H$_2$O] which has been shown earlier to readily produce
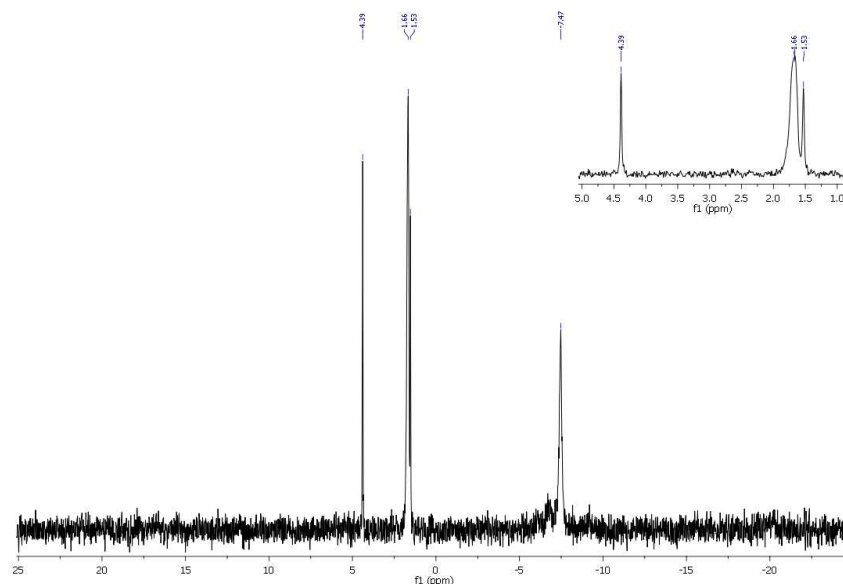
Spectrum 2.23: ^{31}P NMR spectrum (D$_2$O, 300 K, 202.46 MHz) of pH adjusted sodium phosphate dibasic dry heated on a sand bath to 160℃ under flowing N$_2$ for 7 days. A singlet peak for phosphate is visible at 1.66 ppm and also a broader singlet peak at -7.47 ppm for pyrophosphate is also visible. There is also an indication of the presence of phosphite in the sample (δ3.0, d, $^1J_{\text{P-H}}$= 579 Hz).

pyrophosphite at temperatures of *ca.* 90℃.

Initially two sets of two experiments were set up. One set used iron (II) chloride tetrahydrate (4.3 mmol) and the other set used iron (III) chloride (4.3 mmol) mixed with calcium phosphite monohydrate (1 mmol). One experiment of each set was mixed in deionised water while the other was mixed in SMOW to see if there were different effects (as previous work in this chapter had shown beneficial effects on pyrophosphite production in the presence of SMOW residues than without). The solutions were mixed for 30 minutes then dehydrated on a rotary evaporator before being heated on a sand bath at 90℃ for 72 hours under flowing N$_2$. A small portion (0.5 g) of each sample was dissolved in 1 mL deionised water, the dissolved iron removed by pH adjustment using sodium hydroxide (1 M), and the solutions filtered. The samples were then adjusted back to pH 7.5 using HCl then submitted for ^{31}P NMR analysis using D$_2$O insets for locking purposes.

Both the ferrous ion samples showed no conversion of phosphite to pyrophosphite or reduction to hypophosphite at 90℃ with only phosphite visible in the relevant ^{31}P NMR spectra (Spectrum 2.24, δ 6.6 and Spectrum 2.26, δ 6.6). In the ferric ion samples this was not the case. Phosphite was again visible in both spectra but also pyrophosphite was present in both samples (Spectrum 2.25, δ-5.1 and Spectrum 2.27, δ-2.8. Full NME data are shown in Table 6.31.).

This was an interesting and somewhat unexpected result. Ferric iron, being fully oxidised, was not expected to reduce phosphite to hypophosphite as seen with ferrous iron but it showed no effects, beneficial or inhibitory, on the condensation reaction to pyrophosphite. Ferrous iron however, appeared to inhibit the formation of pyrophosphite at low temperatures even in the presence of SMOW (which has previously been shown to aid the formation of pyrophosphite).

As shown previously, at temperatures above 160℃, ferrous ions facilitate the reduction
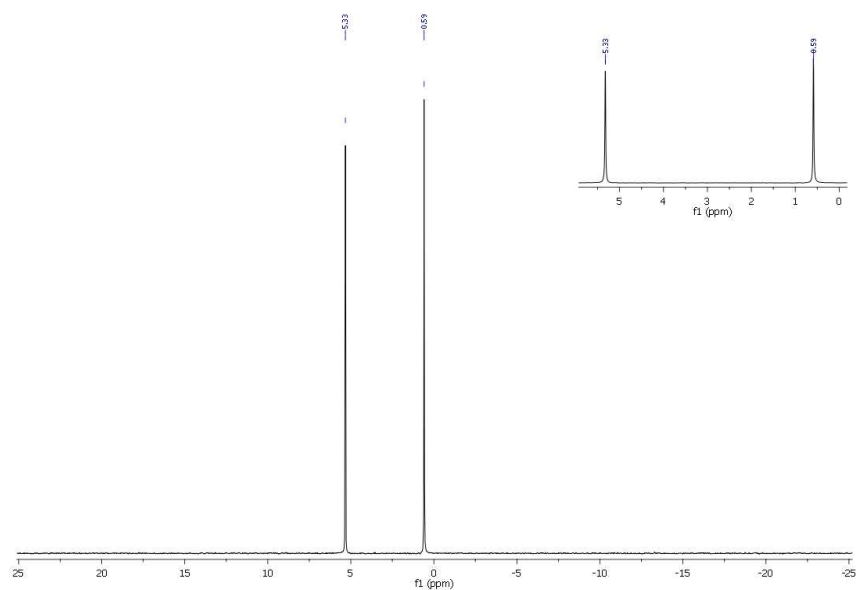
Spectrum 2.24: ^{31}P NMR spectrum (D$_2$O, 300 K, 202.46 MHz) of calcium phosphite monohydrate mixed with ferrous chloride then dry heated on a sand bath at 90℃ under flowing N$_2$ for 72 hours. The sample shows no reduction to phosphite or conversion to pyrophosphite. The spectrum only shows a doublet of peaks at 4.21 ppm (d, $^1J_{\text{P-H}}$= 566 Hz) indicating only the starting material phosphite present. Full NMR data are shown in Table 6.31.
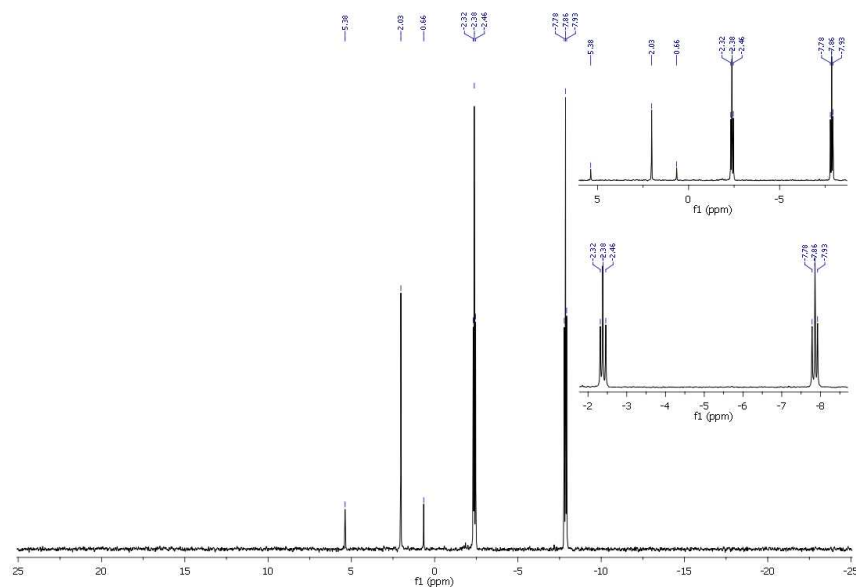
Spectrum 2.25: ^{31}P NMR spectrum (D$_2$O, 300 K, 202.46 MHz) of calcium phosphite mixed with ferric chloride then dry heated on a sand bath to 90℃ under flowing N$_2$ for 72 hours. The spectrum shows condensation of phosphite to pyrophosphite (δ-5.1, AA'XX', $^1J_{\text{P-H}}$= 666 Hz) with the presence of phosphite (δ3.0, d, $^1J_{\text{P-H}}$= 573 Hz) and phosphate (δ2.0, s). Full NMR data are shown in Table 6.31.
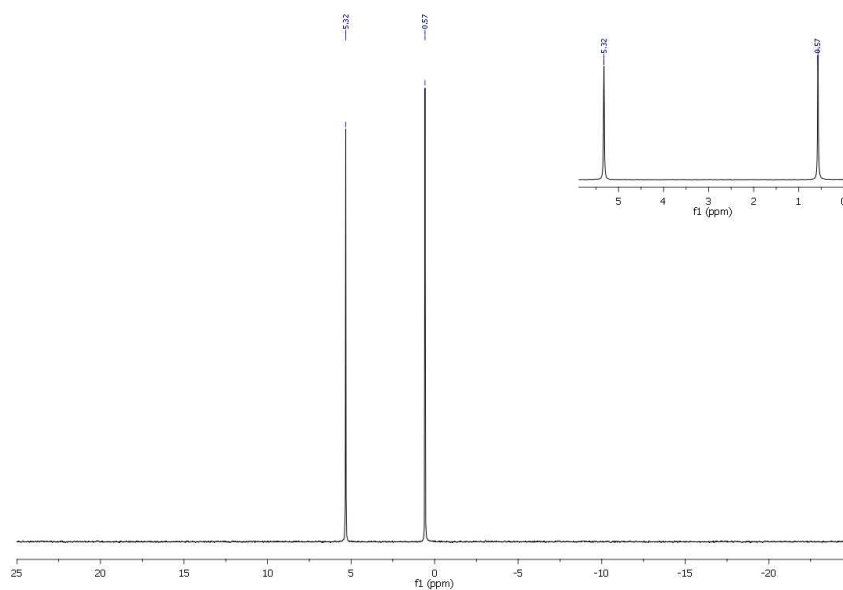
Spectrum 2.26: ^{31}P NMR spectrum (D$_2$O, 300 K, 121.49 MHz) of calcium phosphite/SMOW residues mixed with ferrous chloride then dry heated on a sand bath at 90℃ under flowing N$_2$ for 72 hours. The sample shows no reduction to hypophosphite or condensation to pyrophosphite. The spectrum only shows the presence of phosphite as a doublet of peaks at 3.0 ppm (d, $^1J_{\text{P-H}}$= 576 Hz) which was the starting material. Full NMR data are shown in Table 6.31.
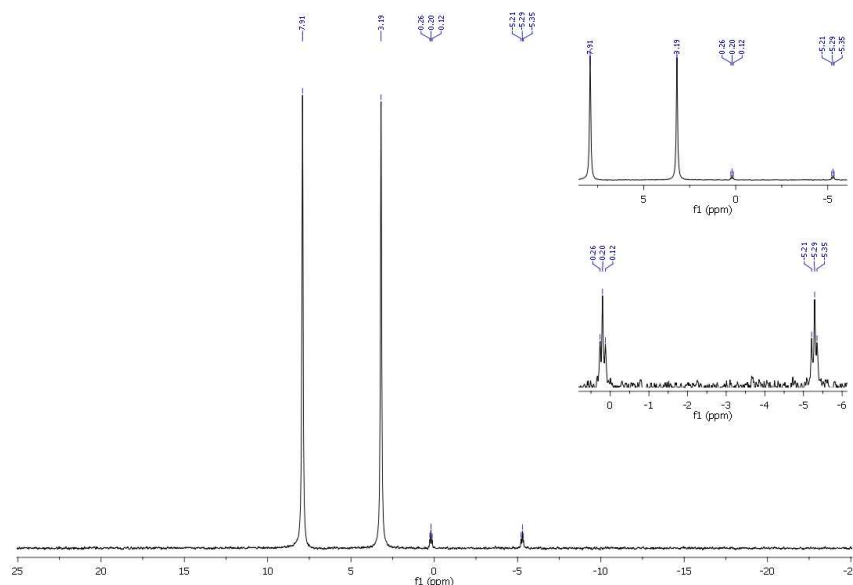
Spectrum 2.27: ^{31}P NMR spectrum (D$_2$O, 300 K, 121.49 MHz) of calcium phosphite/SMOW residues mixed with ferric chloride then dry heated on a sand bath at 90℃ under flowing N$_2$ for 72 hours. The spectrum shows the presence of phosphite (δ5.6, d, $^1J_{\text{P-H}}$= 573 Hz) and also pyrophosphite (δ-2.55, AA'XX', $^1J_{\text{P-H}}$= 667 Hz). Full NMR data are shown in Table 6.31.

of sodium phosphite to hypophosphite. Calcium phosphite (previously shown to produce pyrophosphite by dry heating at 90℃), dry heated in the presence of ferrous ions to 90℃, does not reduce to hypophosphite or produce pyrophosphite. It seems that ferrous iron inhibits any condensation reaction, even with the lower temperature requirements of calcium phosphite to undergo condensation to pyrophosphite. Further investigation of the products obtained by dry heating calcium phosphite between 90℃ and 150℃ was undertaken and the effects temperature has on the products between this range.

Calcium phosphite monohydrate $[Ca(H_2PO_3)_2 \cdot H_2O]$ (0.22 g, 1 mmol) was mixed with ferrous chloride tetrahydrate $[FeCl_2 \cdot 4 H_2O]$ (0.2 g, 1 mmol) in deionised water then reduced to dryness on a rotary evaporator. The residues were ground in a mortar and pestle then dry heated over an oil bath at 90℃ for 10 days. The sample was then dissolved in deionised water and treated via the hydroxide method and filtered to remove iron from the solution. The sample was treated with HCl (1 M) to adjust the pH back to around pH 7.5, then an aliquot of the sample was transferred to an NMR tube and a D_2O insert added and the sample submitted for ^{31}P NMR analysis. This process was repeated for temperatures 120℃ and 150℃ and again the samples submitted for ^{31}P NMR analysis.
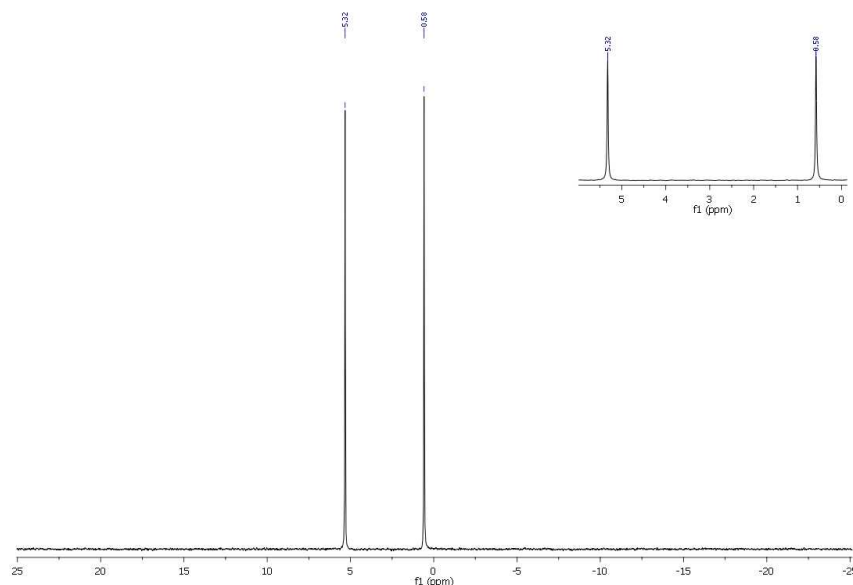
Spectrum 2.28: ^{31}P NMR spectrum (D_2O, 300 K, 202.46 MHz) of calcium phosphite mixed with ferrous chloride then dry heated on a sand bath to 90℃ under flowing N_2 for 72 hours. The spectrum shows the presence of phosphite ($\delta 3.0$, d, $^{1}J_{P-H} = 577$ Hz). Full NMR data are shown in Table 6.32.

The NMR analysis clearly shows (see Spectra 2.28, 2.29 and 2.30) that even up to 150℃ there was no condensation reaction to pyrophosphite in a 72 hour period and no visible reduction of phosphite to hypophosphite (though as before, above 160℃ there was reduction to hypophosphite). As it had previously been shown that calcium phosphite would undergo condensation at temperatures *ca.* 90℃, the only conclusion is that ferrous iron inhibits the condensation reaction but will, given enough energy input, reduce phosphate and phosphite to phosphite and hypophosphite respectively.

Having established the effects of ferrous iron it was decided to further investigate the low temperature effects of ferric iron on the formation of sodium pyrophosphite. It has been shown previously that addition of SMOW to sodium phosphite will reduce the temperature
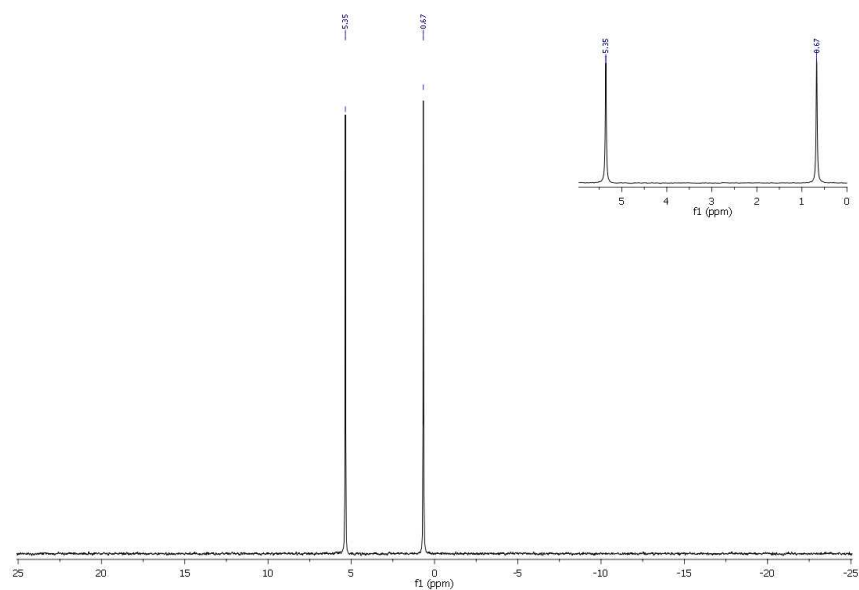
Spectrum 2.29: ^{31}P NMR spectrum (D$_2$O, 300 K, 121.49 MHz) of calcium phosphite mixed with ferrous chloride then dry heated on a sand bath at 120℃ under flowing N$_2$ for 72 hours. The spectrum only shows the presence of phosphite as a doublet of peaks at 3.0 ppm (d, $^1J_{\text{P-H}}=$ 578 Hz) which was the starting material. Full NMR data are shown in Table 6.32.
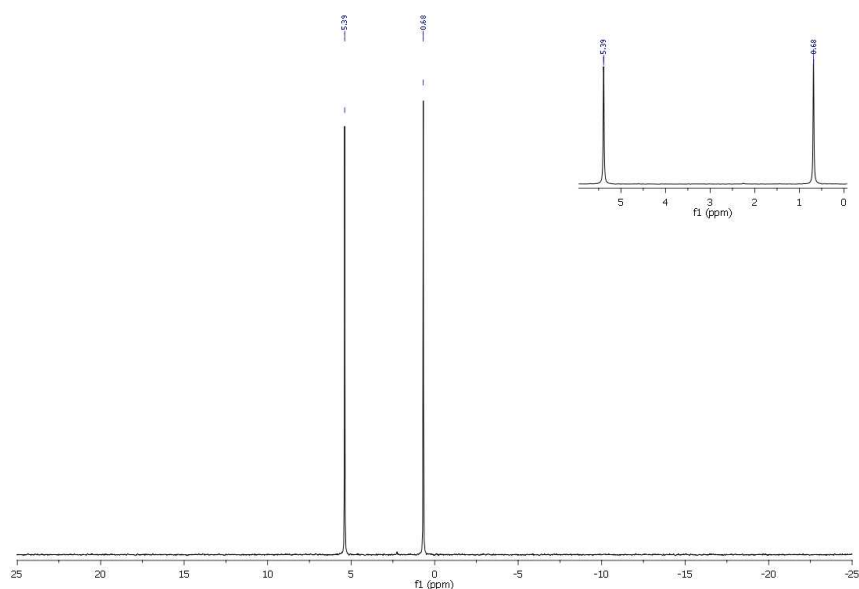
Spectrum 2.30: ^{31}P NMR spectrum (D$_2$O, 300 K, 121.49 MHz) of calcium phosphite mixed with ferrous chloride then dry heated on a sand bath at 150℃ under flowing N$_2$ for 72 hours. The spectrum shows the presence of phosphite (δ3.1, d, $^1J_{\text{P-H}}=$ 571 Hz). Full NMR data are shown in Table 6.32.

required for the condensation to pyrophosphite to occur. Hence, it was decided to see if SMOW in the presence of ferric ions would do the same and aid the formation process.

Two experiments were set up using sodium phosphite (0.104 g, 1 mmol) and ferric chloride hexahydrate (0.27 g, 1 mmol), one was mixed in deionised water and the other in SMOW. Both samples were reduced to dryness on a rotary evaporator and then ground using a mortar and pestle. The samples were both then dry heated on an oil bath at 90℃ under flowing N_2 for 72 hours. After heating, a portion of each sample (0.5 g) was dissolved in deionised water (2 mL) then treated using the hydroxide method to remove dissolved iron. The samples were adjusted using HCl to *ca.* pH 7.5 then submitted for ^{31}P NMR analysis using D_2O inserts for locking purposes.
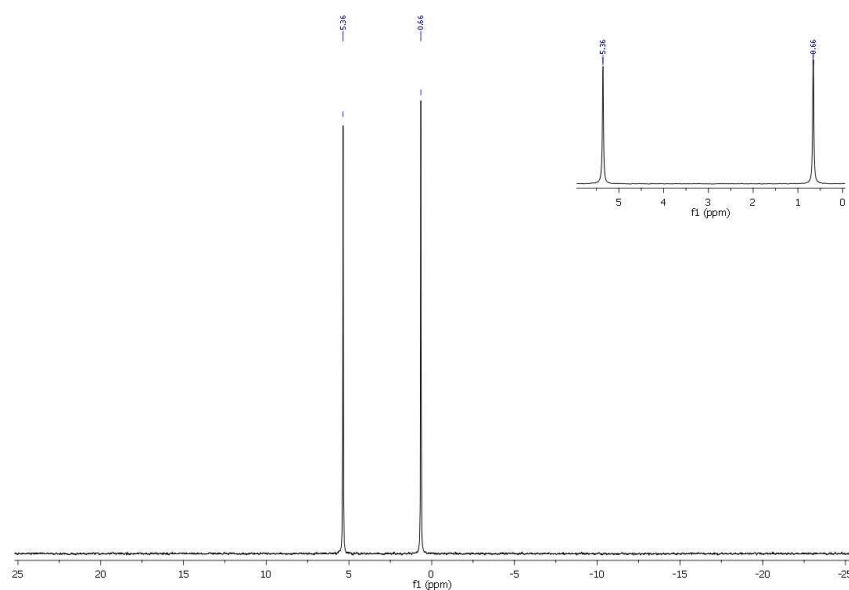
Spectrum 2.31: ^{31}P NMR spectrum (D_2O, 300 K, 121.49 MHz) of sodium phosphite mixed with ferric chloride dry heated on a sand bath to 90℃ under flowing N_2 for 72 hours. The spectrum shows the presence of phosphite ($\delta 3.0$, d, $^1J_{\text{P-H}}$= 571 Hz). Full NMR data are shown in Table 6.33.
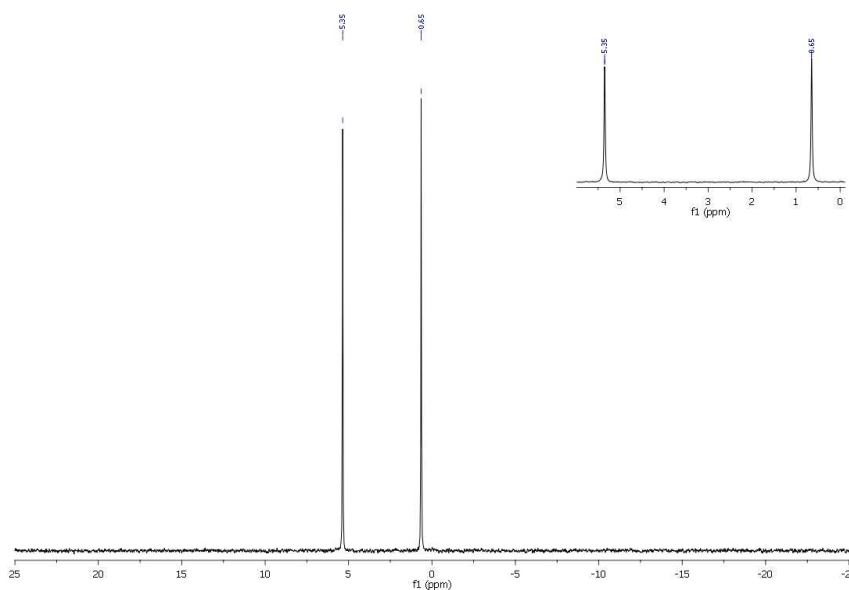
Spectrum 2.32: ^{31}P NMR spectrum (D_2O, 300 K, 121.49 MHz) of sodium phosphite mixed with ferric chloride in SMOW then dry heated on a sand bath to 90℃ under flowing N_2 for 72 hours. The spectrum shows the presence of phosphite ($\delta 3.0$, d, $^1J_{\text{P-H}}$= 571 Hz). Full NMR data are shown in Table 6.33.

The ^{31}P NMR analysis for both samples (Spectrum 2.31 and Spectrum 2.32) only showed the presence of phosphite ($\delta 3.0$, d). Consideration of these data shows that the presence of ferric iron has no beneficial effect on temperature reduction to facilitate the production of pyrophosphite, indicating that though there appears to be no inhibition of the formation of pyrophosphite in the presence of ferric iron, there also seems to be no aid to the formation as there is with magnesium or calcium. Further temperature studies of ferric iron were planned to fully confirm this finding but never completed due to time constraints imposed by other areas of research.

2.3.2 Detection and quantification of pyrophosphite

Up to this point the main methods of analysis used for the detection and quantification of pyrophosphite were ^{1}H and ^{31}P NMR analysis. The identification of pyrophosphite in an NMR spectrum is simple due to the AA'XX' spin system "doublet of triplets" as seen earlier in Spectrum 2.10, but, during later studies where iron was present, the issue of iron removal and the large amount of sample manipulation required meant this method of analysis was much more complex and much less reliable.

As iron is paramagnetic in character, the presence of iron in the sample interferes with this analytical technique and thus it must be fully removed before any NMR analysis can be completed. This posed a problem as the only reliable method for removal of iron involved adjusting to pH 12 then back to pH 7.5. This caused issues as the increase in pH would quickly hydrolyse trace amounts of pyrophosphite, while also diluting the sample further (making trace amounts even more dilute and the weakened signal is less identifiable from the background noise).

Previous work within the Kee group had also shown that the rate of hydrolysis of pyrophosphite depended on pH and the metal ions present. Pyrophosphite was shown to be most stable around pH 7.5 and the rate of hydrolysis would increase rapidly as the solution became more alkaline or more acidic from that median. Pyrophosphite will also hydrolyse more quickly in the presence of Ca^{2+} or Mg^{2+} ions[207] so NMR analysis is not able to give full quantitative data but only semi-quantitative. Knowing the number of moles of phosphite present at the start of the reaction meant that one could calculate the mole percent conversion of phosphite to pyrophosphite, but not get an accurate concentration of pyrophosphite formed. Both of these effects could lead to the assumption of a negative result from a particular experiment or affect the accuracy of the calculated conversion of a particular sample.

Due to these issues it was decided to look for alternative methods of detection for pyrophosphite which would allow for identification and quantification without the need for major sample manipulation. The initial objective was to find a method of analysis which would be suitable to identify pyrophosphite without need for sample manipulation but also, ideally, be able to detect and accurately quantify pyrophosphite in the presence of iron and other possible interferences. After investigation of the literature it was decided to pursue both Raman spectroscopy and fluorometry as potential methods of analysis and the merits and pitfalls of these methods are discussed in the remainder of this chapter.

2.3.2.1   Raman spectroscopy

Raman spectroscopy is a non-destructive technique which can be used to analyse both organic and inorganic samples. The technique works on the principle of light scattering, as the photons from an incident laser interact with individual bonds in a molecule depending on vibrational and rotational modes. Elastic collisions of photons with the molecule result in Rayleigh scattering (which is when the light scattered remains at the same frequency as the incident light) while inelastic collisions are a result of vibrational and rotational inter-actions resulting in a small frequency change between the incident light and the scattered light. The change in frequency of the light is directly proportional to the energy of the interaction with each vibrational or rotational bonding mode in the molecule, which gives a detailed molecular fingerprint of the molecule. Shifts in wavelength to lower frequencies than the incident radiation are known as Stokes lines, while shifts to higher frequencies are known as anti-Stokes lines. The Rayleigh scattered light frequency (equal to the frequency of the incident light) is used as an origin point with all shifts in frequency given relative to that point. The shifts in Raman spectroscopy are generally referred to in wavenumbers (cm^{-1}) from the point of origin (Rayleigh scattered light is 0 cm^{-1}) which are calculated by taking the reciprocal of the wavelength (ν).

As Raman spectroscopy is more sensitive to non-polar molecules than polar molecules it is non-sensitive to water and can be used with no sample preparation. Due to the reliance of photon interaction with bond vibration and rotation, each molecule's Raman signature will be unique, meaning it would be possible to even identify a component molecule from a mixture using this technique. Raman can also be used semi-quantitatively based on intensities of peaks in the Raman spectrum providing you have reasonable calibration data and this was why this technique was selected for further investigation.

Initially it was decided to obtain Raman spectra of pure samples of the phosphorus species of interest which could be encountered during experiments, and try to identify unique peaks in their fingerprints which could be used for easy identification. Samples were analysed using a Renishaw InVia spectrometer using a 785 nm wavelength diode laser and a charge coupled detector (CCD). The samples were analysed using the 20x objective lens and were exposed to 10 acquisitions with a 10 second spot time and 100% laser power. Samples of sodium phosphite monobasic, sodium phosphite dibasic, sodium pyrophosphite and sodium pyrophosphate tetrabasic were subjected to Raman analysis and were prepared by placing a small amount on a glass microscope slide. The sample was pressed flat using a second slide then placed in the spectrometer. The sample was then brought into focus and a wide spectrum scan was taken using Wire 3.0 acquisition software. A stacked plot of the Raman spectra obtained for the named samples is shown in Spectrum 2.33.

As can be seen from comparison of the individual spectra shown in Spectrum 2.33, the fingerprint for pyrophosphite is very different from both pyrophosphate and phosphite. It shows an intense double peak at between 1000–1050 cm^{-1} and another strong single peak at 1140 cm^{-1}. Pyrophosphate on the other hand only showed an intense single peak within this region (*ca.* 1030 cm^{-1}) as did the monobasic phosphite salt. The dibasic phosphite salt had a similar intense peak to the monobasic phosphite salt but was shifted to *ca.*

| | NaH$_2$PO$_3$ | | Na$_2$HPO$_3$ | | Na$_2$H$_2$P$_2$O$_5$ | | Na$_4$P$_2$O$_7$ |
Peak	Assignment	Peak	Assignment	Peak	Assignment	Peak	Assignment
955	P-OH sym str	973	P-OH sym str	1025	P-OH sym str	732	
1033	PO2 sym str	1026	PO2 sym str	1041	PO2 sym str	1029	PO2 sym str
1064	P-O sym str	1042	P-O sym str	1142	P-O-P sym str	1114	P-O-P sym str
1187		1096		1239			
2442	P-H sym str	2343	P-H sym str	2432			
		2395	P-H sym str	2452	P-H sym str		

20x objective lens, 10 acquisitions, 10 second exposure, 100% Laser power. Major peaks recorded (cm-1)

Table 2.4: Table of peak data for Raman spectra of phosphite (monobasic [NaH$_2$PO$_3$] and dibasic [Na$_2$HPO$_3$]), pyrophosphite [Na$_2$H$_2$P$_2$O$_5$] and pyrophosphate [Na$_4$P$_2$O$_7$] using a 785 nm wavelength diode laser (10 acquisitions, 10 second exposure time and 100% laser power) and charge coupled detector (CCD).
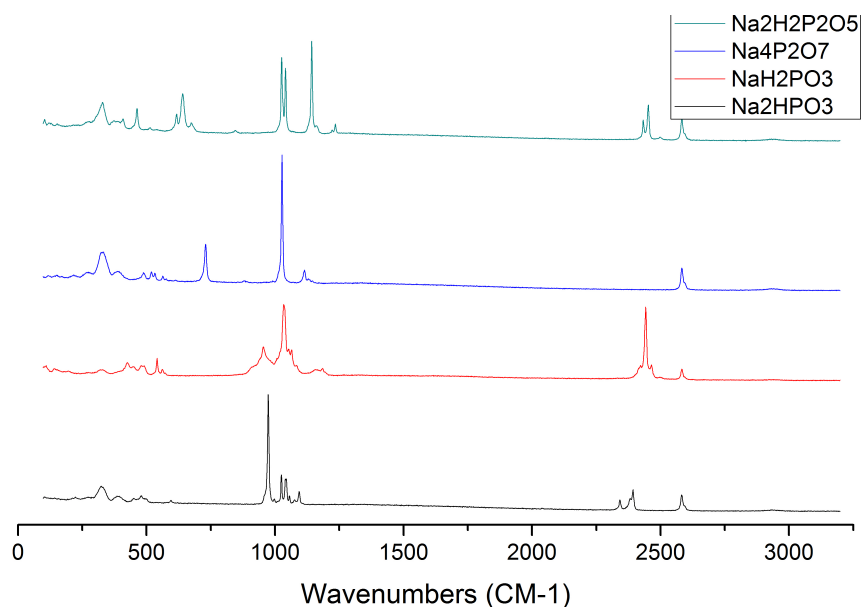
Spectrum 2.33: A stacked plot of Raman spectra obtained for phosphite (monobasic and dibasic), pyrophosphite and pyrophosphate using a 785 nm wavelength diode laser (10 acquisitions, 10 second exposure time and 100% laser power) and charge coupled detector (CCD). Data are tabulated and tentatively assigned in Table 2.4.

975 cm^{-1} showing that Raman was a sensitive enough technique to distinguish between two varieties of the same salt (monobasic and dibasic phosphites) and therefore an ideal technique for identification of pyrophosphite. It appears that there is a distinguishable effect on the signature for the P-O and P=O bonding fingerprint region (1150–950 cm^{-1} region) depending on the atoms directly bonded to the phosphorus which is a feature which warrants further investigation. It is also possible that there is some effect on the spectra from the oxidation state of the phosphorus, which again could be investigated. Unfortunately due to constraints on instrument time, it was not possible to complete this investigation here.

Having identified suitable peaks allowing for identification of phosphite, pyrophosphate and pyrophosphite it was decided to look at powder mixtures of phosphite and pyrophosphite to see if it was possible to identify phosphite and pyrophosphite as the components in a mixture. Sodium pyrophosphite (0.1 g, 0.5 mmol) and sodium phosphite (0.1 g, 1 mmol) were mixed in a mortar and pestle and ground until a fine powder was obtained. A small amount of powder was transferred to a clean microscope slide and pressed flat using another microscope slide. The slide was then transferred to the Raman spectrometer for analysis. One issue with this method became apparent as soon as the sample was brought into focus, it was possible to identify individual crystals in the sample and focus on them directly giving readings for pure compounds rather than the mixture that had been hoped for. It was decided to regrind a small portion of the sample and try again, but the same issue was encountered. With only pure compound spectra obtained from the mixtures due to the heterogeneity of the sample mixing it was decided to try more "life-like" samples by mixing phosphite and pyrophosphite in acidic SMOW, including iron, then dehydrating the samples and trying to identify them from the resultant Raman spectra.

Sodium pyrophosphite (0.2 g, 1 mmol) and sodium phosphite (0.1 g, 1 mmol) were dissolved

in SMOW (20 mL) and the pH adjusted to *ca.* 4 using HCl. Iron (II) chloride tetrahydrate (0.2 g, 1 mmol) was added and the resultant solution reduced to dryness by heating at 40°C under flowing N_2. Once the sample was dry, the residue was collected and ground in a mortar and pestle. A small portion of the sample was placed onto a glass microscope slide and pressed to give a flat surface. The sample was then placed into the Raman spectrometer for analysis. The scan was taken using a 5x objective lens with the sample exposed to 10 acquisitions at 50% laser power with an exposure time of 10 seconds to produce the top spectrum of the group of spectra shown in Spectrum 2.34.

Spectrum 2.34: A composite image of Raman spectra for comparison of an iron, phosphite, pyrophosphite and SMOW mix against the Raman spectra of the individual components of the mixture to try to ascertain if Raman is a suitable technique for experimental analysis. The spectrum of the iron mix was taken using a 785 nm wavelength diode laser (10 acquisitions, 10 second exposure time and 50% laser power) and was compared to the stacked plot of Raman spectra obtained for sodium phosphite monobasic, sodium pyrophosphite and sodium pyrophosphate using a 785 nm wavelength diode laser (10 acquisitions, 10 second exposure time and 100% laser power) and charge coupled detector (CCD).

The spectrum for the iron mix sample is very noisy, which is thought to be due to some irregular laser scattering caused by the iron/irregular sample surface. There clearly appears to be correlation between the iron mix spectrum and the spectrum for sodium phosphite with apparent peak matches at around 950, 1033 and 2450 cm^{-1} but there appear to be no peaks present to confirm the presence of pyrophosphite. It was later concluded that the presence of pyrophosphite would be very weak or non-existent as the slow evaporation in acidic SMOW would accelerate the rate of hydrolysis of pyrophosphite.

Much thought was put into how to resolve problems to proceed with this method but in the end it was decided there were too many complications, to use this method for analysis. With the spectrometer being situated in another institution, it meant having limited access time plus it again would only give semi-quantitative data which we could get using the NMR analysis method on site. It was decided to look at another method which would

allow for full quantitative analysis while using NMR as the main method for identification.

2.3.2.2 Fluorometry

Careful examination of the literature for a method of quantitative analysis for pyrophosphite proved fruitless as very little investigation into pyrophosphite has been undertaken. There is however a very active community working on the quantitative analysis of pyrophosphate so it was thought logical to find a suitable method which may be adapted to quantify pyrophosphite instead of pyrophosphate. The method chosen was published by Fabbrizzi *et al.* (2002) who used a fluorescence assay in water for the quantification of pyrophosphate.[208] The fluorescence method chosen firstly required the preparation of a macrocyclic compound, 3,6,9,16,19,22-hexa-aza-tri-cyclo-[22.2.2.2(11,14)]-triaconta-1(26),11,13,24,27,29-hexaene bi-copper(II) complex ($[(C_{24}H_{38}N_6)_2Cu^{2+}]$, herein referred to as **Compound 3**, see Figure 2.6). This was originally reported by Chen and Martell (1991) and, in conjunction with cobalt, showed promise as an oxygen absorbing molecule.[209]
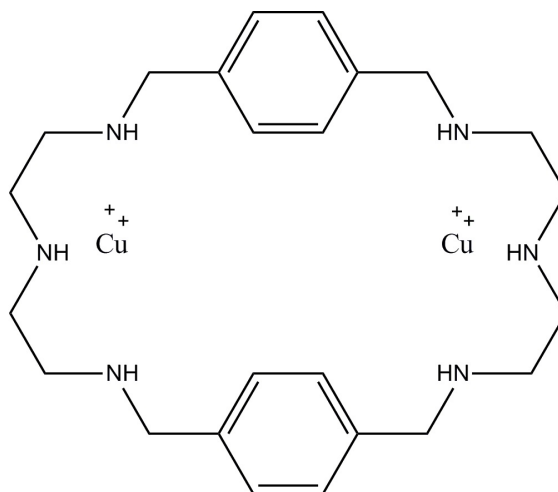
Figure 2.6: Chemdraw image of the copper macrocycle (herein referred to as **Compound 3** used in the fluorescence assay of pyrophosphate. It was hoped that this system could be utilised for the quantification of pyrophosphite too due to the similar molecular structure to pyrophosphate.

Nation *et al.* (1996) looked at copper (II) complexes of the same macrocyclic ligand and their binding energies and selectivity for phosphate, pyrophosphate and tripolyphosphate ions.[210] They reported that the macrocycle preferentially bound to pyrophosphate over phosphate and also a selectivity between pyrophosphate and tripolyphosphate between pH $4-9.3$ which was speculated to be due to the electrostatic affinity for the larger negative charges presented within the pyrophosphate and tripolyphosphate ions under these conditions.[210] Fabbrizzi *et al.* further developed this idea by using the preference of the macrocycle for pyrophosphate to displace a fluorescent indicator (see Figure 2.7 for schematic of chemosensing ensemble taken from Fabbrizzi *et al.* (2002) supplementary information) which could then be used to quantify the concentration of pyrophosphate in solution.[208] The chemosensing ensemble (Compound 3 and fluorescent indicator) sensitivity could be altered by changing the fluorescent indicator to suit the approximate concentration with minimal adjustment to the technique and was able to cover a range of pyrophosphate concentration between 1×10^{-4} and 1×10^{-6} M concentration.[208]
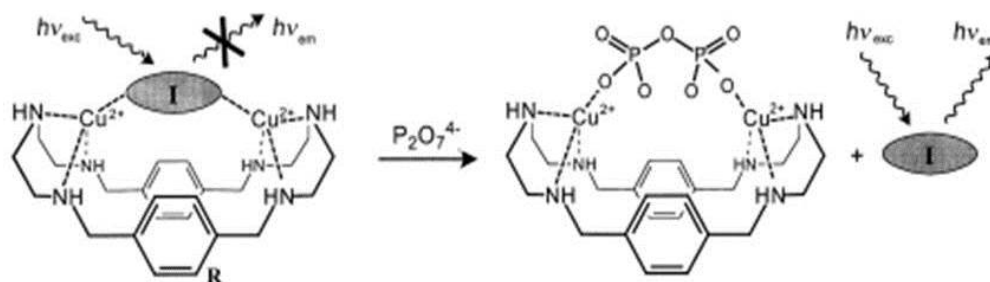
Figure 2.7: Schematic drawing showing the reaction of the chemosensing ensemble reported by Fabbrizzi *et al.* (2002) with pyrophosphate. It can be seen that Compound 3 selectively bonds with the pyrophosphate, displacing the fluorescent indicator thus increasing the fluorescence response of the solution. The stronger the fluorescent response, the greater the concentration of pyrophosphate in solution. Image from supplementary information for Fabbrizzi *et al.* (2002).[208]

The initial step in the preparation of **Compound 3** was to prepare the unsaturated schiff base of the macrocycle 3,6,9,16,19,22-hexa-aza-tri-cyclo-[22.2.2.2(11,14)]-triaconta-1(26),2,8,11,13,15,22,24,27,29-decaene ($[C_{24}H_{30}N_6]$, herein referred to **Compound 1**, see Figure 2.8). This was prepared by slow dropwise addition (over 30 minutes) of teraphtha-laldehyde $[C_6H_4(CHO)_2]$ (0.134 g, 1 mmol) dissolved in acetonitrile (20 mL) to a solution of diethylenetriamine $[NH(CH_2CH_2NH_2)_2]$ (0.103 g, 1 mmol) in acetonitrile (35 mL) which was continuously stirred using a magnetic stirrer. After the two solutions were mixed, the resulting solution was stirred for 24 hours and formed a bright yellow precipitate which was collected by vacuum filtration and washed with chilled acetonitrile to remove any un-reacted materials. Confirmation of the product was obtained by ^{1}H and ^{13}C NMR, mass spectrometry and micro analysis. All analytical data are shown in Table 2.5.
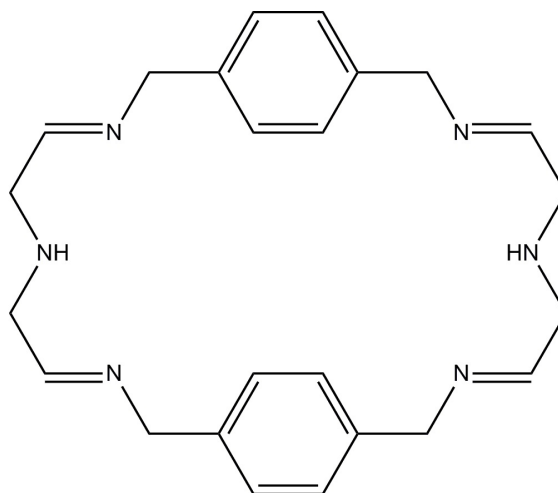
Figure 2.8: Chemdraw image of **Compound 1** which is a precursor of the copper macrocyclic ligand.

An issue was encountered when it came to purification of **Compound 1**. The microanalysis showed the % composition of the sample was not at all close to the expected figures, indicating that there was a level of impurity in the sample. In the literature preparation it stated to recrystallise the yellow solid obtained from dry ethanol[209] but when this was attempted the yellow solid did not dissolve but formed a lump of undissolvable yellow tar in the bottom of the conical flask. As the NMR was clean and the mass spectrometry data were indicative of the product required it was decided to proceed with the next step without any further purification.

NMR:

	^{1}H (CD$_3$OD, 300 K, 500.13 MHz)	^{13}C {^{1}H} (CD$_3$OD, 300 K, 125.72 MHz)
C$_{24}$H$_{30}$N$_6$ - **Compound 1**	3.0 (m, 8H, NH-CH$_2$), 3.8 (m, 8H, =N-CH$_2$), 7.6 (s, 8H, benzene), 8.4 (s, 4H, -CH=N)	48.9 (s, CH$_2$-NH), 60.0 (s, CH$_2$-N=), 129.5 (s, -CH=, benzene), 139.4 (s, -C=, benzene), 164.4 (s, CH=N)

Mass spectrometry:

	Expected	Obtained
ESI$^+$ ([C$_{24}$H$_{30}$N$_6$+H]$^+$)	402.5 ([M+H]$^+$)	403.2 ([M+H]$^+$)

Microanalysis:

	Expected	Obtained
C	71.61	65.00
H	7.50	7.20
N	20.88	14.55

Table 2.5: Table of analytical data for **Compound 1** showing results for the ^{1}H and ^{13}C {^{1}H} NMR analysis, mass spectrometry and microanalysis results. Solvent peaks are at δ4.8 (D$_2$O, H$_2$O and HOD present in D-methanol) and δ3.3 (CD$_3$OD and C(H)D$_2$OD). In ^{13}C NMR, the solvent peak was identified at δ48 for CD$_3$OD (also C(H)D$_2$OD).

Spectrum 2.35: ^{1}H NMR spectrum of **Compound 1**. Full NMR details shown in Table 2.5. Solvent peaks are at δ4.8 (D$_2$O, H$_2$O and HOD present in D-methanol) and δ3.3 (CD$_3$OD and C(H)D$_2$OD).

Spectrum 2.36: ^{13}C {^{1}H} NMR spectrum of **Compound 1**. Full NMR details shown in Table 2.5. The peak at δ48 was identified as for the solvent CD$_3$OD (also C(H)D$_2$OD).

Reduction of **Compound 1** was the next step in the preparation of **Compound 3**. A portion of **Compound 1** (0.1 g, 0.25 mmol) was dissolved in dry methanol and heated to 45°C in the presence of excess sodium borohydride ([NaBH$_4$], 0.25 g, 6.6 mmol) with stirring for 1 hour then allowed to cool to room temperature. When cooled the sample was reduced to dryness on a rotary evaporator and the white solid obtained treated with deionised water (1 mL) and dichloromethane (10 mL). The sample was shaken until all the solid had dissolved then the organic layer [CH$_2$Cl$_2$] was collected using a separating funnel. This was then reduced to dryness on a rotary evaporator. A white solid was obtained of the reduced macrocycle 3,6,9,16,19,22-hexaazatricyclo[22.2.2.2(11,14)]triaconta-1(26),11,13,24,27,29-hexaene ([C$_{24}$H$_{38}$N$_6$], herein referred to as **Compound 2**, see Figure 2.9). Confirmation of the product was obtained by ^{1}H and ^{13}C NMR, mass spectrometry and micro analysis. All analytical data is shown in Table 2.6.
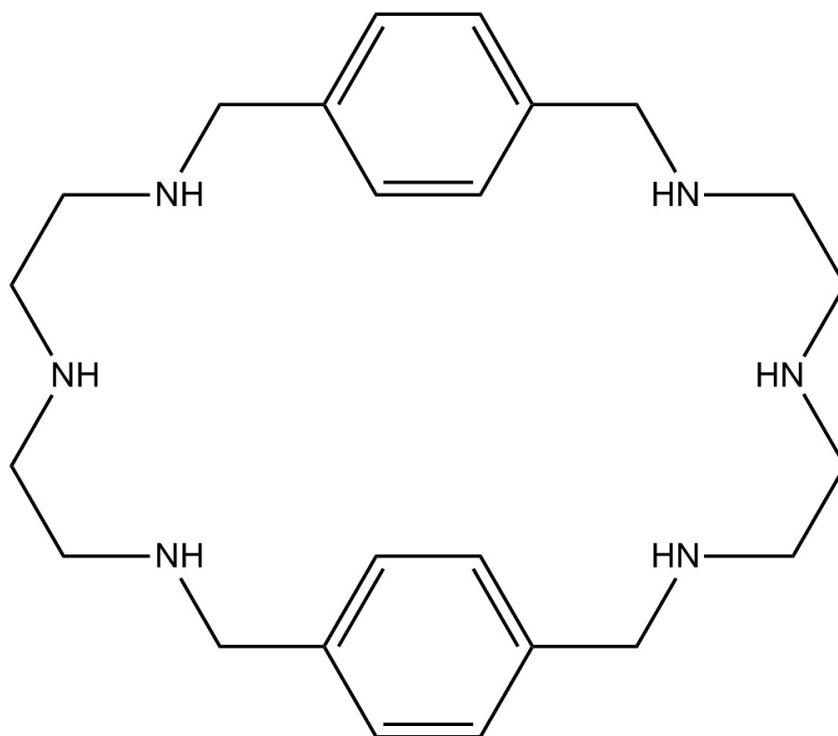
Figure 2.9: Chemdraw image of **Compound 2** which is a precursor of the copper macrocyclic ligand.

Again the issue of purification was a problem. Purification of **Compound 2** by Chen *et al.* (1991)included reacting the macrocycle with excess conc. hydrobromic acid [HBr] to make the the hydrogen bromide salt. When this was attempted, purification appeared to be successful but when it came to conversion back to **Compound 2** using a base, it appeared to completely destroy the structure. Removal of the HBr was attempted by neutralisation first with NaOH (strong base) and then NaHCO$_3$ (weak base) but both seemed to have the same effect. Due to this issue, it was decided to proceed with the crude product through to **Compound 3**, as this seemed relatively pure based on the NMR spectra, rather than keep attempting to purify *via* this method.

The addition of copper to **Compound 2** was undertaken by dissolving copper nitrate trihydrate [Cu(NO$_3$)$_2 \cdot 3$ H$_2$O] (0.76 g, 3.15 mmol) in methanol, adding this to **Compound 2** dissolved in methanol, then refluxing for 30 minutes before allowing to cool. During cooling, deep blue crystals were precipitated and these were collected by vacuum filtration.

NMR:	^{1}H (CD$_3$OD, 300 K, 500.13 MHz)	^{13}C {^{1}H} (CD$_3$OD, 300 K, 125.72 MHz)
C$_{24}$H$_{38}$N$_6$ - Compound 2	2.7 (m, 8H, NH-CH$_2$),3.4 (m, 8H, NH-CH$_2$), 3.8 (m, 8H, benzene-CH$_2$), 7.3 (s, 8H, benzene)	48.6 (s, CH$_2$-NH), 54.2(s, CH$_2$-benzene), 129.7 (s, -CH=, benzene), 139.8 (s, -C=, benzene)

Mass spectrometry:	Expected	Obtained
ESI$^+$ ([C$_{24}$H$_{30}$N$_6$+H]$^+$)	411.6 ([M+H]$^+$)	411.3 ([M+H]$^+$) and 425.4 ([M+BH$_3$]$^+$)

Microanalysis:	Expected	Obtained
C	70.20	67.91
H	9.33	9.74
N	20.47	19.80

Table 2.6: Table of analytical data for **Compound 2** showing results for the ^{1}H and ^{13}C {^{1}H} NMR analysis, mass spectrometry and microanalysis results. Solvent peaks in ^{1}H NMR are at δ4.8 (D$_2$O, H$_2$O and HOD present in D-methanol) and δ3.3 (CD$_3$OD and C(H)D$_2$OD). In ^{13}C NMR, the solvent peak was identified at δ48 for CD$_3$OD (also C(H)D$_2$OD).

Spectrum 2.37: ^{1}H NMR spectrum of **Compound 2**. Full NMR details shown in Table 2.6. Solvent peaks are at $\delta 4.8$ (D$_2$O, H$_2$O and HOD present in D-methanol) and $\delta 3.3$ (CD$_3$OD and C(H)D$_2$OD).
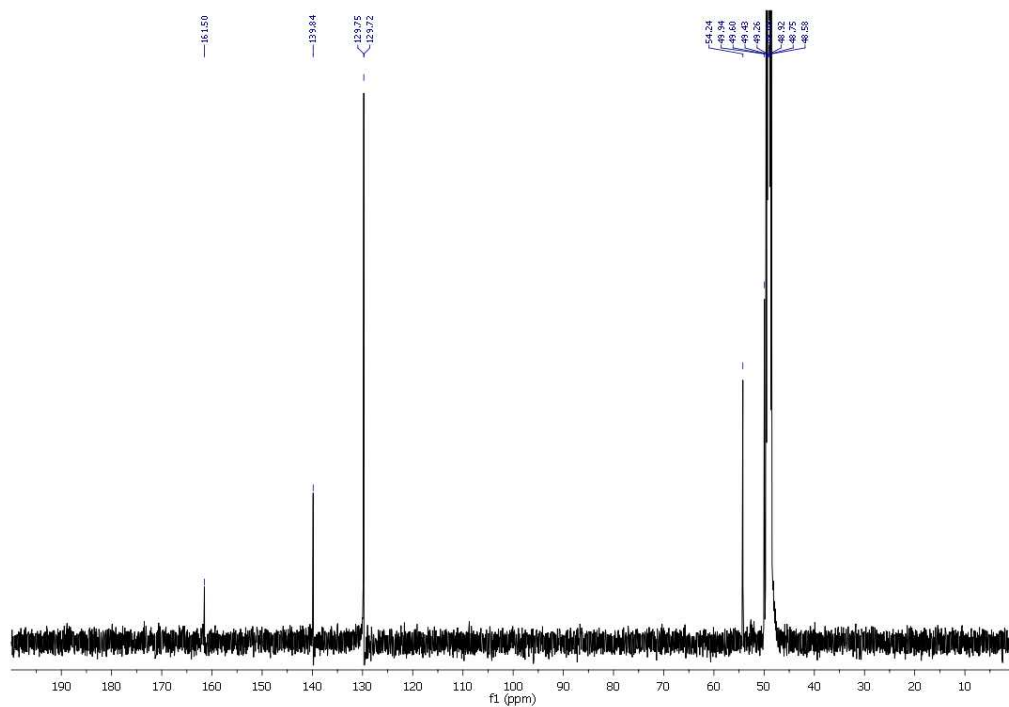
Spectrum 2.38: ^{13}C {^{1}H} NMR spectrum of **Compound 2**. Full NMR details shown in Table 2.6. The peak at $\delta 48$ was identified as for the solvent CD$_3$OD (also C(H)D$_2$OD).

^{1}H and ^{13}C NMR were attempted on the sample but due to the paramagnetic properties of copper (Cu^{2+}, d-9) within the macrocycle it was not possible to collect NMR spectra. Mass spectrometry (ESI+) of the sample showed a [M]++ peak at 192.1 which again was different from the 268.8 expected. The elemental microanalysis was also inconclusive with the expected percentage composition being significantly different to the observed results (see Table 2.7 for results). Several attempts were made and several days were spent trying to figure out the issue with the data but with no success. To prevent any further wasted time it was decided to try using the obtained product "as was", to attempt the fluorescence experiment and see if results were comparable to the findings of Fabbrizzi *et al.* for pyrophosphate and phosphate.

Mass spectrometry:	Expected	Obtained
ESI$^+$ ([(C$_{24}$H$_{38}$N$_6$Cu$_2$)$^{4+}$+H]$^+$)	538.7 ([M+H]$^+$)	192.1 ([M+H]$^+$)
Microanalysis:	Expected	Obtained
C	36.69	35.55
H	4.87	5.20
N	17.68	16.30

Table 2.7: Table of analytical data for the copper macrocycle showing results for the mass spectrometry analysis and elemental microanalysis.

Preparation of the fluorescent indicator solution was completed by dissolving fluorescein [C$_{20}$H$_{12}$O$_5$] (33.23 mg, 10 μmol) in deionised water in a 250 mL volumetric flask. A 25 mL portion of this solution was transferred to a 250 mL volumetric flask creating a 4×10^{-6} M fluorescein solution. The copper macrocycle [C$_{24}$H$_{38}$N$_6$Cu$_2$(NO$_3$)$_4$] (50.28 mg, 64 μmol) was also dissolved in deionised water in a 250 mL volumetric flask. The two solutions were then combined in a 1000 mL volumetric flask and buffered to pH 7 with addition of 0.05 M HEPES solution (4-(2-hydroxyethyl)-1-piperazineethanesulfonic acid, [C$_8$H$_{18}$N$_2$O$_4$S]).

Bulk solutions of orthophosphate (0.1 mM) and pyrophosphate (0.1 mM) were then prepared in volumetric flasks with deionised water. Further dilutions were made to the 1 mM solutions to make solutions of between 1×10^{-6} and 5×10^{-5} M for fluorescence analysis to produce a calibration graph. A 2.5 mL aliquot of the fluorescent indicator was pipetted into a quartz cuvette and 1.5 mL of a standard was added. The cuvette was shaken for 10 seconds to allow mixing and then a reading taken. The fluorescence was recorded in triplicate and an average taken (see Table 6.38). After all 8 samples for each anion were completed the data were plotted in a graph for analysis (see Figure 2.10).

Looking at the graphical data of the recorded fluorescence it can be seen there was an issue. There is wild fluctuation in the sample readings which was not seen in the Fabbrizzi *et al.* data. After consideration of the preparation method and the apparent random variation in the readings, it was concluded that the addition of large amounts of phosphate and pyrophosphate (1.5 mL of sample to 2.5 mL of fluorescent indicator) to the cuvette was causing too great a fluorescent response which saturated the detector taking the spectrometer outwith its linear range. To combat this it was decided to remake the bulk solutions in the fluorescent indicator solution as the solvent and add much smaller amounts of sample per reading thus maintaining the concentrations within the linear range
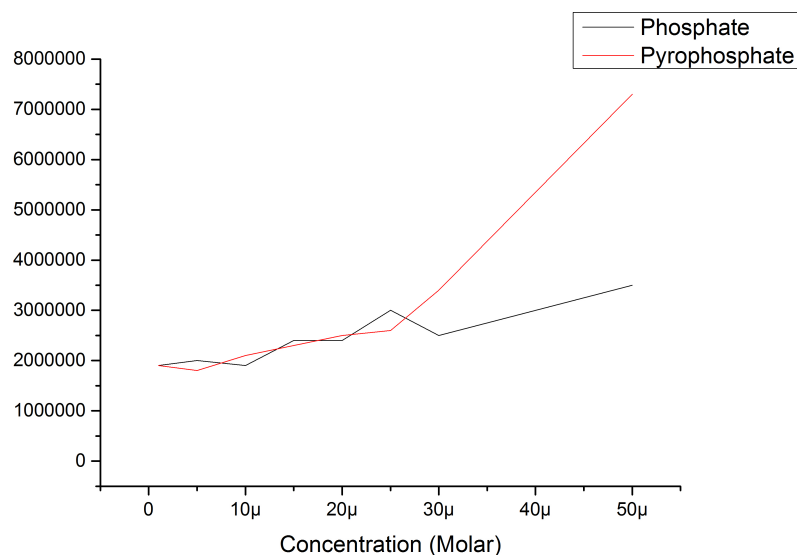
Figure 2.10: Plot of fluorescence date from Table 6.38 showing response for pyrophosphate and phosphate. It is noticed there is an anomaly in the data which is due to the readings being outwith the linear range of the spectrometer. This is thought due to the concentration of phosphate and pyrophosphate added to the cuvette for analysis.

of the spectrometer.

Analysis was conducted by addition of 25 μL of each of the 0.1 mM bulk solutions to 2.5 mL of the fluorescent indicator in the cuvette and the fluorescence recorded. After the reading for each concentration was taken in triplicate, a further 25 μL was added and the process repeated. This was continued until the 4 mL cuvette volume was reached. Once all the data were recorded, a graph of the fluorescence data was produced for analysis.
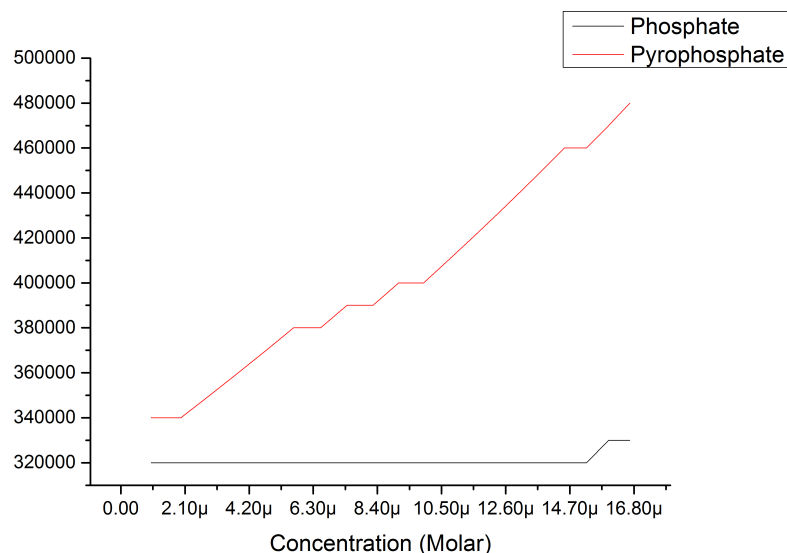
Figure 2.11: Plot of fluorescence date from Table 6.39 showing response for pyrophosphate and phosphate. The graph shows clear distinction in fluorescence response between pyrophosphate and phosphate as in the Fabbrizzi *et al.* paper.[208]

As it was possible to recreate the fluorescence response results for phosphate and pyrophosphate it was then decided to proceed with this method for the comparison of pyrophosphite with phosphite. One issue as mentioned previously is pyrophosphite hydrolysis. Testing

of the stability of pyrophosphite in the chemosensor solution was carried out by initially hourly and then daily[31]P NMR analysis with integration of the peaks for phosphite and pyrophosphite to give percentage conversion. This analysis showed that pyrophosphite was very stable in the chemosensor solution and took over 90 days to undergo 50% hydrolysis. It appeared that the HEPES buffer was stabilising the pyrophosphite against hydrolysis by keeping the pH stable at around pH 7 which kept the rate of hydrolysis slow and constant.

After testing the stability of pyrophosphite the next step was to prepare the analysis. The previous test for phosphate and pyrophosphate took almost 8 hours to complete so working on this timescale it would take 2 days to complete the analysis. To make the results comparable, each solution would need to be made up fresh and run individually so that no solution was sat around awaiting analysis which could affect the fluorescence results. After consideration of the amount of time required to complete this assay, it was decided to look for an alternative method to complete this analysis. During discussion of the options it was suggested to use a Hamilton Star automated liquid handling workstation to complete the analysis as this could be programmed to pipette small volumes for multiple samples and with the inclusion of a plate reader, was able to analyse multiple samples simultaneously. A discussion was held with Dr. Christopher Empson, the robot operator, to discuss the logistics of the analysis confirmed the robot was a suitable method. Dr. Empson wrote a programme to carry out the fluorescence analysis based on the discussion held previously.

Each anion sample was allocated an individual 96 well plate and 1 μL additions of the 0.1 mM stock solutions for each anion were made to each well, topping up to 80 μL with chemosensor solution. After the robot had completed pipetting each sample plate it was sonicated for 2 minutes to remove any bubbles before taking readings for all 80 data points simultaneously on a plate reader reading fluorescent emission at 513 nm. The benefit of using the robot was the high accuracy, high volume throughput that the system allowed meaning all the sample analysis was completed in less than 2 hours. The range of concentrations covered and the number of data points was much greater than the range covered by Fabbrizzi *et al.* and was designed to give maximum coverage to natural expected concentrations.

Comparison of the results for phosphate and pyrophosphate (Figure 2.12) showed the fluorescence difference was only noticeable above *ca.* 10 μM concentration and above this concentration the fluorescence was linear for the range tested. There was a significantly stronger fluorescence response for pyrophosphate than for phosphate. Comparison of the results for phosphite and pyrophosphite showed that even as low as 0.4 μM concentration there was a noticeable fluorescence difference between phosphite and pyrophosphite though the fluorescence response for pyrophosphite was only linear up to a concentration of *ca.* 29 μM concentration. There was some noticeable variation in the data which did not allow for a smooth line to be drawn and this was believed to be caused by microbubbles in the sample wells which were not removed by sonication. To address this issue in the future it was decided to dispense the fluids into the wells more slowly and to sonicate for longer to make sure all bubbles were fully removed.

Further investigation was planned for this system using different fluorescent indicators and a larger range of concentrations to establish accurately the fluorescence response and try to
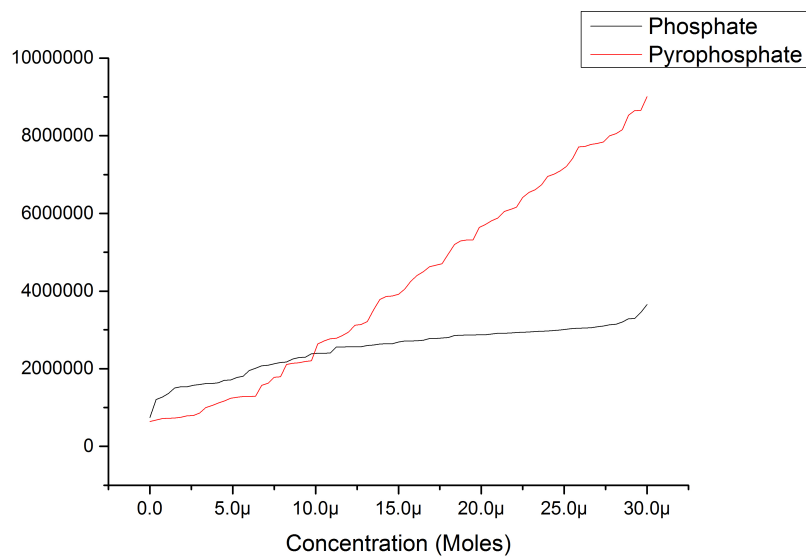
Figure 2.12: Plot of fluorescence date collected by the Hamilton robot comparing pyrophosphate and phosphate. The graph shows a clear distinction in fluorescence response between pyrophosphate and phosphate for concentrations above 15 μmolar.
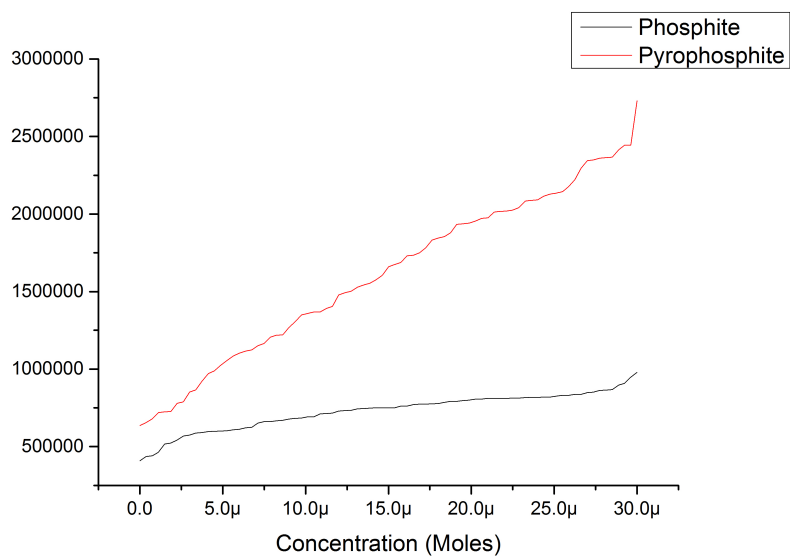
Figure 2.13: Plot of fluorescence date collected by the Hamilton robot comparing fluorescence response for pyrophosphite and phosphite. The graph shows a clear distinction in fluorescence response between pyrophosphite and phosphite.

fine tune to get the biggest difference for a known concentration of sample. Unfortunately however, due to time constraints, it was not possible to continue this investigation though it seems to warrant more extensive study to fully confirm the findings and optimise the process.

2.4   Conclusions

It was shown that the production of reduced oxidation state phosphorus species is possible from acidic hydrothermal corrosion of phosphorus containing minerals such as schreibersite in relatively large quantities in a short period of time. The products of corrosion identified during this research were phosphine gas, a highly reduced (P^{3-} oxidation state) and highly reactive form of phosphorus and phosphite which is a reduced, reactive and water soluble phosphorus acid. Phosphine gas (*ca.* 0.1% available P) released during corrosion into the atmosphere would readily react with a large number of airborne molecules photochemically, especially water, to form reduced, water soluble phosphorus oxy-acids (hypophosphite and phosphite) which can then be included in origin of life reactions. The predominant species produced by acidic hydrothermal corrosion of iron phosphide was phosphite (shown to be *ca.* 10% available P in a 72 hour period). Phosphite is highly soluble in water, and reactive, making it a suitable solution to the "phosphate problem" mentioned in Chapter 1 which makes the inclusion of phosphorus in reactions much easier in the concentrations required by life today.

This research has confirmed that metal phosphite salts are able to undergo condensation reactions to form pyrophosphite by dry heating providing they are acidic salts (monobasic salts) or are in an acidic medium (between pH 3 and pH 6) prior to dehydration. Use of divalent metal ions such as calcium or magnesium significantly reduces the amount of energy required for the condensation reaction to occur (from *ca.* 160℃ to less than 90℃). During these experiments it was proved that, under plausible geological conditions on Earth, pyrophosphite could be formed from corrosion of iron phosphide by evaporative deposition and dry heating of phosphite.

An investigation into the formation of pyrophosphite in the presence of iron gave surprising results. It was shown that in the presence of ferrous iron it was possible to reduce phosphite [P^{3+}] to hypophosphite [P^{1+}] by dry heating at 160℃. This result was very interesting and suggested that, under plausible geological conditions, phosphite could be further reduced to a more soluble and more reactive form. After confirming it was possible to reduce phosphite under plausible geological conditions it was decided to investigate the same effect on phosphate. Again it proved possible to reduce phosphate to phosphite at 160 ℃ in the presence of ferrous iron, which is highly significant as a potential source of reduced phosphorus and could be an explanation for the observation of trace amounts of phosphite in waters of Hot Creek gorge by Pech *et al.* (2009). One other noticeable effect that ferrous iron has on the reactions of phosphite is to inhibit the formation of pyrophosphite. Heating calcium phosphite in the presence of ferrous iron to temperatures greater than 150℃ showed no reaction but, above 160℃, there were signs of phosphite reduction to hypophosphite.

Investigation of the effects of ferric iron on the formation of pyrophosphite showed this had no beneficial or adverse effects on the production. Comparison of a pure calcium phosphite sample and a sample containing ferric iron showed comparable conversion to pyrophosphite at 90℃ showing that, providing you could oxidise the ferrous iron or remove it completely from solution, it would be possible to form pyrophosphite directly from acidic hydrothermal corrosion of iron phosphide minerals.

The majority of analysis carried out during this research involved ^{1}H and ^{31}P NMR spectrometry for identification and quantification of samples. The issue with NMR analysis of samples was apparent when iron was involved as full iron removal was required before NMR analysis could be undertaken (since iron is magnetic and interferes with NMR causing peak broadening or in severe cases, complete magnetic interference resulting in no signal).

Iron removal required large amounts of sample manipulation due to pH adjustment and filtering which not only may have diluted samples but also destroyed them completely. Investigation into alternative analytical methods for identification and quantification of pyrophosphite was undertaken as the issues of sample manipulation and iron removal prior to analysis were a major issue to overcome.

Raman studies showed it was possible to identify individual components from their Raman signatures but when mixing samples for testing, heterogeneity of the sample became an issue. Analysis after mixing with water showed some improvement on this but may also have destroyed the compound we wished to observe. Raman spectrometry was perfectly suited to provide non-destructive analysis with no sample manipulation required, but, with other issues like instrument access and again only semi-quantitative analysis provided, it was decided to look for another alternative.

Fluorometry seemed a good choice for quantification and was shown to be able to provide a visible indicator to the presence of pyrophosphite in solution, although since the assay also produced moderate fluorescence from phosphate and strong fluorescence from pyrophosphate it would not work as an identification tool but only for quantification after identification by another method.

Chapter 3

Kverkfjöll Expedition – June 2011

3.1 Introduction

The aim of this chapter is to report and document the observations made, the conditions encountered and the chemistry undertaken during fieldwork in the Kverkfjöll region of the Vatnajökull glacier, Iceland. The fieldwork was undertaken in conjunction with a research group from UCL/Birbeck College between the 8th and 21st June 2011. The UCL/Birbeck group consisted of Dr. Claire Cousins, the lead researcher and organiser of the expedition; Prof. Ian Crawford, Postdoctoral supervisor of Dr. Cousins and Laura Carmody, a PhD student from UCL operating as field assistant. The Leeds group consisted of Dr. Terence Kee and Barry Herschy. The final member of the group was Magnus Þor Karlsson who was employed as our driver/guide for the expedition. A photograph of the team (Figure 3.1) was taken by Dr. Cousins on the day of departure for the Vatnajökull glacier.

Figure 3.1: Photograph of the expedition team taken by Dr. Claire Cousins in Reykjavik on the day of departure to the Vatnajökull glacier. From left to right: Barry Herschy, Magnus Þor Karlsson, Prof. Ian Crawford, Laura Carmody. Front: Dr Terence Kee. Credit Dr. Claire Cousins

The expedition to Iceland was undertaken to investigate natural volcanic geothermal/hydrothermal

systems, to establish the kind of conditions which may have been present on an early Earth and to investigate the use of natural hydrothermal fluids and geothermal conditions encountered within these systems to perform a variety of experiments, based around elements of prebiotic phosphorus chemistry currently under research within the Kee group.

A recent publication by Mulkidjanian *et al.* identified anoxic geothermal pool systems rather than hydrothermal marine vents as being potentially ideal candidates for breeding grounds of the first cells, due to the ability to concentrate essential ions via vapour deposition.[68] Terrestrial geothermal springs have been shown to contain high concentrations of phosphorus compounds compared to marine hydrothermal systems with 60 to 70 μM measured in Yellowstone springs[211] and concentrations in the region of 1 mM in acidic mud pools in Kamchatka.[212] Pech *et al.* identified similar levels of phosphate but also micromolar concentrations of phosphite, a reduced oxidation state phosphorus species, in pristine geothermal pools in Hot Creek gorge near Mammoth Lakes, California using high performance liquid chromatography.[33] The identification of phosphite in the Hot Creek gorge samples was surprising as it was thought that all phosphorus currently on Earth was locked in the P^{5+} oxidation state, while phosphite is a P^{3+} oxidation state. Consideration of this work led to the undertaking of this project in the hydrothermal and geothermal features of Iceland as it was deemed to be an analogous place to undertake potential prebiotic chemistry.

3.2 Background to the Region

Iceland is an island in the North Atlantic Ocean which is 550 miles North-West of Scotland on the southern edge of the Arctic Circle. It sits on top of the Mid-Atlantic ridge, the divergence point of the North American and Eurasian tectonic plates. Though Iceland is technically nearer to North America, due to its proximity to Greenland, than mainland Europe, it is generally considered to be part of Europe due to cultural similarities with the Scandinavian countries (Norway, Finland, Denmark and Sweden).

As Iceland is situated on the edge of the Arctic Circle it has extended daylight hours during the summer months (*ca.* 20 hours daylight with 4 hours of twilight during the time of the visit) and extended hours of darkness during the winter. It sits at the northern edge of the Gulf Stream, a swift current of warm water which flows up from the southern tip of Florida roughly between the United Kingdom and Iceland. This has a moderating effect on the Icelandic climate. Compared to other land masses on the same latitude it encounters higher than average temperatures resulting in relatively mild winters and damp, cool summers, though there is some climate variation between different areas of the island. Due to the flow of the Gulf Stream around the Icelandic coast, the island usually remains free of ice incursion during the winter months despite its proximity to the Arctic Circle.

Almost half of Iceland's land area is made up of mountainous lava desert which is of recent volcanic origin and approximately 11% of Iceland is covered by glaciers, the three largest of which are at Vatnajökull, Langjökull and Hofsjökull glaciers. The Vatnajökull glacier is the largest in Europe, covering an area of 8,100 km^2 and is situated on the eastern and northern regions of the Icelandic rift zone and also on top of the Icelandic
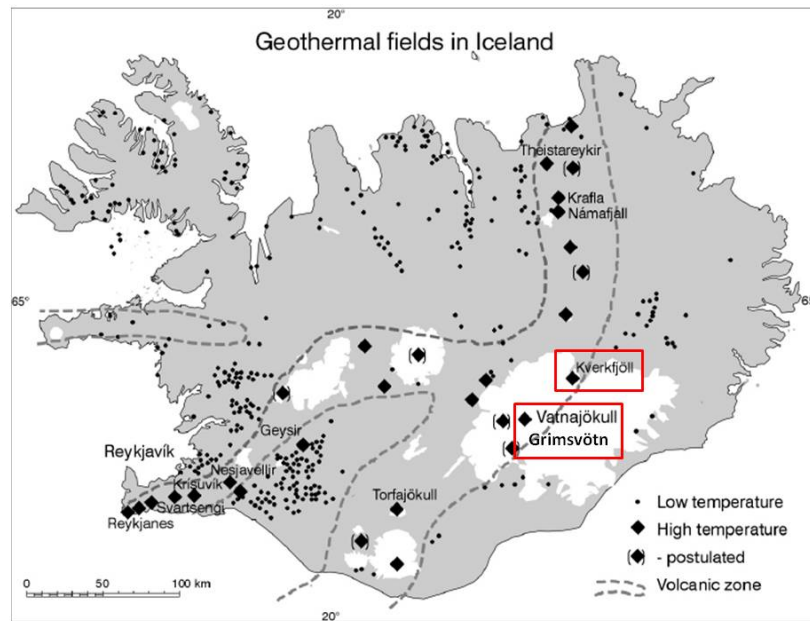
Figure 3.2: Geothermal fields in Iceland and the location of Kverkfjöll and Grimsvötn subglacial volcanoes. Map taken from Ármannsson *et al.* (2000)[183]

hot spot. The Icelandic hotspot is caused by an asthenospheric mantle upwelling due to convective currents causing plate divergence. The upwelling mantle occurs as a plume-like phenomenon which causes the overlying crust to bulge and eventually separate due to gravity - known as ridge push. Due to the rift, which runs from the South-West to the North-East across the island, Iceland is extensively volcanic and highly geothermally active (Figure 3.2). The Vatnajökull glacier sits on top of several active volcanic centres which include the recently erupted Grimsvjötn and the Kverkfjöll sub-glacial volcanoes.

The Grimsvjötn sub-glacial volcano erupted without warning on the 21st May 2011 producing an ash loaded eruption plume which extended *ca.* 17 km in height. Due to prevailing wind conditions and the size of the ash particles ejected, the ash fallout was quick and mainly to the south-east, avoiding any deposition onto the Kverkfjöll site. The disruption to civil aviation was limited due to the large particle size and rapid fallout though some disruption was caused. The eruption started only seven days before the originally planned start of the fieldwork at Kverkfjöll which resulted in a postponement of the expedition while the viability and safety aspects for the expedition were assessed. As the expedition arrived only two weeks after the official end of the eruption on the 28th May 2011, there was still some visible venting of gases in the crater and a newly formed melt-water lake in the crater basin (Figure 3.3).

The Kverkfjöll sub-glacial volcano lies on the on the north-eastern edge of the Vatnajökull glacier, on the Eastern edge of the Icelandic volcanic zone, and on the edge of the Mid-Atlantic rift (Figure 3.4). Kverkfjöll is a stratovolcano which is common in subduction/rift zones. Stratovolcanoes are normally tall, conical in shape and are formed by layered deposits of lava and tephra from periodic eruptions. The lava that usually flows from stratovolcanoes is known as felsic as it contains high to intermediate levels of silica which makes it viscous. This cools rapidly after eruption and thus does not travel far, leading to the classic cone shape formation.
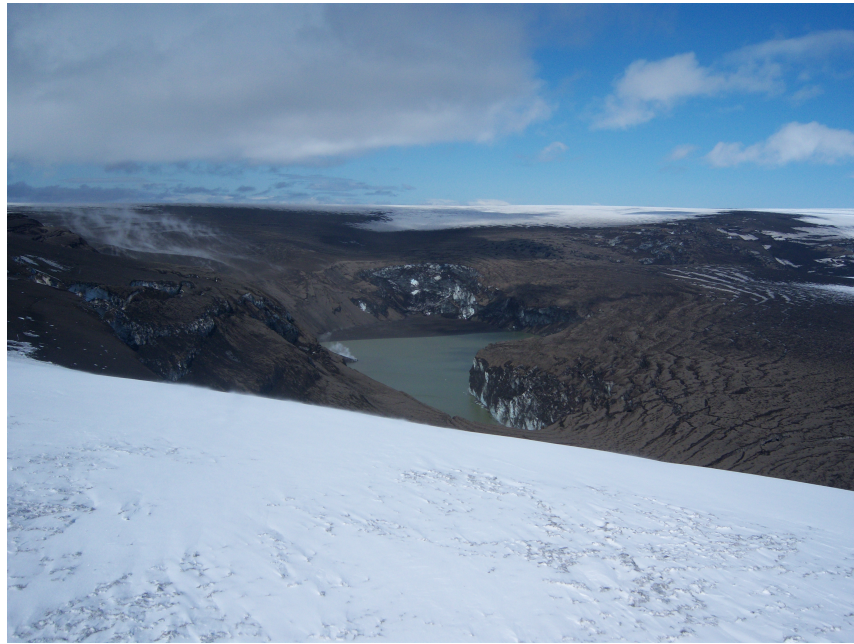
Figure 3.3: Photograph of the recently erupted Grimsvötn eruption crater almost 2 weeks after the eruption officially ended on 21st May 2011, showing the newly formed melt lake and signs of gaseous venting. (Credit: Barry Herschy)
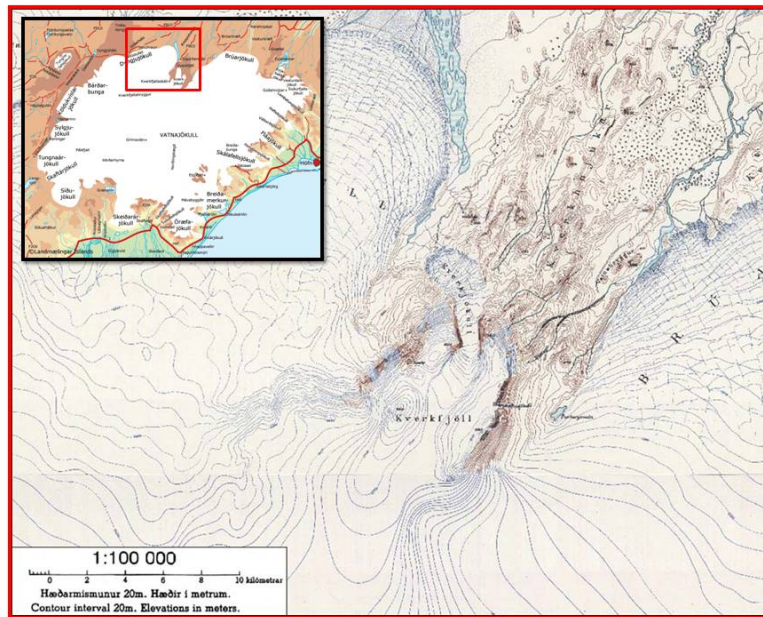
Figure 3.4: Topographic map of Kverkfjöll (1:100000 m scale)with inset picture of the Vatnajökull glacier showing the position of area covered. (Map and inset picture from www.skimountaineer.com)
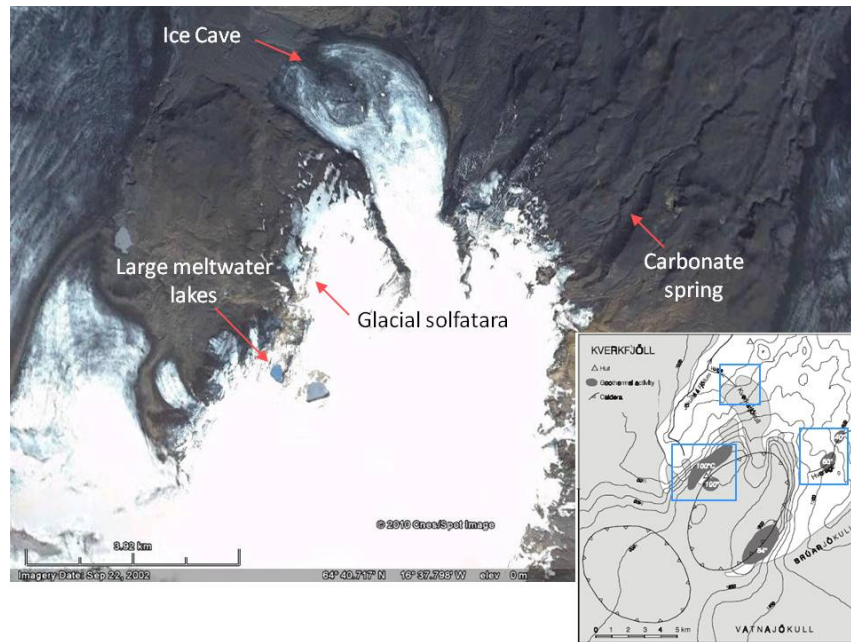
Figure 3.5: Google Earth image and topographic map of Kverkfjöll volcanic region. The Google Earth image was provided by Dr. Claire Cousins to show the areas of interest for the planned fieldwork. The topographical map, reproduced from an article by Ólafsson *et al.* (2000),[184] shows the two subglacial volcanic calderas and the geothermal fields associated with the Northern caldera.
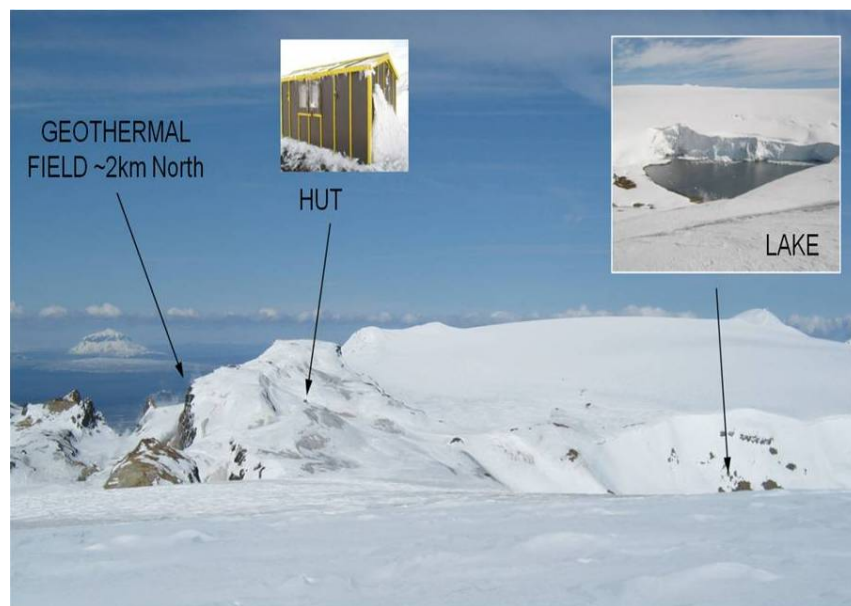
Figure 3.6: Overview of the Kverkfjöll region on the western rim of the northern caldera, showing the geothermal field (see Figure 3.8), the hut where the group was based, and the glacial melt-water lake.

The Kverkfjöll volcano system consists of two sub-glacial volcanic calderas which are elliptical in shape and approximately 8 km x 5 km in size (Figure 3.5). The main area of interest was situated on the western edge of the northern caldera which contains a 3 km long by 1 km wide geothermal zone. Though much of this area is inaccessible due to steep, unstable cliffs , there are partially accessible regions which contain glacial melt lakes (Figure 3.6) and hydrothermal and geothermally active areas. One area of particular interest was the 'glacial solfatara' region at Hveratagl identified by Dr. Claire Cousins during a previous visit to the region in 2007 while completing a PhD fieldwork trip. This contained a number of melt-water pools, fumaroles, sub-glacial melt streams and hot spring environments.[213] It was the proximity and variety of environments which made this site of particular interest due to the wide and varied conditions reported (temperature, pH and redox potential) and also that it was situated on a volcano/glacier boundary.

Previous work in this region of the Vatnajökull was carried out by the Icelandic Glaciological Society to assess the area for hydrothermal and geothermal tapping for use in producing electricity.[183,184] This work found that Kverkfjöll was a highly geothermally active area but was deemed too remote and too costly for viable geothermal harnessing for power.

3.3   Aims and Objectives

Fieldwork was undertaken in the Kverkfjöll region during June 2011 (8th - 21st June). The primary aims of the field campaign were;

1. To understand the plausible natural geological environments which may have been present on the early Earth by investigation of the hydrothermal and geothermal characteristics of the Kverkfjöll volcanic region.

2. To undertake a variety of experiments to assess the plausibility of potential prebiotic chemistry to operate in a natural geological environment.

3. To collect natural fluids for use in laboratory simulation experiments.

4. To analyse the natural fluids to determine base-levels of Fe, Ni, P and S present in the fluids prior to any experiments undertaken.

3.4   Experimental package

The planned experimental work was broken down into three areas:

1. Hydrothermal processing of schreibersite-containing iron meteorites and schreibersite analogue [Fe_3P].

2. Hydrothermal fluid analysis.

3. Reactions of phosphite and pyrophosphite under natural geological conditions.

Once the areas for investigation were established it was necessary to design experiments to fit each section and the methods for analysis of each experiment. The experiments needed to be simple, safe to transport and require no complex preparation or delicate equipment to complete. The idea was to load 50 mL Falcon tubes with all chemicals pre-weighed to which a designated amount of hydrothermal fluid could be added. The experiments could then either be fixed *in situ* (deployed) to maintain temperature of the fluid or removed from the site and packed for return (incubated).

With an outlined experimental package, consideration was then given to safe transportation of the payload. With the fluids coming from natural geological environments there were considerations over (i.) microbiological content, (ii.) sample leakage during transport and (iii.) safety of transport. After consultation with the University safety officer, a protocol for sample packaging and transport was established. Each sample was to be individually packaged into a Whirl-Pak bag then packed into another larger bag containing an absorbent such as vermiculite, capable of fully absorbing all fluid contained within the bag. All samples were to be labelled and a full risk assessment and COSHH form completed for the full experimental set.

The final experimental package is summarised in Table 3.1 and discussed below.

3.4.1 Hydrothermal processing

The aim of these experiments focused on the modification of meteorite and meteoritic inclusions to compare against laboratory simulations. The corrosion of schreibersite [$(FeNi)_3P$] inclusions within iron meteorites and of the analogue, iron phosphide [Fe_3P], is known to produce reduced oxidation state phosphorus species. This has been observed under laboratory conditions. A request was made to the Natural History Museum (NHM) for samples of iron meteorite containing schreibersite for corrosion in natural hydrothermal fluids. Experiments were to be analysed by a variety of methods including ^{31}P NMR spectroscopy, ICP-AES (inductively coupled plasma - atomic emission spectroscopy), infinite focus microscopy (IFM), SEM-EDX (scanning electron microscopy-electron dispersive X-ray) and Raman spectroscopy.

3.4.1.1 Matrix code A - Fe_3P

The purpose of this experiment set was to look at the chemical modification of iron phosphide using natural hydrothermal fluids. Much has already been done on this experiment within a laboratory environment but nothing has been published from real geological sites or fluids. The aim was to determine the phosphorus species produced during corrosion. The individual samples would be exposed to different pH and temperature fluids to investigate the effects on the amount and speciation of P obtained.

3.4.1.2 Matrix code B - Fe_3P + FeS

The purpose of this experiment set was to look at the chemical modification of iron phosphide in the presence of iron sulphide using natural hydrothermal fluids. This was to

Code	# of	Chemicals	Experiment	Environment
A	8	Fe_3P (0.25 g, 1.7 mmol)	Hydrothermal	Volcanic fluids
B	6	Fe_3P (0.25 g, 1.7 mmol) + FeS (0.25 g, 2.8 mmol)	Hydrothermal	Volcanic fluids
C	5	Sikhote Alin meteorite samples (various sizes)	Hydrothermal	Volcanic fluids
D	2	$MgHPO_4$ (0.1 g, 0.8 mmol)	Reduction	Reduced fluids
E	4	$MgHPO_4$ (0.1 g, 0.8 mmol) + FeS (0.1 g, 1.1 mmol)	Reduction	Reduced fluids
F	4	$Ca(H_2PO_3)_2 \cdot H_2O$ (0.1 g, 0.45 mmol) + FeS (0.1 g, 1.1 mmol)	Reduction	Reduced fluids
G	2	$Ca(H_2PO_3)_2 \cdot H_2O$ (0.1 g, 0.45 mmol)	Oxidation	Oxidised fluids
H	4	$Na_2H_2P_2O_5$ (0.1 g, 0.5 mmol)	Oxidation	Oxidised fluids
I	4	$Na_2H_2P_2O_5$ (0.1 g, 0.5 mmol) + Gly (0.94 g, 12.5 mmol)	Coupling chemistry	Glacial/Volcanic fluids
J	2	$Na_2H_2P_2O_7$ (0.1 g, 0.45 mmol) + Gly (0.94 g, 12.5 mmol)	Coupling chemistry	Glacial/Volcanic fluids
K	4	$Na_2H_2P_2O_5$ (0.24 g, 1.3 mmol) + KH_2PO_4 (0.17 g, 1.3 mmol)	Phosphonylation	Glacial/Volcanic fluids
L	4	$Na_2H_2P_2O_5$ (0.24 g, 1.3 mmol) + $Na_2H_2P_2O_7$ (0.28 g, 1.3 mmol)	Phosphonylation	Glacial/Volcanic fluids
M	4	$Na_2H_2P_2O_5$ (0.05 g, 0.25 mmol) + Na_2-ADP (0.1 g, 0.2 mmol)	Phosphonylation	Glacial/Volcanic fluids

Table 3.1: Table of proposed reactions for fieldwork indicating number and type of reactions and conditions required for each reaction type.

determine if the presence of a known reducing agent (sulphide) would alter the nature or quantities of P species produced compared to experiment set (Section 3.4.1.1). The samples would be exposed to different pH and temperature fluids to investigate the effects on the amount and speciation of P obtained and to establish if the presence of sulphide as a reducing agent effects the observed P species.

3.4.1.3   Matrix code C - Sikhote Alin samples

The purpose of this experiment set was to look at the corrosion of *bona fide* meteorite samples in natural hydrothermal fluids. Five samples were obtained of the Sikhote Alin meteorite, an iron meteorite which fell in Siberia, Russia in 1947 and is known to contain the mineral schreibersite ($[FeNi]_3P$, 0.46% Phosphorus w/w.[126]). The samples were to be exposed to different pH and temperature fluids with a view to observing the sites and rates of corrosion. The meteorite samples had previously been weighed to five decimal places and examined by IFM and SEM/EDX around the inclusion sites so that comparisons could be made between samples pre- and post-corrosion.

3.4.1.4   Matrix code D - $MgHPO_4$

The purpose of the experiment set was to look at the potential for reduction of phosphate to phosphite using reducing hydrothermal fluids. It was hoped to establish whether exposure to fluids of reducing quality could provide a route to reduced oxidation state phosphorus species.

3.4.1.5   Matrix code E - $MgHPO_4$ + FeS

The purpose of this experiment set was to look at the possibility of chemical reduction of phosphate to phosphite using natural hydrothermal fluids in the presence of a reducing agent, iron sulphide.

3.4.1.6   Matrix code F - $Ca(H_2PO_3)_2$ + FeS

The purpose of this experiment set was to investigate the potential of iron sulphide as a reducing agent in the presence of phosphite to produce hypophosphite. It was hoped to show the presence of iron sulphide could aid in the production of highly soluble and highly reactive reduced P species.

3.4.1.7   Matrix code G - $Ca(H_2PO_3)_2$

Initially the purpose of this experiment was to investigate the rate of oxidation of phosphite to phosphate in the presence of hydrothermal fluids. The focus of this experiment changed due to the extreme temperature conditions encountered (> 90℃) on site during the fieldwork. The new focus of the experiment set was to investigate the production of

pyrophosphite using geothermal heating. It has been shown to be possible, under laboratory conditions, to produce pyrophosphite [PPi(iii)] from phosphite by dry heating under constant gas flow at *ca.* 90℃. Pyrophosphite is thought to be a plausible prebiotic ancestor to pyrophosphate [PPi(v)].

3.4.2 Hydrothermal fluid analysis

Samples of hydrothermal fluids were to be collected from each chosen sample site and the composition analysed by ^{31}P NMR spectroscopy and ICP-AES to identify and quantify any P-species present within the natural samples and to establish background phosphorus levels for each sample area. The fluid samples were to be collected in sterilised 250 mL Nalgene bottles or 50 mL sterilised Falcon tubes by submersion in the fluid or by disposable sterilised syringe.

The Nalgene bottles and Falcon tubes were sterilised by washing with detergent and water then rinsing with deionised water and allowing to air dry. The bottles were autoclaved for 15 minutes (121℃ at 1.02 bars) then allowed to fully cool before resealing to prevent collapse.

3.4.3 Reactions of condensed phosphorus species – Pyrophosphite [Na$_2$H$_2$P$_2$O$_5$] and pyrophosphate [Na$_2$H$_2$P$_2$O$_7$]

Currently unpublished work within the Kee group has shown that pyrophosphite can participate in interesting and potentially important prebiotic chemical reactions. The Kee group has shown that pyrophosphite can be used to couple amino acids, to aid in acetyl transfer reactions and also used successfully as a phosphonylating agent. It was decided to compare sodium pyrophosphite and sodium pyrophosphate under natural geothermal conditions.

3.4.3.1 Matrix code H - Na$_2$H$_2$P$_2$O$_5$

The purpose of this experiment set was to investigate oxidation of pyrophosphite to pyrophosphate using hydrothermal fluids with an oxidising nature. It was hoped to determine if exposure to oxidising fluids resulted in production of pyrophosphate or if hydrolysis of pyrophosphite to phosphite would be the predominant reaction.

3.4.3.2 Matrix code I - Na$_2$H$_2$P$_2$O$_5$ + Gly

The purpose of this experiment set was to investigate the ability of pyrophosphite to act as a coupling agent for amino acids in natural hydrothermal fluids. It has been shown under laboratory conditions that it is possible to couple amino acids such as glycine in the presence of pyrophosphite at room temperature.

3.4.3.3 Matrix code J - $Na_2H_2P_2O_7$ + Gly

The purpose of this experiment set was to act as a reference for experiment set (3.4.3.2) to confirm whether pyrophosphite was responsible for causing coupling of amino acids. There was also the possibility that due to molecular similarities, pyrophosphate may act as a coupling agent for amino acids. This experiment would then act as a method of comparison between the molecular activity of PPi(iii) and PPi(v).

3.4.3.4 Matrix code K - $Na_2H_2P_2O_5$ + $MgHPO_4$

The purpose of this experiment set was to investigate the potential of pyrophosphite to act as a phosphonylating agent in natural hydrothermal fluids. It was anticipated that pyrophosphite would phosphonylate the phosphate to form isohypophosphate [PPi(iii/v)].

3.4.3.5 Matrix code L - $Na_2H_2P_2O_5$ + $Na_2H_2P_2O_7$

The purpose of this experiment set was to assess the ability of pyrophosphite to phosphonylate pyrophosphate in natural hydrothermal fluids. It was anticipated that phosphonylation would produce linear tripolyphosphate, a long chain polyphosphate, easily identifiable by ^{31}P NMR spectroscopy.

3.4.3.6 Matrix code M - $Na_2H_2P_2O_5$ + ADP

The purpose of this experiment was to investigate the ability of pyrophosphite to act as a phosphonylating agent to convert adenosine diphosphate (ADP) to adenosine triphosphate (ATP) in natural hydrothermal fluids.

With the experimental package outlined, the individual experiments were prepared as shown in Table 3.1. It was planned for all experiments to be conducted in the field and analysed upon return to Leeds.

The remainder of this chapter will outline the localities visited during this expedition, the environmental conditions encountered and the experiments undertaken during the field-work.

3.5 Timeline of events

The group arrived in Iceland on the 8th June 2011 and two days were spent sourcing equipment and supplies for the glacier trip. A series of meetings were held with our guide and driver, Magnus Þor Karlsson and a group from the Icelandic Meteorological Office (IMO) to discuss the weather forecast for the site area, conditions and safety on the glacier and the route of travel. A group from the IMO was to accompany the team to a hut on the glacier near Grimsvötn where it was planned to stay a night before heading on to Kverkfjöll *via* the Grimsvötn eruption site. The following morning the two groups set off in convoy for the Icelandic Glaciological Society (IGS) hut at Grimsfjäll which is on the eastern edge of

the Grimsötn Caldera approximately 6 km from the 21st May 2011 eruption site. The route to Kverkfjöll (shown in Figure 3.7) took the group along the Suðurlandsvegur (Highway 1), Icelands main ring road through Selfoss, then taking the Skeiða-og Hrunamannavegur (Highway 30) and Þjórsárdalsvegur (Highway 32) towards the interior before heading on to unmarked gravel tracks leading to the IGS hut at Jökulheimar on the western edge of the Vatnajökull glacier.

Figure 3.7: GPS map showing the route taken from Reykjavik to Kverkfjöll with stop areas highlighted. Map provided by Magnus Þor Karlsson.

After a brief stop at Jökulheimar, the group then headed onto the glacier towards the IGS hut at Grimsfjäll on the eastern edge of the Grimsvötn caldera. Progress over the glacier was initially slow due to melting snow and ice at the edges and was further hampered by a blizzard which blew in reducing visibility to less than 20 meters. After a *ca.* 10 hour drive the group reached the IGS hut at Grimsfjäll. The next morning the weather had cleared and the team set off for Kverkfjöll with a short stop at the Grimsvötn eruption site. The fresh snowfall made for difficult driving conditions as drifts of *ca.* 2 m caused the vehicles to bottom out and become such fast in the snow. The journey from Grimsvötn to Kverkfjöll took close to 6 hours and upon arrival the hut had to be cleaned, the vehicles unpacked and the equipment supplies sorted. A total of seven days was spent in the Kverkfjöll area before heading back to Reykjavik *via* Grimsvötn and Jökulheimar. The group returned to the UK on the 21st June 2011 after a two night stopover in Reykjavik.

3.6 Preliminary site investigation

The primary site at Hveratagl (Figure 3.8) identified for investigation and sampling was *ca.* 2 km to the north of the IGS hut at Kverkfjöll. The site was identified by Dr. Claire Cousins during her PhD fieldwork trip to Iceland in 2007 and was shown to have a wide variety of pH and temperature environments suitable for prebiotic chemistry, including high temperature fumaroles (acidic, *ca.* pH 3.5), glacial melt-water streams (neutral, *ca.* pH 7) and a carbonate spring (alkaline, *ca.* pH 8.5).[213]

Based on the observations by Dr. Cousins in 2007, an experimental package was designed to incorporate a variety of different types of experiments which could exploit the conditions available. An initial attempt to access the site was hampered by bad weather and poor visibility though after a second successful attempt, again in poor weather conditions, the site was found to be completely covered in snow (Figure 3.9). The site was unfortunately declared unsafe as the geothermal features, hydrothermal pools and melt water streams which were of interest were hidden by a covering of snow which meant there was a danger of falling through the snow into boiling hydrothermal fluids or other geothermal features.

Figure 3.8: The geothermal field photographed during the 2007 field trip by Dr. Claire Cousins that formed the basis of this fieldwork. (Credit: Dr. Claire Cousins)

Figure 3.9: Photographs taken of the primary hydrothermal site showing deep snow cover. This was attributed to a very cold spring in Iceland and increased snow fall through this period.

A secondary site was discovered next to the Hveradalur melt water lake approximately 0.5 km to the east of the IGS hut. The secondary site was first visited on the same day as the first failed attempt to access the primary sampling site and now that this was declared unworkable and time was limited, the new site became the area of focus for all experiments and sampling. The hydrothermal/geothermal area was situated on an elevated plateau *ca.* 3 m above lake level and *ca.* 20 m west from the edge of the lake. The plateau was approximately 30 m (north to south) by 15 m (west to east) and was roughly elliptical in shape. On the plateau there were three large interlinked pools to the north side which
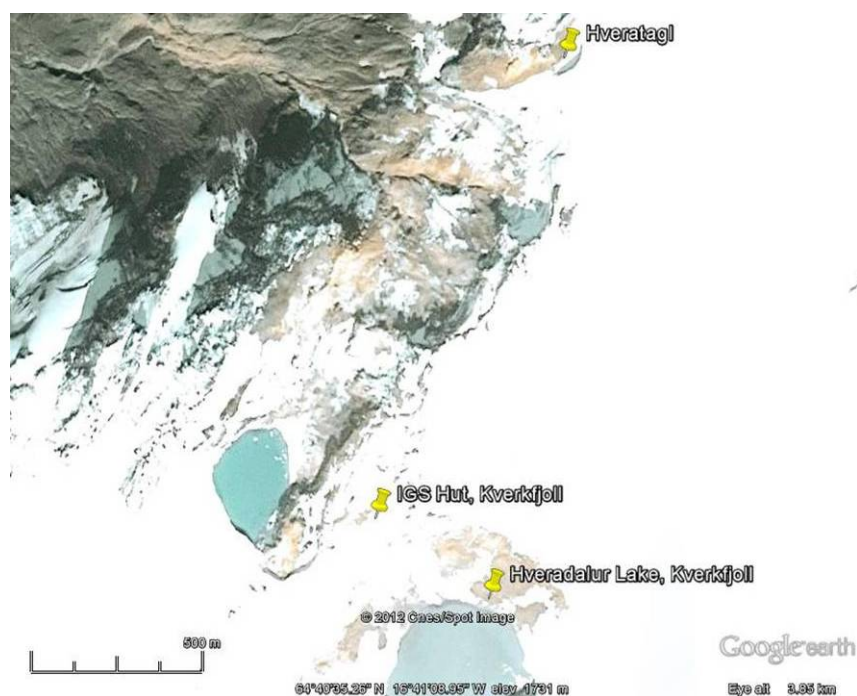
Figure 3.10: Google Earth image of the Kverkfjöll area showing the locations of the primary site at Hveratagl and the secondary site at Hveradalur Lake.

appeared to have fluids close to boiling. Initial investigation of the large and small pools on the plateau showed a wide variety of pH and temperature (pH range 1 to 5 and temperatures between 40°C and 90°C) environments. Due to the favourable conditions present at this site it was decided to deploy a small number of experiments with a view to returning and collecting these experiments prior to leaving the glacier.

To the south of the pool system was a "honeycomb" area of interlinked small pools, mud bubblers and steam/gas vents. There was also a small melt-water stream which ran from west to east across the honeycomb area into the snow line. A larger stream ran from the large pool system over a small waterfall and down over the shore into the melt water lake. Approximately 20 m to the north of the stream on the lake shore was an area of geothermally heated sand which felt hot under foot and also seemed to be heating the lake water in the vicinity of the shore edge. This area was considered for further investigation prior to leaving the glacier, providing there was sufficient time available for analysis, as temperatures around 95°C approximately 2cm below the surface of the sand were observed using a soil thermometer. To the south of the stream, *ca.* 60 m along the shore of the lake was the glacier edge which had small ice caves present. During the time working at the site, the glacier could be heard cracking and there were also calving events in which large blocks of ice fell into the lake causing mini tsunami events, some of which would cover the beach area completely. All around the site there was evidence of degassing of hydrogen sulphide [H_2S]. This could be identified by smell but also by small amounts of elemental sulphur deposited on rocks around vent areas.

As the UCL team required a pristine site for biological sampling our access to the site was limited until all essential work was completed by the UCL team. This resulted in time where no sampling or deployment of experiments could be undertaken, though this did allow for a thorough examination of the site and discussion and planning for deployment

Figure 3.11: Panoramic photograph of the hydrothermal plateau area at Hveradalur Lake taken from the southern tip of the hydrothermal area. The photograph was taken to show the working environment and conditions on the site. The photograph has two members of the team in for scale.
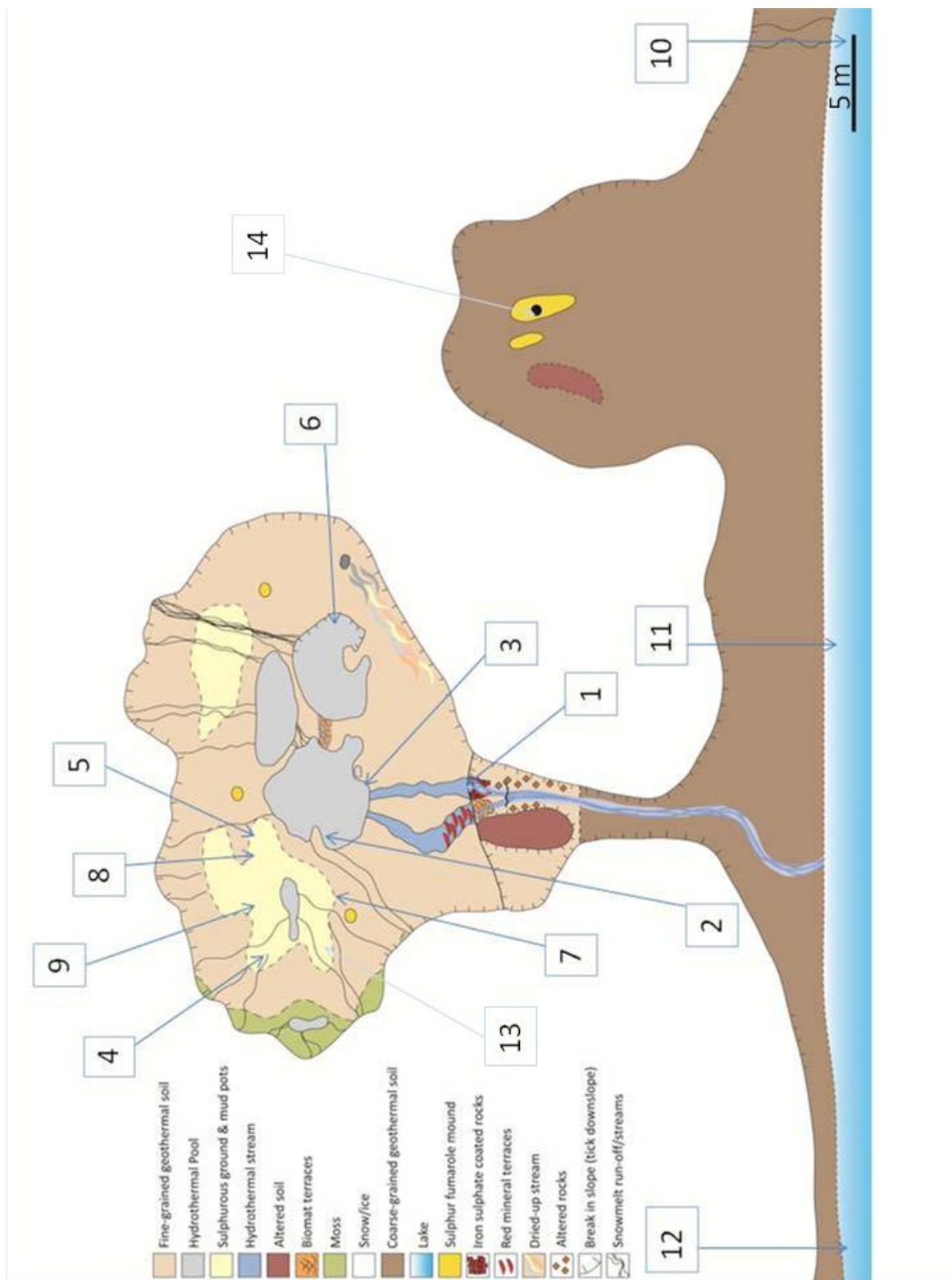
Figure 3.12: Scale map of the sample area indicating sample points referred to in Table 3.2. A photograph of one of the sample points with experiments deployed is shown in Figure 3.13. Used with alteration from publication by Cousins *et al.* (2013).[214]

Fine-grained geothermal soil
Hydrothermal Pool
Sulphurous ground & mud pots
Hydrothermal stream
Altered soil
Biomat terraces
Moss
Snow/ice
Coarse-grained geothermal soil
Lake
Sulphur fumarole mound
Iron sulphate coated rocks
Red mineral terraces
Dried-up stream
Altered rocks
Break in slope (tick downslope)
Snowmelt run-off/streams

5 m

103

and sampling. It was decided to utilise the site to explore the broadest range of pH and temperature conditions possible.

3.7   Observations and experimental deployment

All sites sampled, the conditions observed, the experiments deployed (see Figure 3.13 for example of experimental deployment) and the reasons for choosing the site are detailed below. All fluid samples were collected directly from the site in a sterile 250 mL Nalgene bottle unless otherwise stated. All fluids were added to the experiments using a 50 mL sterile disposable syringe without filtering. A summary of conditions and experiments undertaken are show in Table 3.2.

Figure 3.13: Photograph of experiments deployed in hydrothermal fluid areas for maintaining temperature of fluids sampled for reaction.

Map Ref	Site Ref	pH	Temp.	Date	Time
1	KHL-UCL-3	3.6	40.0℃	12/06/2011	19.30
2	KHL-BPR	4.0	79.5℃	12/06/2011	20.00
3	KHL-UCL-4	3.5	55.0℃	12/06/2011	20.30
4	KHL-MP1	1.6	87.4℃	14/06/2011	12.00
5	KHL-LP1	3.1	93.5℃	14/06/2011	12.30
6	KHL-UCL-5	4.7	89.2℃	16/06/2011	13.40
7	KHL-LP3	2.5	79.2℃	16/06/2011	14.45
8	KHL-LP4	3.3	87.8℃	16/06/2011	16.00
9	KHL-MP3	2.7	84.7℃	16/06/2011	16.05
10	KHL-LAG-1	5.0	21.0℃	14/06/2011	15.55
11	KHL-LAG-2	5.7	20.9℃	16/06/2011	11.30
12	KHL-LAG-3	5.3	11.0℃	18/06/2011	10.40
13	KHL-MP2	2.7	92.6℃	14/06/2011	13.00
14	KHL-UCL-18	N/A	94.3℃	14/06/2011	13.30
N/A	KHL-MEL	5.5	4.7℃	18/06/2011	10.40

Table 3.2: Table of all sample sites showing conditions at the time of sampling. The position of the sample sites is shown on Figure 3.12

3.7.1   KHL-UCL-3 - (DO 4 mg/L, 40.0℃, pH 3.6)

This site was situated in the UCL designated "lower stream" area and was a small waterfall which connected the upper and lower stream areas. The site was chosen due to the low pH recorded by the UCL team and was the first area on the site given clearance for sampling by the UCL team. Due to the nature of the site, only incubation of the experiments was possible.

3.7.2   KHL-BPR - (79.5℃, pH 4.0)

This site was situated on a peninsular on the southern edge of the largest of the three hydrothermal pools which extended to within 2 meters of an area which appeared to be boiling vigorously. This site was chosen due to the combination of high temperature and low pH. Due to the nature of the site, deployment of experiments was possible to maintain temperature.

3.7.3   KHL-UCL-4 - (DO 0.2 mg/L, 55.0℃, pH 3.5)

This site was on the eastern edge of the largest hydrothermal pool close to the stream which runs from the elevated geothermal area to the lake. The site was chosen as the fluids were deemed to be reducing in quality due to the low levels of dissolved oxygen (DO). Due to the nature of the site, deployment of experiments was possible to maintain temperature.

3.7.4   KHL-MP1 - (87.4℃, pH 1.6)

This site was a small mud pool (*ca.* 10 cm diameter) situated to the south of the large hydrothermal pools on the north-eastern edge of a honeycomb of apparently interconnected

fumaroles, steam vents and bubbling mud pools. Due to the size of the pool it was not possible to collect a 250 mL water sample but a 50 mL sample was collected in a 50 mL Falcon tube. The site was chosen due to the low pH and high temperature measured and was comparable to the conditions in which experiments had been conducted in the laboratory. Due to the size of the site, only two experiments were incubated with fluid.

3.7.5 KHL-LP1 - (93.5℃, pH 3.1)

This site was a small pool (*ca.* 30 cm diameter) and was *ca.* 3 m south of the large hydrothermal pools which was part of a stream running from the melting snow line, through the honeycomb area. Due to the size of the pool it was only possible to collect a 50 mL fluid sample in a 50 mL Falcon tube. The site was chosen due to the very high temperature and relatively low pH encountered. Again, only two experiments were selected, one incubated in fluid, the other deployed in the pool to maintain temperature.

3.7.6 KHL-UCL-5 - (89.2℃, pH 4.7)

This site was on the northern edge of the three large hydrothermal pools. The site was difficult to access with a *ca.* 50 cm drop from ground level to the pool edge. The site was chosen due to the combination of low pH and high temperature. The chosen experiments were incubated due to difficulty in accessing the site though it was possible to deploy the meteorite sample to maintain temperature.

3.7.7 KHL-LP3 - (79.2℃, pH 2.5)

This site was situated on the north-east edge of the honeycomb area *ca.* 6 m from the KHL-BPR (map site 2) on the largest hydrothermal pool. The site was a small pool (*ca.* 15cm diameter) situated in a small stream system which ran from the melting snow line through the honeycomb area towards the lake. The site was chosen as it was vigorously bubbling so hot and also low pH observed. Due to the size of the pool all samples were incubated in fluids apart from the meteorite sample which was deployed to maintain temperature. A 50 mL sample of fluid was also collected.

3.7.8 KHL-LP4 - (87.8℃, pH 3.3)

This site was on the north-west edge of the honeycomb area within 50 cm of KHL-LP1 (map site 5). The pool was *ca.* 20 cm diameter and was vigorously bubbling. The site was chosen due to the low pH and high temperature observed. The size and depth of the pool dictated that all samples had to be incubated. A 50 mL sample of fluid was collected in a 50 mL Falcon tube.

3.7.9   KHL-MP3 - (84.7℃, pH 2.7)

This site was on the western edge of the honeycomb area and *ca.* 6 m north from KHL-MP1 (map site 4). The site was a bubbling grey mud pool *ca.* 15 cm in diameter. This site was chosen due to the low pH and high temperature recorded. Due to the size and depth of the pool all experiments from this site were incubated in fluids. A 15 mL fluid sample was collected in a sterile 15 mL Falcon tube.

3.7.10   KHL-LAG-1 - (21.0℃, pH 5.0)

This site was the most northerly of the lake sites and was situated on top of geothermally heated sands. All samples were collected *ca.* 25 cm from the shore line above a bubbling area of the lake bed. The lake was much cooler than the hydrothermal pools and a higher pH and was sampled for this reason. Due to the dynamic nature of the lake and the large amounts of glacial break-off causing sporadic tidal waves, all experiments were incubated in lake fluids.

3.7.11   KHL-LAG-2 - (20.9℃, pH 5.7)

This site was close to the outflow stream from the upper hydrothermal area. Again the samples were collected *ca.* 25 cm from the shore line and all experiments were incubated in the lake fluids due to the dynamic nature of the lake.

3.7.12   KHL-LAG-3 - (11.0℃, pH 5.3)

This site was the most southerly of the lake sites and was situated close to the edge of the glacier. The samples were collected *ca.* 25 cm from the edge of the shore line and all experiments were incubated in lake fluids due to the dynamic nature of the lake.

3.7.13   KHL-MP2 - (92.6℃, pH 2.72)

This site was on the south-eastern edge of the honeycomb area *ca.* 3 m east of KHL-MP1 (map site 4) and 8 m south-east of KHL-MP3 (map site 9). Due to the high temperature encountered it was decided to deploy experiment G1 (calcium phosphite) at this site to heat without addition of fluids in an attempt to produce pyrophosphite in a natural geological environment. This experiment was lost as the Falcon tube containing the experiment became flooded and the contents spilled out into the pool.

3.7.14   KHL-UCL-18 - (93.4℃)

This site was observed during investigation of the geothermal sand area on the shore of the lake. The site is an area of high geothermal activity with hot rocks and sand ($>$90℃), too hot to touch with bare hands. The temperature was measured *ca.* 5 cm depth below the surface at 93.4℃. it was decided to deploy experiment G2 at this site again due to

the very high temperature observed in an attempt to produce pyrophosphite in a natural geological environment.

3.7.15   KHT-MEL - (4.7℃, pH 5.5)

This was collected as snow from a site *ca.* 10 m south of the IGS hut. This sample was collected as a reference sample as it was less likely to contain dissolved ions and metals which would be contained in the hydrothermal fluids. The experiments were incubated in the melt-water fluid for comparison to the lake water samples.

3.8   Summary

This chapter details the information about site conditions and experiments undertaken during the June 2011 field expedition to the Kverkfjöll region of the Vatnajökull glacier, Iceland. The experimental package was returned to Leeds for analysis and this is described in detail in Chapter 4. A summary of all the experiments undertaken and the conditions under which the experiments were undertaken are shown in Table 3.3.

Map Ref:	Site Ref:	pH	Temp.	Samples
1	KHL-UCL-3	3.6	40.0	A1
2	KHL-BPR	4.0	79.5	A2, B1, C5
3	KHL-UCL-4	3.5	55.0	D1, E1, F1
4	KHL-MP1	1.6	87.4	A3, B2
5	KHL-LP1	3.1	93.5	A4, C1
6	KHL-UCL-5	4.7	89.2	A5, B3, C2, E2, F2
7	KHL-LP3	2.5	79.2	A6, B4, C4, E3, F3
8	KHL-LP4	3.3	87.8	A7, B5, E4
9	KHL-MP3	2.7	84.7	A8, B6, F4
10	KHL-LAG-1	5.0	21.0	H1, I1, J1, K1, L1, M1
11	KHL-LAG-2	5.7	20.9	H2, I2, J2, K2, L2, M2
12	KHL-LAG-3	5.3	11.0	H3, I3, K3, L3, M3
13	KHL-MP2	2.7	92.6	G1
14	KHL-UCL-18	n/a	94.3	G2
n/a	KHL-MEL	5.5	4.7	H4, I4, K4, L4, M4

Table 3.3: Table giving locations of fluids collected for each sample and the pH and temperature of the fluids recorded at these locations. The locations can be seen in Figure 3.12

Chapter 4

Kverkfjöll expedition sample analysis

4.1 Introduction

As discussed in Chapter 3, the purpose of the Kverkfjöll expedition was to undertake experiments to simulate prebiotic chemistry and investigate the dynamics and products of meteoritic corrosion under natural geological conditions. The experimental work was carried out in three main areas: 1) Hydrothermal processing of iron meteorites and in particular the phosphorus containing components therein, 2) Hydrothermal fluid analysis and 3) Reactions of phosphite and pyrophosphite, all to be conducted under natural geological hydrothermal conditions. The design of each experiment chosen was based on the differing hydrothermal conditions expected to be encountered on site based on the report of Dr. Claire Cousins in her Ph.D. thesis[213] (later published in Cousins *et al.* (2013)[214]).

The site at Hveratagl was identified as having both acidic and alkaline conditions with acidic hydrothermal pools (pH 4-6), glacial melt-water streams (*ca.* pH 7) and an alkaline carbonate stream (pH 8-9). Unfortunately, due to being snow covered after a cold hard winter and spring, the primary site was unworkable and it was necessary to select a secondary site to complete the work. The site chose was at Hveradalur Lake, which was less than 500 m from the IGS hut which was base camp. During preliminary investigation of this site it became apparent that the full range of expected pH s was not available which led to an alteration in the chemistry which could be undertaken on this site. The site proved ideal for the hydrothermal corrosion experiments as it was highly acidic (pH 1.5-6) and hot (temperatures between 40-95℃ were available) though less useful for the solution chemistry experiments as the majority required either neutral or alkaline fluids. It was decided to attempt the solutions chemistry experiments in fluids as close to the required pH/temperature as was possible to see what reactions, if any, would take place under such conditions (to save on potential experimental losses due to the site change).

4.2 Reactions of phosphite and pyrophosphite

A suite of experiments was designed to investigate potential prebiotic chemistry of phosphorus species such as phosphite, pyrophosphite and pyrophosphate under natural geological

conditions. The experiments had initially been successfully tested in the lab by other members of the Kee group and the trip to Iceland gave the opportunity to try these experiments in natural fluids in an environment which could be considered as an analogue to early Earth conditions.

The experiments (sample matrix codes D, E, F, H, I, J, K, L and M) were conducted in 50 mL Falcon tubes. The fluids for each experiment were collected using 50 mL disposable plastic syringes and the locations and fluid conditions are recorded in Table 4.1 while the locations of the sites are shown in Figure 4.1.
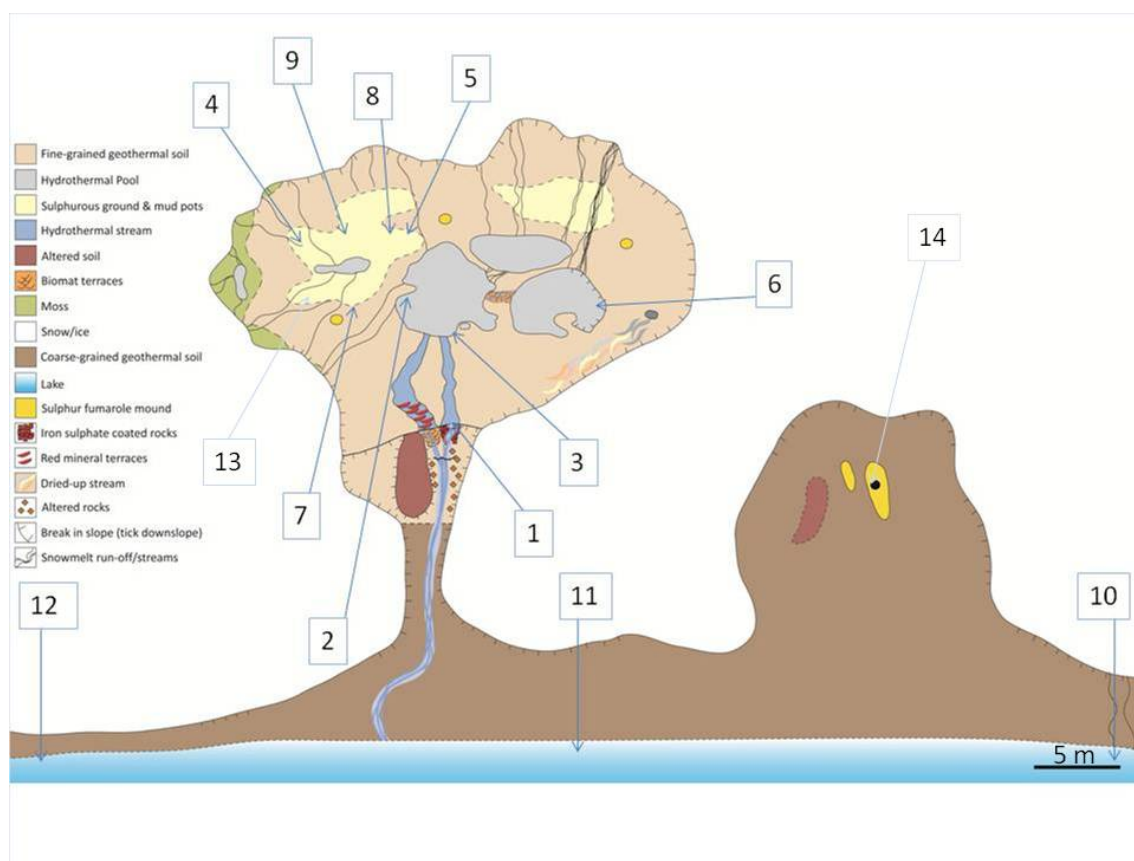
Figure 4.1: Map of the sample site showing locations in which fluid samples for the experiments were collected. Details of pH and temperature conditions recorded are shown in Table 4.1. Map has been used from Cousins *et al.* (2013).[214]

The samples were initially stored under ambient conditions until arrival back in Leeds upon which they were stored in a fridge at *ca.* 8°C while awaiting processing and analysis. The analysis of each sample was conducted by either ^{1}H or ^{31}P NMR depending on the expected target molecules. Initially the NMR analysis was hampered by an issue with small levels of dissolved iron present in the natural waters. Iron removal (discussed in Chapter 2) was undertaken by addition of sodium hydroxide (2 M, *ca.* 1 mL) to obtain pH 12 then gravity filtered through Whatman No. 1 filter papers to remove any precipitate before a usable NMR spectrum could be obtained.

Upon interpretation of the NMR spectra it became apparent that only starting materials, hydrolysis products and/or oxidation products of the reduced oxidation state species were present in the fluids in all cases. It appeared that, due to the site move and the lack of suitable conditions required for the chemistry to be undertaken, the attempts to conduct the solution chemistry in natural fluids had failed. Considering why the reactions did not

Map Ref:	Site Ref:	pH	Temp.	Samples
1	KHL-UCL-3	3.6	40.0	A1
2	KHL-BPR	4.0	79.5	A2, B1, C5
3	KHL-UCL-4	3.5	55.0	D1, E1, F1
4	KHL-MP1	1.6	87.4	A3, B2
5	KHL-LP1	3.1	93.5	A4, C1
6	KHL-UCL-5	4.7	89.2	A5, B3, C2, E2, F2
7	KHL-LP3	2.5	79.2	A6, B4, C4, E3, F3
8	KHL-LP4	3.3	87.8	A7, B5, E4
9	KHL-MP3	2.7	84.7	A8, B6, F4
10	KHL-LAG-1	5.0	21.0	H1, I1, J1, K1, L1, M1
11	KHL-LAG-2	5.7	20.9	H2, I2, J2, K2, L2, M2
12	KHL-LAG-3	5.3	11.0	H3, I3, K3, L3, M3
13	KHL-MP2	2.7	92.6	G1
14	KHL-UCL-18	n/a	94.3	G2
n/a	KHL-MEL	5.5	4.7	H4, I4, K4, L4, M4

Table 4.1: Table giving locations of fluids collected for each sample and the pH and temperature of the fluids recorded at these locations. The locations can be seen in Figure 4.1

work under the new site conditions led to the conclusion that the acidic fluids had resulted in either protonation of the reactive species or rapid hydrolysis of reactive species which were then incapable of undergoing any further reactions.

There was only one set of experiments which showed some success. The G- samples which were initially intended to look at the rate of oxidation of phosphite under natural geological conditions was reassigned and used to try to determine whether it was possible to produce pyrophosphite under natural geological conditions by dry heating open to the atmosphere using either hydrothermal or geothermal heating.

4.3 Dry heating of phosphite using a geothermal heat source

As discussed in Chapter 2, the formation of pyrophosphite from sodium phosphite requires heating to 160℃ for the condensation reaction to occur effectively. Mixing the sodium phosphite with SMOW afforded a lowering of the temperature required for the formation of pyrophosphite from 160℃ to 90℃. Investigation by the Kee group on why SMOW has this effect on the formation showed that the presence of certain divalent cations such as magnesium and calcium allowed for the lowering of temperatures to the much more prebiotically reasonable 90℃. Work was then undertaken within the group to produce pure metal phosphites which could be used in experiments at lower temperatures. Some of this work is shown in Chapter 2. It has been shown in Chapter 2 that dry heating of calcium phosphite at *ca.* 90℃ under flowing N_2 gas will result in the effective condensation of phosphite to pyrophosphite. The idea was to attempt to reproduce this experiment and form pyrophosphite under natural geological conditions by finding suitable sites in the Kverkfjöll area in which temperatures exceeded 90℃. Samples of calcium phosphite could be dry heated for a few days to see if production of pyrophosphite was possible under these conditions.

Figure 4.2: Photograph of experiment G2 shown *in situ* in the geothermally heated sand at site KHL-UCL-18. As can be seen from the thermometer the temperature of the sand is 94.3℃. Credit: Barry Herschy

The first sample (G1) was placed and secured in a hot hydrothermal pool (designated KHL-LP2, 92.7℃) using rocks to keep it in position. The sample was to be heated dry for a period of 4 days then sealed and returned to Leeds for analysis. The second sample (G2) was initially deployed into hot sand on the shore of the lake where the sand temperature *ca.* 2 cm below the surface was 93.8℃. The sample was pushed into the sand to a depth of *ca.* 5 cm and left there overnight. Due to fracturing of the glacier into the lake overnight, the water level of the lake had risen to within *ca.* 20 cm of the sample and thus was in danger of flooding the experiment. It was decided to move the sample to UCL site 18 (see Figure 4.2) which was well up the beach, away from the rising water line and close to the snow line. The temperature of the sand at this site was 94.7℃ so was equivalent to the temperature of the original site meaning the integrity of the experiment was not compromised.

Upon return to collect the experiments from their deployment sites it was found the Falcon tube for sample G1 had fallen over into the pool and spilled its contents into the water meaning the experiment was lost. Sample G2 was still safe and intact and was sealed and packed away for transport back to Leeds where it was analysed by ^{1}H and ^{31}P NMR.

Initial attempts of ^{1}H and ^{31}P NMR analysis (300 MHz) were inconclusive. The spectra showed peaks in the right regions and with appropriate shifts to be the AA'XX' spin system indicative of pyrophosphite, but they were too weak to be certain. The ^{1}H and ^{31}P NMR analysis (500 MHz) were repeated with an extended number of scans in an attempt to maximise resolution from the sample and increase the chance of pyrophosphite observation (if it was present in the sample). Full NMR data are shown in Table 6.48.

Analysis of the ^{1}H NMR spectrum (Spectrum 4.1) showed the presence of phosphite ($\delta6.7$, d) and also the AA'XX' spin coupling system ($\delta6.9$, AA'XX') characteristic of pyrophosphite. The presence of pyrophosphite was confirmed with analysis of the ^{31}P NMR spectrum (Spectrum 4.2) which showed the presence of the AA'XX' spin system peaks (δ-4.4).
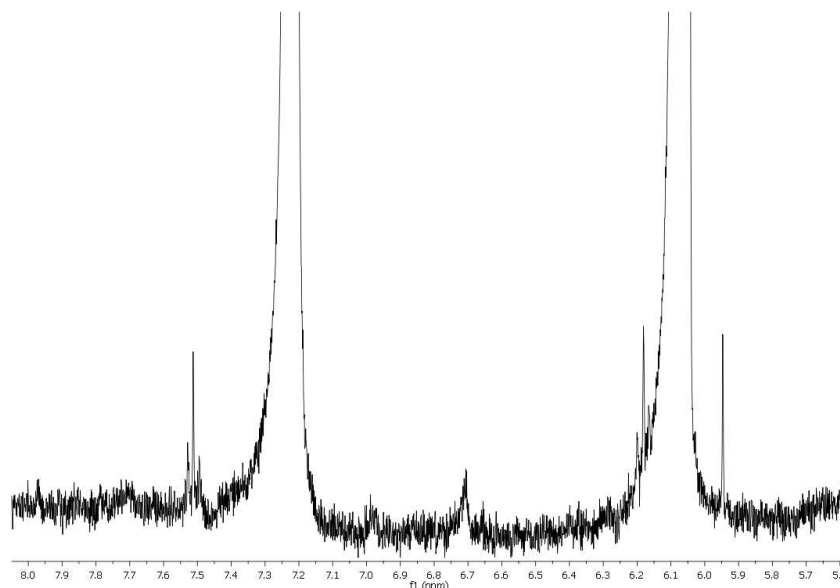
Spectrum 4.1: ^{1}H NMR spectrum (300 K, D_2O, 500.57 MHZ) of sample G2 which was dry heated by geothermally heated sand at 94.7℃ for *ca.* 72 hours. Phosphite ($\delta6.7$, d, $^1J_{\text{P-H}}$= 575 Hz) and pyrophosphite ($\delta6.9$, AA'XX', $^1J_{\text{P-H}}$= 666 Hz, $^2J_{\text{P-P}}$= 10 Hz, $^3J_{\text{P-H}}$= 8 Hz) can be identified in the spectrum.

The presence of pyrophosphite in the ^{1}H and ^{31}P NMR spectra was very exciting as it appeared to prove that the production of pyrophosphite under natural geological conditions was possible. To confirm the production of pyrophosphite in sample G2 it was firstly decided to conduct NMR analysis on a blank sample of the calcium phosphite used in the Iceland experiments (which had not been heated), to confirm that there was no contamination of the starting sample. It was also decided to conduct a dry heating experiment to simulate heating of calcium phosphite under the conditions originally used in Iceland to heat the G2 sample. It was thought that, if it was possible to repeat the result under similar conditions in the laboratory, then this would confirm it was possible to produce pyrophosphite under those conditions.

The simulation experiment was conducted by taking calcium phosphite (0.1 g, 450 μmol) which was placed in a 50 mL Falcon tube. The sample was dry heated at *ca.* 95℃ using a sand bath open to the atmosphere inside a fume hood. The sample was heated for a period of 72 hours, the same time as the G2 sample in Iceland, allowed to cool to ambient temperature then analysed by ^{1}H and ^{31}P NMR. The starting material was also analysed by ^{31}P NMR to confirm no contamination of the experiment.

The ^{31}P NMR spectrum of the unreacted calcium phosphite showed only the presence of phosphite ($\delta2.6$, d) confirming there was no contamination of the sample prior to the experiment. The ^{1}H NMR spectrum (Spectrum 4.3) of the simulation experiment showed the presence of phosphite ($\delta6.7$, d) and pyrophosphite ($\delta6.9$, AA'XX'). The presence of pyrophosphite was again confirmed by the presence of the AA'XX' spin system (δ-5.5, AA'XX') in the ^{31}P NMR spectrum (Spectrum 4.4). Full NMR data are shown in Ta-
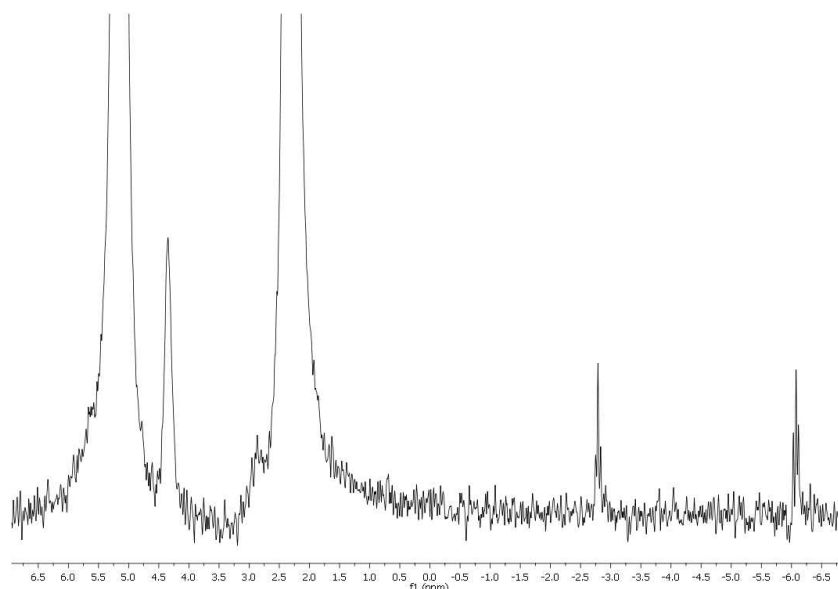
Spectrum 4.2: ^{31}P NMR spectrum (300 K, D$_2$O, 202.63 MHz) of sample G2 which was dry heated by geothermally heated sand at 94.7℃ for *ca.* 72 hours. As with the ^{1}H NMR spectrum, both phosphite (δ3.7, d, $^1J_{\text{P-H}}$= 573 Hz) and pyrophosphite (δ-4.4, AA'XX', $^1J_{\text{P-H}}$= 666 Hz, $^2J_{\text{P-P}}$= 10 Hz, $^3J_{\text{P-H}}$= 8 Hz) are identifiable in the spectrum which confirms the ability to produce pyrophosphite under natural geological conditions.

ble 6.49.

The results of the analysis of the starting material and simulated Iceland heating proved that it was indeed possible under natural geological conditions to produce pyrophosphite from phosphite. Based on this evidence, if it were possible to produce large amounts of phosphite in a natural pool then allow this pool to evaporate to dryness then it would be feasible that, if the dry phosphite was exposed to geothermal heating in excess of *ca.* 90℃, there would be natural production of pyrophosphite. This pyrophosphite could then be redissolved in natural fluids as they returned (i.e. rainfall or tidal systems) and then able to participate in prebiotic chemistry reactions such as amino acid coupling and phosphonylation reactions.

4.4 Hydrothermal reactions

Due to the lack of positive results from the solution chemistry samples which made up the bulk of the experimental package, the decision was made to try to maximise the data obtained from the remaining experiments. It was decided to establish an experimental analysis protocol for the A-, B- and C- samples and a schedule for analysis to maximise the data that could be obtained from each remaining experiment. An analytical protocol was produced for each experiment to encompass a multitude of analytical techniques to return the maximum amount of data possible. Priority samples were identified and timescales for analysis established.

The purpose of the hydrothermal reactions was to look at the phosphorus species released during hydrothermal corrosion of iron phosphide and samples of Sikhote Alin meteorite containing the mineral schreibersite. Using natural acidic fluids, the aim was to identify
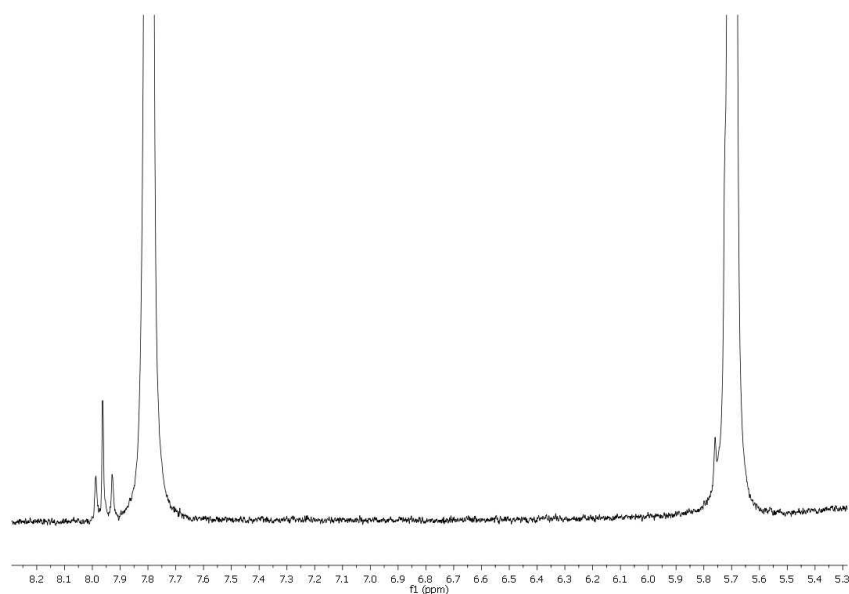
Spectrum 4.3: ^{1}H NMR spectrum (300 K, D$_2$O, 500.57 MHZ) of the lab based simulated repeat of sample G2 which was dry heated over a sand bath at 95℃ for *ca.* 72 hours. Phosphite (δ6.7, d, $^1J_{P\text{-}H}$= 630 Hz) and pyrophosphite (δ6.8, AA'XX', $^1J_{P\text{-}H}$= 672 Hz, $^2J_{P\text{-}P}$= 10 Hz, $^3J_{P\text{-}H}$= 8 Hz) can be identified in the spectrum.
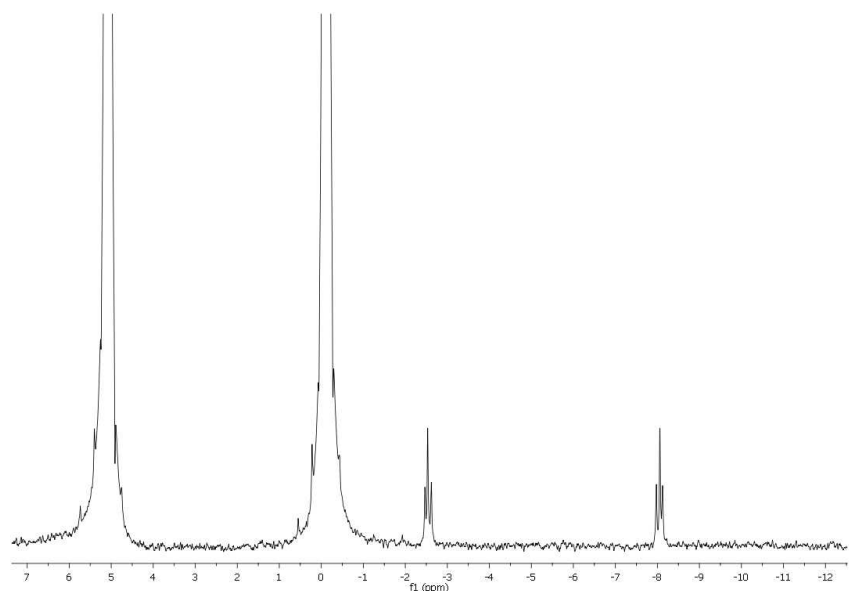
Spectrum 4.4: ^{31}P NMR spectrum (300 K, D$_2$O, 202.63 MHz) of the lab based simulated repeat of sample G2 which was dry heated over a sand bath at 95℃ for *ca.* 72 hours. As with the ^{1}H NMR spectrum, both phosphite (δ2.6, d, $^1J_{P\text{-}H}$= 631 Hz) and pyrophosphite (δ-5.5, AA'XX', $^1J_{P\text{-}H}$= 672 Hz, $^2J_{P\text{-}P}$= 11 Hz, $^3J_{P\text{-}H}$= 7 Hz) are identifiable in the spectrum.

the species produced and to quantify the amount over a given time period. As stated in Chapter 3, the chosen hydrothermal area was surveyed and specific sites chosen to give the widest variety of pH and temperature available for comparison of results.

The pH and temperature of each site was recorded prior to collection of fluids for each sample and were again recorded prior to sample preparation for sample analysis. The pH and temperature data are shown in Table 6.42 (Sectionhydroexptsiceland).

The pH of each sample was compared to the pH measured *in situ* at the time the sample was collected. In the majority of samples the pH had increased slightly since the time of collection in the field. This was an expected occurrence due to liberation of hydrogen during an acid/metal reaction though it was also considered that the decrease in temperature to room temperature could also have allowed for precipitation of some of the dissolved ions from solution which would also affect the pH of the sample.

Once the pH and temperature of each sample had been recorded, the next step was to begin sample analysis to confirm the presence of phosphorus species and to quantify the amounts released by hydrothermal corrosion. The first analytical method chosen for analysis was ICP-AES (Inductively Coupled Plasma - Atomic Emission Spectroscopy) and was chosen to identify and quantify the ionic composition of the water samples pre- and post-corrosion.

4.4.1 Water chemistry

The ICP-AES analysis of the water chemistry of the samples was conducted by Dr. Claire Cousins (UCL). Each water sample was first prepared by pre-filtering with Whatman Number 1 filter papers to remove any large solids from the fluid. The fluid was diluted to 70 mL using deionised water, then filtered through a Pall Corporation Acrodisc 32 mm 0.45 μm syringe filter to remove undissolved particulates. The 70 mL sample was then split between two 30 mL Nalgene bottles (35 mL in each bottle, filled up to the brim of the bottle to remove excess oxygen) which were acid washed by soaking in 50% HCl for 24 hours then rinsed with tap water (three times) and deionised water (three times) and left to air dry. One of the bottles for each sample was acidified by adding 2 drops of Conc. nitric acid while 2 drops of toluene were added to the other to prevent microbial growth. The samples were tightly sealed, the lids taped with Parafilm and each bottle labelled. The samples were then shipped to Dr. Cousins for subsequent analysis.

The levels of iron (Fe), nickel (Ni), phosphorus (P) and sulphur (S) were observed for each sample *via* this method and the contents of the sample were then compared to blank fluids from the source fluids from where the sample was collected, to map any changes to the composition of the fluids during the reaction process. The data are shown in Table 6.43.

Initial inspection of the data showed that the water samples all had quite large amounts of dissolved sulphur. This was thought to be due to the high amounts of H_2S gas which was bubbling though the system from volcanic venting. It was also noted that there was evidence of elemental sulphur deposits all around the sample site so the observation of high sulphur content was expected. The B- samples were also loaded with FeS which could account for the much higher sulphur content in these samples. Analysis of the hydrothermal mud by powder X-ray diffraction was conducted and is discussed later in this chapter. The

spectrum identified elemental sulphur as a major component of the mud present around the hydrothermal system (see Spectrum 4.35 and 4.8.0.2 for full details).

Analysis of the A- samples [Fe$_3$P (1.25 mM)] data showed there was an increase in both iron and phosphorus concentrations. Closer analysis of these data (Table 4.2) showed that in all cases there was an increase in the concentrations of dissolved iron and phosphorus in each sample compared to the background water sample. This would be expected as corrosion of iron phosphide in an acidic medium would liberate both into solution. It was also noticed that the samples which were maintained at temperature also had a larger increase. However, it was pH which showed the greatest effect on the amount of iron and phosphorus in solution. The general trend shows that the more acidic the fluid, the greater the concentration of phosphorus and iron in solution. It was also noticed that there were anomalies to the general rule and this was put down to precipitation of iron phosphates by oxidation which were then removed by filtration during sample preparation.

Analysis of the B- sample [Fe$_3$P (1.25 mM) + FeS (2.84 mM)] data (Table 4.2) showed a much higher level of dissolved iron in solution, with only a small increase in the dissolved phosphorus concentration. The high concentration of iron can be explained by the addition of iron sulphide which would dissolve readily in the acidic fluids. The low concentration of phosphorus on the other hand was somewhat perplexing. It was thought that the high concentration of iron and sulphur either inhibited corrosion of the iron phosphide or that the phosphorus was precipitated out of solution as ferric salts, due to the oxidation of iron.

The C- sample [Sikhote Alin meteorite pieces] data (Table 4.2) showed mixed results. The iron concentration in each sample showed an increase compared to the background sample and the nickel concentration has increased dramatically compared to the background readings, and compared to the iron phosphide experiments. This shows that there is definitely corrosion of the meteorite occurring as this is the only source of nickel present. The phosphorus concentrations only showed an increase in the most acidic of the samples. It is shown later in this chapter, that when an iron meteorite with schreibersite inclusions is corroded the iron matrix will corrode preferentially to the schreibersite. This would account for the increase in iron concentration in the samples with little or no visible increase in the phosphorus concentration. While the meteorite samples had been sectioned to expose the schreibersite inclusions for corrosion, the P-concentrations were expected to be small as the exposed schreibersite contributed only a fraction of the exposed surface area.

The increase in phosphorus concentration in only the most acidic sample shows that lower pH is required to accelerate corrosion to liberate P from the schreibersite inclusion while still embedded within the matrix. It is also possible that this meteorite sample had inclusions with a larger surface area than the other three samples allowing for better corrosion of the schreibersite. It is clear however that for rapid, consistent liberation of phosphorus from meteorite samples, the schreibersite inclusion would need to be liberated from the iron matrix and then allowed to corrode independently as this would maximise the surface area available for corrosion resulting in more rapid production of P.

While completing the water data analysis, an opportunity arose to analyse the fluid samples by Ion chromatography *via* Prof. Matthew Pasek at the University of South Florida

Sample	Fe	Background	+/-	P	Background	+/-
A1	3.25	1.27	1.98	0.53	0.53	0.00
A2	39.96	4.11	35.85	1.01	-0.01	1.02
A3	72.11	2.23	69.89	2.20	0.03	2.17
A4	9.56	3.35	6.22	0.53	-0.04	0.57
A5	6.20	1.26	4.94	1.20	0.54	0.66
A6	17.28	31.40	-14.13	0.62	0.08	0.53
A7	16.10	1.51	14.59	0.77	0.00	0.77
A8	48.22	4.15	44.07	2.28	0.25	2.04
B1	73.00	4.11	68.89	0.00	-0.01	0.01
B2	71.05	2.23	68.82	0.01	0.03	-0.01
B3	33.01	1.26	31.75	0.11	0.54	-0.43
B4	66.70	31.40	35.29	0.18	0.08	0.10
B5	71.41	1.51	69.90	0.10	0.00	0.10
B6	67.33	4.15	63.18	1.34	0.25	1.10
C1	7.82	3.35	4.48	16.78	-0.04	16.82
C2	0.35	1.26	-0.91	0.17	0.54	-0.37
C4	68.01	31.40	36.61	-0.01	0.08	-0.10
C5	11.97	4.11	7.86	0.06	-0.01	0.07

Table 4.2: Table comparing levels of iron and phosphorus present in hydrothermal samples (sample sets A, B and C) compared to the untreated water samples from the respective sample sites. It can be seen that there is generally an increase in both iron and phosphorus concentrations but which is dependent on pH and temperature of sample site.

	UCL (ICP-AES)	USF (IC)	ESD
A1	0.53	0.40	0.10
A2	1.01	0.92	0.06
A3	2.20	1.72	0.34
A4	0.53	0.20	0.23
A5	1.20	1.50	0.21
A6	0.62	0.47	0.10
A7	0.77	0.70	0.05
A8	2.28	2.00	0.20
B1	0.00	0.08	0.06
B2	0.01	0.10	0.06
B3	0.11	0.20	0.06
B4	0.18	0.16	0.02
B5	0.10	0.16	0.04
B6	1.34	1.01	0.24
C1	16.78	14.30	1.75
C2	0.17	0.06	0.08
C4	-0.01	0.04	0.04
C5	0.06	0.07	0.01

Table 4.3: Table comparing the phosphorus concentrations obtained from the UCL sample analyses (Inductively Coupled Plasma- Atomic Emission Spectroscopy [ICP-AES]) with those from the USF sample analyses (Ion Chromatography [IC]). Concentrations in mg/L and have been fully adjusted for dilution. The ESD value shown is the standard deviation calculated for the difference between UCL and USF data for the phosphorus concentration.

(USF). The aim of this analysis was to both to duplicate the UCL results using a slightly different technique (IC) and also to attempt to identify and quantify the different phosphorus oxidation states present in the fluids giving individual quantities for P_{III} and P_V species present in each sample.

This technique was originally reported by Pech *et al.* (2009) and was used to identify the presence of phosphite $[P^{3+}]$ in hydrothermal fluids from Hot Creek Gorge, California at low nanomolar levels.[33] A follow up paper by Pech *et al.* in 2011 (which included Prof. Pasek) used ion chromatography to investigate the redox cycle of phosphorus present in the environment. It showed the presence of hypophosphite $[P^{1+}]$, phosphite $[P^{3+}]$ and phosphate $[P^{5+}]$ in water samples with hypophosphite and phosphite detected at levels up to 1.3 μM and 2.0 μM respectively.[215] Two 1.5 mL portions of each acidified sample were packaged into Eppendorf vials and sent to Prof. Pasek at USF for ICP-MS and ion chromatography analysis.

Quantitative data on the phosphorus quantities present in each sample were measured by ICP-MS to compare to the ICP-AES water data obtained by Dr. Cousins at UCL. The data were corrected for dilution, averaged for the number of results per sample and then compared to the UCL concentration data (see Table 4.3). The concentration data from USF showed good correlation with the initial concentration data obtained by UCL though lower values were obtained on all samples. This is believed to be due to the time difference between analysis of the samples and the precipitation of phosphate from the samples. With good data correlation of the two different analytical methods, it was decided to continue with the analysis of phosphorus species on each sample.

4.4.2 Ion chromatography speciation analysis

Analysis of the phosphorus speciation was conducted by Prof. Matt Pasek at USF on a Perkin Elmer S-200 HPLC fitted with an IonPac AS17-C ion chromatography column with the total phosphorus measured on the attached, in-line Perkin Elmer Elan DRC II ICP-MS. The system was calibrated using standards for hypophosphite, phosphite and phosphate ($\times 10^{-3}$ to $\times 10^{-7}$ M), using 50μL injections, monitoring m/z= 31 with a 250 ms dwell time. The mobile phase was run at 1.5 mL/min using 3.5 mM KOH for 2 minutes then increased linearly to 35 mM concentration over 10 minutes. The concentration was then held at 35 mM for a further 10 minutes to ensure all species were eluted. Previous investigation of this method of analysis by Prof. Pasek, published in Pech *et al.* (2011) has shown that speciation data can be obtained for samples as low as $\times 10^{-6}$ M (μM) concentrations.[215]

As with the sample preparation for the ICP-AES analysis, the samples were diluted with ultra-pure deionised water then filtered using Millipore 0.45μm syringe filters to remove any undissolved particulates. The samples were analysed using the same injection method as the standards and the data obtained are shown in Table 6.45. Examples of the ion chromatography can be seen in Spectrum Figure 4.3.

The data obtained from USF by this method was far in excess of expectations as it allowed for detection of the various P species to sub-ppm levels. Upon analysing the data it can
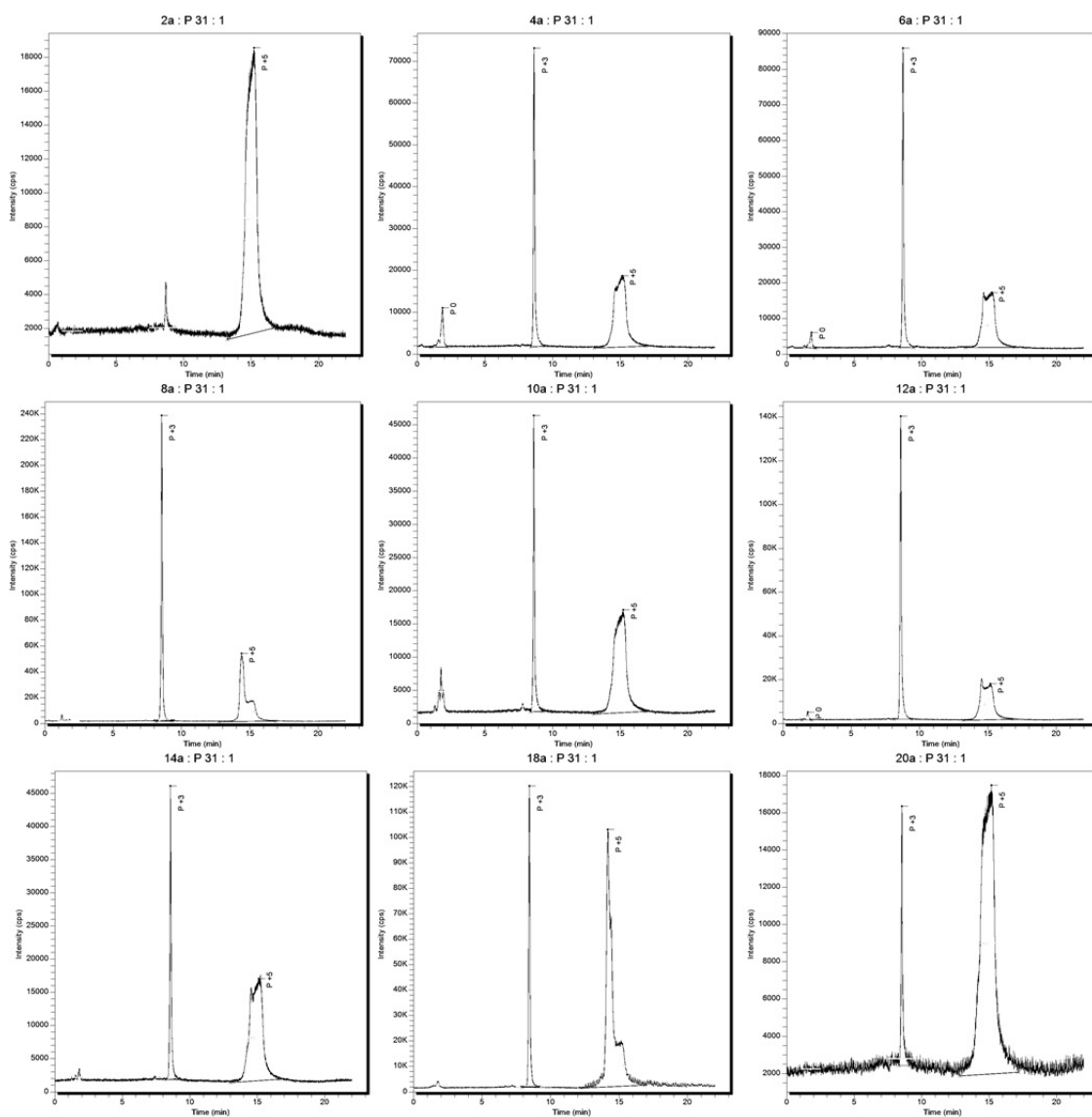
Figure 4.3: Examples of HPLC ion chromatography traces produced for the A samples analysed by Prof. Matt Pasek at USF. The traces shows peak elution times of the individual oxidation state species. The lower oxidation state species elute first and the higher oxidation state species eluting last. Standards of the various oxidation state species were run as references in different concentrations to give expected elution times for each species for comparison to the sample results while the area under each peak can be integrated and compared to the standard samples to calculate the concentration of each species present in the sample. Typical results show the elution of hypophosphite [P^{1+}] at *ca.* 2 mins, phosphite [P^{3+}] at *ca.* 8.5 minutes and phosphate [P^{5+}] as a broad/double peak at *ca.* 14 minutes. Phosphate elutes broadly due to an increasing pH corresponding to increasing concentration of potassium hydroxide. At the time of elution, the system is approaching pH 12, is around the pK_{a3} of phosphate so there is co-elution of HPO_4^{2-} and PO_4^{3-} species. (Sample correlation: 2a= DI water, 4a= A1, 6a= A2, 8a= A3, 10a= A4, 12a= A5, 14a= A6, 16a= A7, 18a= A8, 20a= DI water.)

clearly be seen that both phosphite [P^{3+}] and phosphate [P^{5+}] are present in all samples and in significant amounts. In some samples it was even possible to identify hypophosphite [P^{1+}] in solution though in very small quantities. The speciation data confirmed that, during the corrosion of iron phosphide [Fe$_3$P] or schreibersite [(FeNi)$_3$P], the main corrosion product is phosphite. Phosphate is naturally produced by further oxidation though at a much slower rate. One issue with this method was that, although it was able to specify the oxidation state of the phosphorus, it did not tell you the exact speciation and thus it has to be assumed that the concentrations given for [P^{3+}] and [P^{5+}] are indeed phosphite and phosphate. With the apparent success of the quantitative species analysis of phosphorus in the samples by ion chromatography, it remained to confirm the structural speciation by ^{31}P NMR analysis.

4.4.3 NMR analysis

ICP-AES data from UCL and ICP-MS data from USF had been used to quantify the amount of phosphorus available in each sample and then ion chromatography used to quantify the oxidation state of phosphorus present in each sample but the actual phosphorus species had not been fully identified. As discussed in the previous section, both P^{3+} and P^{5+} species were observed and were quantifiable though this method was not able to confirm without doubt if they are phosphite and phosphate, this was only assumed. ^{31}P NMR analysis was utilised to fully identify and confirm the species obtained in the samples.

Each sample was treated using the hydroxide method (used previously, see Chapter 2) for removal of iron from the samples to allow NMR analysis to be undertaken. Each sample was analysed initially using a 300 MHz NMR spectrometer for 320 scans for quick confirmation of species present. An insert of deuterium oxide [D$_2$O] was inserted into the NMR tube of each sample for locking purposes.

4.4.3.1 A Samples - Fe$_3$P

The initial attempts at NMR analysis were very hit and miss due to the presence of dissolved iron in the samples. Attempts were made to remove all the iron though it was realised that full removal would be impossible due to the nature of the samples. In some cases multiple treatments of hydroxide were required and filtration using Millipore 0.45μm filters were required to remove fine suspended particulate iron before a clean NMR could be obtained.

^{31}P NMR analysis was completed on all samples (A1-A8). It was clear that the spectra showed the main species present in all the samples was phosphite [H$_2$PO$_3^-$]. Phosphate was also visible in some of the spectra taken at 300 MHz but not visible in all. This was due to a change of chemical shift of phosphate and phosphite with changing pH of the sample. This effect led to the phosphate peak merging with one of the phosphite peaks so that it was no longer visible in the spectrum, although it could be identified by integration of the phosphite peaks (as this would result in one peak having a larger peak area than the other).

The presence of phosphite was expected as the main product from these experiments based on previous laboratory work while phosphate was also expected to be present in small amounts due to its presence in the natural fluids. A typical NMR spectrum from these samples is shown in Spectrum 4.5 and 4.6. The full NMR data for the A samples is shown in Table 6.46.
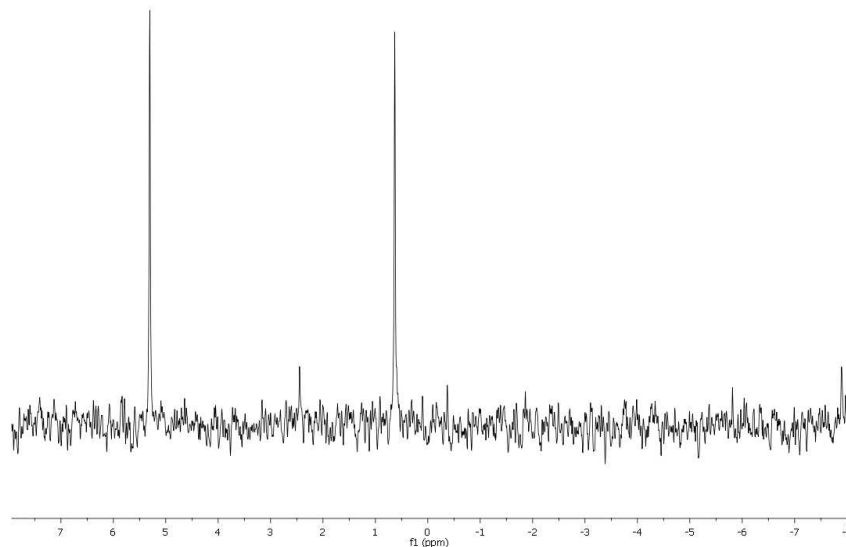
Spectrum 4.5: ^{31}P NMR spectrum (300 K, D_2O, 121.46 MHz) of sample A1 showing the presence of phosphite ($\delta 3.0$, d, $^1J_{P\text{-}H}$= 568 Hz) and possibly phosphate ($\delta 2.5$, s). Phosphate cannot be absolutely confirmed in this spectrum due to the low resolution of the spectrum (peak signal is barely above the background signal). The resolution and clarity of the spectrum could be improved by increasing the number of scans (to 2048 scans) or by increasing the frequency of the instrument (using 500 MHz instead of 300 MHz instrument).

As can be seen from Spectrum 4.5 the presence of phosphite is clearly visible as a doublet in the NMR spectrum ($\delta 3.0$, d) and what appears to be a peak indicating phosphate ($\delta 2.5$, s), while in Spectrum 4.6 phosphite ($\delta 3.2$, d) and phosphate ($\delta 3.0$, s) are both clearly visible. It was possible to identify phosphite and phosphate in all A- samples analysed either by chemical shifts or by peak area integration.

The ^{31}P NMR data were obtained using a 300 MHz instrument and only 320 scans which means the sample strength of phosphorus in solution must be quite strong. The quality of the spectra obtained could be improved by using a higher resolution instrument (500 MHz) or by increasing the number of scans (from 320 to 2048 for example). Increasing the resolution and the scans would give the optimal improvement in the quality of the spectra allowing for very low concentration samples to be analysed. One major issue faced by these samples was the presence of iron which is known to interfere with NMR spectroscopy. The presence of only a small amount of iron in the sample can lead to peak broadening, poor resolution and in some cases the instrument will fail to observe any signals in the spectrum so the full removal of iron is required to observe high quality spectra.

4.4.3.2 B Samples - Fe$_3$P + FeS

As with the A samples, iron was a major issue with the B samples. The levels of iron in each sample were very high due to the addition if iron sulphide, meaning that two or three
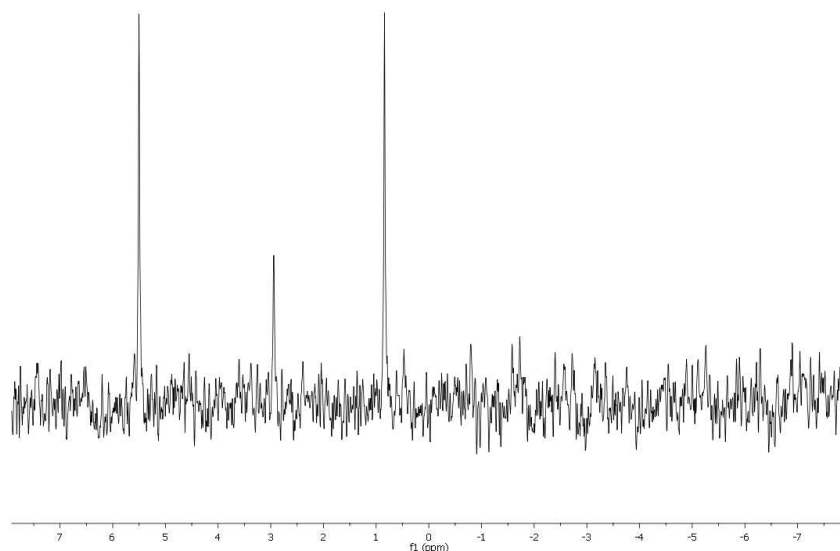
Spectrum 4.6: ^{31}P NMR spectrum (300 K, D$_2$O, 121.46 MHz) of sample A5 showing the presence of phosphite (δ3.2, d, ^{1}J$_\text{P-H}$= 565 Hz) and phosphate (δ3.0, s). A low concentration of phosphate was expected in the samples as there should be an amount of dissolved phosphate present in natural water samples.

treatments with sodium hydroxide were required to remove enough iron from the sample to obtain a usable spectrum. A second issue was the concentration of phosphorus in the samples. Looking at the data from ICP-AES and IC analysis, the B samples are clearly much lower in concentration than the A samples. Either they have corroded much less than the pure iron phosphide samples, or the phosphite and phosphate have precipitated out of solution in greater quantities.

Using the 300 MHz spectrometer it was almost impossible to identify the signals from the background noise so it was required to use the 500 MHz spectrometer and an extended number of scans (2048 scans) to obtain clear and usable spectra. As with the A samples, it was possible to identify phosphite and/or phosphate in all samples (B1-B6) either by chemical shift or by peak area integration. Examples of the spectra obtained are shown in Spectrum 4.7 and Spectrum 4.8. The full NMR data for the B samples are shown in Table 6.46.

As can be seen in Spectrum 4.7, phosphite (δ5.2, d) is easily visible in the spectrum though there is no indication of phosphate in this spectrum. In Spectrum 4.8 it is possible to see a trace of phosphate (δ2.7, s. Tentative assignment as a very weak signal) as well as the expected phosphite (δ3.1, d) signal. The lack of identifiable phosphate peaks in the B samples was believed to be due to the highly reduced conditions in which the samples have been corroded (due to the presence of iron sulphide in the sample solutions). However, based on the ion chromatography data, the levels of phosphate present in the B samples were similar to the levels found in the A samples which would discount this theory. An explanation of this may be the difference in time (*ca.* 6 weeks) between NMR analysis and species analysis by ion chromatography allowing for further sample oxidation or that the sample preparation for NMR analysis aids in the precipitation of phosphate from solution.
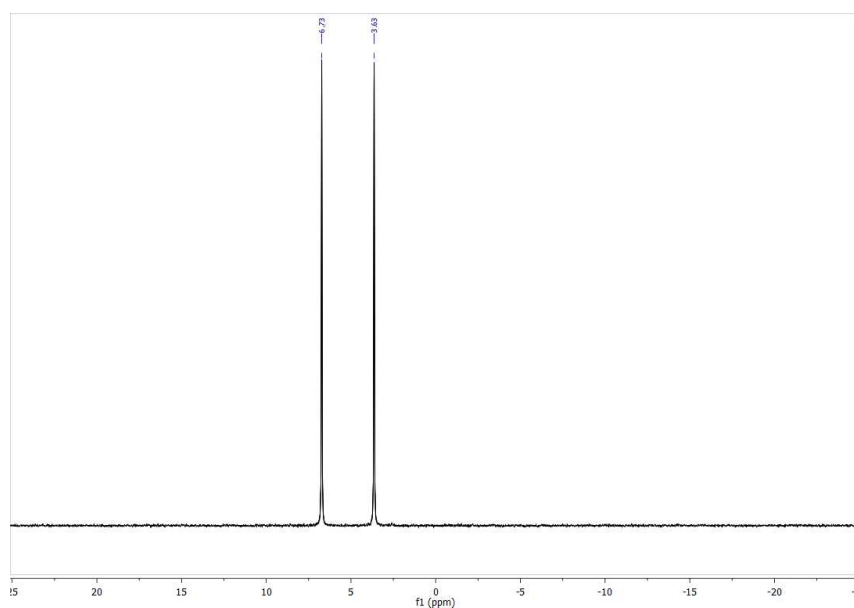
Spectrum 4.7: ^{31}P NMR spectrum (300 K, D$_2$O, 202.63 MHz) of sample B1 (2,048 scans) showing the presence of phosphite (δ5.2, d, ^{1}J$_{P\text{-}H}$= 628 Hz). No phosphate is visible in this spectrum suggesting that the phosphate peak is under one of the phosphite peaks, or that no phosphate was present due to the added sodium sulphide and the reducing nature of the experiment.
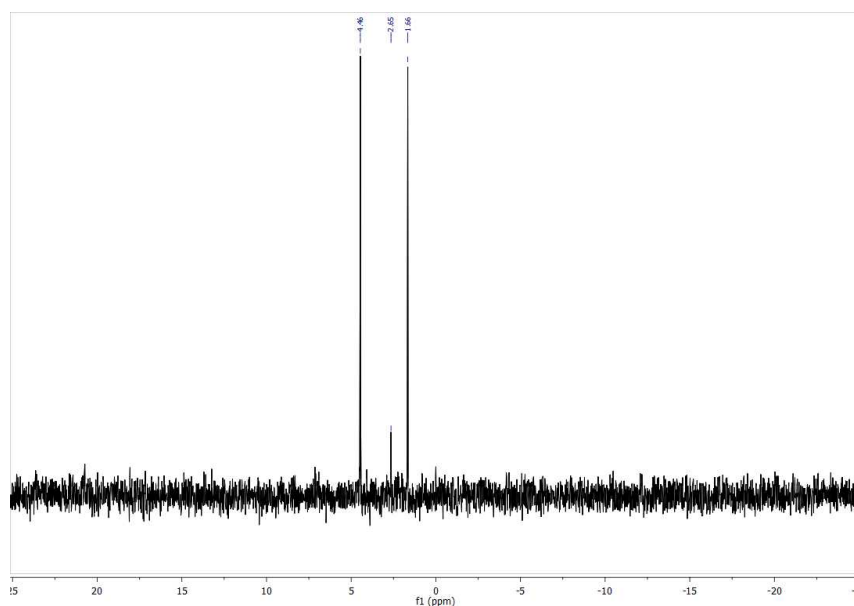
Spectrum 4.8: ^{31}P NMR spectrum (300 K, D$_2$O, 202.63 MHz) of sample B2 (2,048 scans) showing the presence of phosphite (δ3.1, d, ^{1}J$_{P\text{-}H}$= 567 Hz) and a very small amount of phosphate (δ2.7, s) is visible in the spectrum.

4.4.3.3   C Samples - Sikhote Alin meteorite samples

The C samples were prepared for NMR using the same method as for the A and B samples. Due to the low concentrations of the samples identified in the ICP-AES and IC data it was decided to analyse the samples using the 500 MHz spectrometer for 2048 scans as with the B samples to obtain usable spectra. The iron removal was conducted using the sodium hydroxide method as stated previously and after filtering a drop of sodium sulphide was added to confirm the full removal of iron from the sample. Examples of the NMR spectra obtained are shown in Spectrum 4.9 and Spectrum 4.10. The full NMR data for the C samples are shown in Table 6.46.
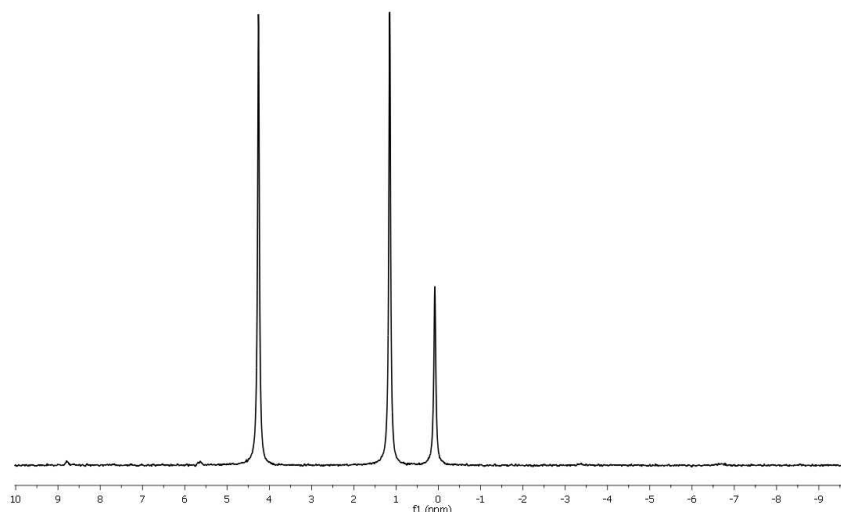
Spectrum 4.9: ^{31}P NMR spectrum (300 K, D_2O, 202.63 MHz) of sample C1 showing the presence of phosphite (δ2.7, d, $^1J_{P\text{-}H}$= 629 Hz) and phosphate (δ0.1, s). This spectrum was significant proof that it is possible to produce a reduced oxidation state phosphorus species in significant amounts by hydrothermal corrosion (weathering) of an iron meteorite containing schreibersite under natural geological and prebiotically plausible conditions.

Analysis of Spectrum 4.9 confirmed the presence of both phosphite (δ2.7, d) and phosphate (δ0.1, s) while Spectrum 4.10 also showed phosphite (δ2.7, d) and phosphate (δ0.0, s). It was possible to identify both phosphite and phosphate in all four C samples from the respective NMR spectra.

It was noticed that the NMR spectra shown in Sections 4.4.3.1, 4.4.3.2 and 4.4.3.3 that the proportion of phosphate looked much higher than the speciation data observed by ion chromatography. Investigation of this was undertaken by calculating the percentage composition for each phosphorus species present in the NMR spectra by integration of the peak areas for each sample and comparing this to the percentage of total phosphorus for phosphite and phosphate present in the IC data. The comparison data is shown in Table 6.47.

The data shows that, in almost all cases, the percentage of phosphate is smaller in samples than the observed percentage in the IC data. The NMR analysis was completed much earlier than the IC analysis which could suggest that some oxidation of the samples has occurred between the NMR analysis and the IC analysis. The levels of total phosphorus
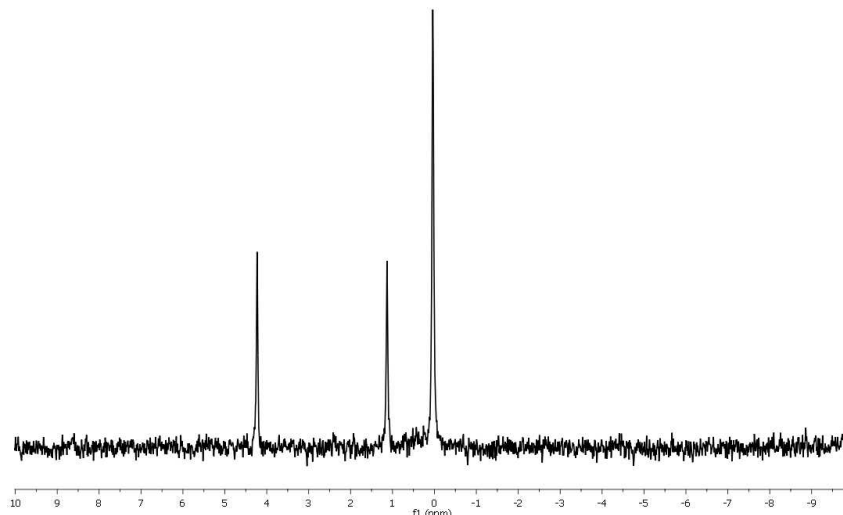
Spectrum 4.10: ^{31}P NMR spectrum (300 K, D$_2$O, 202.63 MHz) of sample C4 showing the presence of phosphite (δ2.7, d, ^{1}J$_{P-H}$= 628 Hz) and phosphate (δ0.0, s). This spectrum was further proof of the ability to produce reduced oxidation state phosphorus species directly from iron meteorites by weathering under natural geological and plausible prebiotic conditions.

observed in the IC analysis are comparable (though slightly lower) to the total P observed by ICP-AES which was conducted prior to the NMR analysis which would seem to confirm that oxidation is responsible for the change in speciation over time.

Now, with good quality NMR spectra identifying the phosphorus species present in the samples, it shows without doubt that acidic hydrothermal corrosion of iron phosphite and schreibersite will produce significant amounts of reduced oxidation state phosphorus for inclusion in prebiotic chemical reactions. The next step was to use the phosphite produced by these reactions in an attempt to simulate prebiotic chemistry such as the production of pyrophosphite or the formation of isohypophosphate.

4.5 Formation of pyrophosphite by simulated geothermal heating of phosphite

As discussed in Chapter 2 and shown earlier in this chapter, it is possible to produce pyrophosphite by dry heating of phosphite. The temperature required to facilitate the formation of pyrophosphite is strongly dependent on the metal ions present and also the degree of solid dispersion achieved in the sample. The temperature required has been shown to be between 90℃ (Ca and Mg) and 160℃ (Na) for effective condensation to occur. The presence of iron in the sample can have a significant effect on the formation of pyrophosphite and is dependent on the oxidation state. Earlier work in this thesis has shown that the presence of Fe^{3+} has little effect on the formation of pyrophosphite while Fe^{2+} will inhibit the formation of pyrophosphite up to *ca.* 180℃. It has also been shown that above 180℃, the reduction of phosphite to hypophosphite will occur in the presence of Fe^{2+}. As the hydrothermal corrosion samples all contained iron mainly in the Fe^{2+} form, formation of pyrophosphite would require either oxidation of the iron to the Fe^{3+} oxidation

state, or its removal from the system. As it would be difficult to oxidise Fe^{2+} present in the samples without oxidising the phosphite it was decided to remove the ferrous iron for the following experiments.

4.5.1 A Samples

Each sample was filtered to remove any unreacted Fe_3P and a 5 mL aliquot of the fluids was taken. Each sample was adjusted to *ca.* pH 12 using NaOH (1 M, dropwise addition), filtered and then re-adjusted to *ca.* pH 4 using HCl (1 M, dropwise addition). The sample was reduced to dryness on a rotary evaporator and the residues of each sample were ground using a mortar and pestle, placed into a round-bottomed flask, and dry heated under flowing N_2 to 90℃ over a sand bath for 72 hours. Each sample was dissolved in D_2O (1 mL) then transferred to an NMR tube using a long-nose Pasteur pipette and analysed using the 500 MHz NMR spectrometer. Examples of the obtained spectra are shown in Spectrum 4.11 and Spectrum 4.12. Full NMR data are shown in Table 6.50.
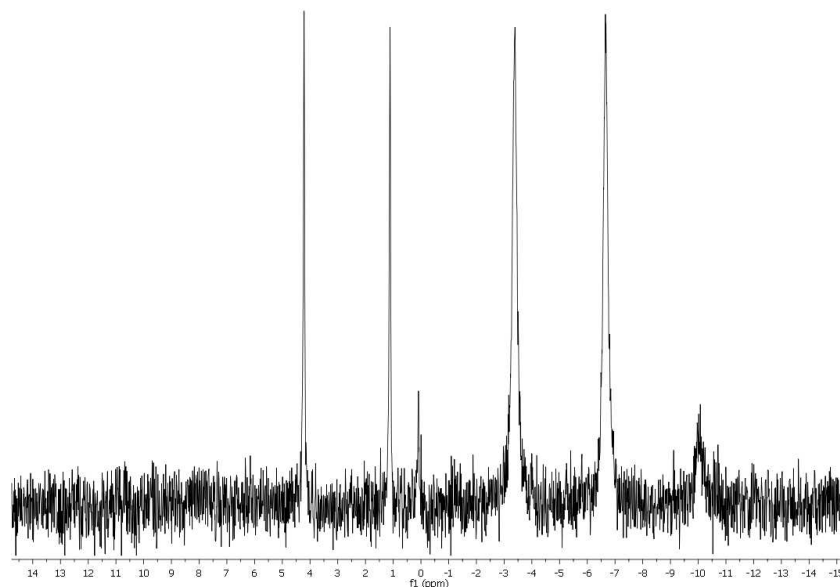
Spectrum 4.11: ^{31}P NMR spectrum (300 K, D_2O, 202.63 MHz) spectrum of sample A1 fluid residues which was dry heated in a round bottom flask to 90℃ for 72 hours under flowing N_2. There is a visible presence of phosphite ($\delta 2.7$, d, $^1J_{P-H}= 628$ Hz) and phosphate in the sample. There is also an unresolved doublet at -5.0 ppm which is assumed to be pyrophosphite though there is no visible AA'XX' spin system.

It is seen from Spectrum 4.11 that the dry heating of sample A1 appears to have produced pyrophosphite (δ-5.0, d) though the resolution of the spectrum is poor. This visible doublet has a coupling constant of 668 Hz which is indicative of pyrophosphite though without the tell-tale AA'XX' spin system splitting it is unconfirmed. However, in Spectrum 4.12 the spectrum shows the presence of pyrophosphite (δ-5.0, AA'XX'), phosphite ($\delta 3.0$, d) and phosphate ($\delta 1.2$, s). There are also indications of the presence of either pyrophosphate (δ-6.1, s) or isohypophosphate though the peak definition is such that it is impossible to give a clear assignment due to poor resolution.

The AA'XX' spin system is clearly visible in the A5 sample spectrum which confirms without doubt that pyrophosphite was produced by dry heating this sample. Using this result as indication of the expected chemical shifts and coupling constants for pyrophosphite un-
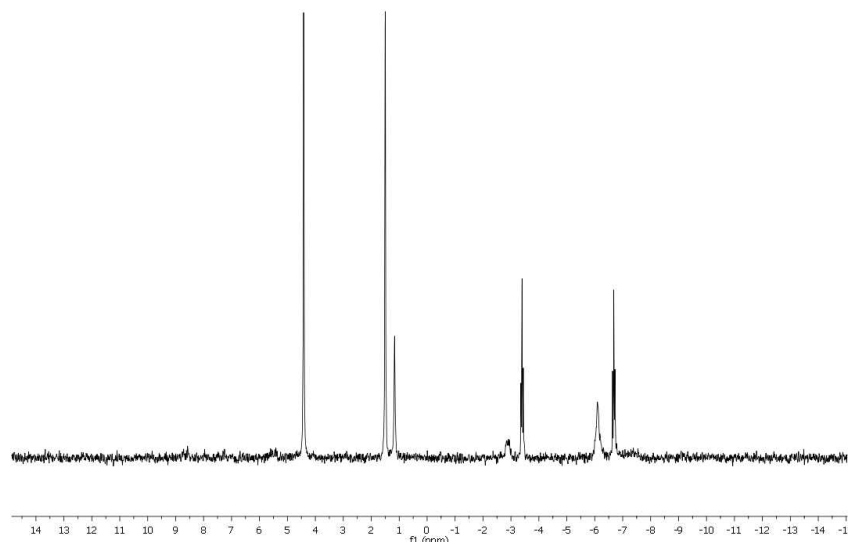
Spectrum 4.12: ^{31}P NMR spectrum (300 K, D$_2$O, 202.63 MHz) spectrum of sample A5 fluid residues which was dry heated in a round bottom flask to 90℃ for 72 hours under flowing N$_2$. The AA'XX' spin system indicative of pyrophosphite (δ-5.0, AA'XX', $^1J_{\text{P-H}}$= 665 Hz, $^2J_{\text{P-P}}$= 10 Hz, $^3J_{\text{P-H}}$= 8 Hz) is clearly visible in the spectrum while phosphite (δ3.0, d, $^1J_{\text{P-H}}$= 594 Hz) and phosphate (δ1.2, s) are also present.

der these experimental conditions, there is no doubt that pyrophosphite has been observed in the other samples. Five of the A samples (A1-A5) were subjected to dry heating and all heated samples successfully produced pyrophosphite. This shows that naturally produced phosphite from hydrothermal corrosion of iron phosphide is capable of production of pyrophosphite under plausible prebiotic conditions. The poor resolution in some of the dry heated spectra was thought due to small amounts of iron still present in the samples despite best efforts to remove all iron from the fluids.

4.5.2   B Samples

The B samples were again filtered to remove all unreacted material. A 5 mL aliquot of each sample was taken and treated with NaOH via dropwise addition to pH 12 to remove dissolved iron from the fluids. The samples were then filtered and adjusted back to pH 4 using dropwise addition of HCl. The sample was then reduced to dryness on a rotary evaporator and ground using a mortar and pestle. The sample was then dry heated in a round bottom flask at 90℃ for 72 hours under flowing N$_2$. The samples were then dissolved in D$_2$O (1 mL) and subjected to ^{31}P NMR analysis.

The samples were first analysed on the 500 MHz instrument using 2048 scans with no usable spectra obtained. The sample spectra showed no presence of phosphorus which seemed odd as they had been previously confirmed to contain phosphite prior to heating. Thinking that there was an issue with iron content in the samples suppressing the spectrum, it was decided to again treat the samples with NaOH to pH 12 and also treat them with sodium sulphide [NaS] in an attempt to make sure all dissolved iron was removed. The samples were again filtered, dehydrated, ground and dry heated as done previously. The residues were again dissolved in D$_2$O (1 mL) and this time analysed on the 500 MHz instrument

using 8192 scans.

Again the spectra showed no phosphorus peaks. Two possibilities remained, first that there was still iron present in the sample interfering with the instrument, or second that there was very little or no phosphorus present in the sample. Based on previous experience of sample analysis, it was possible that there was an amount of iron still suspended in the samples causing the interference. It was noted that the phosphite levels in the B samples were quite low and there was the possibility that during treatment of the samples the phosphite had precipitated out of solution. It was decided, due to analysis issues, to abandon further attempts at pyrophosphite production from the B samples and move on to the C samples.

4.5.3   C Samples

As with the A samples, the C samples were filtered and the iron meteorite samples placed in a vacuum desiccator to dry. Each sample was adjusted to *ca.* pH 12 using NaOH (1 M, dropwise addition), filtered and then re-adjusted to *ca.* pH 4 using HCl (1 M, dropwise addition). The sample was reduced to dryness on a rotary evaporator and the residues of each sample were ground using a mortar and pestle, placed into a round-bottomed flask, and dry heated under flowing N_2 to 90℃ over a sand bath for 72 hours. Each sample was dissolved in D_2O (1 mL) then transferred to an NMR tube using a long-nose Pasteur pipette and analysed using ^{31}P NMR spectroscopy using the 500 MHz spectrometer. Full NMR data are shown in Table 6.51.
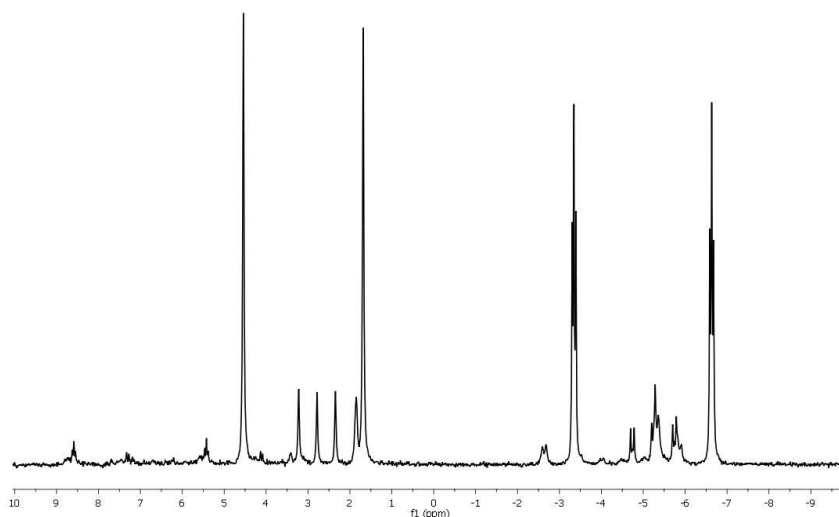
Spectrum 4.13: ^{31}P NMR spectrum (300 K, D_2O, 202.63 MHz) spectrum of sample C1 fluid residue which was dry heated in a round bottom flask to 90℃ for 72 hours under flowing N_2. The AA'XX' spin system indicative of pyrophosphite (δ-5.0, AA'XX', $^{1}J_{P-H}$= 665 Hz, $^{2}J_{P-P}$= 10 Hz, $^{3}J_{P-H}$= 8 Hz) is clearly visible in the spectrum with phosphite (δ3.1, d, $^{1}J_{P-H}$= 582 Hz) and phosphate (δ1.8, s) also clearly visible. What appear to be linear polyphosphates are also present in the sample with which have been tentatively assigned as isohypophosphate [$HP_2O_6^{3-}$], pyrophosphate [$P_2O_7^{4-}$] and linear tripolyphosphate [$P_3O_{10}^{5-}$] though with significant overlap these species have not been fully confirmed.

Spectrum 4.13 is of a dry heated phosphite produced from hydrothermal corrosion of sample C1, a piece of Sikhote Alin meteorite which contains an inclusion of schreibersite [$(FeNi)_3P$]. The spectrum very much resembles that of the iron phosphite with phosphite (δ3.1, d),

phosphate ($\delta 1.8$, s) and pyrophosphite (δ-5.0, AA'XX') all visible. There were other species visible in the spectrum which were tentatively assigned and include isohypophosphate [$HP_2O_6^{3-}$], pyrophosphate [$P_2O_7^{4-}$] and linear tripolyphosphate [$P_3O_{10}^{5-}$], though there was some significant overlap on the peaks so it was not possible to work out all the chemical shifts and give coupling constants.

The production of pyrophosphite directly from the hydrothermal corrosion of schreibersite from the Sikhote Alin meteorite was a result with great significance as this showed it is possible to go from a meteorite to a reduced oxidation state and activated phosphorus species under prebiotic conditions. The three other meteorite samples (C2, C4 and C5) were all analysed under dry-heating conditions with the view of forming condensed $PPi_{(III)}$. The major issue with that the meteorite samples was the rate of corrosion of schreibersitic minerals in the meteorites is much slower than that of pure iron phosphide (due to the presence, in the former, of nickel). The surface area of schreibersite available for corrosion was one issue and presence of nickel in the schreibersite made the inclusion more noble than the iron matrix and thus the matrix corroded preferentially. This meant that for these samples there was a greater concentration of iron in solution while only a small amount of phosphorus was liberated during corrosion. The slower rate of corrosion meant that either the concentration of phosphite in solution in the C samples was too low to successfully produce pyrophosphite, or the amount produced was below the sensitivity of the NMR analysis. The C1 sample was successful as corrosion has been induced at the lowest pH at high temperature meaning accelerated corrosion of this sample was possible.

The surprise found during analysis of Spectrum 4.13 was the presence of isohypophosphate (tentatively assigned as δ-4.2, dd, J_{P-H} = 641 Hz $^2J_{P-P}$ = 18 Hz), δ-5.7, d, $^2J_{P-P}$ = 24 Hz), pyrophosphate (δ-10.4, s) and linear tripolyphosphate (presence indicated by visible triplet δ-21.6 though not possible to assign all chemical shifts as significant overlap with the isohypophosphate peaks).

This shows something not really witnessed before, as the formation of isohypophosphate was thought to be a reaction between pyrophosphite and phosphate in solution while pyrophosphate and linear tripolyphosphate were only thought to be formed by heating phosphate to over 180℃. It was decided to investigate further the production of these species to try to identify the mechanism for their production in the system.

4.6   Production of isohypophosphate

The initial investigation was to look at the reaction of pyrophosphite with phosphate to see how rapidly this would produce isohypophosphate. This involved dissolving sodium phosphate dibasic [Na_2HPO_4, 0.142 g, 1 mmol] and sodium pyrophosphite [$Na_2H_2P_2O_5$, 0.198 g, 1 mmol] in deionised water (20 mL) and adjusting to pH 4 with HCl (1 M, dropwise addition). An aliquot (1 mL) of the solution was taken for analysis by ^{31}P NMR spectroscopy. The sample was incubated at room temperature and was resubmitted for analysis by ^{31}P NMR every 30 minutes for 2.5 hours (Full NMR data are shown in Table 6.52). This timescale was chosen as the NMR instrument was open access and this was considered to be the longest time possible for a sample to be in solution (after heating

and dissolving) and completion of analysis by NMR. A table of the percentage composition of the sample for this experiment is shown in Table 4.4.

Sample	PO_4^{3-} (%)	$H_2P_2O_5^{2-}$ (%)	HPO_3^{2-} (%)	Total	$HP_2O_6^{3-}$ (%)
0	26.21	68.94	4.85	100.00	0.00
30	26.45	69.07	4.48	100.00	0.00
60	25.34	71.23	3.42	99.99	0.01
90	24.52	70.75	4.72	99.99	0.01
120	25.40	69.11	4.88	99.39	0.61
150	26.19	69.84	3.97	100.00	0.00

Table 4.4: Table of composition of the time analysis NMR samples for the production in solution of isohypophosphate [$HP_2O_6^{3-}$] by the reaction of pyrophosphite [$H_2P_2O_5^{2-}$] with phosphate [PO_4^{3-}]. The sample was analysed every 30 minutes up to 150 minutes. The Percentages allocated to each sample run was calculated by integration of the peak areas for each identified component in the spectrum and is the percentage of available phosphorus in solution.

Analysis of the NMR spectra showed that even after 2.5 hours, isohypophosphate was not visible or identifiable in the spectrum. With no visible peaks for isohypophosphate it was hoped to use the calculated percentage composition from the peak area integration to confirm production of isohypophosphate but this proved to produce highly variable results and was therefore unreliable for absolute identification. As the amount of isohypophosphate produced in the C1 sample was visible in the NMR spectra and it was not visible in this experiment, it would seem that the solution method of production for isohypophosphate could not produce the levels observed in the C1 sample. This would indicate that there is an alternative method of production for isohypophosphate to produce the levels observed.

The next step in the investigation of the production of isohypophosphate was to dry heat the phosphite and the phosphate together to see if this method produce commensurate amounts of isohypophosphate as those identified in the C1 sample. This experiment involved dissolving sodium phosphate dibasic [Na_2HPO_4, 0.142 g, 1 mmol] and calcium phosphite [$Ca(H_2PO_3)_2 \cdot H_2O$, 0.220 g, 1 mmol] in deionised water (20 mL) then adjusting to pH 4 using HCl (1 M, dropwise addition). A 5 mL aliquot was taken and reduced to dryness at 40℃ on top of a drying oven. The sample was collected and ground using a mortar and pestle then placed in a round bottom flask and dry heated at 90℃ on a sand bath under flowing N_2 for 72 hours. An aliquot of the sample (*ca.*0.5 g) was then dissolved in 1 mL D_2O and analysed by ^{31}P NMR spectroscopy.

Analysis of Spectrum 4.14 shows the presence of pyrophosphate (δ-7.1, s), pyrophosphite (δ-4.9, AA'XX') and isohypophosphate (δ-4.1, dd) though the signals are very weak (*ca.* 1% total available phosphorus) and barely distinguishable from the baseline. Based on this evidence it appeared that the dry heating of phosphate and phosphite together was the method for the production of isohypophosphate at the concentrations observed in the dry heated C1 sample.

To further confirm this theory, sodium phosphate [Na_2HPO_4, 0.142 g, 1 mmol] and calcium phosphite [$Ca(H_2PO_3)_2 \cdot H_2O$, 0.220 g, 1 mmol] were mixed by milling in a mortar and pestle for 5 minutes then transferred to a round bottom flask then dry heated on a sand bath at 90℃ under flowing N_2 for 72 hours. An aliquot of the sample (*ca.* 0.5 g) was then dissolved in 1 mL of D_2O and analysed by ^{31}P NMR spectroscopy. Full NMR data
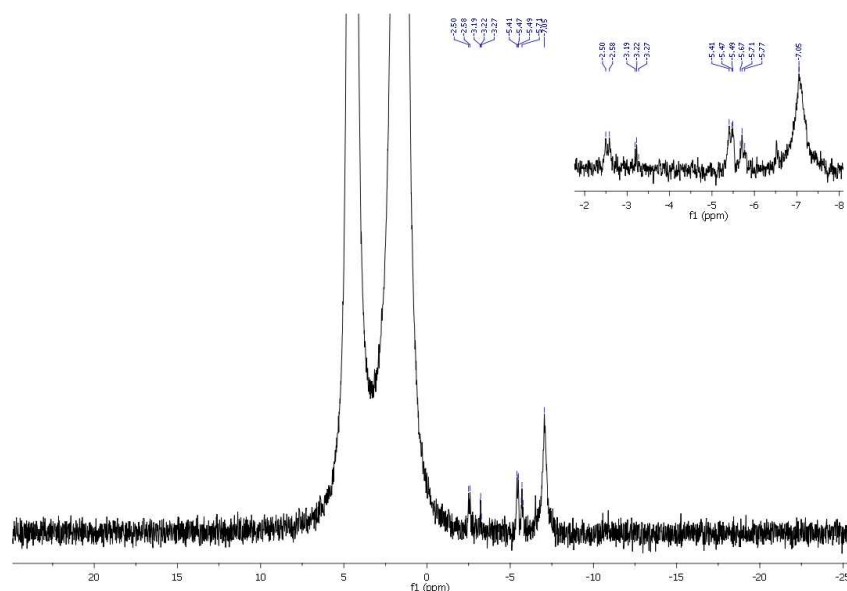
Spectrum 4.14: ^{31}P NMR spectrum (300 K, D_2O, 202.63 MHz) of phosphate and phosphite dissolved in deionised water, adjusted to pH 4 and was reduced to dryness by heating at 40℃ under aerobic conditions on top of a drying oven. The sample was then dry heated under anaerobic conditions at 90℃ for 72 hours. Signals representative of pyrophosphite (δ-4.9, AA'XX', $^1J_{P\text{-}H}$= 673 Hz, $^2J_{P\text{-}P}$= 8 Hz, $^3J_{P\text{-}H}$= 6 Hz), isohypophosphate (δ-4.1, dd, $J_{P\text{-}H}$ = 648 Hz $^2J_{P\text{-}P}$ = 16 Hz), δ-5.6, d, $^2J_{P\text{-}P}$ = 12 Hz) and pyrophosphate (δ-7.1, s) are visible in the spectrum though the signals are weak.

are shown in Table 6.52.

Upon analysis of the spectrum (Spectrum 4.15) it was clear that the dry heating alone of phosphate and phosphite was not the method of production of isohypophosphate observed in the dry heating experiments. Only phosphate, phosphite and pyrophosphite were visible in the sample. After careful consideration of each step of the process it was identified that in all the samples where the isohypophosphate was observed, the solvated samples had first been reduced to dryness on top of the drying oven at 40℃ before dry heating. It seemed implausible that this step was responsible, but as the only remaining option this was the next step to investigate.

Sodium phosphate dibasic [Na_2HPO_4, 0.142 g, 1 mmol] and calcium phosphite [$Ca(H_2PO_3)_2 \cdot H_2O$, 0.220 g, 1 mmol] were dissolved in deionised water (20 mL) and then adjusted to pH 4 using HCl (1 M, dropwise addition). A 5 mL aliquot was taken and reduced to dryness at 40℃ on top of a drying oven. The sample was collected and ground using a mortar and pestle then an aliquot of the sample (*ca.* 0.5 g) was dissolved in 1 mL of D_2O and analysed by ^{31}P NMR spectroscopy. Full NMR data are shown in Table 6.52.

Analysis of the spectrum showed the presence of the starting materials, phosphate (δ0.7, s) and phosphite (δ2.9, d). The spectrum also shows the presence of isohypophosphate (δ-4.1, dd) along with pyrophosphate (δ-6.2, s) which confirmed that dehydration of the sample on the oven at 40℃ was responsible for the production of the observable quantities of isohypophosphate visible in the dry heating samples. This was very unexpected as it was believed that the production of isohypophosphate was only possible by reaction in solution between pyrophosphite and phosphate. Granted, only 1% of total available phosphorus was converted to isohypophosphate but it was produced in less than 24 hours and by slow evaporation of the sample at 40℃.
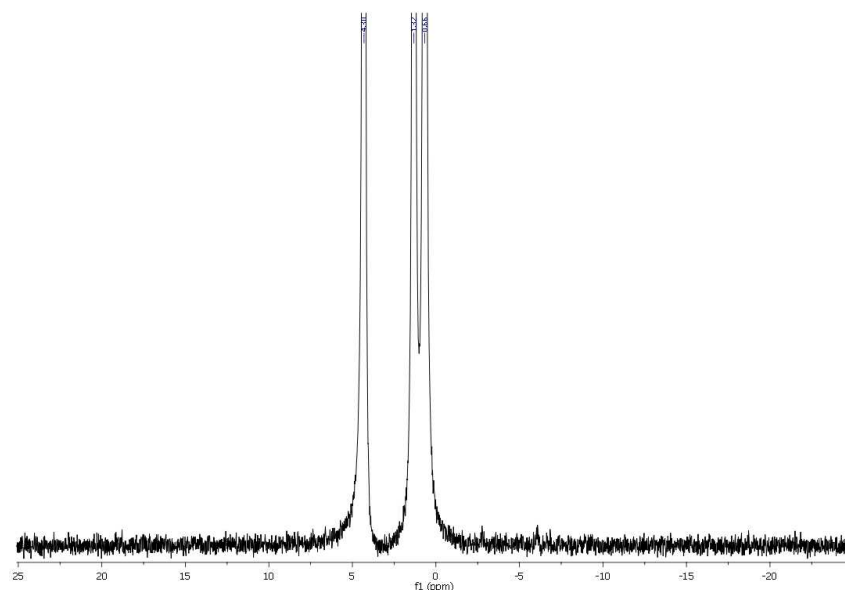
Spectrum 4.15: ^{31}P NMR spectrum (300 K, D_2O, 202.63 MHz) which was heated at 90℃ under aerobic conditions in a sand bath. The spectrum clearly shows the presence of the starting materials with phosphite ($\delta 2.8$, d, $^{1}J_{P-H}$= 598 Hz) and phosphate ($\delta 0.7$, s) visible in the spectrum. There are also peaks visible in the baseline which are indicative of pyrophosphite (δ-4.46, $^{1}J_{P-H}$= 675 Hz. No further coupling constants are reportable due to the quality of the spectrum) but as the spectrum is not sufficiently clear, the AA'XX' spin system is not visible.
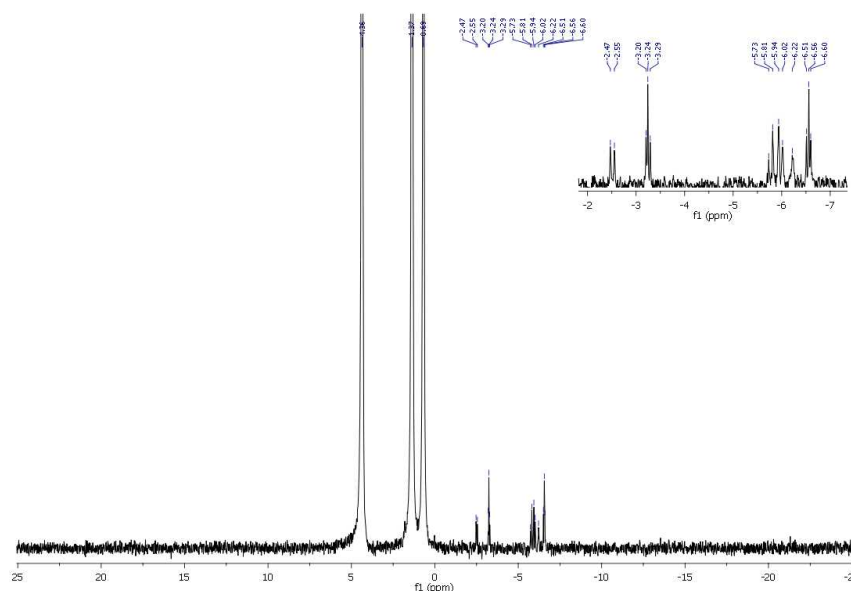
Spectrum 4.16: ^{31}P NMR spectrum (300 K, D_2O, 202.63 MHz) of phosphite and phosphate dissolved in deionised water, adjusted to pH 4 and heated at 40℃ under aerobic conditions on top of a drying oven. The sample spectrum clearly shows the presence of pyrophosphite (δ-4.9, AA'XX', $^{1}J_{P-H}$= 673 Hz, $^{2}J_{P-P}$= 10 Hz, $^{3}J_{P-H}$= 8 Hz), isohypophosphate (δ-4.1, dd, J_{P-H} = 662 Hz $^{2}J_{P-P}$ = 17 Hz, δ-6.0, d, $^{2}J_{P-P}$ = 17 Hz), δ-5.6, d, $^{2}J_{P-P}$ = 12 Hz) and pyrophosphate (δ-6.2, s) in the sample. This confirms that it is the process of dehydration of the sample that is responsible for the production of isohypophosphate.

This condensation reaction gives rise to a product in isohypophosphate which is capable of both phosphorylation and phosphonylation reactions. Isohypophosphate has the same P-O-P bonding system as pyrophosphite meaning it has the same potential as an energy currency and is less susceptible to hydrolysis than pyrophosphite but is also less reactive than pyrophosphite. There is work ongoing within the Kee group to fully investigate isohypophosphate and its potential in prebiotic chemistry. Having discovered the apparent mechanism for its production it was decided to further investigate the conditions required for isohypophosphate production to try to increase yield of this very interesting product.

4.6.1 pH Effects on the formation of isohypophosphate by evaporation method

The effects of pH on the formation of isohypophosphate were investigated by preparation of two samples. for the first sample, sodium phosphite [NaH_2PO_3, 0.05 g, 0.5 mmol] and sodium phosphate dibasic [Na_2HPO_4, 0.07 g, 0.5 mmol] were dissolved in deionised water and adjusted to pH 4 using dropwise addition of HCl (1 M). The second sample was prepared in the same manner though the pH was adjusted to pH 7 using dropwise addition of NaOH (1 M). Both samples were transferred to a petri dish and heated at 40℃ on top of a drying oven for 72 hours. Both samples were allowed to cool to room temperature, ground in a mortar and pestle and then dissolved in D_2O (1 mL) and analysed by ^{31}P NMR spectroscopy. Full NMR details are shown in Table 6.53.
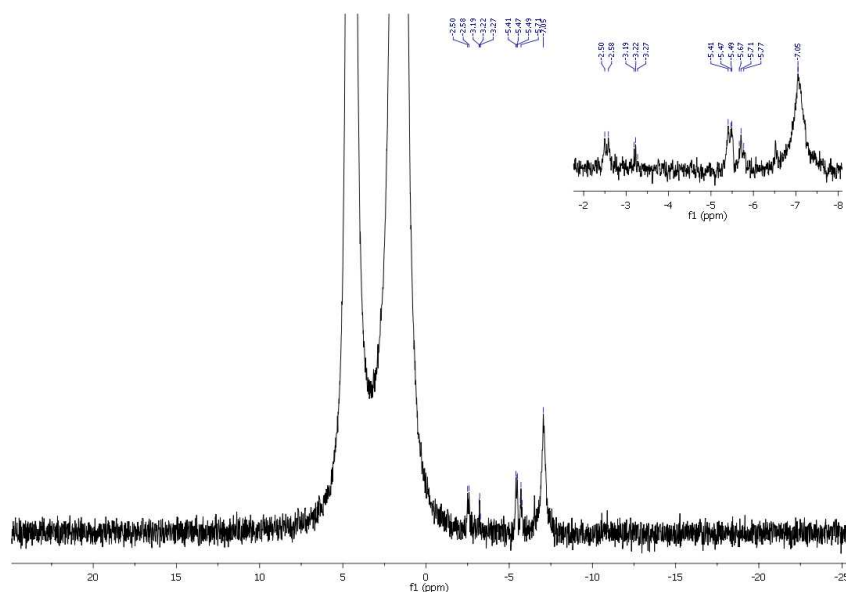
Spectrum 4.17: ^{31}P NMR spectrum (300 K, D_2O, 202.63 MHz) for the pH 4 sample which was heated at 40℃ under aerobic conditions on top of a drying oven. The sample spectrum clearly shows the presence of phosphite (δ3.1, d, $^1J_{P\text{-}H}$= 585 Hz) and phosphate (δ1.6, s) and weak signals in the baseline which are representative of pyrophosphite (δ-4.9, AA'XX', $^1J_{P\text{-}H}$= 673 Hz, $^2J_{P\text{-}P}$= 8 Hz, $^3J_{P\text{-}H}$= 6 Hz), isohypophosphate (δ-4.1, dd, $J_{P\text{-}H}$ = 648 Hz $^2J_{P\text{-}P}$ = 16 Hz), δ-5.6, d, $^2J_{P\text{-}P}$ = 12 Hz) and pyrophosphate (δ-7.1, s).

Interpretation of the pH 4 spectrum (Spectrum 4.17) showed the presence of phosphite (δ3.1, d,) and phosphate (δ1.62, s) but there were also weak signals in the baseline of the spectrum which were indicative of isohypophosphate (δ-4.1, dd), pyrophosphite (δ-4.9, AA'XX') and pyrophosphate (δ-7.1, s). Analysis of the pH 7 spectrum (Spectrum 4.18)
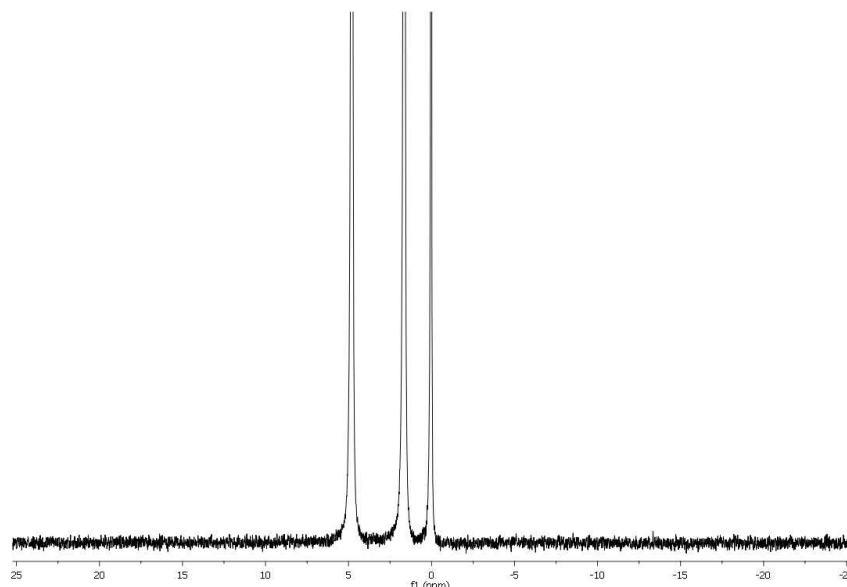
Spectrum 4.18: ^{31}P NMR spectrum (300 K, D$_2$O, 202.63 MHz) for the pH 7 sample which was heated at 40°C under aerobic conditions on top of a drying oven. The sample only shows the presence of the starting materials, phosphite ($\delta 3.2$, d, $^1J_{\text{P-H}}=$ 640 Hz) and phosphate ($\delta 0.0$, s).

showed only the presence of phosphite ($\delta 3.2$, d) and phosphate ($\delta 0.0$, s). The presence of isohypophosphate, pyrophosphite and pyrophosphate was confirmed in the pH 4 sample using a spiking technique in which each suspected component was added individually from a known sample and the spiked sample then analysed by ^{31}P NMR after each addition. The final spectrum obtained of the pH4 sample with all successful spikings is shown in Spectrum 4.19 (see Table 6.53 for full details)..

The spiked sample spectrum (Spectrum 4.19) confirmed the presence of pyrophosphite (δ-4.8, AA'XX'), isohypophosphate (δ-4.1, dd) and pyrophosphate (δ-7.4, s) in the sample. The results show that an acidic pH (*ca.* pH 4) is required for the formation of isohypophosphate as is required for the formation of pyrophosphite. This experiment also showed that it was possible to produce both pyrophosphite and pyrophosphate via this evaporation method at 40°C, although the total condensed phosphorus species present in the sample was only around 1% of the total available phosphorus in the sample.

4.6.2 Effects of SMOW on the formation of isohypophosphate by evaporation method

An investigation of the effects of SMOW on the formation of isohypophosphate was undertaken using two samples which were prepared by taking sodium phosphite [NaH$_2$PO$_3$, 0.05 g, 0.5 mmol] and sodium phosphate dibasic [Na$_2$HPO$_4$, 0.07 g, 0.5 mmol] and dissolving in SMOW (5 mL) and deionised water (5 mL) respectively. Both samples were transferred to petri dishes with no further manipulation of the samples and heated at 40°C on top of a drying oven for 72 hours. The samples were allowed to cool to room temperature before being ground by mortar and pestle, dissolved in D$_2$O and submitted for ^{31}P NMR analysis. Full NMR data are shown in Table 6.55.

Interpretation of the spectrum of the SMOW sample (Spectrum 4.20) showed the presence
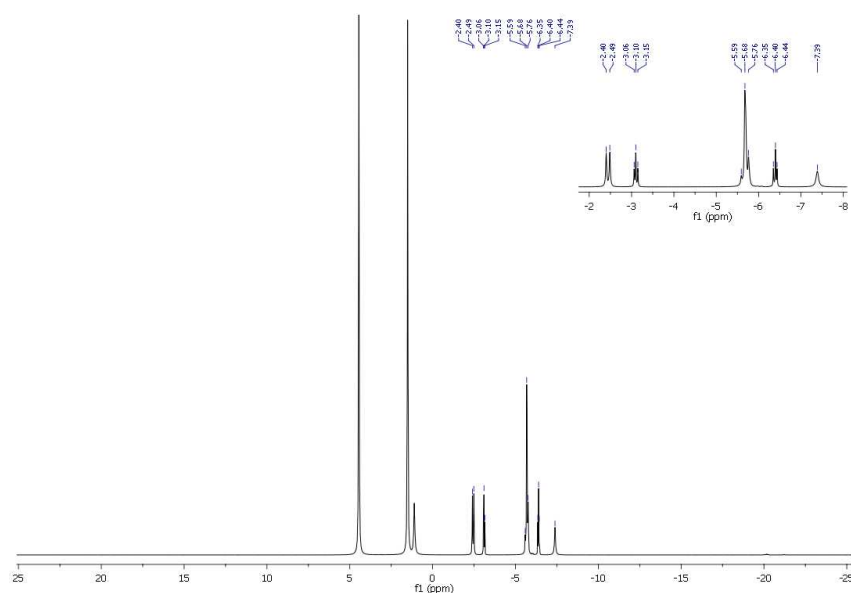
Spectrum 4.19: ^{31}P NMR spectrum (300 K, D$_2$O, 202.63 MHz) of the spiked pH 4 sample. The process of spiking the sample with known samples of the suspected constituents was used to confirm their presence in the sample. This process was used to confirm the presence of pyrophosphite (δ-4.8, AA'XX', $^1J_{P-H}=$ 669 Hz, $^2J_{P-P}=$ 10 Hz, $^3J_{P-H}=$ 8 Hz), isohypophosphate (δ-4.1, dd, $J_{P-H}=$ 654 Hz $^2J_{P-P}=$ 18 Hz), δ-5.7, d, $^2J_{P-P}=$ 18 Hz) and pyrophosphate (δ-7.4, s) in the pH 4 sample.

Spectrum 4.20: ^{31}P NMR spectrum (300 K, D$_2$O, 202.63 MHz) of phosphite and phosphate dissolved in SMOW which was heated at 40℃ under aerobic conditions on top of a drying oven. The sample spectrum clearly shows the presence of phosphite (δ2.9, d, $^1J_{P-H}=$ 608 Hz), phosphate (δ0.7, s), pyrophosphite (δ-4.9, AA'XX', $^1J_{P-H}=$ 673 Hz, $^2J_{P-P}=$ 10 Hz, $^3J_{P-H}=$ 8 Hz), isohypophosphate (δ-4.1, dd, $J_{P-H}=$ 662 Hz $^2J_{P-P}=$ 17 Hz, δ-6.0, d, $^2J_{P-P}=$ 17 Hz), δ-5.6, d, $^2J_{P-P}=$ 12 Hz) and pyrophosphate (δ-6.2, s).

Spectrum 4.21: ^{31}P NMR spectrum (300 K, D$_2$O, 202.63 MHz) of phosphite and phosphate dissolved in deionised water which was heated at 40℃ under aerobic conditions on top of a drying oven. The sample spectrum clearly shows the presence of phosphite (δ2.8, d, ^{1}J$_{P-H}$= 577 Hz) and phosphate (δ0.7, s) but no other products are visible in the spectrum.

of phosphite (δ2.9, d) and phosphate (δ0.7, s), isohypophosphate (δ-4.1, dd), pyrophosphite (δ-4.9, AA'XX') and pyrophosphate (δ-6.2, s). The deionised water sample (Spectrum 4.21) showed only the presence of phosphite (δ2.8, d) and phosphate (δ0.7, s). The amount of condensed phosphorus species in the SMOW sample was roughly calculated to be again *ca.* 1% of the total available phosphorus. It can be seen that in the presence of SMOW, phosphate and phosphite will undergo reaction to form isohypophosphate and other condensed phosphorus species without need of pH adjustment while phosphate and phosphite in deionised water will not react without pH adjustment to pH 4. To confirm this, the above experiments were repeated and the samples adjusted to pH 4.

Analysis of the spectrum for the pH adjusted deionised water sample (Spectrum 4.22) showed the presence of phosphite (δ3.3, d), isohypophosphate (δ-4.1, dd) and pyrophosphite (δ-4.8, AA'XX'). The presence of phosphate in the sample was confirmed by integration of the sample peaks and is hidden under the phosphite peak at 1.8 ppm. The pH adjusted SMOW sample spectrum (Spectrum 4.23) identified the presence of phosphite (δ2.9, d) and phosphate (δ0.8, s), isohypophosphate (δ-4.4, dd), pyrophosphite (δ-4.9, AA'XX') and pyrophosphate (δ-8.0, s). The amount of condensed phosphorus species in the deionised water and SMOW samples was calculated to be around 1% in both cases.

It appears that though the presence of SMOW will aid in the formation of isohypophosphate without any sample alteration or preparation it is the pH which is the more important factor in the formation of isohypophosphate and pyrophosphite. Along with the production of isohypophosphate in the SMOW experiment, there is also observed production of pyrophosphite and pyrophosphate. It has been shown in previous work in Chapter 2 that pyrophosphite can be produced at 90℃ by dry heating in SMOW but never at such low temperatures. The production of pyrophosphate at these mild temperatures is very surprising as generally pyrophosphate is produced by heating phosphate to over 180℃. It was

Spectrum 4.22: ^{31}P NMR spectrum (300 K, D$_2$O, 202.63 MHz) of phosphite and phosphate dissolved in deionised water which was heated at 40℃ under aerobic conditions on top of a drying oven. The sample spectrum clearly shows the presence of phosphite (δ2.8, d, ^{1}J$_{P-H}$= 577 Hz) and phosphate (δ0.7, s) and also pyrophosphite (δ-4.8, AA'XX', ^{1}J$_{P-H}$= 671 Hz, ^{2}J$_{P-P}$= 10 Hz, ^{3}J$_{P-H}$= 8 Hz) and isohypophosphate (δ-4.1, dd, J$_{P-H}$ = 662 Hz ^{2}J$_{P-P}$ = 17 Hz, δ-6.0, d, ^{2}J$_{P-P}$ = 17 Hz).

Spectrum 4.23: ^{31}P NMR spectrum (300 K, D$_2$O, 202.63 MHz) of phosphite and phosphate dissolved in SMOW which was heated at 40℃ under aerobic conditions on top of a drying oven. The sample spectrum clearly shows the presence of phosphite (δ2.9, d, ^{1}J$_{P-H}$= 608 Hz), phosphate (δ0.7, s), isohypophosphate (δ-4.4, dd, J$_{P-H}$ = 650 Hz ^{2}J$_{P-P}$ = 15 Hz, δ-6.6, d, ^{2}J$_{P-P}$ = 17 Hz), pyrophosphite (δ-4.9, AA'XX', ^{1}J$_{P-H}$= 668 Hz, ^{2}J$_{P-P}$= 10 Hz, ^{3}J$_{P-H}$= 8 Hz) and pyrophosphate (δ-8.0, s).

decided to look closer at these individual reactions to try to determine the mechanism for production of the different species.

A series of four experiments was set up, two to look at the heating of phosphate in SMOW and deionised water while the remaining two would look at the heating of phosphite, again in SMOW and deionised water. As before, sodium phosphate dibasic [Na_2HPO_4, 0.1 g, 0.7 mmol] or sodium phosphite [NaH_2PO_3, 0.1 g, 1 mmol] was dissolved in either SMOW (5 mL) or deionised water (5mL) then adjusted to pH 4 using dropwise addition of HCl (1 M). The samples were heated at 40℃ on top of a drying oven for 72 hours. All samples were then allowed to cool to room temperature then ground in a mortar and pestle. An aliquot of each sample was taken (*ca.* 0.5 g) and dissolved in D_2O for ^{31}P NMR analysis. Full NMR data are shown in Table 6.55.
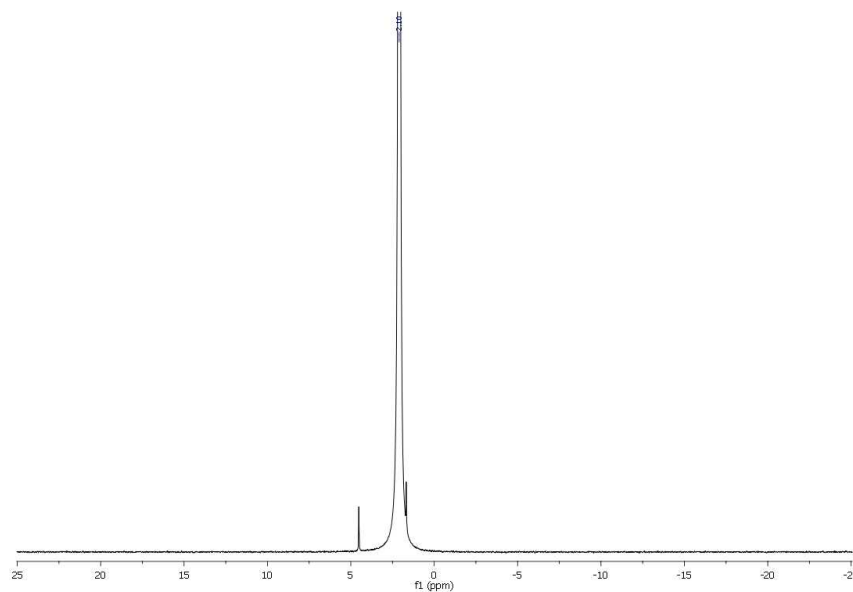
Spectrum 4.24: ^{31}P NMR spectrum (300 K, D_2O, 202.63 MHz) of sodium phosphate dibasic prepared in deionised water which was dry heated at 40℃ on top of a drying oven for 72 hours. The sample was adjusted to pH 4 using HCl (1 M) and then dehydrated prior to heating on top of the drying oven. The spectrum only shows the presence of phosphate (δ2.6, s).

Analysis of the spectra of the phosphate samples showed only phosphate present in both the SMOW (Spectrum 4.25, δ1.53, s) and deionised water (Spectrum 4.24, δ2.6, s) samples. It means therefore that there is an alternative mechanism for the production of pyrophosphate in these low temperature samples other than simple condensation. It would seem that the production of pyrophosphate requires the presence of phosphite in the sample though no obvious explanation could be found or given for this phenomenon. The mechanism for production of pyrophosphate in these samples may be due to oxidation or possibly the phosphite acts as a catalyst to the formation. This effect requires further investigation but due to limited time it was not possible to pursue this investigation further.

The analysis of the spectra from the phosphite samples however showed a different story. In previous work it was shown that sodium phosphite would produce pyrophosphite at temperatures of around 160℃ when adjusted to pH 4 but in the presence of SMOW, the formation of pyrophosphite was observed at 90℃. The spectrum of sodium phosphite in deionised water (Spectrum 4.26) showed only phosphite present (δ3.1, d) which was as expected due to the low temperature but the SMOW experiment spectrum (Spectrum
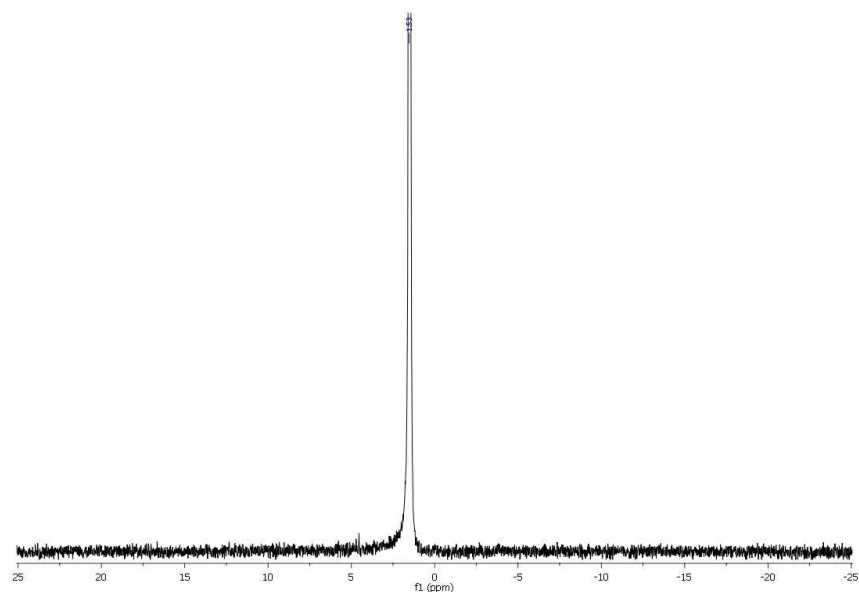
Spectrum 4.25: ^{31}P NMR spectrum (300 K, D_2O, 202.63 MHz) of sodium phosphate dibasic in SMOW which was dry heated at 40°C on top of a drying oven for 72 hours. The sample was adjusted to pH 4 using HCl (1 M) and then dehydrated prior to heating on top of the drying oven. The spectrum only shows the presence of phosphate (δ1.53, s).
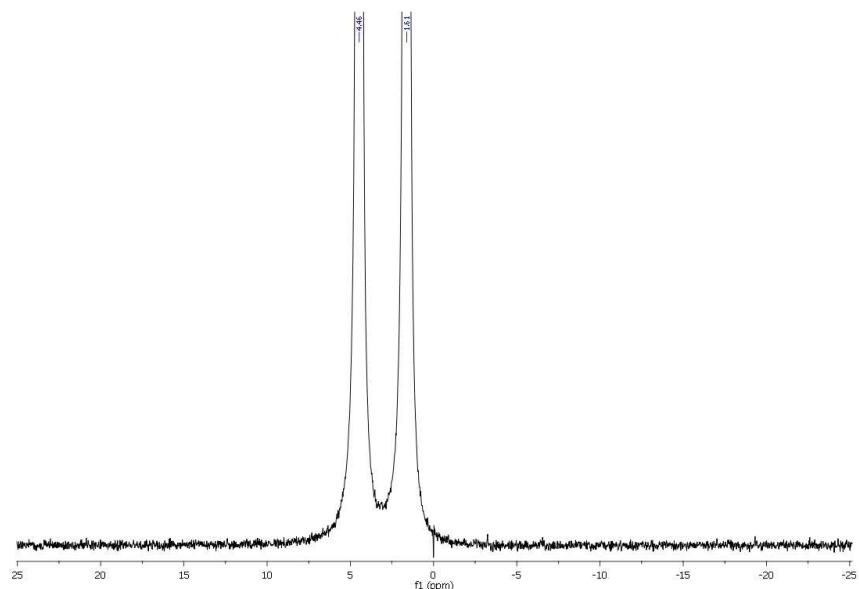
Spectrum 4.26: ^{31}P NMR spectrum (300 K, D_2O, 202.63 MHz) of sodium phosphite prepared in deionised water which was dry heated at 40°C on top of a drying oven for 72 hours. The sample was adjusted to pH 4 using HCl (1 M) and then dehydrated prior to heating on top of the drying oven. The spectrum only shows the presence of phosphite (δ3.1, d, $^1J_{P-H}$= 577 Hz).
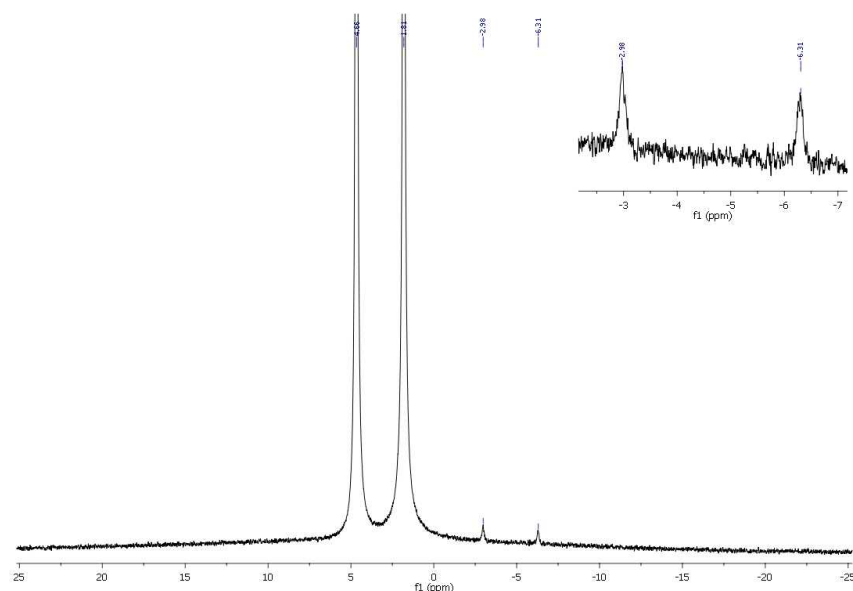
Spectrum 4.27: ^{31}P NMR spectrum (300 K, D$_2$O, 202.63 MHz) of sodium phosphite prepared in SMOW which was dry heated at 40℃ on top of a drying oven for 72 hours. The sample was adjusted to pH 4 using HCl (1 M) and then dehydrated prior to heating on top of the drying oven. The spectrum shows the presence of phosphite (δ3.2, d, ^{1}J$_{P-H}$= 577 Hz) and pyrophosphite (δ-4.6, AA'XX', ^{1}J$_{P-H}$= 673 Hz, further coupling constants were not able to be calculated due to the quality of spectrum) in the sample.

4.27) showed the presence of pyrophosphite (δ-4.6, AA'XX') though in very small amount even when heating to 40℃ for 72 hours.

It has been shown in the above experiments when heating at 40℃ in aerobic conditions that the amount of condensed phosphorus species produced was very small (*ca.* 1% total available P). It was decided to attempt to increase the yield of isohypophosphate and other condensed phosphorus species by increasing the temperature of the dry heating reaction from 40℃ to 60℃. It was hoped that the increase in temperature would increase the observed yield of isohypophosphate as was previously shown for the production of pyrophosphite.

4.6.3 Temperature effects on the formation of isohypophosphate by evaporation method

Having repeatedly observed the production of isohypophosphate and other condensed phosphorus species at 40℃ it was decided to try a slight increase of temperature to 60℃ to see if this would increase the yield obtained. One concern was that the previous reactions had been conducted under aerobic conditions which would not be the case on the early Earth so it was decided to conduct the reactions under anaerobic conditions to keep the chemistry more in line with all previous work in this thesis. The experiments would be carried out using the same reagents and quantities as the 40℃ experiments, under a constant flow of N$_2$ (*ca.* 1 bubble per second flow) to ensure anaerobic conditions with the samples analysed by ^{31}P NMR post-heating to confirm if any increase in yield of condensed phosphorus species was obtained.

Sodium phosphite [NaH$_2$PO$_3$, 0.05 g, 0.5 mmol] and sodium phosphate dibasic [Na$_2$HPO$_4$, 0.07 g, 0.5 mmol] were dissolved in SMOW (5 mL) and adjusted to pH 4 by dropwise

addition of HCl (1 M). The sample was then heated over a sand bath at 60℃ under flowing N_2 for 72 hours. A second experiment was set up using the same components but dissolved in deionised water (5 mL) for comparison. This sample was again heated over a sand bath at 60℃ under flowing N_2 for 72 hours. The samples were allowed to cool to room temperature then ground with a mortar and pestle. The samples were dissolved in D_2O (1 mL) and analysed by ^{31}P NMR spectroscopy. Full NMR data are shown in Table 6.56.
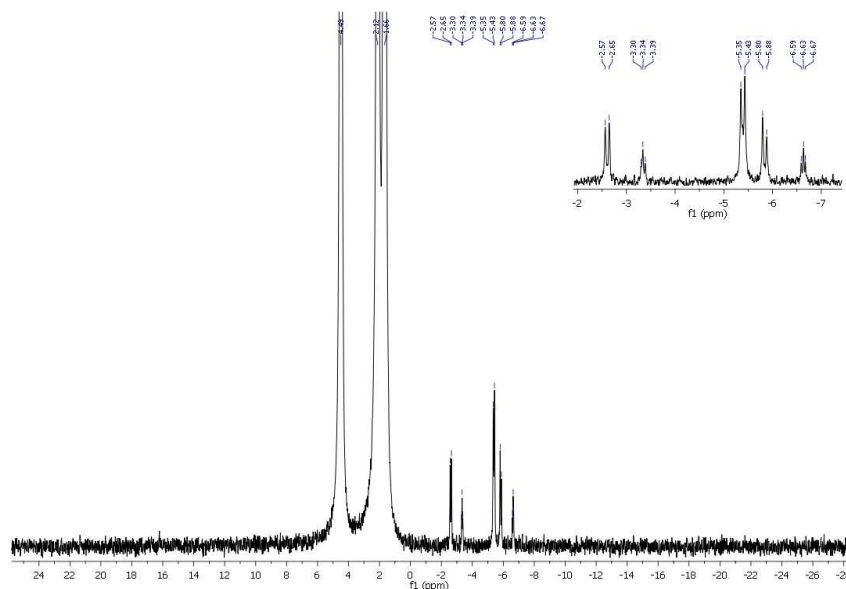
Spectrum 4.28: ^{31}P NMR spectrum (300 K, D_2O, 202.63 MHz) of the phosphite and phosphate sample prepared in SMOW and adjusted to pH 4 then heated to 60℃ for 72 hours under flowing N_2. The sample showed the presence of phosphate ($\delta 2.1$, s) and phosphite ($\delta 3.1$, d, $^1J_{P-H}$= 575 Hz) as well as the presence of pyrophosphite (δ-5.0, AA'XX', $^1J_{P-H}$= 671 Hz, $^2J_{P-P}$= 10 Hz, $^3J_{P-H}$= 8 Hz) and isohypophosphate (δ-4.0, dd, J_{P-H} = 563 Hz $^2J_{P-P}$ = 17 Hz, δ-5.8, d, $^2J_{P-P}$ = 17 Hz).

Analysis of the spectrum for the deionised water sample showed the presence of phosphate ($\delta 2.1$, s) and phosphite ($\delta 3.1$, d) and also the presence of pyrophosphite (δ-5.0, AA'XX') and isohypophosphate (δ-4.0, dd). The spectrum of the SMOW sample again showed the presence of pyrophosphite (δ-5.0, AA'XX') and isohypophosphate (δ-4.0, dd) as well as phosphate ($\delta 2.1$, s) and phosphite ($\delta 3.1$, d). Integration of the peak areas for both the deionised water and SMOW samples showed very little difference to those at 40℃ with still only around 1% of total phosphorus being converted to condensed P species though the ratio of isohypophosphate produced to pyrophosphite is smaller (*ca.* 3:1 from *ca.* 1:1).

It appears that the increase in temperature results in the solutions evaporating to dryness much quicker which limits the amount of isohypophosphate which can be produced by the experiment. Once the experiment is dry and providing the temperature is sufficient, then the formation of pyrophosphite becomes the dominant reaction. This would account for why there are only very small amounts visible in experiments where heating was conducted at 90℃.

The experiments in this section have shown that the slow evaporation (40℃) of phosphite and phosphate in solution are responsible for the formation of small amounts (*ca.* 1% available phosphorus) of both pyrophosphite and isohypophosphate, and that increasing the temperature of the system only succeeds in drying the samples faster, not generating
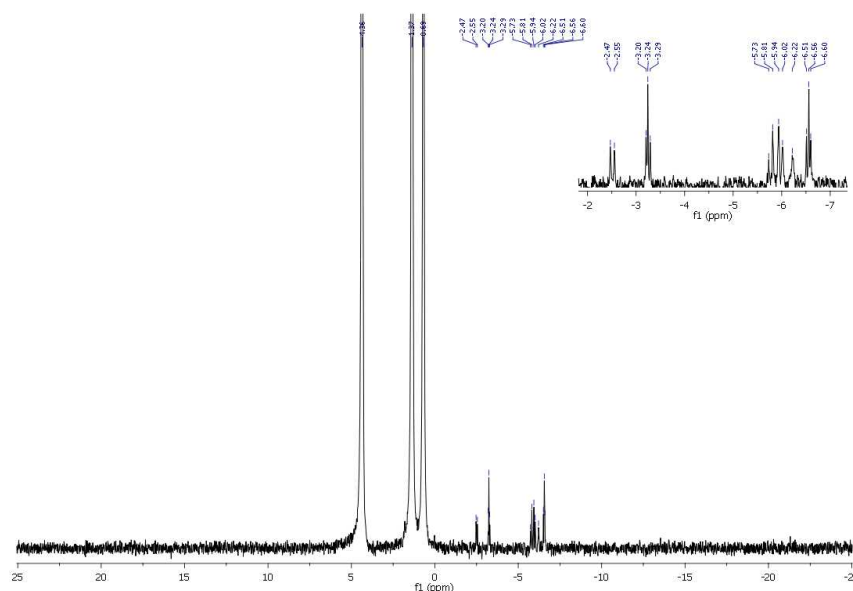
Spectrum 4.29: ^{31}P NMR spectrum (300 K, D$_2$O, 202.63 MHz) of the phosphite and phosphate sample prepared in deionised water and adjusted to pH 4 then heated to 60°Cfor 72 hours under flowing N$_2$. The sample showed the presence of phosphate (δ2.1, s) and phosphite (δ3.1, d, $^1J_{\text{P-H}}$= 573 Hz) and also the presence of pyrophosphite (δ-5.0, AA'XX', $^1J_{\text{P-H}}$= 671 Hz, $^2J_{\text{P-P}}$= 10 Hz, $^3J_{\text{P-H}}$= 8 Hz) and isohypophosphate (δ-4.0, dd, $J_{\text{P-H}}$ = 563 Hz $^2J_{\text{P-P}}$ = 17 Hz, δ-5.8, d, $^2J_{\text{P-P}}$ = 17 Hz).

isohypophosphate. As the temperature increases and the samples dry out, the production of pyrophosphite becomes the dominant reaction.

The pH of the system is also very important. At pH 4, the condensation reaction is at its best and as the pH increases the reaction is hindered. This effect is thought to be due to the corresponding pK_{a2} values as it is for pyrophosphate formation. The presence of SMOW also facilitates the formation of isohypophosphate and this also puts less emphasis on the requirement for an acidic pH, although the SMOW solution is naturally acidic (*ca.* pH 5). The findings raise the possibility of repeated cycles of wetting and evaporation to increase yields of isohypophosphate in the samples, though due to time constraints this was not undertaken.

4.7 Simulated anaerobic corrosion of schreibersite

Up to this point, all work carried out has been using natural hydrothermal fluids under aerobic conditions to simulate reactions which would be prebiotically plausible for the formation of reduced, activated phosphorus species. However, it is widely accepted that there was very little or no free oxygen in the early Earth atmosphere. To fully investigate the prebiotic plausibility of the route from meteorite to activated condensed phosphorus species it would be required to conduct experiments using natural hydrothermal fluids, natural geological conditions and in the absence of free oxygen.

Previous work has been conducted on the anaerobic corrosion of iron phosphide by Pasek and Lauretta (2005).[28] Pasek and Lauretta conducted both aerobic and anaerobic corrosion of iron phosphide in deionised water and reported that the products of corrosion under aerobic were the same as under anaerobic conditions but in significantly greater quantities.

It was proposed that the presence of oxygen rapidly accelerated the oxidation of iron thus releasing the phosphorus present in the iron phosphide into solution. However, it has been shown in this chapter (see Sections 4.4.1 and 4.8.0.3 for evidence) that the rate of corrosion of schreibersite $[(FeNi)_3P]$ in an iron meteorite is considerably slower than that of the synthetic analogue iron phosphide $[Fe_3P]$ used by Pasek. This is partly due to the nickel content of the schreibersite making it nobler in character but mainly due to the fact that, due to the potential difference between the iron matrix and the schreibersite, the iron matrix will preferentially corrode. This effect will be further discussed later in this Chapter (4.8.0.3).

4.7.1 Simulated anaerobic corrosion of Sample C3

A sample of the Sikhote Alin meteorite (Sample C3) containing schreibersite was placed inside a 50 mL Falcon tube under an atmosphere of N_2. 50 mL of naturally acidic Icelandic fluid was added and the tube was then sealed with PTFE tape. The Icelandic fluid used was from site KHL-LP3 (originally recorded at pH 2.5, 79.2℃) which was reheated to its original temperature before the sample was taken to redissolve all the salts present then degassed by bubbling N_2 though the fluid for a period of 30 minutes prior to addition to the reaction vessel.

The Falcon tube was then suspended inside a test tube containing silicon oil and fitted with a gas inlet cap which allowed for flowing N_2 to be fed into the vessel to sustain a N_2 atmosphere. To retain the anaerobic conditions inside the vessel, all joints were greased and tied using copper wire. The test tube containing the sample was suspended in an oil bath and heated to 80℃ for a period of 28 days to simulate anaerobic corrosion in natural hydrothermal fluids.

After the 28 day heating period, the sample was allowed to cool to room temperature under the N_2 atmosphere. The sample vessel was then transported to an anaerobic glove box where the meteorite sample was removed and dried for surface analysis and the fluids were re-sealed inside the Falcon tube and removed to a fridge at 8℃ for storage while awaiting analysis.

As with the previous samples, it was planned to conduct ICP-AES analysis to obtain quantification on the iron and phosphorus content of the sample post corrosion but the service was no longer available via UCL due to the closure of the facility. It was decided to send the sample to Prof. Pasek at USF for ICP-MS analysis. Due to technical issues on site the analysis could not be completed as expected so no results regarding the water chemistry of the sample were obtained.

Due to the lack of water chemistry analysis it was decided to conduct ^{31}P NMR analysis of the sample to try to obtain data on the phosphorus species present in the sample and possibly some semi-quantitative data on the phosphorus concentration of the sample. The NMR analysis was conducted utilising the same tried and tested method used with the previous iron-bearing samples.

The iron was removed by adjusting the sample to pH 12 using dropwise addition of sodium hydroxide (1 M) then filtering the precipitate. An aliquot of the sample (*ca.* 0.5 mL) was

transferred to an NMR tube and a D_2O insert used for locking purposes.

The spectrum was very poor and showed no phosphorus peaks. Two possibilities existed. One was that there was no phosphorus present in the sample, the other was that there was still a large amount of iron present in the sample which was interfering with the instrument and obstructing the successful acquisition of the NMR spectrum. It was decided to assume the latter and re-treat the sample with NaOH (1 M) and filter using a 0.45μm syringe filter. An aliquot (5 mL) was then taken and reduced to dryness by evaporation on top of the drying oven then dissolved in D_2O (1 mL). The sample was then re-submitted for ^{31}P NMR analysis. Full NMR data are shown in Table 6.57.
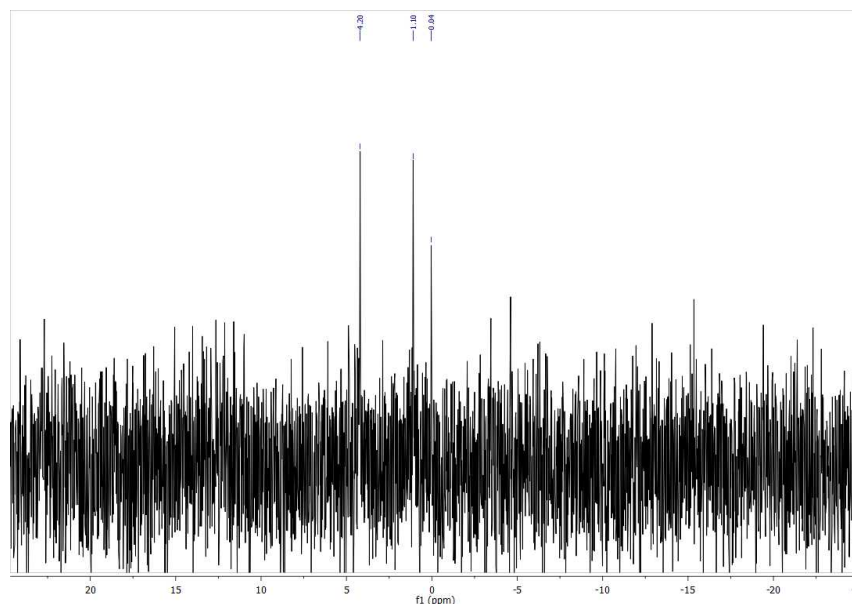
Spectrum 4.30: ^{31}P NMR spectrum (300 K, D_2O, 202.63 MHz) of sample C3 (2,048 scans) after further treatment to remove iron from the fluids. Though the spectrum is still very poor, there is both phosphite (δ2.7, d, ^{1}J$_{\text{P-H}}$= 628 Hz) and phosphate (0.0, s) visible in the spectrum.

As before, the spectrum quality is very poor (see Spectrum 4.30) and has a very high background signal but there is both phosphite (δ2.7, d) and phosphate (0.0, s) visible in the spectrum. The signal to noise ratio (S/N) is very low (*ca.* 3:1) but the peaks are easily definable in the spectrum. The reason for the poor S/N ratio is due either to the low concentration of phosphite and phosphate in the sample or due to continued interference of iron in solution. Based on the knowledge of the slow corrosion of schreibersite in an iron matrix and that according to the findings of Pasek (2005),[28] the rate of corrosion of iron phosphide is much slower in anaerobic conditions, it would seem very likely that the main issue will be the low concentration of phosphorus in solution though the presence of iron may also be a contributing factor. Without ICP-AES or ICP-MS data, the true concentration of phosphorus and iron in solution could not be confirmed.

4.8 Surface analysis of Sikhote Alin samples

As part of the investigation into the products of hydrothermal corrosion of iron meteorites, it was also decided to look at the effects of corrosion on the meteorite surface. It was hoped to build a corrosion profile of the meteorite samples due to the effects of acidic hydrothermal

corrosion. The aims were; to look at how the matrix and the inclusion were affected by acidic hydrothermal corrosion; to identify differences in susceptibility to corrosion between the matrix and the inclusion; to identify any surface chemistry which may be taking place, and, to identify what ultimately may affect the levels of iron and phosphorus observed in each samples fluids. All five of the Sikhote Alin meteorite samples used (C1-C5) were provided by Dr. Caroline Smith of the Natural History Museum, London.

Each of the Samples (C1-C5) was cleaned upon receipt using water and ethanol. The intention of the cleaning was to remove any fingerprint residues (sweat and sebum) and other contamination which may have been present as a result of cutting and handling. The samples were then only handled using nitrile gloves from this point to try to limit further contamination. A later reflection of the washing protocol used concluded that ethanol was not the correct solvent for cleaning the meteorite samples as sebum (an organic fatty acid) is not soluble in ethanol. Methanol or dichloromethane would have been a more suitable choice for removal of such contamination from the samples though by this point the experiment and subsequent analysis was already undertaken.

Each sample was fully analysed using Raman spectroscopy, Scanning Electron Microscopy/Energy Dispersive X-ray spectroscopy (SEM/EDX) and Infinite Focus Microscopy (IFM), and then weighed on a five figure analytical balance pre- and post-corrosion. Each sample was fully cleaned with water and ethanol after each analysis and stored under vacuum while not in use. After full analysis of the samples, they were again washed and dried using water and ethanol then vacuum desiccated for 2 days before being placed into 50 mL falcon tubes and sealed under N_2. PTFE tape was used to completely seal the samples from oxygen for transport to Iceland for experimentation.

4.8.0.1   Raman

Raman analysis pre- and post-corrosion of the inclusions and surrounding matrix was undertaken by Prof. Ian Scowen and his group at the University of Bradford. Raman analysis was conducted on samples C1 to C5 prior to sealing in the Falcon tubes and was undertaken at the University of Bradford using a Renishaw InVia spectrometer and a 633 nm He-Ne laser. The purpose of the Raman investigation pre-corrosion was to look at the surface areas around the matrix/inclusion boundary, to identify the presence of any oxidation products on the surface prior to corrosion and to give a base level for post-corrosion analysis. It was thought that post-corrosion it would be possible to observe reduced oxidation state phosphorus species on the surface of the meteorite and establish the method of corrosion and compounds produced by corrosion.

The Raman analysis was conducted using the 20x objective lens at 100% laser power. The sample was exposed with a 1 second exposure time and the data collected in 1 acquisition over a 100-1200 cm^{-1} range as this allowed for rapid collection of data over multiple points. The analysis was conducted on cleaned, dry samples with areas of analysis selected and focused manually. Analysis of the matrix/inclusion boundaries of the samples showed some evidence of iron oxidation products such as the minerals magnetite [Fe_3O_4] and hematite [Fe_2O_3] with evidence for the mineral goethite [α- FeO(OH)] also present. Examples of

the Raman spectra obtained post-corrosion can be seen in Spectrum 4.31. Raman analysis was also conducted on the matrix and inclusion areas but due to the metallic nature of the samples this resulted in a phenomenon called "flaring" which is caused by saturation of the detector due to reflection of light which resulted in no usable data for these areas.

The analysis on sample C1 post corrosion at 633 nm gave very poor results (Spectrum 4.32). The sample again "flared" badly causing over-saturation of the detector though in this case this was caused by a mineral clay deposit which covered the surface of the meteorite sample. The mineral was believed to be an aluminosilicate which was deposited onto the samples from the fluids used in the experiment. It was decided to attempt analysis at a shorter wavelength (514.5 nm) but with the same result. Due to the poor quality of spectra obtained by the analysis it was decided to abandon the Raman studies of the meteorite samples and try SEM/EDX analysis to confirm the nature of the clay deposit on the surface and to get a closer look at the inclusion area in an to attempt to identify changes to the mineral composition around the inclusion.

With little data obtained using Raman analysis on the meteorite samples it was decided to use other techniques to characterise the surface of the samples prior to corrosion. The next method chosen was SEM/EDX which would give not only optical images of the surfaces in great detail but also elemental composition data for each sample.

4.8.0.2 SEM/EDX

Scanning Electron Microscopy (SEM) is an optical method which provides high resolution imaging of a surface by scanning a focused electron beam over the surface of the sample and detecting secondary (electrons emitted from atoms in the sample surface by impact of an electron beam with sufficient energy) and back-scattered (electrons involved in elastic collision with the sub-atomic particles in the surface of the sample) electrons. The use of SEM with Energy Dispersive X-ray (EDX) analysis is a very powerful tool in surface analysis of samples which allows for high quality imagery of a sample's surface along with the identification of elemental composition and quantitative compositional information of the selected area of analysis. Because of this it was selected as a method for analysis of the meteorite samples.

The aim of the preliminary analysis (pre-corrosion) was to get optical images of the matrix and inclusion areas on the surface of the meteorite samples. The surface investigation was used to identify prominent features which could then be used post corrosion for analysis and comparison of the pre- and post-corrosion surfaces. Once the prominent features were identified the elemental composition was mapped using EDX analysis. This would give indicators to how the elemental composition of the surface changed during corrosion. The EDX analysis also allowed the confirmation that the inclusions were indeed schreibersite as believed.

As expected, the SEM/EDX analysis confirmed the presence of schreibersite in all the meteorite samples. An example of the SEM data obtained can be seen in Figure 4.4 and Figure 4.5 taken of sample C3. The images were taken using the Back Scatter Electron (BSE) detector which means that elements of a lighter colour have a higher atomic mass.
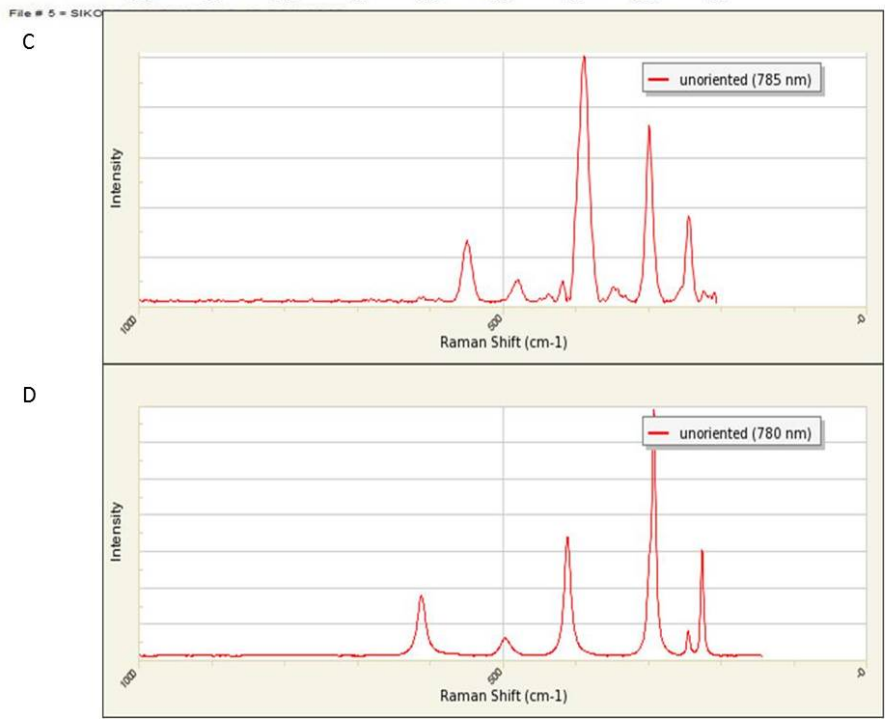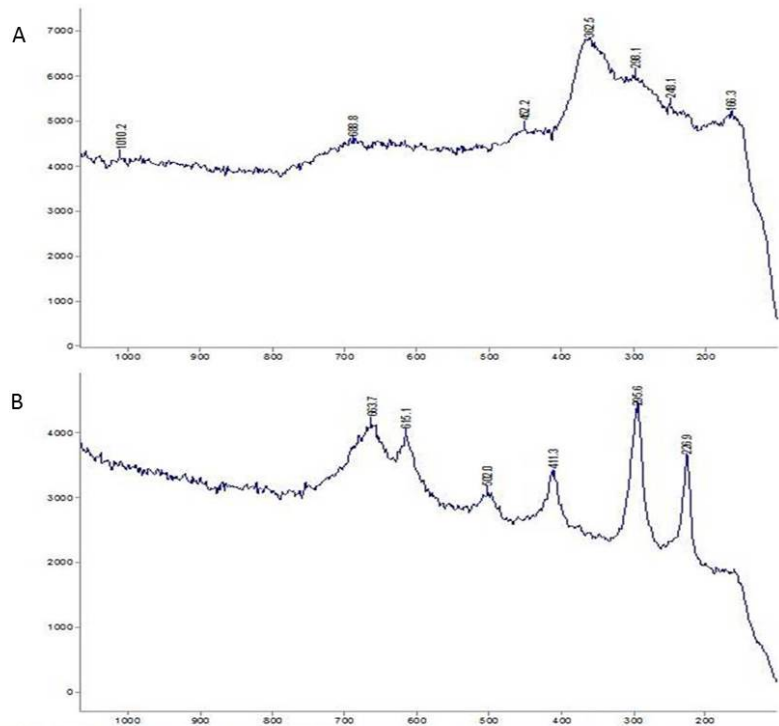
Spectrum 4.31: Raman spectra obtained of sample C1 using 633 nm laser in 1 acquisition with 100% power and a sample an exposure time of 1 second. The spectra shows what is thought to be the presence of hematite and goethite on the surface of the meteorite sample close to the inclusion boundary. The assignment is based on comparison to spectra obtained for each of these minerals from the RUFF database. A. and B. Raman spectra from sample C1 of the matrix-inclusion boundary, C. Raman spectrum of goethite from the RUFF database, D. Raman spectrum of hematite from the RUFF database.

File # 7 = SIKOTE ALIN EX ICELAND -1993 4315 -167 X 10
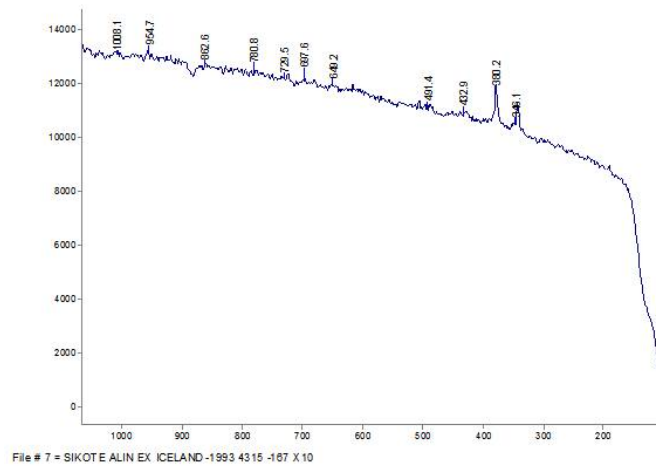
Spectrum 4.32: Raman spectrum obtained from sample C1 post-corrosion. Due to the issue of 'flaring", there are no clear peaks though some tentative peaks can be identified as appearing from the baseline suggesting the presence of pyrite (FeS_2, cubic) or marcasite (FeS_2, orthorhombic) in the clay coating. Due to the quality of the obtained spectrum it is very difficult to identify the minerals responsible for the signals.

1mm   Electron Image 1
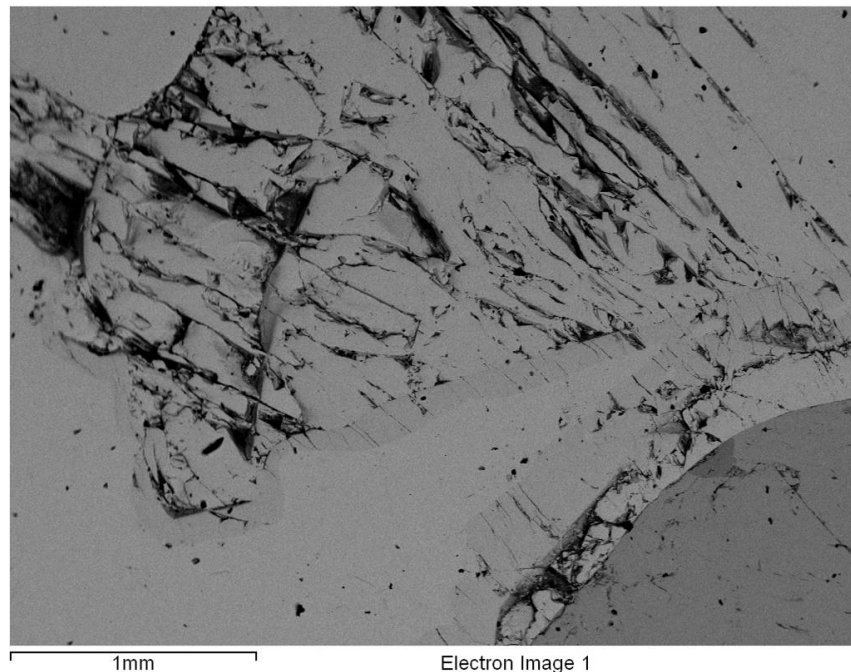
Figure 4.4: SEM image of a schreibersite inclusion from the surface of the C3 meteorite sample. The image clearly shows an area with a cracked, brittle looking surface which is schreibersite and a darker area in the bottom right hand corner which was assumed to be troilite. EDX analysis was carried out on this site of interest and can be seen in Figure 4.6 Part A. The image was obtained using the BSE detector to give the best contrast between different phases present on the surface of the meteorite.
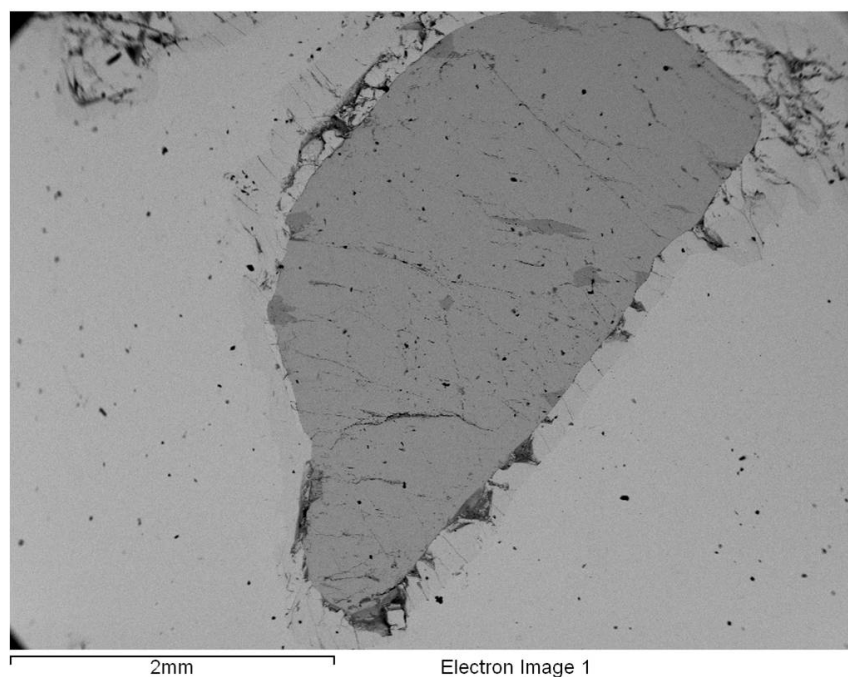
Figure 4.5: SEM image of the troilite inclusion from the surface of the C3 meteorite sample. EDX analysis was carried out on this site of interest to confirm if the inclusion was indeed troilite as predicted and can be seen in Figure 4.6 Part B. The image was obtained using the BSE detector to give the best contrast between different phases present on the surface of the meteorite.

This gives greater contrast to the inclusions while analysing the meteorite surfaces making them easier to find than with the Secondary Electron (SE) detector. Once the inclusion is found it is then possible to proceed with the EDX (Energy Dispersive X-ray) analysis to show elemental composition of the site of interest.

It can be seen in Figure 4.6 (Part A) the inclusion area is higher in concentration of phosphorus (P) and nickel (Ni) and poor in iron (Fe) compared to the matrix which is indicative of schreibersite. There is also an area next to the schreibersite which is rich in sulphur (S) which is thought to be the mineral troilite. The sulphur inclusion is shown full in Figure 4.6 (Part B) and is seen to have a rim of schreibersite surrounding the inclusion. Due to the presence of both schreibersite and troilite in the C3 sample, it was decided to keep back the sample for a controlled anaerobic experiment rather than use it in aerobic condition experiments in Iceland. The samples were then analysed using Infinite Focus Microscopy by Dr. David Greenfield from the Materials Engineering Research Institute at Sheffield Hallam University.

The meteorite samples were collected from the fluids post corrosion by filtration. They were then dried and stored in a vacuum desiccator until ready for analysis. The analysis of the samples was to look at the inclusion/matrix boundaries for changes in chemical composition caused by corrosion of the sample. The samples were analysed in order C1, C2, C4, and C5.

The analysis of sample C1 proved to be very difficult as the surface of the meteorite was covered in a layer of clay. The clay was initially responsible for hampering and eventually causing the abandonment of the analysis by Raman and again proved a source of frustration as it made finding the inclusion very difficult. Time was spent slowly scouring over the
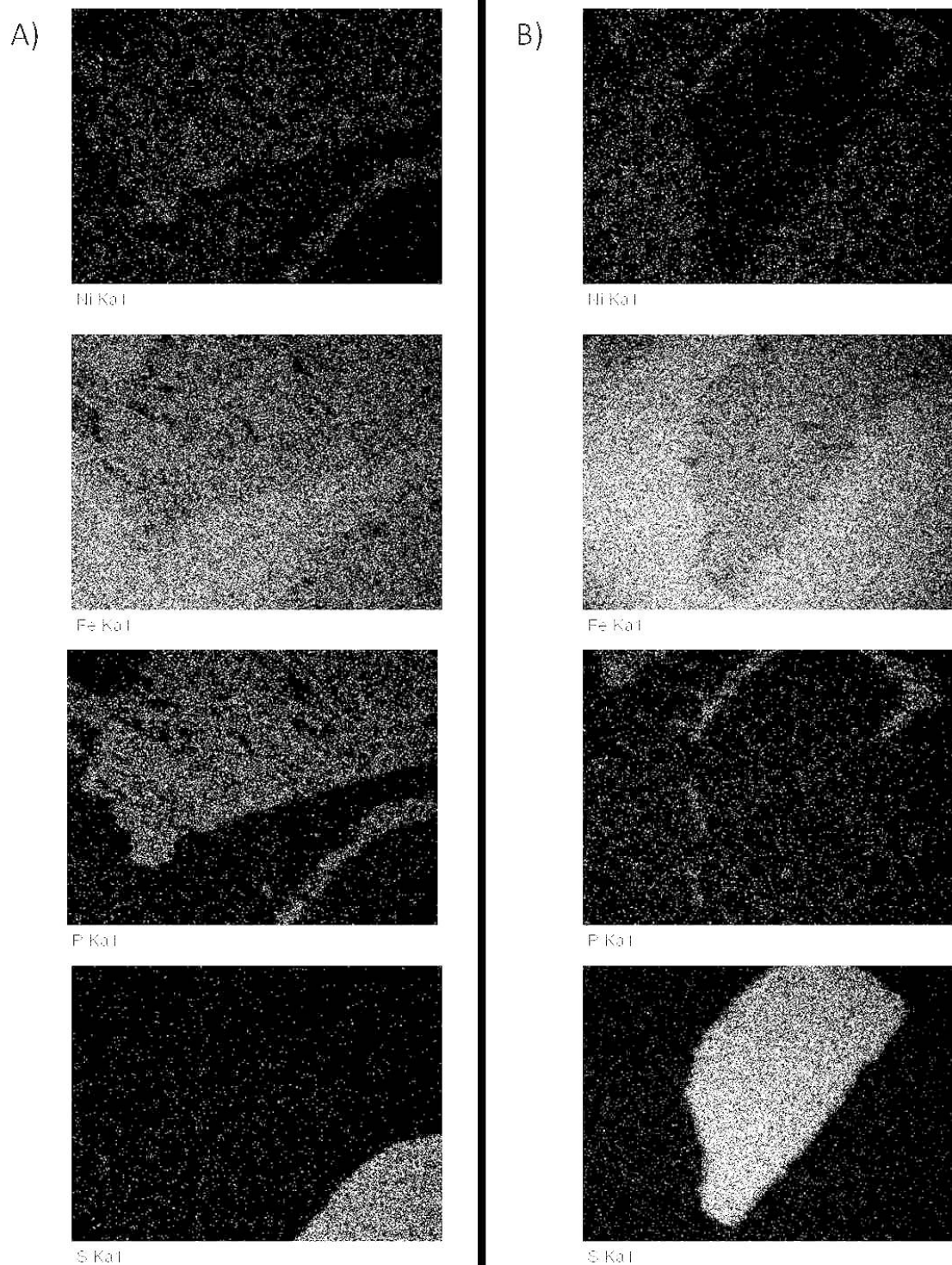
Figure 4.6: A) EDX map of Figure 4.4 from meteorite sample C3 showing an area of schreibersite which is enriched in nickel (Ni) and phosphorus (P) compared to the matrix which is rich in iron (Fe). There is also an inclusion in the bottom corner which is enriched in sulphur (S) thought to be the mineral troilite. **B)** EDX map of Figure 4.5 from meteorite sample C3 showing the troilite inclusion which is rich in sulphur (S) and depleted in iron (Fe), nickel (Ni) and phosphorus (P). Interestingly, the troilite inclusion is surrounded by a thin band of schreibersite as can be seen by the rich phosphorus and nickel signal around the sulphur inclusion area.

inclusion surface of the meteorite looking for signs of schreibersite to no avail. However, while looking for the schreibersite it was decided to use the SEM/EDX to investigate the composition of the clay to try to identify the composition and its potential origins.
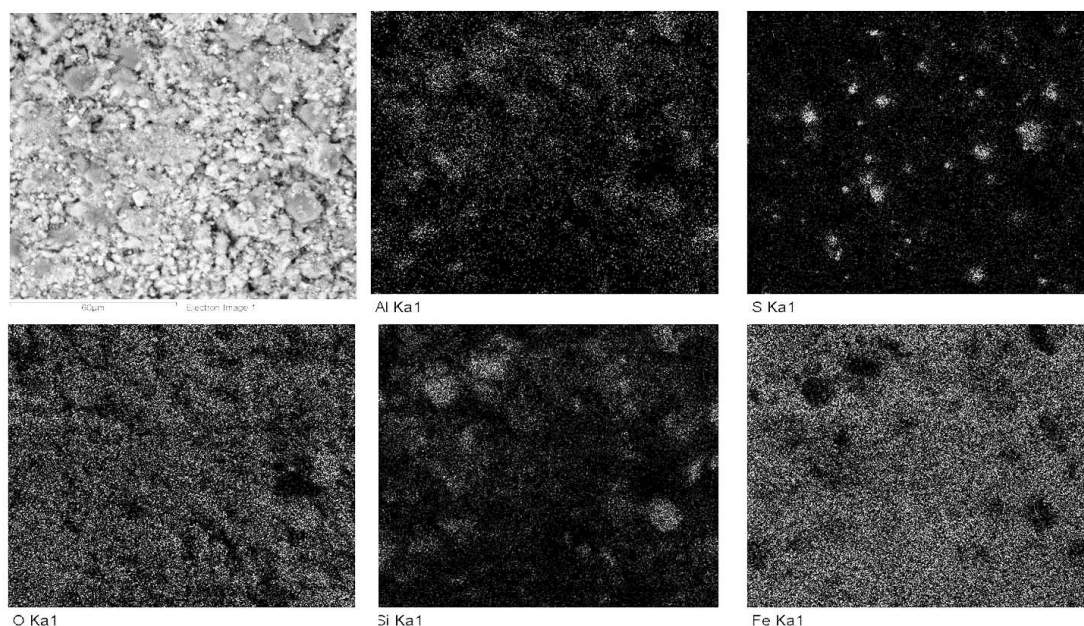
Figure 4.7: SEM image and related EDX maps of the clay on the surface of the C1 meteorite sample. It can be seen from the EDX analysis that the clay appears to be an aluminosilicate based on the relatively uniform distribution of aluminium (Al), silicon (Si) and oxygen (O) present over the map area. There is also a very uniform distribution of iron (Fe) which is most likely to be corrosion products of the iron meteorite surface such as hematite [Fe_2O_3] and magnetite [Fe_3O_4]

The SEM/EDX of the meteorite surface confirmed the composition of the clay as an aluminosilicate base with amounts of titanium present. The clay was in an apparently uniform deposit all over the surface of the meteorite. There were areas of the meteorite however which were high in concentration of sulphur which was of interest and it was decided to look closer at one of these rich sulphur areas to identify the cause.

Focusing the SEM on one particularly large bright area which was visible in Figure 4.7 it was noticed there was a group of six cubic crystals visible against the background clay. The cubic crystal formation was subjected to EDX analysis to try and confirm the elemental composition. The analysis showed a strong presence of iron and sulphur and the crystals were, thus, believed to be pyrite [FeS_2, cubic] and also marcasite [FeS_2, orthorhombic]. This can be seen quite clearly in the EDX map of the crystal area (Figure 4.8).

The presence of pyrite and marcasite was confirmed by Raman analysis of the crystals. The Raman spectra were obtained of the cubic crystals and also of a dark crystal next to the cubic crystals and can be seen in Spectrum 4.33 and Spectrum 4.34. The spectrum obtained for the cubic crystal was compared to known iron sulphides present on the RUFF database and was confirmed as pyrite while the spectrum obtained for the dark crystal was confirmed to be marcasite *via.* the same method.

The presence of pyrite and marcasite on the surface of the meteorite was considered to be an interesting phenomenon as it introduced a new aspect to sulphur chemistry which has not been previously considered. With sulphide deposition on the surface of the mete-
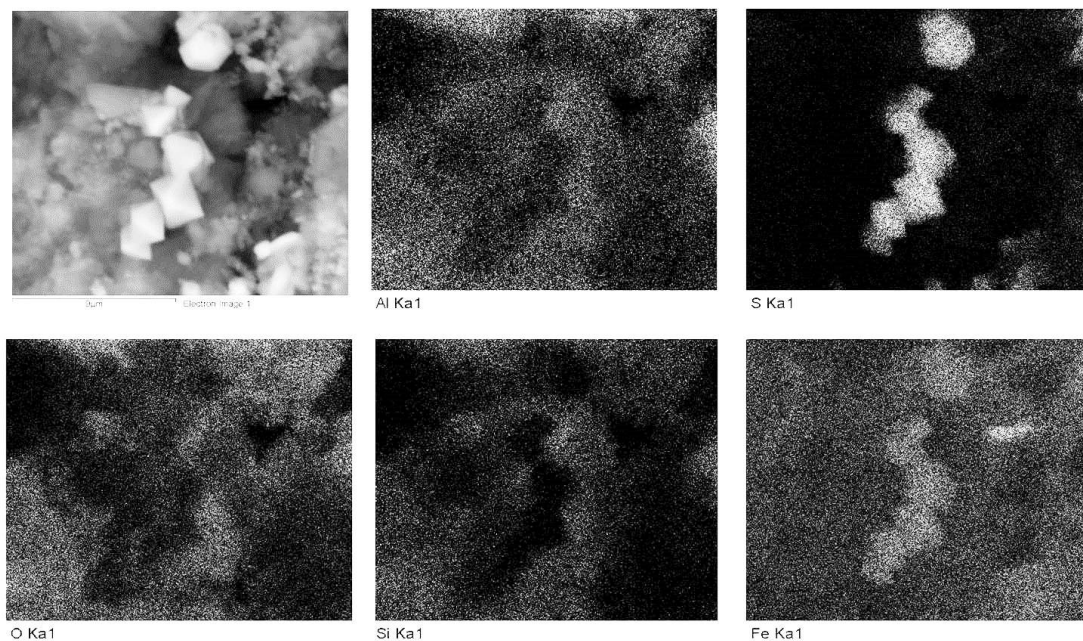
Figure 4.8: SEM image and related EDX maps of the cubic crystals found in the clay on the surface of the C1 meteorite sample. The crystals are observed to be both rich in iron (Fe) and sulphur (S) which, given the cubic structure, would be an excellent indication that they were pyrite crystals [FeS$_2$].
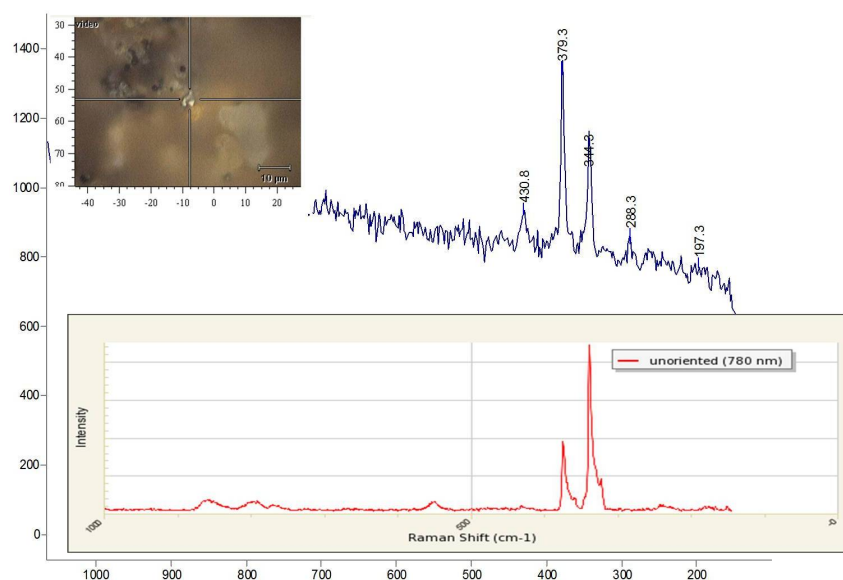
Spectrum 4.33: Raman spectrum obtained using a 633 nm laser of the cubic crystals present in the clay on the surface of meteorite sample C1. The spectrum was compared to known iron sulphides in the RUFF database and was deemed to be most similar to pyrite [FeS$_2$, cubic]. Inset: Raman spectrum of pyrite taken using a 780 nm laser from the RUFF database for comparison.
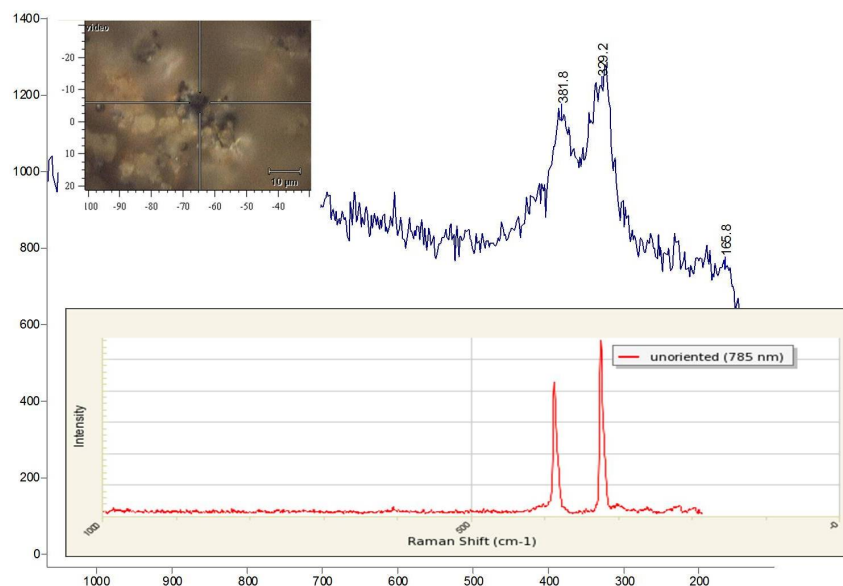
Spectrum 4.34: Raman spectrum obtained using 633 nm laser of the dark crystals adjacent to the cubic crystals present in the clay on the surface of meteorite sample C1. The spectrum was also compared to known iron sulphides in the RUFF database and was deemed to be most similar to marcasite [FeS_2, orthorhombic]. Inset: Raman spectrum of marcasite taken using a 785 nm laser from the RUFF database for comparison.

orite it is possible the meteorites could become catalytic centres for a wealth of prebiotic chemistry as has been proposed by Günter Wäctershäuser. For many years, Wäctershäuser has postulated that iron/nickel sulphides are highly efficient catalytic centres (see Wächtershäuser (1988),[216] Wächtershäuser (1990)[217] and Wächtershäuser (1990a)[218] for examples) capable of involvement in variety of prebiotic chemical reactions including carbon fixation. This was reported by Huber and Wächtershäuser (1997) who showed production of methyl thioacetate from the reaction of carbon monoxide and methyl sulphide in the presence of iron/nickel sulphide.[219]

The formation of the crystals would require a redox reaction between iron and sulphur to form pyrite or marcasite. The analysis of the hydrothermal mud showed the presence of elemental sulphur but there were also large amounts of H_2S evolved on the site which may react with the iron meteorite surface. There was also the possibility that the crystals were a deposit of organic origin caused by sulphur metabolising organisms present in the fluids. Due to the very clean, cubic nature of the crystals, it is thought that they were most likely to be of abiotic origin based solely on the morphology. To say undoubtedly whether the sulphur was of organic or inorganic origin would require sulphur isotope analysis but there were insufficient crystals for this to be easily completed so this was not pursued.

The mineral clay deposit on the surface of the meteorite was also a previously unconsidered effect of the corrosion and it was decided to try to identify the mineral components of this clay. The grey clay mud from one of the water samples was collected by filtration and dried. This was then ground to a fine powder and subject to powder XRD analysis.

The resulting powder pattern spectrum (Spectrum 4.35 was then compared to minerals in a crystallographic database (identification courtesy of Prof. Liane Benning, School of Earth Sciences, University of Leeds). There were three minerals formally identified from the pow-

der pattern; heulandite [$(CaNa)_2Al_3(SiAl)_2Si_{13}O_{36} \cdot 12\,H_2O$], clinochlore [$Mg_5Al(SiAl)_4O_{10}(OH)_8$] and sulphur (orthorhombic). There was also some similarity shown towards montmorillonite [$(NaCa)(AlMg)_6(Si_4O_{10})_3(OH)_6 \cdot nH_2O$] though this was not formally identified.
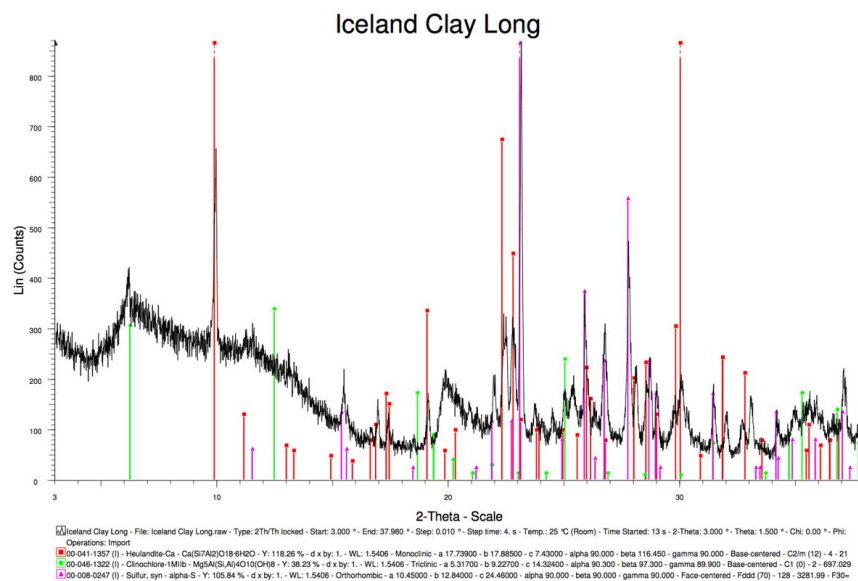
Spectrum 4.35: Powder X-ray diffraction spectrum for the Iceland clay present in the collected fluids. The spectrum was collected using a Bruker D8 Powder X-ray spectrometer. The spectrum was run through a crystallographic database and the minerals heulandite [$(CaNa)_2Al_3(SiAl)_2Si_{13}O_{36} \cdot 12\,H_2O$], clinochlore [$Mg_5Al(SiAl)_4O_{10}(OH)_8$] and sulphur (orthorhombic) were identified. There was also some similarity of the spectrum towards the mineral montmorillonite [$(NaCa)(AlMg)_6(Si_4O_{10})_3(OH)_6 \cdot nH_2O$] though this was not formally identified. Identification courtesy of Prof. Liane Benning, School of Earth Sciences, University of Leeds.

Analysis of the other meteorite samples showed a similar clay deposit on all the meteorites but no further evidence of pyrite crystals was found. Again the clay hampered the identification of the inclusions on the meteorite surface so it was not possible to accurately assess the surface changes caused by corrosion using this method. It was decided to continue analysis of the meteorites it would be necessary to clean the meteorite surfaces prior to further analysis.

The cleaning of the meteorite samples was conducted by Dr David Greenfield at SHU using a process known as cathodic depolarisation. This involved the samples being connected to a cathode and submerged in a solution of sodium hydroxide, sodium carbonate and sodium sulphate. A current is then passed through the sample as a part of a Galvanic cell which causes the corrosion products on the surface of the meteorite to be blown off into the solution. The process can be seen in Figure 4.9. After the sample has been cleaned it was rinsed with deionised water, then ethanol and allowed to dry. The samples were then ready to be analysed by IFM.

4.8.0.3   IFM

Infinite Focus Microscopy (IFM) is another optical analytical method which is used for specifically mapping alterations and defects in surfaces such as metals. The instrument operates using a working distance which is set by focusing the microscope on the lowest point on the viewable surface of the sample then again focusing on to the highest point
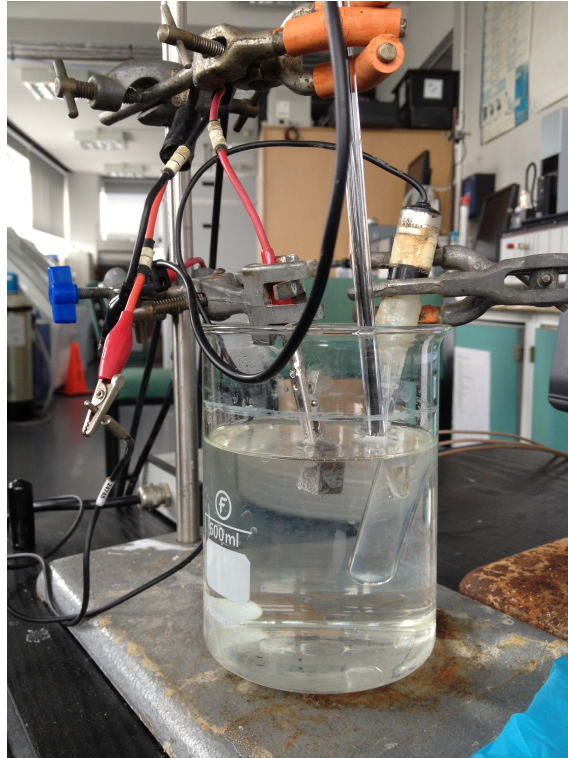
Figure 4.9: Photograph of the apparatus used for the cleaning of the meteorite samples by cathodic depolarisation. The equipment turns the meteorite sample into a cathode in a galvanic cell which causes all of the corrosion products to be "blown" off of the surface leaving clean metal behind.
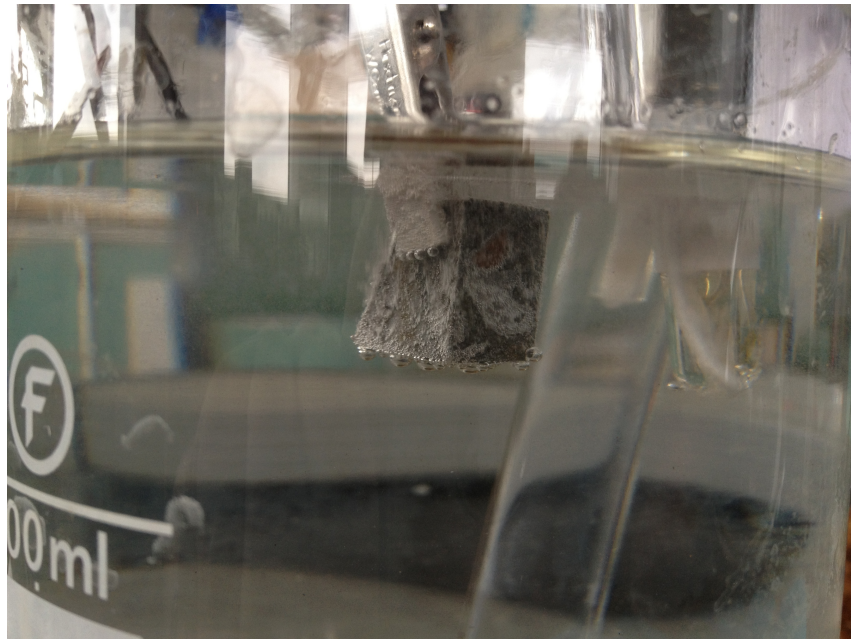
Figure 4.10: Photograph close up of the meteorite sample being cleaned in Figure 4.9. It can be seen that during the cleaning process that hydrogen gas is given off as an electric current is passed through the meteorite sample. This aids in the cleaning of the corrosion products from the meteorite surface as the hydrogen is generated on the metal surface below the corrosion surface.

of the sample of the surface. A series of images is collected by taking very small focus steps through the working distance then the images are stitched together to form a three dimensional image of the surface which gives very high levels of detail about the topography of the surface.

The initial analysis of the meteorite samples was conducted by Dr. David Greenfield at SHU and was to be used for comparison to the meteorite samples post corrosion to try to identify how the corrosion affected the topography of the meteorite surface. It was hoped to identify areas of rapid corrosion, whether the exposed face corroded uniformly or if there were areas of the surface more liable for corrosion than others.

Investigation of each meteorite inclusion was completed looking at easily identifiable points of interest which would be easy to identify for comparison after corrosion. It was possible to generate 3D images of sites and use line scans to measure how the topography of the surface changed over the matrix/inclusion boundaries. Examples of the 3D images and line scans can be seen in Figure 4.11 and Figure 4.12.
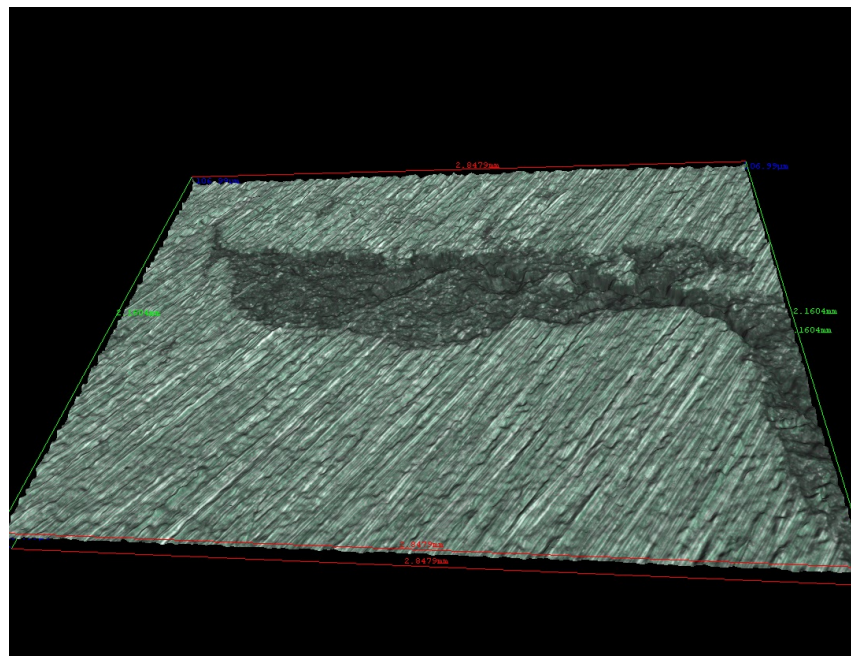
Figure 4.11: 3D IFM image of the inclusion on the surface of sample C4 pre-corrosion. The image is composed of a large number of images taken within a working distance. The working distance is set by focusing on the bottom most and then the top most point visible on the surface. The technique of IFM is perfect for analysis of surface topography and ideally suited for pre- and post- corrosion analysis of metals

Inspection of each of the IFM images for each meteorite showed that the inclusion generally sat proud of the matrix and that the boundary was usually a slight depression. The inclusion itself was much more textured than the matrix and generally quite pitted and cracked, looking much more brittle than the matrix. The matrix seemed to have a large number of horizontal ridges on the surface which was an effect of the cutting technique used when preparing the samples.

IFM analysis of the post-corrosion meteorite samples was conducted after cleaning by cathodic depolarisation due to the visual inhibitory effects of the aluminosilicate clay deposited on the surfaces by the hydrothermal fluids. For each sample, the points of interest identified in the pre-corrosion analysis were found and analysed to confirm changes to
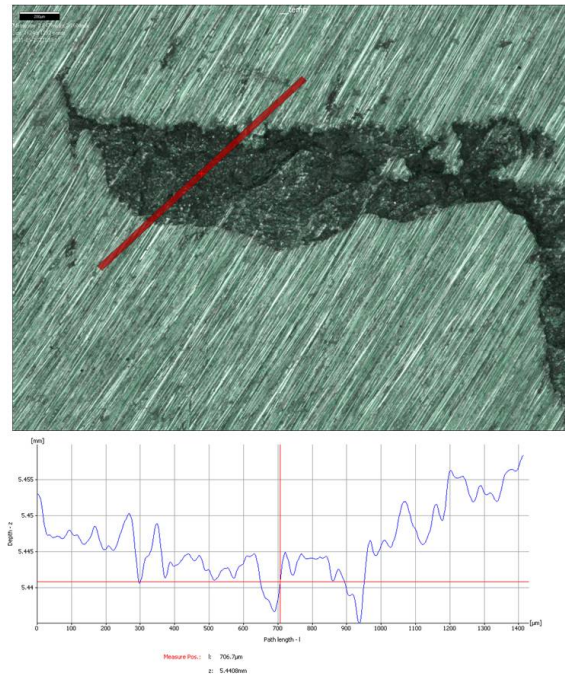
Figure 4.12: IFM image of the inclusion on the surface of sample C4 pre-corrosion. The red line visible in the image is taking a linescan which uses the IFM data to calculate the topography of the surface over the length of the line. The topography profile is shown below the IFM image. The linescan can be used to map changes in topography pre- and post- corrosion.

the surface topography of the inclusion and matrix with special interest paid to the matrix/inclusion boundaries.

Comparison of pre- and post-corrosion images of sample C1 shows quite a change in the surface topography pre- and post-corrosion. As can be seen from the images (Figure 4.13 and Figure 4.14), the post corrosion sample shows significant alteration of the matrix surface which shows signs of pitting and much more defined edges to the matrix/inclusion boundary. In one section, defined the "duck's head", the overlying matrix has been corroded away exposing more inclusion surface. This becomes even more apparent when you look at the 3D IFM image of the surface (Figure 4.14). It is seen that what was originally thought to be two separate inclusion areas is now just one large inclusion which was covered by overlying matrix.

The inclusion was subjected to SEM/EDX analysis by Dr. David Bryant to try and show this elementally. It is seen in the EDX map (Figure 4.15 of the inclusion area that the "duck's head" is now connected to what was originally a second smaller inclusion due to the corrosion of the overlying matrix. The map shows the inclusion has enriched in phosphorus and nickel while depleted in iron. It can also be seen that the matrix/inclusion boundary is enriched in oxygen, as is the matrix surface which coincides with the areas of highest visible corrosion. The image seems to show that the matrix, especially around the inclusion is more susceptible to corrosion than the inclusion.

The IFM analysis of the other meteorite samples showed the same phenomena though to a varying degree, dependent on the pH and temperature conditions to which they were subjected. It followed that the more acidic the fluids used for corrosion, the more corrosion of the matrix and matrix/inclusion boundary was observed. Sample C1 was incubated in
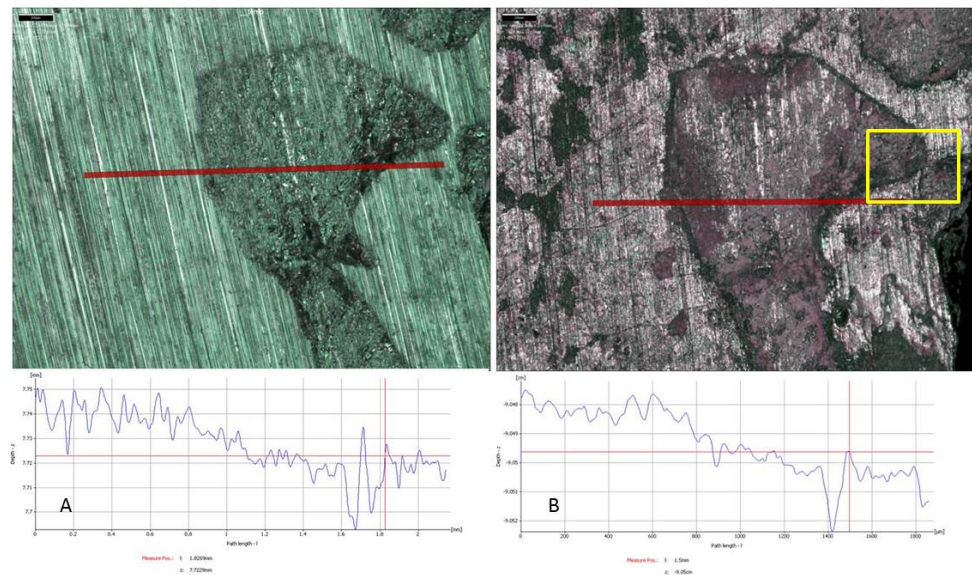
Figure 4.13: Composite image showing the IFM analysis of sample C1 (A) pre- and (B) post-corrosion. Comparison of the pre- and post-corrosion images shows how much the surface has been altered during corrosion. It is noticed that there has been significant alteration of the meteorite surface with clearly defined corrosion around the matrix/inclusion boundary. There is one section to the right of the image where the matrix has corroded away between two separate inclusions to show that it is actually one large inclusion which was underlying the matrix. The box highlighted on the post-corrosion image is shown in Figure 4.14 as a 3D image.
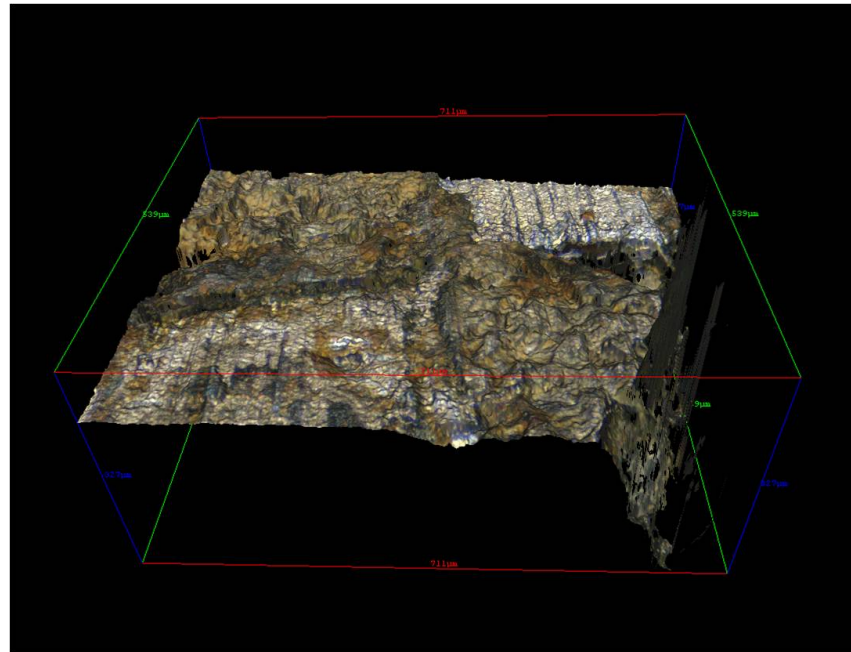
Figure 4.14: 3D IFM image focusing on the area of corrosion highlighted in Figure 4.13 which has revealed where what was thought to be two separate inclusions are actually one large one which was underlying the matrix.
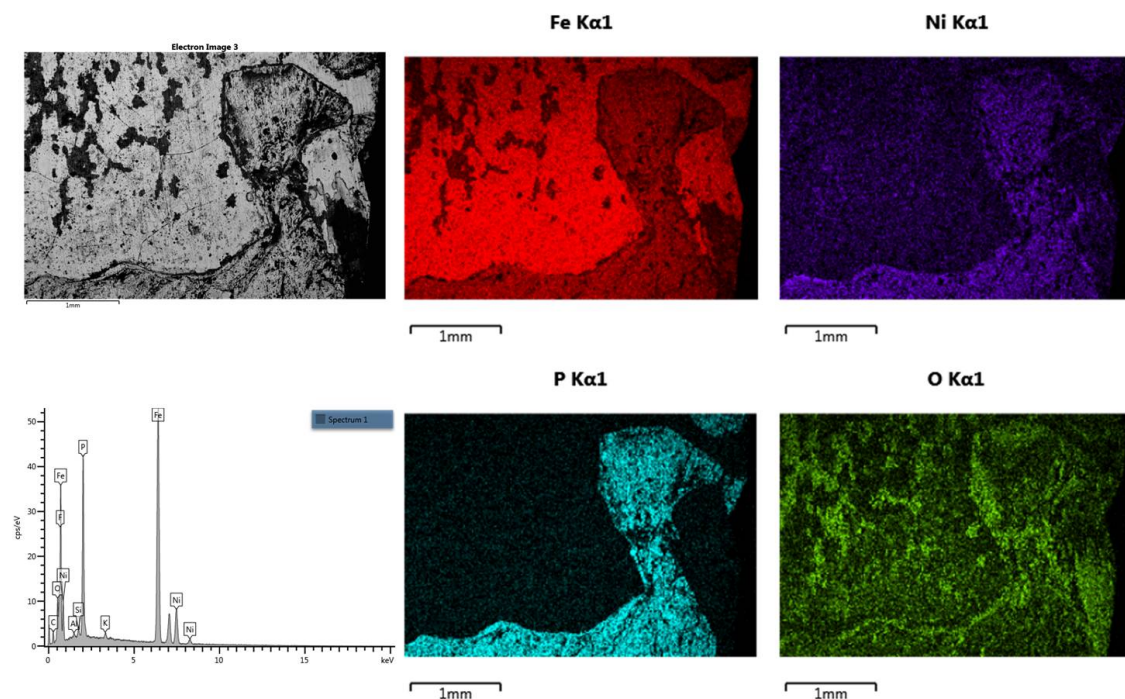
Figure 4.15: False colour EDX maps of the "duck's head" region of the C1 meteorite sample conducted by Dr David Bryant. The EDX analysis shows that the larger inclusion is now connected to what was originally thought to be a second smaller inclusion due to the corrosion of the overlying matrix. The map shows the inclusion is rich in phosphorus (P) and nickel (Ni) while depleted in iron (Fe) compared to the matrix which is rich in iron.

fluids at pH 3.1 for 35 days while sample C4, which showed the biggest changes in surface topology pre- and post-corrosion, was incubated in fluids at pH 2.5 for 82 days. It can be seen from the pre- (Figure 4.16) and post-corrosion (Figure 4.17) images that there is major evidence of corrosion of both the matrix surface and the matrix/inclusion boundary.

The evidence shows that the inclusion corrodes much slower than the matrix. The rate of corrosion of the inclusion is hampered due to the high nickel content making it much nobler in character than the matrix which has a higher iron content. The matrix will corrode quite rapidly dependent on pH and temperature conditions but it is the matrix/inclusion boundary which is much more susceptible to corrosion and that will corrode preferentially allowing for the eventual release of the inclusion into the fluids where it will then corrode without inhibition.

The analysis of the anaerobic corrosion sample C3 showed a much slower corrosion rate even though it was incubated in fluids at 80℃ and pH 2.7 for 28 days. By comparison of the pre-corrosion image (Figure 4.18) with the post-corrosion image (Figure 4.19) it can be seen that though there has been obvious alteration of the surface due to the corrosion that the rate of corrosion is much slower. There was potential evidence for this earlier in this chapter by the weak ^{31}P NMR spectra obtained on the fluid samples of the C3 anaerobic corrosion experiment. The lack of oxygen slows down the rate of corrosion of the iron in the meteorite and though it still allows for corrosion, the amount observed is much smaller than corrosion in aerobic conditions. From the results obtained it is clear that the anaerobic corrosion of iron meteorites to release phosphite would be a very slow process though the above experiment was only run for a period of 28 days which in geological time
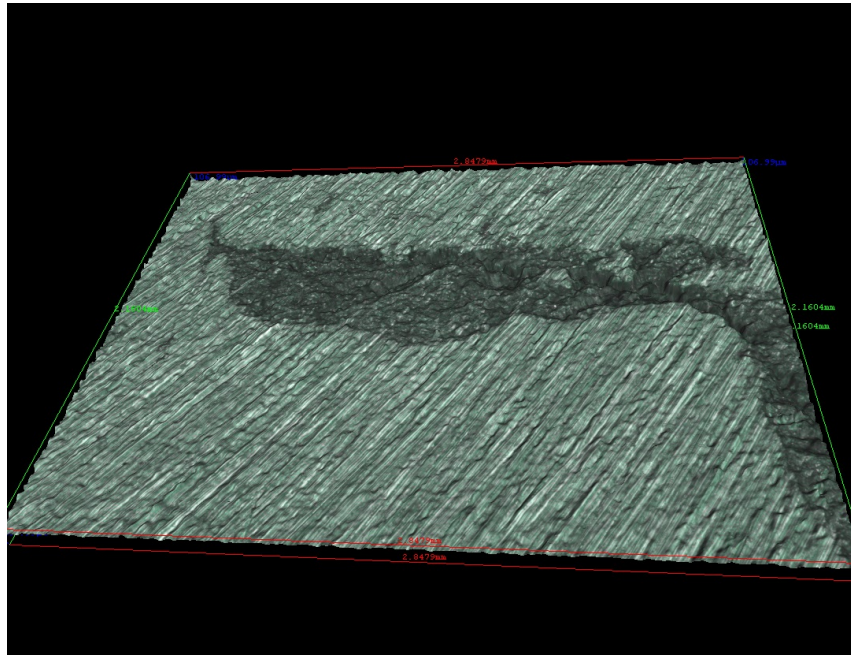
Figure 4.16: 3D IFM image of the C4 sample showing the inclusion area pre-corrosion. The diagonal lines on the matrix are from the cutting of the meteorite sample to expose the inclusion. It is seen that the cutting process has caused chunks of the inclusion to break out as the inclusion is much more brittle than the matrix.
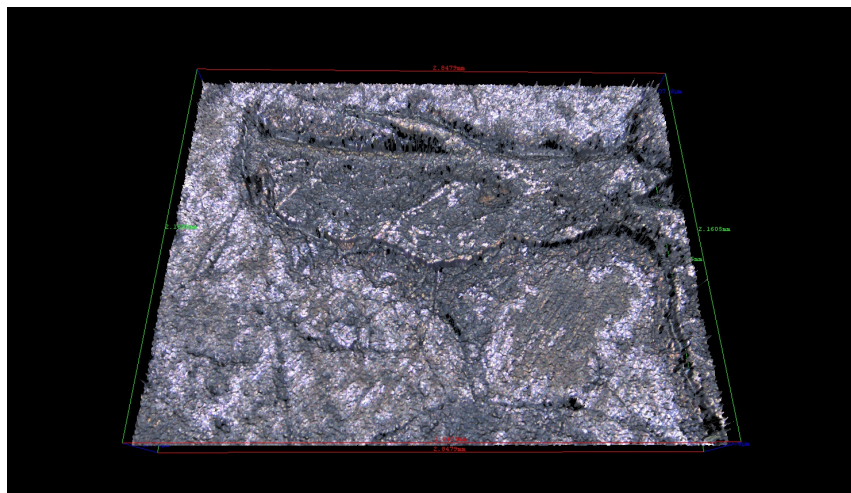
Figure 4.17: 3D IFM image of the C4 sample showing the inclusion area post-corrosion. It is noticed that the corrosion process has caused significant alteration to the matrix surface when compared to Figure 4.16. The inclusion has also grown in size with much of the overlying matrix having corroded away completely. There is also evidence suggesting the formation of troughs at the matrix/inclusion boundary indicating that corrosion is much more rapid at the boundary than on the inclusion or matrix surfaces separately.
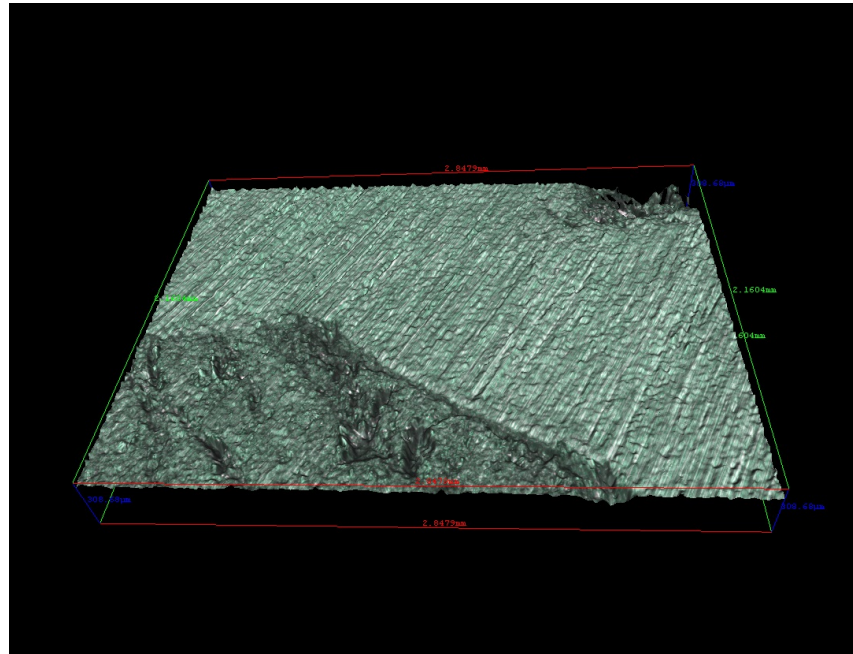
Figure 4.18: 3D IFM image of the C3 sample showing an area with two schreibersite inclusions. The cutting lines are visible on the surface as in Figure 4.16 as are the chunks of missing inclusion which have fallen out during cutting.
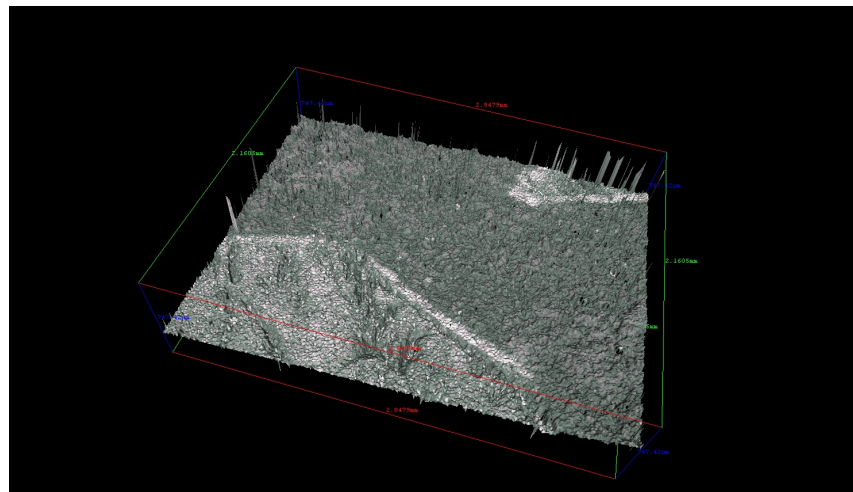
Figure 4.19: 3D IFM image of the C3 meteorite sample showing an area with two schreibersite inclusions post-corrosion. Again there is visible corrosion of the matrix surface though the corrosion is much less extensive than the meteorite samples which were corroded under aerobic conditions. It is clear from the image that the rate of anaerobic corrosion is much slower than that of aerobic corrosion even at low pH and high temperatures.

is extremely insignificant.

4.9   Conclusions

The work in this Chapter clearly shows there is the potential for the production of reduced oxidation state phosphorus species and also activated condensed phosphites and phosphates under natural geological conditions. Production of reduced oxidation state phosphorus species, primarily phosphite [HPO_3^{2-}], is possible by acidic hydrothermal corrosion in natural fluids. The levels of phosphorus released into the water samples were quantified by ICP-AES by Dr. Claire Cousins (UCL) and the phosphorus oxidation states quantified by Prof. Matt Pasek (USF) using Ion Chromatography. The water chemistry analysis confirmed increases in the amounts of iron and phosphorus present in the fluid samples, and that the rate of release of iron and phosphorus was directly linked to the pH and temperature conditions to which the sample was exposed. The oxidation state analysis conducted by Prof. Pasek confirmed the main phosphorus oxidation state observed was the P^{3+} oxidation state which was indicative of phosphite. The confirmation of the actual speciation present in the samples was completed using ^{31}P NMR analysis which confirmed that phosphite was indeed the main phosphorus species present in the fluid samples.

It was shown that it was possible to produce pyrophosphite, a low oxidation state, highly reactive and highly soluble condensed phosphorus species under natural geological conditions by dry heating calcium phosphite in geothermally heated sand at *ca.* 95℃. This experiment proved that, given the correct conditions (correct pH, correct divalent cations present, sufficient heat and a naturally flowing atmosphere) in the natural environment, it was possible to produce pyrophosphite. The formation of pyrophosphite is aided by the presence of divalent cations (such as Mg^{2+} and Ca^{2+} present in SMOW) to lower the required energy of formation and facilitate the reaction. Without the presence of divalent metal ions, the condensation reaction of sodium phosphite to pyrophosphite will only occur at higher temperatures (formation occurs above 140℃).

Based on the successful heating under natural geothermal conditions it was then appropriate to heat the phosphite produced by corrosion to try and obtain pyrophosphite. The phosphite produced in the fluids was concentrated by evaporation and dry heated to 90℃ on a sand bath to produce pyrophosphite. This temperature was lower than those observed on the Kverkfjöll site and thus seemed a good geological analogue for comparison. As reported in Chapter 2, pyrophosphite is capable of some very interesting prebiotic chemistry such as amino acid coupling to form proteins but also provides a P-O-P bond system similar to that found in ATP which could provide a useful energy currency molecule for the development of metabolism.

As discussed in Chapter 2, pyrophosphite can undergo reaction with phosphate in solution to produce isohypophosphate which would also be beneficial to prebiotic chemistry due to the release and recovery of chemical energy first by hydrolysis and then formation of P-O-P bonds in the reaction. Work in this Chapter also showed that it was possible to produce *ca.* 1% of condensed P species by heating at very mild temperatures (40℃) in natural fluids which would be of great benefit to origin of life reactions. The investigation

showed that during the process of evaporation, direct coupling of phosphite and phosphate would take place during the dehydration process, but, once the sample is dry, the favoured condensation product is pyrophosphite. The investigation also showed that, like pyrophosphite, the production of isohypophosphate was favoured at low pH (*ca.* pH 4) and that the presence of divalent cations in SMOW also favoured the formation of isohypophosphate under these conditions. The effects of increasing temperature on the formation of isohypophosphate were negligible as there was no apparent increase in products for the increase in temperature from 40℃ to 60℃ though it would seem prudent to consider lower temperatures which may yield different results. It is thought that the increase in temperature only speeds up the rate of dehydration of the sample so the amount of time available for reaction is reduced in what is assumed a linear fashion.

Based on these findings it is thought that the ideal natural environment for this chemistry to proceed would be an acidic (*ca.* pH 4), tidal environment in which salt water (SMOW) could be evaporated by gentle heating (to *ca.* 40℃ by either geothermal or solar energy) which would lead steady and repeated production of isohypophosphate and pyrophosphite. This repeated production of even small amounts would mean that high energy, condensed P species would be continuously available for utilisation in prebiotic chemistry though this theory is still to be tested.

The corrosion of iron meteorites in natural, acidic hydrothermal fluids has been shown to release phosphorus into the fluids but in much smaller amounts than that of pure iron phosphide, a schreibersite analogue. It has been shown that the corrosion of iron meteorites in hot (40-95℃), acidic fluids (<pH 4) would preferentially corrode the iron matrix but would also result in accelerated corrosion on the inclusion/matrix boundary. This is believed due to the inclusion being nobler in character due to the higher concentration of nickel than the matrix. Though the inclusion will corrode in the presence of acidic, hydrothermal fluids, it is only at a slow rate. The release of phosphorus is then greatly increased by the corrosion of the inclusion/matrix boundary exposing more of the inclusion surface up to the point when, sufficiently corroded, it would release the schreibersite inclusions into the fluids to corrode independently of the matrix.

During corrosion of the meteorite samples it was found that mineral contents of the fluid interacted and deposited on the surface of the meteorite. Analysis of the surface deposits established that an aluminosilicate clay was deposited on the surface and was fixed by some form of electrostatic interaction with the metal surface. It is not known what kind of effect this clay deposit has on the corrosion of the meteorite surface and this would require further investigation. The clay was identified by powder x-ray diffraction to be a mixture of heulandite [a$(Si_7Al_2)O_{18} \cdot 6\,H_{20}$], clinochlore [$Mg_5Al(SiAl)_4O_{10}(OH)_8$] and sulphur (orthorhombic). There was also evidence on sample C1 of pyrite [FeS_2] and marcasite deposition though it was not established if this was abiotic or biogenic in origin. The production of iron sulphides in the surface could make iron meteorites catalytic centres in a variety of prebiotic chemical reactions such as carbon fixation (Fischer-Tropsch synthesis) and synthesis of acetyl phosphate or methyl thioacetate, all of which according to Huber and Wäctershäuser (1997) can be utilised in origin of life reactions.[219]

In this Chapter it has been shown possible to go from a phosphorus containing iron mete-

orite to pyrophosphite by hydrothermal corrosion, evaporation and then dry heating using fluids and conditions found in the natural geological environment, specifically volcanic, acidic hydrothermal systems such as those encountered in the Kverkfjöll region of Iceland. The ability to produce phosphite and pyrophosphite in a natural environment using natural fluids and natural geothermal conditions from schreibersite shows that iron meteorites were a potential abundant source of reduced oxidation state phosphorus species. Geothermal and hydrothermal induced chemical reactions can then manipulate the phosphite produced into reduced, condensed phosphorus species which are highly reactive, soluble and useful in potential prebiotic chemistry.

Chapter 5

Conclusions and Future Work

5.1 Conclusions

This research has shown it possible to produce reduced oxidation state phosphorus species from acidic hydrothermal corrosion of phosphorus containing compounds such as iron phosphide and schreibersite, in relatively large quantities over a short period of time. The corrosion products identified were phosphine gas (*ca.* 0.1% available P), a highly reduced (P^{3-} oxidation state) and highly reactive form of phosphorus, and phosphite (*ca.* 10% available P in a 72 hour period), a reduced, reactive and water soluble phosphorus oxy-acid.

Phosphine gas released during corrosion into the atmosphere would readily react with a large number of airborne molecules photochemically, especially water, to form reduced, water soluble phosphorus oxy-acids (hypophosphite and phosphite) which could then be included in origin of life reactions.

The predominant species produced by acidic hydrothermal corrosion of iron phosphide was phosphite which is highly soluble in water and reactive making it a suitable solution to the "phosphate problem" mentioned in Chapter 1. The inclusion of phosphorus in reactions would therefore be much easier in the concentrations required by life today.

This research has confirmed that metal phosphite salts are able to undergo condensation reactions to form pyrophosphite by dry heating providing they are acidic salts (monobasic salts) or were in an acidic medium (between pH 3 and pH 6) prior to dehydration. Use of divalent metal ions, such as calcium or magnesium, significantly reduces the amount of energy required for the condensation reaction to occur (from *ca.* 160℃ to less than 90℃).

An investigation into the formation of pyrophosphite in the presence of iron showed that in the presence of ferrous iron it was possible to reduce phosphite [P^{3+}] to hypophosphite [P^{1+}] by dry heating at 160℃. It appears that the oxidation of ferrous iron caused the reduction of phosphite to hypophosphite during the heating process. This suggests that under plausible geological conditions, phosphite could be further reduced to a more soluble and more reactive form.

Ferrous iron was also shown to inhibit the formation of pyrophosphite. Heating calcium phosphite (usually forms pyrophosphite at 90℃) in the presence of ferrous iron to temperatures of 150℃ showed no reaction, but once temperatures exceeded 160℃, there was

signs of phosphite reduction to hypophosphite.

Having shown it to be possible to reduce phosphite under plausible geological conditions it was prudent to investigate the same effect on phosphate. Again it proved possible to reduce phosphate to phosphite at 160 ℃ in the presence of ferrous iron which is highly significant as a potential source of reduced phosphorus and could be an explanation for the observation of trace amounts of phosphite in waters of Hot Creek gorge by Pech *et al.* (2009).[33]

Investigation of the effects of ferric iron on the formation of pyrophosphite showed no beneficial or adverse effects on the production. This proved that production of condensed phosphorus species (such as pyrophosphite) from acidic hydrothermal corrosion of iron phosphide would either require oxidation of the ferrous to ferric iron or complete iron removal from solution.

The major analytical method used this research for identification and quantification of samples was NMR spectroscopy. NMR analysis of samples containing iron was an issue due to paramagnetism. Full iron removal was required before NMR analysis could be undertaken due to interference of iron with NMR (causing peak broadening or in severe cases, complete magnetic interference resulting in no signal). Iron removal required large amounts of sample manipulation due to pH adjustment and filtering, which may not only have diluted samples, but destroyed them completely. Investigation into alternative analytical methods for identification and quantification of pyrophosphite was undertaken as the issues of sample manipulation and iron removal prior to analysis were major problems.

Raman spectrometry seemed perfectly suited to provide non-destructive analysis with no sample manipulation required. Raman studies showed it was possible to identify individual components but when mixing samples for testing, heterogeneity of the sample became an issue. Mixing samples in water then dehydrating showed improvement on this but also destroyed the compound we wished to observe. |Issues with instrument access and only semi-quantitative analysis possible *via* this method, it was decided to look for an alternative.

Fluorometry was tested for quantification and was shown to provide visible indication to the presence of pyrophosphite in solution. Unfortunately, as phosphate also showed moderate fluorescence response and, though pyrophosphate response was much stronger, it could not be used for identification but only for quantification after identification by another method.

Production of reduced oxidation state phosphorus species, primarily phosphite [HPO_3^{2-}], is possible by acidic hydrothermal corrosion in natural fluids. This was quantified using ICP-AES by Dr. Claire Cousins (UCL) and the phosphorus oxidation states quantified by Prof. Matt Pasek (USF) using ion chromatography. The oxidation state analysis conducted by Prof. Pasek confirmed the main phosphorus oxidation state observed was P^{3+}, which was indicative of phosphite. The confirmation of the actual speciation present in the samples was completed using ^{31}P NMR spectroscopy for analysis, which confirmed that phosphite was indeed the main phosphorus species present in the fluid samples.

It was shown that it was possible to produce pyrophosphite, a low oxidation state, highly

reactive and highly soluble condensed phosphorus species under natural geological conditions by dry heating calcium phosphite in geothermally heated sand at *ca.* 95℃. The formation of pyrophosphite is aided by the presence of divalent cations (such as Mg^{2+} and Ca^{2+} present in SMOW) which lower the required energy of formation and facilitate the condensation reaction. Without the presence of divalent metal ions, the condensation reaction of sodium phosphite to pyrophosphite will only occur at higher temperatures (formation occurs above 140℃).

Based on the successful heating under natural geothermal conditions, phosphite produced by corrosion in natural fluids was concentrated by evaporation and dry heated to 90℃ in a sand bath to produce pyrophosphite. As reported in Chapter 2, pyrophosphite is capable of some very interesting prebiotic chemistry such as amino acid coupling to form proteins but also provides a P-O-P bond system similar to that found in ATP, which could provide a useful energy currency molecule for the development of metabolism.

It has also been shown possible by this research to produce *ca.* 1% of condensed P species by heating at very mild temperatures (40℃) in natural fluids. The investigation showed that during the process of evaporation, coupling of phosphite and phosphate would take place during the dehydration process. Once the sample is completely dried, the favoured condensation product is pyrophosphite.

The investigation also showed that, like pyrophosphite, the production of isohypophosphate was favoured at low pH (*ca.* pH 4) and that the presence of divalent cations in SMOW also favoured the formation of isohypophosphate under these conditions. The effects of temperature on the formation of isohypophosphate were shown to be negligible as there was no apparent increase in products for the increase in temperature from 40℃ to 60℃. It is thought that the increase in temperature only speeds up the rate of dehydration of the sample so the amount of time available for reaction is reduced in what is assumed to be a linear fashion.

Based on findings it is thought that the ideal natural environment for this chemistry to proceed would be an acidic (*ca.* pH 4), tidal environment in which salt water (SMOW) could be evaporated by gentle heating (to *ca.* 40℃ by either geothermal or solar energy), which would lead to steady and repeated production of isohypophosphate and pyrophosphite. This repeated production of even small amounts would mean that high energy, condensed P species would be continuously available for utilisation in prebiotic chemistry. This theory is yet to be thoroughly tested.

The corrosion of iron meteorites in natural, acidic hydrothermal fluids has been shown to release phosphorus but in much smaller amounts than that of pure iron phosphide. The corrosion of iron meteorites in hot (40-95℃), acidic fluids (<pH 4), has been shown to preferentially corrode the iron matrix but also accelerate corrosion of the inclusion/matrix boundary. This is believed to be due to the inclusion being nobler in character due to the higher concentration of nickel than the matrix. The release of phosphorus would be greatly increased by release of the inclusion into the hydrothermal fluids by corrosion of the matrix. At this point the inclusion will corrode independently of the matrix at a greatly increased rate due to the surface area.

It was found that the mineral content of the fluids would interact and be deposited on the surface of the meteorite during corrosion. Surface analysis by SEM/EDX established that aluminosilicate clay was deposited on the surface, fixed by electrostatic interaction with the metal surface. It is not known what effect the clay deposit has on the corrosion of the meteorite surface and this would require further investigation.

The clay, identified by X-ray diffraction to be a mixture of heulandite, clinochlore and elemental sulphur (orthorhombic). There was also evidence on sample C1 of pyrite [FeS_2, cubic] and marcasite [FeS_2, orthorhombic] deposition though it was not established if this was abiotic or biogenic in origin.

The production of iron sulphides on the surface could make iron meteorites catalytic centres in a variety of prebiotic chemical reactions such as carbon fixation (Fischer-Tropsch synthesis) and synthesis of acetyl phosphate or methyl thioacetate, all of which, according to Huber and Wäctershäuser (1997), can be utilised in origin of life reactions.[219]

The work in this thesis shows it is highly plausible to go from phosphorus containing iron meteorite to activated, reduced oxidation state phosphorus species. This is possible by hydrothermal corrosion, evaporation and dry heating, using fluids and conditions found in the natural geological environment. These conditions are encountered in volcanic, acidic hydrothermal systems such as those observed in the Kverkfjöll region of Iceland.

The work in this thesis clearly shows there is the potential for the production of reduced oxidation state phosphorus species and also activated condensed phosphites and phosphates under natural geological conditions. The ability to produce phosphite and pyrophosphite from schreibersite in the natural environment using hydrothermal fluids and geothermal conditions indicates that iron meteorites were a potentially abundant source of reduced oxidation state phosphorus species. These species can then be subject to hydrothermal/geothermal manipulation to produce condensed phosphorus species which are highly reactive, high energy, soluble and useful in prebiotic chemistry.

5.2 Future Work

Ideas and considerations for future work required to take this research forward are specified below;

1. The direct observation of phosphine gas was one objective not met during this research. One issue of direct phosphine observation is highly toxicity. Safety concerns were paramount when attempting direct observation. Phosphine is produced over a period of time, inside a flow reaction system using N_2 gas to keep the reaction system anaerobic. This means the phosphine produced is always below limits of detection for the Universal Gas Analyser. Attempts were made to collect or concentrate the gas without success. One possible solution would be to bubble the gas flow through a vessel containing cyclohexane, in which phosphine is highly soluble, then to use GC-MS analysis via a liquid injection method to look for phosphine dissolved in the cyclohexane.

2. The investigation of the effects of ferric iron [Fe^{3+}] on the production of condensed phosphorus species requires further investigation. It has been shown that ferrous iron [Fe^{2+}] when heated with sodium or calcium phosphite hinders formation of pyrophosphite up to *ca.* 180°C, and that, above this temperature, phosphite is reduced to hypophosphite. It was also shown that ferric iron would not hinder production of pyrophosphite from sodium or calcium phosphite at 160°C and 90°C, respectively, but it did not lower the temperature of formation of sodium phosphite unlike the presence of magnesium or calcium. Further investigation of the effects of ferrous and ferric iron on the formation of isohypophosphate, produced by the condensation method, is required to fully assess the plausibility of the prebiotic chemistry reported in Chapter 4.

3. The use of fluorescence spectroscopy was attempted for the quantification of pyrophosphite in solution. The fluorescence system chosen was originally reported by Fabbrizzi *et al.* (2002) for the quantification of pyrophosphate produced as a by-product of metabolic action under physiological conditions.[208] It was hoped adaptation of this method would allow quantification of pyrophosphite and isohypophosphate, due to the similarity in structures. The method was successfully tested for pyrophosphite but isohypophosphate was not tested due to time constraints. The method still requires optimisation for quantification purposes, with different fluorescent indicators and different quenching ensembles available for testing. The method showed potential for quantification of pyrophosphite in concentration ranges between 0.4 and 30 μM, but with other quenching ensembles or by using a different fluorescent indicator such as Coumarine-343 or Eosine-Y, which were also reported by Fabbrizzi *et al.* (2002), to tailor the sensitivity of the method for varying concentrations.[208]

4. The production of condensed phosphorus species, namely isohypophosphate and pyrophosphite, at low temperatures (40°C) in the presence of divalent cations was significant and requires further investigation. The mechanism for formation needs to be established. The question 'Would a repeated wetting and drying cycle in conditions analogous to tidal, evaporative pool systems, result in greater quantities of these molecules being produced as a cumulative effect?' need to be addressed. An experiment was planned and designed to investigate this theory but was never undertaken due to time constraints. The experiment was to repeatedly wet and allow to dry a mixture of phosphite and phosphate on a rotary evaporator at 40°C taking a small aliquot (0.5 g) of residues after each wetting and drying cycle to see whether, by repeated reaction of the same components, a noticeable accumulation of the reaction products would occur.

5. The failure of the solution chemistry experiments conducted in Kverkfjöll, Iceland was a disappointment. It would be beneficial to repeat this expedition to the original site of interest and to try to repeat these experiments under favourable naturally occurring geological conditions. The experience gained by the initial expedition allows for much better planning and preparation for a second visit allowing for much higher chances of success.

Chapter 6

Experimental

All chemicals used in this work were used as supplied without any preparation or purification unless stated otherwise.

A twin-columned drying column containing molecular sieves (4Å) and phosphorus pentoxide (P_2O_5) was used to dry dinitrogen gas (N_2) which was used in some reactions. PureShield Argon (Ar, 99.998%) and Oxygen Free Nitrogen (OFN, N_2, 99.998% minimum nitrogen) compressed gases supplied by BOC were also used in this work where stated.

All pH data was recorded using a Jenway Model 350 pH meter using either a standard epoxy bodied glass electrode or a NMR micro-probe glass electrode, both with a silver chloride internal reference electrode. Calibration was undertaken daily using standard solutions of phosphate buffer tablets (pH 7, Fisher Chemicals) and phthalate buffer tablets (pH 4, Fisher Chemicals) as specified in the operating manual. The buffer solutions were prepared by dissolving a single buffer tablet in a 100 mL volumetric flask and making up to the line with deionised water.

All deionised water used in this work was purified in-house using a Purite Select Analyst 100 combined reverse osmosis-deionisation system (1 – 10 MΩ.cm).

Standard mean ocean water (SMOW) was prepared using the ASTM International standard specification for substitute ocean water (D 1141) for guidance. The composition was adapted as not all chemicals required were available and were hence omitted from the solution. The composition of SMOW is shown in Table 6.1.

6.1 Methodology

All ^{1}H, ^{13}C{^{1}H}, ^{31}P and ^{31}P{^{1}H} NMR spectra were recorded on either a Bruker Avance 500 MHz spectrometer (operating frequencies: ^{1}H = 500.57 MHz, ^{13}C = 125.88 MHz and ^{31}P = 202.46 MHz), a Bruker DPX400 spectrometer (operating frequency: ^{1}H = 400.132 Hz) or a Bruker Ultrashield 300 MHz (operating frequencies: ^{1}H = 300.13 MHz, ^{13}C = 75.48 and ^{31}P = 121.49 MHz). Both the Avance 500 MHz and the Ultrasheild 300 MHz were using a 5 mm multi-nuclear Bruker BDFO$^{\text{PLUS}}$ SmartProbe™. All spectra were recorded at 300 K in D_2O unless otherwise stated. Chemical shifts (δ) stated are given in parts per

Chemical name	Formula	Mass (Mr)	Added (g/L)	Conc. (mM)
Sodium chloride	NaCl	58.443	24.534	419.794
Magnesium chloride hexahydrate	$MgCl_2 \cdot 6H_2O$	203.302	11.112	54.658
Sodium sulphate	Na_2SO_4	142.043	4.094	28.822
Calcium chloride	$CaCl_2$	110.983	1.158	10.434
Potassium chloride	KCl	74.551	0.695	9.322
Sodium hydrogen carbonate	$NaHCO_3$	84.007	0.200	2.381
Potassium bromide	KBr	119.002	0.100	0.840
Boric acid	H_3BO_3	61.833	0.027	0.437
Strontium chloride hexahydrate	$SrCl_2 \cdot 6H_2O$	266.617	0.042	0.158
Sodium fluoride	NaF	41.988	0.003	0.071

Table 6.1: The chemical composition of standard mean ocean water (SMOW) used in experiments. Heavy metals such as iron were omitted from the SMOW solution as they are paramagnetic and would interfere with analysis of the experiments which was mainly conducted by Nuclear Magnetic Resonance (NMR) spectroscopy. Full discussion of the effects of paramagnetic materials and NMR spectroscopy are discussed in Section 2.2.2.

million (ppm), coupling constants (J) stated in Hertz (Hz) and multiplicities are reported as singlet (s), doublet (d), triplet (t), quartet (q) and multiplet (m) and combinations of these as appropriate. All NMR spectra were recorded by the author or Mr. Simon Barrett (School of Chemistry NMR Service technician).

Infrared spectra were recorded using a Prospect FT-IR spectrometer over a range of 4000 cm^{-1} to 400 cm^{-1}. The spectral data was collected and processed using Galactic Industries MIDAC GRAMS/32 software (Version 4.11). All IR spectra were collected using KBr discs. Only principal absorptions are reported.

UV/Vis spectroscopy was conducted on a Thermo Spectronic Heλios γ fixed wavelength UV/Vis spectrometer. Absorption readings were taken at 880 nm, the stated absorption maxima for the molybdenum blue colorimetric method, using blank reagent as the reference solution.

Raman spectroscopy was carried out using a Renishaw InVia Micro-Raman spectrometer at the University of Bradford Analytical Centre. Raman analysis was carried out using laser wavelengths of either 633 nm (He-Ne laser) or 785 nm (diode laser) using a charge coupled detector (CCD). The data was collected using Wire 3.0 spectral acquisition software. Exposure time, laser power and the number of acquisitions used are stated within this chapter and were varied to obtain the best possible resolution. Calibration of the instrument was carried out before each use using a silicon wafer as a standard reference. The instrument was set to obtain a static scan at 1% laser power and 10 second exposure time to obtain a spectrum using the 50x objective lens which was focussed on the surface of the silicon wafer. A sharp intense peak at 520.5 cm^{-1} +/- 0.5 cm^{-1} was expected with any variation in the spectrum outside these parameters offset using the Wire 3.0 software. All spectra were obtained by the author unless otherwise credited.

Fluorometry was initially undertaken using a Perkin Elmer Lambda 900 UV/Vis/NIR spectrometer. Data was collected and processed using DataMax software (version 2.20) provided by Industries SA Inc. Fluorescein was used as the fluorescent indicator and the instrument was set to an excitation wavelength of 489 nm and set to observe emission at a wavelength of 513 nm. A later fluorometry assay was undertaken with the assistance of Dr. Christopher Empson at the University of Leeds. The assay was completed using a Hamilton Star automated liquid-handling robot and a Perkin-Elmer EnVision plate reader using an excitation wavelength of 489 nm and an observation wavelength of 513 nm.

Atomic absorption spectroscopy was conducted with an AAnalyst 100 spectrometer using AA Winlab acquisition and control software (version 3.2). Calibration was conducted as per the manufacturer operating instructions using standard solutions of iron at concentrations 1, 2, and 5 ppm; prepared by dilution in 100 mL volumetric flasks from a stock solution of 1000 ppm concentration iron. The calibration produced had a linear range between 0 and 5 ppm.

Elemental analyses (C, H and N) were conducted by Mr. Ian Blakeley (School of Chemistry Analytical Service) using a Thermo Electron Flash EA 1112 series analyser.

Mass spectroscopy was conducted by Miss Tanya Marinko-Covell (School of Chemistry Mass Spectrometry Service) using a Micromass ZMD spectrometer. Electrospray (ES)

ionisation technique was used with acetonitrile (CH_3CN) and water as solvents.

Powder X-ray data was collected on a Bruker D8 diffractometer. The diffractometer was controlled by computer running the Bruker XRD Commander software. The experimental parameters (scanning range, step size and collection time) were selected based on the sample type and the information required. X-rays of wavelength 0.154 nm were emitted from a Cu X-ray tube (voltage 40 kV, filament emission 30 mA). The instrument was set up in a Bragg-Brentano geometry, the receiving slit and scatter slit were 1 mm and 0.1 mm respectively. Data was manipulated using Bruker Evaluation and Thermo Grams AI software, figures for display were created in QTI Plot.

SEM/EDX analysis was undertaken on two separate instruments. The first was a Carl Zeiss EVO MA15 variable pressure W SEM with Oxford Instruments AztecEnergy EDX system with 80 mm X-Max SDD detector. The second was a Philips XL30 ESEM system fitted with an Oxford Instruments INCA250 EDX. Images are routinely acquired in backscatter electron (BSE) mode unless otherwise stated. Elemental X-ray data were compiled into 2D maps using the Oxford Instruments INCA software. Samples were analysed with a 20 kV accelerating voltage and a 10-12 mm working distance. Samples were carbon coated to prevent surface charging where specified.

IFM analysis was conducted using a Alicona InfiniteFocus Standard microscope running Alicona InfiniteFocus software (version 3.5.1.5) at the Materials Engineering Research Institute at Sheffield Hallam University. The Infinite Focus Microscope was used to construct a high resolution 3D image from a number of 2D images that have been captured between the lowest and highest focal plane. Areas of the sample that are determined to be in focus are compiled by the microscope software to produce a repeatable, sharp and accurate reconstruction of the surface of the sample.

Dissolved ion chemistry of water samples collected from Kverkfjöll were analysed at the Wolfson Geochemistry Laboratory by Dr. Claire Cousins at UCL using a Dionex Ion Chromatograph and Horoba JY Ultima 2C ICP-AES for dissolved anion and cation analyses respectively. The fluids were filtered through 0.45 μm in-line syringe filters to remove large solids prior to analysis. Dissolved phosphorus and phosphorus speciation of water samples collected from Kverkfjöll were analysed by Prof. Matt Pasek at the University of South Florida, Tampa using a Perkin Elmer S-200 HPLC fitted with an IonPac AS17-C ion chromatography column. Total phosphorus was measured on the attached, in-line Perkin Elmer Elan DRC II ICP-MS. The fluids were filtered through 0.45 μm in-line syringe filters to remove large solids prior to analysis.

6.2   Laboratory Work

6.2.1   Hydrothermal treatment of iron phosphide

6.2.1.1   Hydrothermal treatment of iron phosphide. Use of silver nitrate to observe phosphine gas generation.

Iron phosphide (Fe_3P, 1.27 g, 6.4 mmol) was placed in a side-arm Schlenk under nitrogen in a glove box and connected to a bubbler system. The bubbler system was a series of three 250 mL glass bubblers connected with 10 mm bore PVC tubing *ca.* 50 cm in length. The three bubblers contained deionised water (40 mL) in bubbler 1, silver nitrate solution (5% solution, 40 mL) in bubbler 2 and standard bleach in bubbler 3 (40 mL). Bubbler 2 was wrapped in aluminium foil to prevent reaction of the silver nitrate with light. A second sample was also wrapped in aluminium foil as a control sample for comparison after the completion of the experiment. Degassed sulphuric acid (H_2SO_4, *ca.* pH 4.6, 5 ml) was added to the reaction vessel *via* a positive pressure transfer method.

The reaction vessel was then heated rapidly to 90℃ with the acid being sparged by the argon flow to prevent re-gassing of the acid. After *ca.* 6 hours the heating the system was allowed to cool to 25℃ for running overnight and after 15 hours the experiment was stopped. Bubbler 2 and the control sample were both visibly inspected for the presence of silver metal. Silver metal was visible in bubbler 2 but not in the control sample. The pH of the water in bubbler 1 was also taken for comparison to the starting pH. The pH of the water in bubbler 1 before the experiment = pH 6.4 → The pH of the water in bubbler 1 after the experiment = pH 7.1

The previous experiment was repeated using the same set-up. The experiment was undertaken using deionised water in bubbler 1, silver nitrate solution (5% solution, 40 mL) in bubbler 2 and standard bleach (40 mL) in bubbler 3. A duplicate system was set up using iron filings (1.227 g) rather than iron phosphide with degassed sulphuric acid (H_2SO_4, *ca.* pH 4.6, 5 ml) to confirm if hydrogen produced was able to reduce silver nitrate or whether it was phosphine gas responsible for the reduction of silver nitrate. Both experiments were run simultaneously under the same conditions and gas flow.

Both systems were run without heating for *ca.* 43 hours then rapidly heated to 90℃ for *ca.* $6\frac{1}{2}$ hours before cooling to 25℃ for *ca.* $71\frac{1}{2}$ hours at which point the experiment was stopped. Both silver nitrate bubblers were checked for visible signs of silver metal. No silver metal was observed in either reaction trap.

6.2.1.2   Hydrothermal treatment of iron phosphide. Use of sodium hypochlorite to confirm the production of phosphine gas

Iron phosphide (Fe_3P, 1.288 g, 6.5 mmol) was placed in a side-arm Schlenk under nitrogen in a glove box and connected to a bubbler system specified previously. The bubbler system contained deionised water (40 mL), sodium hypochlorite solution (NaOCl, 4% available chlorine, 40 mL) and a final bubbler containing sodium hypochlorite (NaOCl, 4% available chlorine, 40 mL) as a final safety measure to ensure no phosphine could escape into the

atmosphere. The system was allowed to equilibrate under an argon flow of *ca.* 1 bubble per second for 15 minutes. Degassed sulphuric acid (H_2SO_4, *ca.* pH 4.6, 5 ml) was added to the reaction vessel *via* positive pressure method and the system given 15 minutes to equilibrate with the argon flow sparging the acid to prevent re-gassing of the acid.

The reaction vessel was then heated to 70℃ using a pre-heated oil bath to aid in corrosion of the metal phosphide and generation of phosphine. Heating was continued for *ca.* $4\frac{1}{2}$ hours then allowed to cool to 25℃ overnight. In the morning the sample was heated to 90℃ using the same pre-heated oil bath for *ca.* 9 hours. The reaction vessel was again allowed to cool to 25℃ overnight and after 48 hours the heating and gas flow was stopped.

The bleach in bubbler 2 was transferred to a 100 ml round bottomed flask and reduced to dryness on a rotary evaporator and the residue re-dissolved in a minimum of water (*ca.* 15 ml). A 2 ml aliquot was taken by volumetric pipette and again was reduced to dryness on a rotary evaporator then re-dissolved in 2 ml of D_2O. A 0.5 ml sample was taken by volumetric pipette for analysis by[31]P NMR spectroscopy. NMR spectroscopy was conducted by Mr. Simon Barrett, NMR technician. All NMR data is reported in Table 6.2.

To confirm the source of the phosphorus peak obtained was indeed phosphorus transfer from the reactor vessel and not contamination of the trapping fluid, a second NMR was run on a sample of NaOCl residue prepared by the same method as the sample for comparison. The NMR results are shown in Table 6.2. It was noticed that the stock NaOCl solution has phosphorus present prior to reaction as a contaminant. An alternative source of bleach was sought to solve this problem with $Ca(OCl)_2$ chosen as an alternative. Analysis by ^{31}P NMR spectroscopy (see Table 6.2 showed that the prepared $Ca(OCl)_2$ was clear from phosphorus contamination and thus could be used in place of NaOCl solution.

The pH of bubbler 1 was taken before and after the experimental run to confirm if any transfer of acidic gases such as hydrogen sulphide (H_2S) had taken place. The pH of the water in bubbler 1 before the experiment = pH 6.4 → The pH of the water in bubbler 1 after the experiment = pH 7.1.

^{31}P {^{1}H} NMR (D$_2$O, 300 K, 202.46 MHz)	
Conditions: pH 4.6, 90℃, 120 hours, anaerobic	
Analysis	
Bubbler 2	phosphate (δ5.1, s)
NaOCl	Phosphate (δ6.0, s)
Ca(OCl)$_2$	no visible phosphorus peaks

Table 6.2: Table of NMR data for the experiment to confirm the production of phosphine gas using sodium hypochlorite as a trapping agent. δ given in ppm.

6.2.1.3 Hydrothermal treatment of iron phosphide. Use of calcium hypochlorite to confirm the production of phosphine gas

Iron phosphide (Fe_3P, 2.25 g, 11.3 mmol) was placed into the reactor vessel from a glove box under nitrogen and degassed sulphuric acid (H_2SO_4, 2 M, 5 mL) was added by syringe. The reaction vessel was connected an altered experimental set-up in the same configuration as used in previous experiments. The altered experimental set-up used 50 mL test tubes

with a custom-built glass bubbler train which minimised dead space within the system and significantly reduced the required volumes in the bubbler system. The three bubblers contained deionised water (5 mL) in bubbler 1, calcium hypochlorite [$Ca(OCl)_2$, 1 mmol, 5 mL] in bubbler 2 and NaOCl (5 mL) in bubbler 3. Nitrogen gas was then bubbled through the system for 15 minutes and the reactor then heated rapidly to 90℃ in an oil bath for 72 hours. The reaction vessel looked to have completely dried of acid leaving a white, ash-like solid formed during this reaction.

The deionised water from bubbler 1 and the calcium hypochlorite solution from bubbler 2 were placed in 10 mm NMR tubes using 5 mm NMR tubes containing D_2O as inserts and analysed by ^{31}P-NMR spectroscopy. Full results of NMR analysis are shown in Table 6.3.

The white, ash-like solid was washed with deionised water (10 mL) and filtered by gravity to remove the solid from the washings. The solid was transferred to a watch glass and placed in the oven for 72 hours and the dry weight of the solid taken. The washings were treated with sodium sulphide (Na_2S, 1 M, *ca.* 10 mL in 1 mL additions) until no solid precipitated. The solid was filtered off by gravity and the sample lyophilised, the solid residue redissolved in D_2O (5 mL) and placed in a 10 mm NMR tube and submitted for analysis by[31]P NMR spectroscopy. The results of NMR analysis are shown in Table 6.3.

Analysis of reactor sample could not be completed due to still having high dissolved iron content. The sample was treated with sodium hydroxide (NaOH, 1 M, 50 mL) until pH 12 was obtained, the solution was then gravity filtered to remove the solid. The sample was then again lyophilised, the solid residue redissolved in D_2O and resubmitted for analysis by ^{31}P NMR spectroscopy. See Table 6.3 for NMR results.

	^{31}P NMR (D_2O, 300 K, 202.46 MHz)
	Conditions: pH 1, 90℃, 72 hours, anaerobic
	Analysis
Bubbler 1	no visible phosphorus peaks
Bubbler 2	hypophosphate ($\delta 7.7$, t, $^1J_{\text{P-H}} = 518$ Hz); phosphate ($\delta 3.03$, s)
Reaction Vessel	phosphite $\delta 4.0$, d, $^1J_{\text{P-H}} = 566$ Hz); phosphate ($\delta 6.3$, s)
	^{31}P{^{1}H} NMR (D_2O, 300 K, 202.46 MHz)
Bubbler 2	hypophosphite ($\delta 7.7$, s); phosphate ($\delta 3.1$, s)

Table 6.3: Table of NMR data for the experiment to confirm phosphine gas production using calcium hypochlorite as a trapping agent. δ given in ppm.

6.2.1.4 Use of calcium hypochlorite to confirm the production of phosphine gas

Repeat of experiment (6.2.1.3) was conducted to repeat confirmation of phosphine observation. Iron phosphide (Fe_3P, 1.009 g, 5.1 mmol) was placed in the reactor and degassed sulphuric acid (5 mL) added by syringe. Nitrogen carrier gas was bubbled through the system for 15 minutes then the reactor rapidly heated to 90℃ in an oil bath for 72 hours.

The bubblers dried out before 72 hours were reached. The nitrogen flow was stopped and

the reactor system taps closed. The traps were refilled as they were originally and the reaction restarted. The ambient temperature in the lab was very high (around 30℃) so the bubblers were submerged in a water bath to control temperature fluctuations.

Again the bubblers dried out before 72 hours were reached, the experiment was abandoned while the issue of the drying bubblers was investigated. The reaction vessel did not dry out as in the previous experiment. Deionised water (10 mL) was added to the reactor vessel and then filtered to remove solid. The washings were treated with sodium hydroxide (2 M, 30 mL) until pH 12 was obtained and the solid produced filtered by gravity. The solution was then lyophilised, the solid residue redissolved in D_2O and placed in a 10 mm NMR tube and submitted for analysis by ^{31}P-NMR spectroscopy. The results of the NMR analysis are shown in Table 6.4

31P NMR (D2O, 300 K, 202.46 MHz)
Conditions: pH 1, 90textcelsius, 72 hours, anaerobic
Analysis
Reaction Vessel   phosphite ($\delta 4.0$, d, $J_{P\text{-}H} = 566$ Hz); phosphate ($\delta 5.5$, s)

Table 6.4: Table of NMR data for the failed phosphine trapping experiment using calcium hypochlorite solution. δ given in ppm.

6.2.1.5   Use of calcium hypochlorite to confirm the production of phosphine gas – Repeat

Second repeat of experiment (6.2.1.3) was conducted to repeat confirmation of phosphine observation. Iron phosphide (Fe_3P, 2.25 g, 11.3 mmol) was placed in the reactor inside a glove box under nitrogen and degassed sulphuric acid (H_2SO_4, 5 mL) added by syringe under a flow of nitrogen. The bubbler system contained deionised water (5 mL) in bubbler 1, calcium hypochlorite ($Ca(OCl)_2$, 5 mL) in bubbler 2 and again calcium hypochlorite (5 mL) in bubbler 3. The reactor was rapidly heated to 90℃ using an oil bath and was heated continuously for 72 hours then the reactor was allowed to cool to room temperature and the taps on the reactor vessel closed to minimise oxygen exposure. The contents of bubblers 2 and 3 were transferred into 10 mm NMR tubes and submitted for analysis by ^{31}P NMR spectroscopy. Full NMR results are shown in Table 6.5.

The reactor vessel was dried out as in the original experiment. The contents of the reactor vessel were treated with deionised water (10 mL) and gravity filtered to remove any solids. Sodium hydroxide (NaOH, 2 M, *ca.* 15 mL) was added changing the pH of the washings from pH 3 to pH 12. A grey/green precipitate was formed which was removed by gravity filtration. The sample was then placed in a 100 mL round bottomed flask and reduced to dryness using a rotary evaporator. The residue was re-dissolved in deionised water (5 mL) and placed in a 10 mm NMR tube and submitted for ^{31}P NMR analysis. The sample from bubbler 2 was resubmitted for ^{31}P {^1H} NMR analysis to confirm the products and aid in identification of the unknown doublet at 3.4 ppm. See Table 6.5 for full NMR results.

^{31}P NMR (D$_2$O, 300 K, 202.46 MHz)	
Conditions: pH 1, 90℃, 72 hours, anaerobic	
Analysis	
Bubbler 2	phosphite (δ3.4, d, $^1J_{\text{P-H}}$ = 627 Hz); hypophosphite (δ7.9, t, $^1J_{\text{P-H}}$= 519 Hz); phosphate (δ0.8, s)
Bubbler 3	No visible phosphorus peaks after 16,384 scans. Assume no phosphorus presence
31P1H NMR (D2O, 300 K, 202.46 MHz)	
Bubbler 2	phosphite (δ3.4, s), hypophosphite (δ7.9, s); phosphate (δ0.8, s)

Table 6.5: Table of NMR data for second repeat attempt to confirm production of phosphine using calcium hypochlorite solution as a trapping agent. δ given in ppm.

6.2.1.6 Attempts to directly observe phosphine production using a Universal Gas Analyser (UGA)

The Universal Gas Analyser (UGA) is a quadrupole mass spectrometer which can be used to analyse and observe gas flows for composition. It is possible to select specific mass channels to observe and this allows real-time observation of gas flow systems. A quadrupole mass spectrometer works by drawing a small amount of the gas flow into the ionisation chamber. The gas molecules are ionised by electron impact (EI) removing electrons from the gas molecules giving them a positive charge. The gas ions are then accelerated into the quadrupole chamber by accelerator and repulsion plates.

The different mass:charge ratios (m/Z) are separated by four parallel metal rods which run the length of the quadrupole chamber. The opposing rod pairs are connected electrically and a RF voltage applied to each pair of rods alternately with a super-imposed DC current applied. As the ion stream passes down the centre axis of the rods, only ions of the correct mass:charge ratio pass through to the detector. Ions of incorrect mass:charge ratio undergo unstable trajectory and collide with the rods so not reaching the detector.

The UGA has the benefit of being able to observe isotopic exchange so substitution of deuterated sulphuric acid [D$_2$SO$_4$] to produce deuterated phosphine [PD$_3$] (M$_r$= 37) could also be observed to fully confirm the production of phosphine in the system. The UGA was used to observe both of the attempted silver nitrate reduction experiments and also the sodium hypochlorite experiment so full details of the experimental contents and conditions are described in Sections 6.2.1.1 and 6.2.1.2 above.

The UGA was started and allowed to run for $1\frac{1}{2}$ hours to allow temperatures and readings to reach equilibrium in air prior to use in the experiments.

6.2.1.6.1 UGA analysis of the silver nitrate experiment

The experiment was set up and conducted as discussed in 6.2.1.1. The system was degassed prior to beginning the experiment with argon for 15 minutes at a rate of 1 bubble per second. The system was then left to run for *ca.* 92 hours without heating to check the effects of the laboratory ambient conditions on the UGA traces. A timeline of the UGA events is shown in Table 6.6.

After the 92 hour observation period, rapid heating of the experiment to 90℃. It can be

Time	Action taken/Observation
00:16:30	Needle inserted into system
92:12:00	System checked. Channels 18 amu and 34 amu show correlation with turbo pump temperature
92:40:00	Started rapid heating to 90℃
93:00:00	Started gas sparging acid in reaction vessel
98:54:00	Started cooling to 25℃ for overnight run
120:00:00	Experiment stopped

Table 6.6: Time correlation data for the observation of the silver nitrate experiment. The table details actions taken during experiment based on UGA timings.
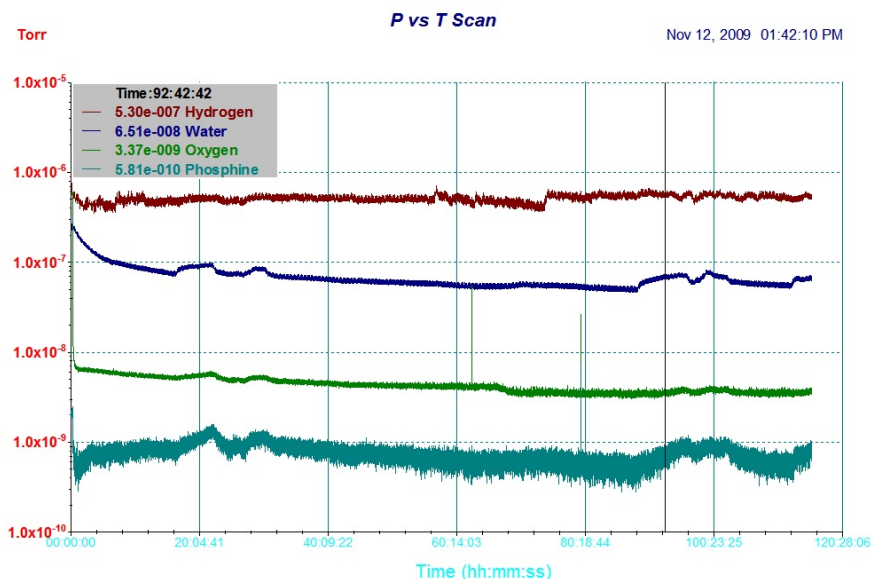
Figure 6.1: UGA trace of silver nitrate experiment.

seen from the UGA trace (see /reffig:EXPTBH002) that this resulted in a steady increase in the observed mass channels 18 (water) and 34 (phosphine). The experiment was heated for a period of 6 hours before cooling to room temperature. The experiment was formally stopped after 120 hours running. An overview of the gas trace shows that the increases in concentration shown on mass channels 18 and 34 coincide with the natural increase in the daytime temperature of the lab and not directly to the heating of the reaction vessel.

The repeat silver nitrate experiment involved two systems running independently, one with iron phosphide and the other with pure iron filings. Only the iron phosphide system was monitored *via* the UGA. The experiment was set up and conducted as discussed in 6.2.1.1. The system was degassed prior to beginning the experiment with argon for 15 minutes at a rate of 1 bubble per second. A timeline of the UGA events is shown in Table 6.7.

The system was heated rapidly to 90℃ after a period of 43 hours. It can be seen from the UGA trace (see /reffig:EXPTBH003) that this again resulted in a steady increase in the observed mass channels 18 (water) and 34 (phosphine) as in the previous attempt. After 6.5 hours heating the system was allowed to cool to room temperature and after 121 hours the experiment was stopped. Again the increases observed in the mass channels could not be directly attributed to the direct heating of the experiment and was comparable only to the fluctuations in lab temperature over the period of a day. With the data once again

Time	Action taken/Observation
00:05:30	Needle inserted in the system
00:09:00	Argon flow slowed to 1 bubble/second
19:32:00	Sample needle fell out of system
19:41:00	Sample needle reinserted into system
43:03:00	Started rapid heating to 90℃
49:36:00	Started cooling to 25℃
121:06:40	Experiment ended

Table 6.7: Time correlation data for the observation of the repeat silver nitrate experiment. The table details the actions taken during experiment based on UGA timings.
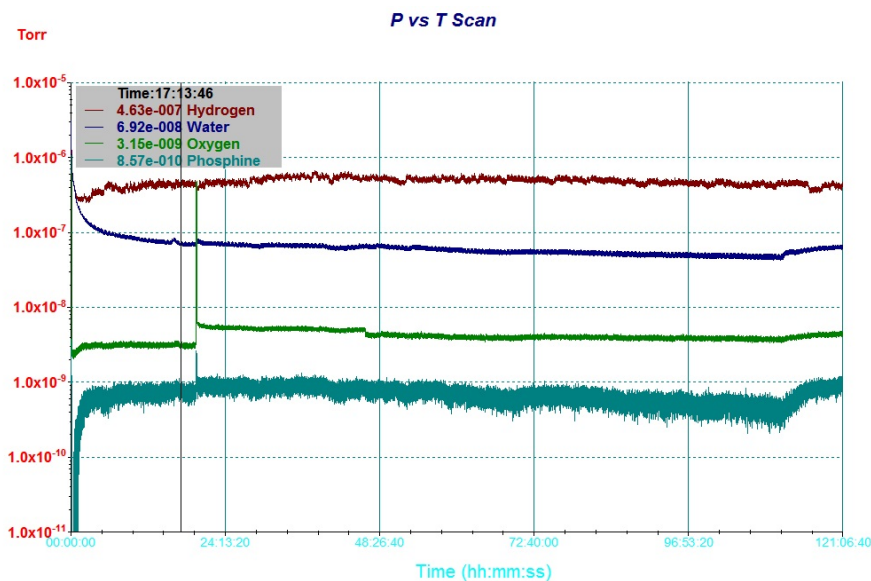
Figure 6.2: UGA trace of the repeat silver nitrate experiment.

inconclusive it was decided to have one last attempt to directly observe phosphine using the UGA setup.

The final experiment to attempt to directly observe for phosphine using the UGA was the sodium hypochlorite experiment. The experiment was set up and conducted as discussed in 6.2.1.2. The system was degassed prior to beginning the experiment with argon for 15 minutes at a rate of 1 bubble per second. The sample needle was then inserted into the system and the resting state of the reaction monitored for *ca.* 2 hours. A timeline of the UGA events is shown in Table 6.8.

The system was heated rapidly to 70℃ after a period of almost 3 hours then further heated to 90℃ after a period of 23 hours. It can be seen from the UGA trace (see /reffig:EXPTBH001) that this again resulted in a steady increase in the observed mass channels 18 (water) and 34 (phosphine) as in the previous attempt but also in a marked increase in the 2 mass channel. At just over 31 hours in the system was cooled and after a period of 48 hours the experiment was stopped. Once again the increases observed in the mass channels could not be directly attributed to the direct heating of the experiment and was comparable only to the fluctuations in lab temperature over the period of a day and as the results were inconclusive the attempts to directly observe phosphine production by this method were abandoned.

Time	Action taken/Observation
01:13:00	Sample needle inserted into system
01:15:30	Acid added to reaction vessel
01:44:30	Started gas sparging acid in reaction vessel
02:19:00	Sudden drop in O_2 (32 amu) channel
02:52:00	Started heating reaction vessel to 70°C
06:44:30	Visible increase in H_2 (2 amu) channel
07:23:00	Started cooling to 25textcelsius for overnight run
22:59:30	Starting rapid heating to 90°C
26:46:00	Increased argon flow to 2 bubbles/second
31:14:00	Started cooling to 25°C for overnight run
48:37:00	Experiment stopped

Table 6.8: Time correlation data for the observation of the sodium hypochlorite experiment. The table details the actions taken during experiment based on UGA timings.
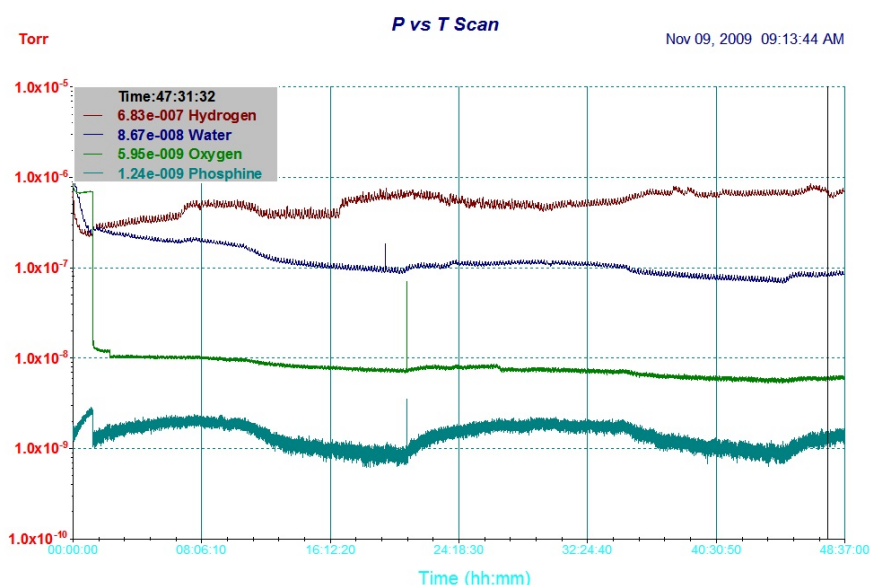
Figure 6.3: UGA trace of the sodium hypochlorite experiment.

6.2.1.7 Rate of phosphine production *via* hydrothermal processing of iron phosphide

Iron phosphide [Fe_3P, 2.25 g, 11.3 mmol] was placed into the reactor from a glove box under nitrogen and degassed sulphuric acid [H_2SO_4, 2M, 5 mL] was added by syringe. The reaction vessel was connected to the altered experimental set-up. The three bubblers contained deionised water (5 mL) in bubbler 1, calcium hypochlorite [$Ca(OCl)_2$, 1 mmol, 5 mL] in bubbler 2 and standard bleach (5 mL) in bubbler 3. Nitrogen gas was then bubbled through the system for 15 minutes and the reactor then heated rapidly to 90°C in an oil bath. After 24 hours, the taps to the reactor vessel were closed and bubbler 2 removed and swapped for another 50 mL test tube containing calcium hypochlorite [$Ca(OCl)_2$, 1 mmol, 5 mL]. The taps on the reactor vessel were reopened and the experiment allowed to run for a further 24 hours where again the taps on the reactor vessel were closed and bubbler 2 removed and swapped as previously stated. This step was repeated a further two times and after heating for a total of 96 hours the experiment was stopped.

The bleach samples collected (numbered $1-4$) were analysed quantatively for total phosphorus content by phosphomolybdate colorimetry.

6.2.2 Colorimetric Analysis of Dissolved Reactive Phosphorus Species

Concentration (ppm)	Reading 1	Reading 2	Reading 3	Average
1.500	0.797	0.795	0.796	0.796
1.250	0.693	0.695	0.694	0.694
1.000	0.580	0.581	0.580	0.580
0.750	0.413	0.414	0.413	0.413
0.625	0.354	0.353	0.354	0.354
0.500	0.304	0.304	0.303	0.304
0.375	0.269	0.270	0.270	0.270
0.250	0.133	0.133	0.131	0.132
0.125	0.066	0.067	0.067	0.067

Table 6.9: Table of absorbance recorded using the phosphomolybdate colorimetric method required for the calibration curve. The data were collected for concentrations of phosphorus between 1.5 ppm and 0.125 ppm with an average of 3 readings taken after allowing a 20-25 minute development time. The average absorption was then plotted on a graph (Figure 6.4) giving a straight line through the origin.
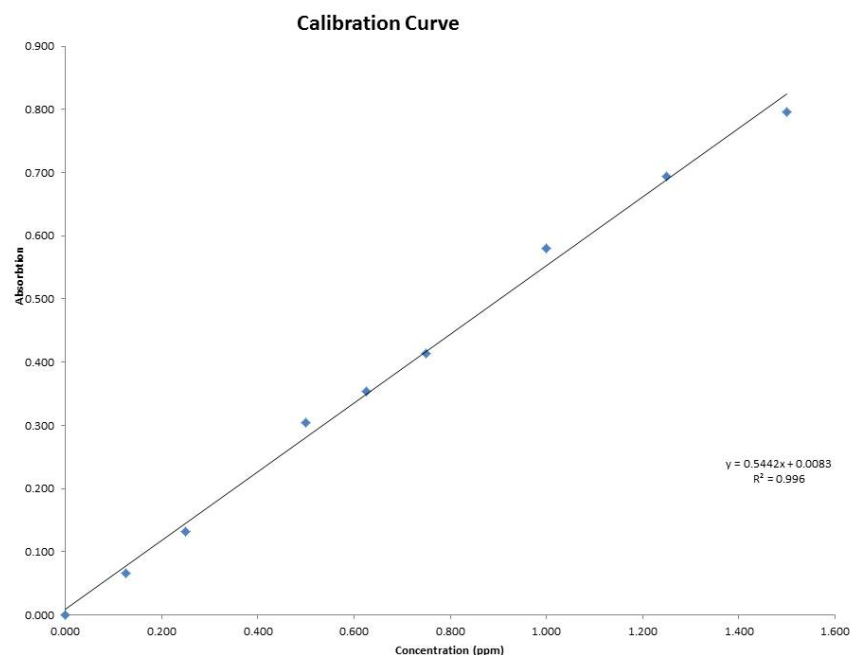
Figure 6.4: Calibration curve produced from absorption data of the known standards recorded in Table 6.9. The graph shows a linear response between 0 and 1.5 ppm for phosphate and $R^2 = 0.996$ calculated.

Colorimetric analysis was undertaken using the standard method for phosphorus analysis (4500-P) stated in "Standard Methods for the Examination of water and Wastewater" published by the American Public Health Association, Water Environment Federation.[188] The persulphate digestion method was used for oxidation of the standards and samples and the ascorbic acid method used for development of the molybdenum blue complex. Measurement of the absorption of each sample was taken after allowing 25 minutes for developing colour.

A series of standard solutions was prepared from a 200 ppm stock solution of potassium

phosphate monobasic (KH_2PO_4, 0.2195 g in 250 mL). Standards were used to produce a calibration curve from which the concentration of the samples could then be extrapolated. The initial set standard solutions were prepared in 100 mL volumetric flasks to concentrations of 100, 50, 20, 10, 5, 2 and 1 ppm. A second set of standards with concentrations of 2.5, 2, 1.5, 1.25, 1, 0.75, 0.5 and 0.25 ppm were prepared to refine the calibration curve and a final set of standards with concentrations of 1.5, 1.25, 1, 0.75, 0.625, 0.5, 0.375, 0.25 and 0.125 ppm were then used to create the calibration curve. The absorption data is shown in Table 6.9 and the calibration curve is shown in Figure 6.4. The calibration curve shows a linear absorption response in the 0 to 1.5 ppm range and an $R^2 = 0.996$ calculated.

6.2.2.1 Phosphomolybdate colorimetric analysis of hydrothermal corrosion experiments

The contents of bubbler 2 from the hydrothermal experiments 6.2.1.3 and 6.2.1.4 and also the washings from the reaction vessels from the same experiments were digested using the persulphate method and analysed as stipulated in 6.2.2. The absorption measured by UV/Vis spectroscopy was used to extrapolate the concentration for each sample to give the total amount of phosphorus liberated by acid hydrolysis. Dilution of the samples was required to bring the absorption within a linear range to allow extrapolation of the concentration. All extrapolated concentrations were then multiplied by a dilution factor to give the true concentration for each sample. Two samples of deionised water, one freshly prepared and one which was 5 days old from the storage vessel were also analysed to get background phosphorus content for the water used. The absorption data and calculated concentrations are shown in Table 6.10.

Source	Abs	Conc. (ppm)	Dil.	Conc. (ppm)
Bubbler (1)	0.214	0.378	20	7.6
Reactor (1)	0.828	1.506	4500	6778
Bubbler(2)	0.201	0.354	20	7.0
Reactor (2)	0.768	1.396	4500	6282
Blank (fresh)	0.012	0.007	1	0.007
Blank (5 days)	0.081	0.134	1	0.134

Table 6.10: Table of absorption data for the reaction vessels and phosphorus bubbler traps of the two successful calcium hypochlorite hydrothermal corrosion experiments. Concentrations calculated by extrapolation using calibration curve obtained and expressed in ppm after adjustment for any dilution required.

6.2.2.2 Phosphomolybdate colorimetric analysis of the hydrothermal corrosion of iron phosphide to determine the rate of phosphine production

Four samples were collected from bubbler 2 during the hydrothermal corrosion of iron phosphide as specified in 6.2.1.7. The fluids of each of the four samples collected from bubbler 2 were digested using the persulphate method and analysed as stipulated in 6.2.2. The absorption measured by UV/Vis spectroscopy was used to extrapolate the concentration for each sample to give the total amount of phosphorus liberated by acid hydrolysis.

Dilution of the samples was required to bring the absorption within a linear range to allow extrapolation of the concentration. The absorption data and calculated concentrations are shown in Table 6.11.

Sample	Abs 1	Abs 2	Abs 3	Ave.	Conc. (ppm)	Dil.	Conc. (ppm)
1	0.140	0.141	0.141	0.141	0.244	20	4.88
2	0.018	0.019	0.018	0.018	0.018	20	0.36
3	0.029	0.029	0.029	0.029	0.038	20	0.76
4	0.012	0.012	0.013	0.012	0.007	20	0.14

Table 6.11: Table of absorption data for the phosphorus bubbler trap of the phosphine production rate hydrothermal corrosion experiment designed to look at the evolution of phosphine over time. Concentrations calculated using calibration curve obtained and expressed in ppm after adjustment for dilution.

6.2.3   Preparation of sodium phosphite

Sodium phosphite was prepared by the method stipulated by Amat (1888a).[201] Phosphinic acid (H_3PO_3, 4.1 g, 50 mmol) and sodium hydroxide (NaOH, 2 g, 50 mmol) were slowly dissolved in 50 mL deionised water in a 250 mL conical flask. Once dissolved completely the solution was reduced to dryness on a rotary evaporator and then transferred to a 50℃ oven and allowed to dry further overnight. The resultant white solid was ground in a mortar and pestle to a fine powder. A small portion of the crystals were dissolved in D_2O (*ca.* 0.5 mL) and submitted for analysis by ^{31}P NMR spectroscopy. NMR data is shown in Table 6.12.

^{31}P NMR (D$_2$O, 300 K, 121.49 MHz)	
H$_3$PO$_3$ (4.1 g, 50 mmol) + NaOH (2 g, 50 mmol)	
Analysis	
NaH$_2$PO$_3$	δ3.1, d, $^{1}J_{\text{P-H}}$ = 566 Hz

Table 6.12: Table of NMR data for sodium phosphite prepared from 1:1 mixing of phosphonic acid and sodium hydroxide in 50 mL deionised water. δ given in ppm.

6.2.4   Preparation of magnesium phosphite

6.2.4.1   Preparation of magnesium phosphite monobasic – Magnesium chloride and phosphonic acid

An attempt was made to produce magnesium phosphite by the adaptation of a method stipulated by Ortiz-Avila *et al.* (1989).[204] Magnesium chloride hexahydrate ($MgCl_2 \cdot 6\,H_2O$, 0.51 g, 2.5 mmol) and sodium phosphite (NaH_2PO_3, 0.52 g, 5 mmol) were dissolved in 5 mL deionised water in a 25 mL conical flask and stirred for 6 hours. After 6 hours the stirring was stopped and the solution left to crystallise. No crystals formed after 2 months.

6.2.4.2 Preparation of magnesium phosphite monobasic – Magnesium oxide and phosphonic acid

Magnesium oxide [MgO, 0.1 g, 2.5 mmol] and phosphonic acid [H_3PO_3, 0.41 g, 5 mmol] were dissolved in 5 mL deionised water in a 25 mL conical flask and stirred for 6 hours under a constant flow of nitrogen. After 6 hours the stirring was stopped and the solution left to crystallise. After 3 days a white micro-crystal precipitate formed which was collected by vacuum filtration using a Hirsch funnel then dried in a vacuum desiccator. A small portion of the crystals were dissolved in D_2O (*ca.* 0.5 mL) and submitted for analysis by ^{31}P NMR spectroscopy. NMR data is shown in Table 6.13.

^{31}P NMR (D_2O, 300 K, 121.49 MHz)
H_3PO_3 (0.41 g, 5 mmol) + MgO (0.1 g, 2.5 mmol)
Analysis
Mg(H_2PO_3)$_2$ δ2.6, d, $^1J_{P\text{-}H}$ = 632 Hz

Table 6.13: Table of NMR data for magnesium phosphite prepared from 2:1 mixing of phosphonic acid and magnesium oxide in 5 mL deionised water. δ given in ppm.

6.2.4.3 Preparation of magnesium phosphite monobasic – Magnesium metal and phosphonic acid

Magnesium turnings (Mg, 1.22 g, 50 mmol) were added slowly to phosphonic acid (H_3PO_3, 8.2 g, 100 mmol) dissolved in 50 mL deionised water in a 250 mL conical flask. The turnings were added in small portions over a period of 2 days until there was no evolution of hydrogen by further addition. The resultant solution was filtered to remove any unreacted metal and left to crystallise. Within 48 hours there was a large mat of crystals formed on the bottom of the conical flask. The crystals were harvested by vacuum filtration using a Buchner funnel and dried in a vacuum desiccator. A small portion of the crystals were dissolved in D_2O (*ca.* 0.5 mL) and submitted for analysis by ^{31}P NMR spectroscopy. NMR data is shown in Table 6.14.

^{31}P NMR (D_2O, 300 K, 121.49 MHz)
H_3PO_3 (4.1 g, 50 mmol) + Mg (1.22 g, 25 mmol)
Analysis
Mg(H_2PO_3)$_2$ δ2.9, d, $^1J_{P\text{-}H}$ = 592 Hz

Table 6.14: Table of NMR data for magnesium phosphite prepared from 2:1 mixing of phosphonic acid and magnesium turnings in 50 mL deionised water. δ given in ppm.

6.2.5 Preparation of calcium phosphite

6.2.5.1 Preparation of calcium phosphite monobasic – Calcium chloride and phosphonic acid

It was attempted to produce calcium phosphite monobasic by the adaptation of a method stipulated by Ortiz-Avila *et al.* (1989).[204] Calcium chloride ($CaCl_2$, 2.78 g, 25 mmol) and

phosphonic acid (H_3PO_3, 450 g, 50 mmol) was dissolved in 50 mL deionised water in a 250 mL conical flask. A colourless solution was formed. The flask was sealed with parafilm and a small syringe needle fitted to allow slow evaporation. The flask was then placed at the back of a fume cupboard at room temperature and checked on periodically. There was no formation of crystals after 3 months just a translucent gum in the bottom of the flask.

6.2.5.2 Preparation of calcium phosphite monobasic – Calcium carbonate and phosphonic acid

It was attempted to produce calcium phosphite monobasic by a method published by Larbot *et al.* (1984).[206] Calcium carbonate ($CaCO_3$, 5 g, 50 mmol) and phosphonic acid (H_3PO_3, 8.2 g, 100 mmol) were dissolved in 50 mL deionised water in a 250 mL conical flask. The solution was placed in a 60℃ oven for 4 hours then removed and allowed to cool to room temperature. Within 3 days a white microcrystal precipitate was observed. This was collected by vacuum using a Buchner funnel and dried in a vacuum desiccator. The liquor was left to see if there would be any further crystallisation. After 2 weeks a crop of thick rod-like translucent crystals were collected by vacuum in a Buchner funnel and dried in a vacuum desiccator. Again the liquor was left and after a further 2 weeks another crop of the rod-like crystals was obtained. The white micro-crystals and the translucent rod-like crystals were ground to a fine powder using a mortar and pestle and dissolving a small amount in D_2O (*ca.* 0.5 mL) and analysed by ^{31}P NMR spectroscopy. NMR data is shown in Table 6.15.

^{31}P NMR (D_2O, 300 K, 121.49 MHz)	
H_3PO_3 (8.2 g, 100 mmol) + $CaCO_3$ (5 g, 50 mmol)	
Analysis	
$Ca(H_2PO_3)_2$	$\delta 2.6$, d, $^1J_{\text{P-H}}= 627$ Hz

Table 6.15: Table of NMR data for calcium phosphite monobasic prepared from 2:1 mixing of phosphonic acid and calcium carbonate in 50 mL deionised water. δ given in ppm.

6.2.6 Formation of sodium pyrophosphite *via* dry heating method

6.2.6.1 Formation of sodium pyrophosphite – Dry heating of 1:1 prepared sodium phosphite

Sodium phosphite was prepared as per 6.2.3. The sodium phosphite kept dry by storing in a 50℃ oven and was prepared by grinding in a mortar and pestle to a fine powder. The ground sodium phosphite (*ca.* 10 g) was then loaded into quartz tube and heated to between 180-220℃ in a tube furnace for 72 hours under a constant flow of nitrogen. The furnace was allowed to cool to room temperature and the tube removed. The sodium phosphite powder had taken a light orange colour during heating. The sample was analysed by ^{31}P NMR spectroscopy to confirm conversion to sodium pyrophosphite and to establish the purity of the sample. NMR data is shown in Table 6.16 (NMR data for clean conversion) and Table 6.17 (NMR data showing sample impurities). The sample impurities are investigated in Sections 6.2.6.2 and 6.2.6.3.

Compound:	Pyrophosphite $[\mathbf{H_2P_2O_5^{2-}}]$	Phosphite $[\mathbf{HPO_3^{2-}}]$
Conditions:	160°C, 72 hours, N_2 flow	
Composition (%):	94	6
Analysis		
^{1}H NMR (D$_2$O, 300 K, 300.13 Hz)	δ6.9 (AA'XX', $^1J_{\text{P-H}}=$ 663 Hz, $^2J_{\text{P-P}}=$ 9 Hz, $^3J_{\text{P-H}}=$ 9 Hz	δ6.8 (d, $^1J_{\text{P-H}}=$ 597 Hz)
^{31}P NMR (D$_2$O, 300 K, 121.49 Hz)	δ-5.0 (AA'XX', $^1J_{\text{P-H}}=$ 663 Hz, $^2J_{\text{P-P}}=$ 10 Hz, $^3J_{\text{P-H}}=$ 9 Hz	δ6.8 (d, $^1J_{\text{P-H}}=$ 596 Hz)

Table 6.16: Table of NMR data for ^{1}H and ^{31}P NMR spectroscopic analysis of the condensation of sodium phosphite to form sodium pyrophosphite. δ given in ppm

^{31}**P NMR (D$_2$O, 300 K, 121.49 MHz)**	
NaH$_2$PO$_3$ (10 g, 96 mmol), 180°C, 72 hours, N$_2$	
Analysis	
Na$_2$H$_2$P$_2$O$_5$	cyclotrimetaphosphate (δ-21.3, s); pyrophosphate (δ-10.6, s); Pyrophosphite (δ-5.0, AA'XX', $^1J_{\text{P-H}} = 667$ Hz, $^2J_{\text{P-P}}=$ 9 Hz, $^3J_{\text{P-H}}=$ 8 Hz); phosphate (δ0.0, s); phosphite (δ2.84, d, $^1J_{\text{P-H}}=$ 633 Hz); other minor peaks indicative of small amounts of linear tri- and tetra-polyphosphates.

Table 6.17: Table of NMR data for the preparation of sodium pyrophosphite by dry heating sodium phosphite at 180°C for 72 hours in a tube furnace. δ given in ppm.

6.2.6.2 Formation of sodium pyrophosphite – Dry heating of sodium phosphite prepared with 5% wt. excess acid

The previous experiment (6.2.6.1) was repeated with sodium phosphite which was prepared as in 6.2.3 but with a 5% by wt. excess of acid. Phosphonic acid (H$_3$PO$_3$, 8.6 g, 105 mmol) and sodium hydroxide (NaOH, 4 g, 100 mmol) were slowly dissolved in 20 mL deionised water. Once dissolved completely the solution was reduced to dryness on a rotary evaporator and then dried overnight in a 50°C oven. The resultant white solid was then ground to a fine powder in a mortar and pestle then loaded into a 100 mL round bottom flask fitted with a gas inlet allowing a constant flow of nitrogen through the flask. The solid was then heated on a sand bath at 240°C for 72 hours. The solid had taken on a heavy orange colour during heating. The composition of the sample was analysed by ^{31}P NMR spectroscopy to confirm the conversion to sodium pyrophosphite and to establish the purity of the sample. NMR data is shown in Table 6.18.

31P NMR (D2O, 300 K, 121.49 MHz)
NaH2PO3 (5% wt excess acid, 10 g, 96 mmol), 240°C, 72 hours, N_2
Analysis
Na2H2P2O5   pyrophosphite (δ-5.1, AA'XX', $^1J_{P\text{-}H}$= 666 Hz, $^2J_{P\text{-}P}$= 9 Hz, $^3J_{P\text{-}H}$= 8 Hz); phosphite (δ3.1, d, $^1J_{P\text{-}H}$= 577 Hz); other peaks indicative of small amounts of linear tri- and tetra-polyphosphates.

Table 6.18: Table of NMR data for the preparation of sodium pyrophosphite by dry heating sodium phosphite which was prepared with a 5% wt excess of phosphonic acid. The phosphite was heated to 240°C for 72 hours on a sand bath under flowing nitrogen. δ given in ppm.

6.2.6.3 Formation of sodium pyrophosphite – Dry heating of sodium phosphite prepared with 5% wt. excess hydroxide

The previous experiment (6.2.6.1) was again repeated with sodium phosphite which was prepared as in 6.2.3 but with a 5% by wt. excess of hydroxide. Phosphonic acid (H_3PO_3, 8.2 g, 100 mmol) and sodium hydroxide (NaOH, 4.2 g, 105 mmol) were slowly dissolved in 20 mL deionised water. Once dissolved fully the solution was reduced to dryness on a rotary evaporator and the dried overnight in a 50°C oven. The resultant white solid was ground in a mortar and pestle to a fine powder then loaded into a 100 mL round bottomed flask and fitted with a gas inlet allowing a constant flow of nitrogen over the solid. The solid was then heated to 240°C on a sand bath for 72 hours. The composition of the sample was analysed by ^{31}P NMR spectroscopy to confirm the conversion to sodium pyrophosphite and to establish the purity of the sample. NMR data is shown in Table 6.19.

^{31}P NMR (D_2O, 300 K, 121.49 MHz)
NaH$_2$PO$_3$ (5% wt excess hydroxide, 10 g, 96 mmol), 240°C, 72 hours, N_2
Analysis
Na$_2$H$_2$P$_2$O$_5$ pyrophosphite (δ-5.06, AA'XX', $^1J_{P\text{-}H}$= 666 Hz, $^2J_{P\text{-}P}$= 9 Hz, $^3J_{P\text{-}H}$= 8 Hz); phosphite (δ3.05, d, $^1J_{P\text{-}H}$= 577 Hz)

Table 6.19: Table of NMR data for the preparation of sodium pyrophosphite by dry heating sodium phosphite which was prepared with a 5% wt excess of sodium hydroxide. The phosphite was heated to 240°C for 72 hours on a sand bath under flowing nitrogen. δ given in ppm.

6.2.7 Formation of magnesium pyrophosphite *via* dry heating method

6.2.7.1 Formation of magnesium pyrophosphite – Magnesium oxide prepared phosphite

Magnesium phosphite [assumed $Mg(H_2PO_3)_2$, 5 g, 27 mmol] prepared using the method specified in 6.2.4.2 was ground in a mortar and pestle to a fine powder and transferred to a 50 mL round bottomed flask fitted with a gas inlet allowing a constant flow of nitrogen through the flask. The solid was then heated on a sand bath at 90°C for 72 hours. An aliquot (*ca.* 0.5 g) was taken and dissolved in D_2O (0.5 mL) and analysed by ^{1}H NMR spectroscopy. NMR data is shown in Table 6.20.

Compound:	Pyrophosphite $[\mathrm{H_2P_2O_5^{2-}}]$	Phosphite $[\mathrm{HPO_3^{2-}}]$
Conditions:	MgO(1):(2)H$_3$PO$_3$, deionised water, N$_2$ flow **Analysis**	
1H NMR (D$_2$O, 300 K, 300.13 Hz)	n/a	δ6.7 (d, $^1J_{\mathrm{P\text{-}H}}=$ 633 Hz)
Conditions:	90℃, 72 hours, N$_2$ flow	
Composition (%):	8.3	91.7
^{1}H NMR (D$_2$O, 300 K, 300.13 Hz)	δ6.8 (AA'XX', $^1J_{\mathrm{P\text{-}H}}=$ 669 Hz, $^2J_{\mathrm{P\text{-}P}}=$ 9 Hz, $^3J_{\mathrm{P\text{-}H}}=$ 9 Hz)	δ6.7 (d, $^1J_{\mathrm{P\text{-}H}}=$ 633 Hz)

Table 6.20: Table of NMR data for ^{1}H NMR spectroscopic analysis of the formation and condensation of magnesium phosphite prepared by magnesium oxide/phosphonic acid reaction. δ given in ppm

6.2.7.2 Formation of magnesium pyrophosphite – Study of formation over time

The remaining dry heated magnesium phosphite sample from the previous experiment (6.2.7.1) was resealed and the sample heated for a further 72 hours at 90℃ under flowing nitrogen. An aliquot (*ca.* 0.5 g) was taken and dissolved in D$_2$O (0.5 mL) and analysed by ^{1}H NMR spectroscopy. This process was continued for a period of 21 days in total to monitor the generation of pyrophosphite over time. NMR data is shown in Table 6.21.

6.2.7.3 Formation of magnesium pyrophosphite – Magnesium metal prepared phosphite

Magnesium phosphite [assumed Mg(H$_2$PO$_3$)$_2$, 5 g, 27 mmol] prepared using the method specified in 6.2.4.3 were ground in a mortar and pestle to a fine powder and transferred to a 50 mL round bottomed flask fitted with a gas inlet allowing a constant flow of nitrogen through the flask. The solid was then heated on a sand bath at 90℃ for 72 hours. An aliquot of sample (0.5 g) was dissolved in D$_2$O (0.5 mL) and analysed by ^{1}H NMR spectroscopy. Full NMR data are provided in Table 6.22.

6.2.7.4 Formation of magnesium pyrophosphite – Study of formation issues

With no pyrophosphite visibly generated in the previous experiment it was decided to continue heating the sample to see if any pyrophosphite was produced. The remaining dry heated magnesium phosphite sample from the previous experiment (6.2.7.3) was resealed and the sample heated for a further 72 hours at 90℃ under flowing nitrogen. An aliquot (*ca.* 0.5 g) was taken and dissolved in D$_2$O (0.5 mL) and analysed by ^{1}H NMR spectroscopy. This process was continued for a period of 21 days in total to monitor for generation of pyrophosphite. After 18 days as no pyrophosphite was observed, the sample was dissolved in deionised water (10 mL) and adjusted to pH 4 using HCl (1 M, dropwise addition), dried on a rotary evaporator then ground to a fine powder using a mortar and pestle. The

^{1}**H NMR (D$_2$O, 300 K, 300.13 MHz)**			
Conditions: Mg(H$_2$PO$_3$)$_2$ (5 g, 27 mmol), 90℃, N$_2$			
Analysis			
Compound:	**Phosphite [HPO$_3^{2-}$]**	**Pyrophosphite [H$_2$P$_2$O$_5^{2-}$]**	**% Conv.**
3 days	δ6.7, d, $^1J_{\text{P-H}}$ = 626 Hz	δ6.8, AA'XX', $^1J_{\text{P-H}}$ = 669 Hz, $^2J_{\text{P-P}}$ = 10 Hz, $^3J_{\text{P-H}}$ = 8 Hz	9.1
6 days	δ6.7, d, $^1J_{\text{P-H}}$ = 633 Hz	δ6.8, AA'XX', $^1J_{\text{P-H}}$ = 673 Hz, $^2J_{\text{P-P}}$ = 10 Hz, $^3J_{\text{P-H}}$ = 8 Hz	25.3
9 days	δ6.7, d, $^1J_{\text{P-H}}$ = 634 Hz	δ6.8, AA'XX', $^1J_{\text{P-H}}$ = 672 Hz, $^2J_{\text{P-P}}$ = 10 Hz, $^3J_{\text{P-H}}$ = 8 Hz	41.9
12 days	δ6.7, d, $^1J_{\text{P-H}}$ = 634 Hz	δ6.8, AA'XX', $^1J_{\text{P-H}}$ = 672 Hz, $^2J_{\text{P-P}}$ = 10 Hz, $^3J_{\text{P-H}}$ = 8 Hz	41.5
15 days	δ6.7, d, $^1J_{\text{P-H}}$ = 635 Hz	δ6.8, AA'XX', $^1J_{\text{P-H}}$ = 672 Hz, $^2J_{\text{P-P}}$ = 10 Hz, $^3J_{\text{P-H}}$ = 8 Hz	58.7
18 days	δ6.7, d, $^1J_{\text{P-H}}$ = 634 Hz	δ6.8, AA'XX', $^1J_{\text{P-H}}$ = 672 Hz, $^2J_{\text{P-P}}$ = 10 Hz, $^3J_{\text{P-H}}$ = 8 Hz	59.7
21 days	δ6.7, d, $^1J_{\text{P-H}}$ = 635 Hz	δ6.8, AA'XX', $^1J_{\text{P-H}}$ = 672 Hz, $^2J_{\text{P-P}}$ = 10 Hz, $^3J_{\text{P-H}}$ = 8 Hz	64.7

Table 6.21: Table of NMR data for the study of formation of magnesium pyrophosphite over time by dry heating magnesium phosphite prepared using the magnesium oxide method (6.2.4.2). The phosphite was heated to 90℃ for 72 hour periods on a sand bath under flowing nitrogen for a total of 21 days. δ given in ppm.

Table 6.22: Table of NMR data for [^{31}P] NMR spectroscopic analysis of the formation and condensation of magnesium phosphite prepared by magnesium metal/phosphonic acid reaction. δ given in ppm

Compound:	Pyrophosphite $[H_2P_2O_5^{2-}]$	Phosphite $[HPO_3^{2-}]$
Conditions:	**Analysis**	90°C, 72 hours, N_2 flow
MgHPO3 crystals	[^{31}P] NMR (D_2O, 300 K, 121.49 Hz) n/a	$\delta 2.9$, d, $^1J_{\text{P-H}}=$ 592 Hz
MgHPO3 crystals – 90°C	[^{31}P] NMR (D_2O, 300 K, 121.49 Hz) n/a	$\delta 2.6$, d, $^1J_{\text{P-H}}=$ 627 Hz
MgHPO3 crystals – pH 4, 90°C	**Composition (%):** ^{1}H NMR (D_2O, 300 K, 300.13 Hz) 22 $\delta 6.9$, AA'XX', $^1J_{\text{P-H}}=$ 672 Hz, $^2J_{\text{P-P}}=$ 15 Hz, $^3J_{\text{P-H}}=$ 6 Hz	78 $\delta 6.8$, d, $^1J_{\text{P-H}}=$ 624 Hz

192

sample was then heated as before (90℃, 72 hours, N_2 flow) then analysed by ^{1}H NMR spectroscopy. NMR data is shown in Table 6.23.

^{1}H NMR (D$_2$O, 300 K, 300.13 MHz)		
Conditions: Mg(H$_2$PO$_3$)$_2$ (5 g, 27 mmol), 90℃, N$_2$ flow		
	Analysis	
Compound:	Phosphite [HPO$_3^{2-}$]	Pyrophosphite [H$_2$P$_2$O$_5^{2-}$]	% Conv.
3 days	δ6.6, d, $^1J_{\text{P-H}}$= 575 Hz	-	0.0
6 days	δ6.7, d, $^1J_{\text{P-H}}$= 568 Hz	-	0.0
9 days	δ6.6, d, $^1J_{\text{P-H}}$= 568 Hz	-	0.0
12 days	δ6.7, d, $^1J_{\text{P-H}}$= 573 Hz	-	0.0
15 days	δ6.6, d, $^1J_{\text{P-H}}$= 580 Hz	-	0.0
18 days	δ6.7, d, $^1J_{\text{P-H}}$= 618 Hz	-	0.0
21 days	δ6.7, d, $^1J_{\text{P-H}}$= 602 Hz	δ6.9, AA'XX', $^1J_{\text{P-H}}$= 668 Hz, $^2J_{\text{P-P}}$= 9 Hz, $^3J_{\text{P-H}}$= 6 Hz	18.7

Table 6.23: Table of NMR data for the study of formation of magnesium pyrophosphite over time by dry heating magnesium phosphite prepared using the magnesium metal method (6.2.4.3). The phosphite was heated to 90℃ for 72 hour periods on a sand bath under flowing nitrogen for a total of 21 days. δ given in ppm.

6.2.7.5 Investigation of pH effects on production of magnesium pyrophosphite

Seven samples were prepared using magnesium phosphite (0.2 g) prepared from magnesium turnings as in 6.2.4.3 dissolved in deionised water (5 mL) and adjusted using either HCl or NaOH (1M, dropwise addition) to obtain samples covering a pH 4 to pH 10 range. The solutions were reduced to dryness on a rotary evaporator and the residues for each sample were transferred into petri dishes and heated at 85℃ in a vacuum oven at *ca.* 10 mbar pressure for 72 hours. An aliquot (*ca.* 0.5 g) was taken and dissolved in D$_2$O (0.5 mL) and analysed by ^{1}H NMR spectroscopy. NMR data is shown in Table 6.24.

6.2.8 Formation of calcium pyrophosphite *via* dry heating method

Calcium carbonate (CaCO$_3$, 10.4 g, 104 mmol) prepared using the method specified in 6.2.5.2 were ground in a mortar and pestle to a fine powder and transferred to a 50 mL round bottomed flask fitted with a gas inlet allowing a constant flow of nitrogen through the flask. The sample was then heated on a sand bath at 90℃ for 72 hours. An aliquot (*ca.* 0.5 g) was taken and dissolved in D$_2$O (0.5 mL) and analysed by ^{1}H NMR spectroscopy. NMR data is shown in Table 6.25.

6.2.9 Dry Heating of Acid Hydrolysed Iron Phosphide

Iron phosphide [Fe$_3$P, 0.49 g, 2.5 mmol] was placed into a 100 mL two-neck round bottomed flask in the glove box under nitrogen and the two necks sealed with suba seals. Sulphuric acid [H$_2$SO$_4$, *ca.* pH 1, 10 mL] was injected into the flask. Nitrogen gas was then flowed through the flask using a canula inserted through one suba seal with a needle venting the flask. The flask was heated to 90℃ for 7 days in an oil bath. The pH of the flask was

	¹H NMR (D$_2$O, 300 K, 300.13 MHz)		
	Conditions: MgHPO$_3$ (0.2 g, 2 mmol), 85℃, vacuum		
	Analysis		
Compound:	**Phosphite [HPO$_3^{2-}$]**	**Pyrophosphite [H$_2$P$_2$O$_5^{2-}$]**	**% Conv.**
pH 4	δ6.8, d, $^1J_{\text{P-H}}$= 624 Hz	δ6.9, AA'XX', $^1J_{\text{P-H}}$= 672 Hz, $^2J_{\text{P-P}}$= 9 Hz, $^3J_{\text{P-H}}$= 6 Hz	22
pH 5	δ6.7, d, $^1J_{\text{P-H}}$= 600 Hz	δ6.9, AA'XX', $^1J_{\text{P-H}}$= 669 Hz, $^2J_{\text{P-P}}$= 9 Hz, $^3J_{\text{P-H}}$= 6 Hz	18
pH 6	δ6.7, d, $^1J_{\text{P-H}}$= 618 Hz	no chemical shift data available due to only one very weak peak being visible	4
pH 7	δ6.6, d, $^1J_{\text{P-H}}$= 579 Hz	no chemical shift data available due to only one very weak peak being visible	3
pH 8	δ6.7, d, $^1J_{\text{P-H}}$= 573 Hz	-	0
pH 9	δ6.6, d, $^1J_{\text{P-H}}$= 570 Hz	-	0
pH 10	δ6.6, d, $^1J_{\text{P-H}}$= 567 Hz	-	0

Table 6.24: Table of NMR data to study the effect of pH on the formation of magnesium pyrophosphite by dry heating magnesium phosphite prepared using the magnesium metal method (6.2.4.3). The samples were adjusted to cover a range of pH 4 to pH 10 using either HCl or NaOH (1 M, dropwise addition) then reduced to dryness on a rotary evaporator before the phosphite was heated to 85℃ for 72 hours in a vacuum oven. δ given in ppm.

Compound:	**Pyrophosphite [H$_2$P$_2$O$_5^{2-}$]**	**Phosphite [HPO$_3^{2-}$]**
Conditions:	CaCO$_3$(1):(2)H$_3$PO$_3$	
	Analysis	
¹H NMR (D$_2$O, 300 K, 300.13 Hz)	n/a	δ6.8 (d, $^1J_{\text{P-H}}$= 627 Hz)
Conditions:	90℃, 72 hours, N$_2$flow	
Composition (%):	43	57
¹H NMR (D$_2$O, 300 K, 300.13 Hz)	δ6.9 (AA'XX', $^1J_{\text{P-H}}$= 669, $^2J_{\text{P-P}}$= 9, $^3J_{\text{P-H}}$= 6)	δ6.8 (d, $^1J_{\text{P-H}}$= 627 Hz)

Table 6.25: Table of NMR data for ¹H NMR spectroscopic analysis of the formation and condensation of calcium phosphite prepared by reaction of calcium carbonate with phosphonic acid. δ given in ppm

adjusted to pH 4.3 using sodium carbonate, transferred to a 100 mL round bottomed flask and reduced to dryness on a rotary evaporator. The residue was then dry heated on a sand bath to 180℃ for 72 hours under a constant flow of nitrogen. After 72 hours the heat was removed and the flask allowed to cool still under a constant flow of nitrogen. When cool the residue was dissolved in deionised water (20 mL) and the pH of the solution adjusted to pH 8.5 by addition of sodium carbonate to remove dissolved iron. The precipitated iron was filtered by gravity and the solution reduced to dryness on a rotary evaporator. The residue was then dissolved in D_2O (*ca.* 0.5 mL) and submitted for analysis by ^{31}P and ^{31}P $\{^1H\}$ NMR spectroscopy. NMR data is shown in Table 6.26.

Fe_3P hydrothermal residues, 180℃, N_2 flow	
Analysis	
^{31}P **NMR** $(D_2O,$ **300 K, 121.49 MHz)**	phosphite $(\delta 3.9,$ d, $^1J_{P-H} = 567$ Hz); hypophosphite $(\delta 7.9,$ t, $^1J_{P-H} = 516$ Hz)
^{31}P $\{^1H\}$ **NMR** $(D_2O,$ **300 K, 121.49 MHz)**	phosphite $(\delta 4.4,$ s); hypophosphite $(\delta 8.4,$ s)

Table 6.26: Table of NMR data for the dry heating of iron phosphide corrosion residues. The residues were formed by heating iron phosphide in H_2SO_4 (2 M) for 7 days under flowing nitrogen filtering to remove unreacted solid and reducing to dryness on a rotary evaporator. The residues were heated to 180℃ for 72 hours on a sand bath under flowing nitrogen. δ given in ppm.

6.2.10 Investigation of effects of iron and iron (II) on the dry heating of sodium phosphite

A set of two experiments were undertaken using iron chloride [$FeCl_2$, 1.99 g, 15 mmol] and iron powder [Fe, 0.84 g, 15 mmol] mixed in solution with sodium phosphite [NaH_2PO_3, 0.5 g, 5 mmol] and reduced to dryness on a rotary evaporator. The residues were transferred to a 100 mL round-bottomed flask and dry heated at 160℃ for 72 hours under nitrogen flow. After 72 hours the heat was removed and the flask allowed to cool under a constant flow of nitrogen. When cool the residue was dissolved in deionised water (20 mL) and the pH of the solution adjusted to pH 12 by addition of NaOH (1 M, dropwise addition) to remove dissolved iron. The precipitated iron was filtered by gravity and the solution adjusted back to pH 7.5 using HCl (1 M, dropwise addition). The samples were reduced to dryness on a rotary evaporator and a aliquot of each sample (0.5 g) were dissolved in D_2O (0.5 mL) and submitted for analysis by ^1H NMR spectroscopy. NMR data is shown in Table 6.27.

6.2.11 Investigation of redox effects of iron (II) and iron (III) on sodium phosphite and sodium hypophosphite

Two experiments were prepared to investigate the redox effects of ferrous [Fe^{2+}] and ferric [Fe^{3+}] iron on phosphite and hypophosphite. Experiment one used sodium phosphite [NaH_2PO_3, 0.52 g, 5 mmol] and iron (II) chloride tetrahydrate [$FeCl_2 \cdot 4H_2O$, 2.99 g, 15 mmol] dissolved in 10 mL degassed deionised water in a 50 mL round bottomed flask. Experiment two used sodium hypophosphite [NaH_2PO_2, 0.44 g, 5 mmol] and iron (III)

¹H NMR (D₂O, 300 K, 300.13 MHz)

^{1}H NMR (D$_2$O, 300 K, 300.13 MHz)	
Fe metal or FeCl$_2$ + NaH$_2$PO$_3$, 160°C, N$_2$ flow	
	Analysis
Fe metal	water (δ4.7, s); phosphite δ6.6, d, $^1J_{\text{P-H}}$= 567 Hz)
Fe^{2+}	water (δ4.7, s); phosphite (δ6.7, d, $^1J_{\text{P-H}}$= 564 Hz); hypophosphite (δ7.1, d, $^1J_{\text{P-H}}$= 519 Hz)

Table 6.27: Table of NMR data for the dry heating of sodium phosphite in the presence of ferrous iron and iron metal. The samples were heated to 160°C for 72 hours on a sand bath under flowing nitrogen. δ given in ppm.

chloride [FeCl$_3$, 2.43 g, 15 mmol] dissolved in 10 mL degassed deionised water in a 50 mL round bottomed flask. The solutions were stirred overnight under flowing nitrogen then reduced to dryness on a rotary evaporator. The solid residues were transferred to 50 mL round bottom flasks and heated to 160°C on a sand bath for 72 hours. An aliquot of each sample (0.5 g) was then dissolved in *ca.* 2 mL deionised water and treated with *ca.* 1 mL sodium sulphide solution (Na$_2$S, 1 M). The sample was then centrifuged for 1 minute and then filtered by gravity to remove any solid. A *ca.* 0.5 mL portion was taken and submitted for analysis by ^{31}P and ^{31}P{^{1}H} NMR spectroscopy using a D$_2$O capillary insert for locking purposes. NMR data is shown in Table 6.28.

FeCl$_2$ + NaH$_2$PO$_3$, 160°C, 72 hours, N$_2$ flow	
	Analysis
	^{31}P NMR (D$_2$O, 300 K, 202.46 MHz)
Fe^{2+}	phosphite (δ4.3, d, $^1J_{\text{P-H}}$= 564 Hz); hypophosphite (δ8.8, t, $^1J_{\text{P-H}}$= 519 Hz)
	^{31}P{^{1}H} NMR (D$_2$O, 300 K, 202.46 MHz)
Fe^{2+}	phosphite (δ4.3, s,); hypophosphite (δ8.8, s)
FeCl$_3$ + NaH$_2$PO$_2$, 160°C, 72 hours, N$_2$ flow	
	^{31}P NMR (D$_2$O, 300 K, 202.46 MHz)
Fe^{3+}	phosphite (δ4.2, d, $^1J_{\text{P-H}}$ = 564 Hz)
	^{31}P{^{1}H} NMR (D$_2$O, 300 K, 202.46 MHz)
Fe^{3+}	phosphite (δ4.2, s)

Table 6.28: Table of NMR data for the dry heating of sodium phosphite in the presence of ferrous iron and sodium hypophosphite in the presence of ferric iron. The samples were heated to 160°C for 72 hours on a sand bath under flowing nitrogen. δ given in ppm.

6.2.12 Investigation of phosphate reduction using ferrous iron

Sodium phosphate dibasic [Na$_2$HPO$_4$, 0.71 g, 5 mmol] and iron chloride [FeCl$_2 \cdot 4$H$_2$O, 1.99 g, 10 mmol] were dissolved in 10 mL degassed deionised water in a 50 mL round bottomed flask. The solutions were stirred overnight under flowing nitrogen then reduced to dryness on a rotary evaporator. The solid residues were transferred to 50 mL round bottom flasks and heated to 160°C on a sand bath for 7 days. After 7 days the heat was removed and the flask allowed to cool still under a constant flow of nitrogen. When cool the residue was dissolved in deionised water (20 mL) and the pH of the solution adjusted to pH 12 by addition of NaOH (1 M, dropwise addition) to remove dissolved iron. The

precipitated iron was filtered by gravity and the solution adjusted back to pH 7.5 using HCl (1 M, dropwise addition). The sample was reduced to dryness on a rotary evaporator and a aliquot of the sample (0.5 g) were dissolved in D_2O (0.5 mL) and submitted for analysis by ^{31}P NMR spectroscopy. NMR data is shown in Table 6.29.

Compound:	Hypophosphite [$H_2PO_2^-$]	Phosphite [HPO_3^{2-}]
Conditions:	160℃, 72 hours, N_2 flow	
Composition (%):	33	67
Analysis		
^{31}P NMR (D_2O, 300 K, 202.46 Hz)	$\delta7.9$ (t, $^1J_{P\text{-}H}=$ 516 Hz)	$\delta3.9$ (d, $^1J_{P\text{-}H}=$ 567 Hz)
^{31}P NMR {^1H} (D_2O, 300 K, 202.46 Hz)	$\delta7.9$, s	$\delta3.9$, s

Table 6.29: Table of NMR data for ^{31}P NMR spectroscopic analysis of the dry heating of phosphite in the presence of ferrous iron produced by the simulated hydrothermal corrosion of Fe_3P. The sample was heated on a sand bath to 160℃ under flowing N_2 for 72 hours. δ given in ppm

An investigation into whether iron metal or ferrous iron is responsible was conducted. add to this

^1H NMR (D_2O, 300 K, 300.13 Hz)		
Compound	Hypophosphite [$H_2PO_2^-$]	Phosphite [HPO_3^{2-}]
	Conditions: 160℃, 72 hours, N_2 flow	
	Analysis	
Fe	-	$\delta6.6$ (d, $^1J_{P\text{-}H}=$ 568 Hz)
Fe^{2+}	$\delta7.0$ (d, $^1J_{P\text{-}H}=$ 516 Hz)	$\delta6.7$ (d, $^1J_{P\text{-}H}=$ 567 Hz)

Table 6.30: Table of NMR data for ^1H NMR spectroscopic analysis of the dry heating of phosphite in the presence of ferrous ions and iron metal to determine if iron metal or ferrous ions are responsible for the reduction of phosphite to hypophosphite. The samples were heated on a sand bath to 160℃ under flowing N_2 for 72 hours. δ given in ppm

6.2.13 Investigation of effects of iron (II) and iron (III) on the dry heating of calcium phosphite

Four experiments were prepared to study the effects of iron oxidation state on the production of pyrophosphite using calcium phosphite prepared using the calcium carbonate method in 6.2.5.2. Experiments one and two used iron (II) chloride tetrahydrate ($FeCl_2 \cdot 4\,H_2O$, 0.2 g, 1 mmol) and calcium phosphite monohydrate ($Ca(H_2PO_3)_2 \cdot H_2O$, 0.95 g, 4.3 mmol). One was dissolved in 10 mL of degassed deionised water while two was dissolved in 10 mL standard mean ocean water (SMOW) solution. Experiment three and four used iron (III) chloride ($FeCl_3$, 0.16 g, 1 mmol) and calcium phosphite monohydrate ($Ca(H_2PO_3)_2 \cdot H_2O$, 0.95 g, 4.3 mmol) and were also dissolved in 10 mL of degassed deionised water while two was dissolved in 10 mL standard mean ocean water (SMOW) solution respectively.

The solutions were each stirred under flowing nitrogen for 30 minutes then each reduced to dryness on a rotary evaporator. The residues for each experiment were collected and

ground in a mortar and pestle. The powder for each sample was placed in a 50 mL round bottomed flask and fitted with a gas inlet allowing a constant flow of nitrogen through the flask. The residues were then heated at 85℃ for 72 hours on a sand bath.

A small portion of each sample (0.5 g) were dissolved in 1 mL deionised water and the pH of the solution was then adjusted to *ca.* pH 12 by dropwise addition of sodium hydroxide (NaOH, 2 M) then filtered to remove any precipitate formed. The sample was then adjusted to *ca.* pH 7 by dropwise addition of hydrochloric acid (HCl, 1 M). The sample was submitted for ^{31}P NMR using a capillary D_2O insert for locking purposes. NMR data is shown in Table 6.31.

6.2.14 Investigation of effects of iron (II) and temperature on the dry heating of calcium phosphite

Iron (II) chloride tetrahydrate ($FeCl_2 \cdot 4H_2O$, 0.198 g, 1 mmol) and calcium phosphite monohydrate ($Ca(H_2PO_3)_2 \cdot H_2O$, 0.22g, 1 mmol) were dissolved in 10 mL deionised water in a 50 mL round bottomed flask and stirred for 30 minutes. The flask was fitted with a gas inlet allowing a constant flow of nitrogen through the flask. The sample was dried using a rotary evaporator and the residues transferred to a 50 mL round bottom flask. The sample was heated to 90℃ on a sand bath for 10 days under flowing nitrogen. An aliquot of the sample (0.5 g) was taken and the remainder of the residues were heated to 120℃ on a sand bath for 10 days under flowing nitrogen. An aliquot of the sample (0.5 g) was again taken and the remainder heated for a further 10 days at 150℃ on a sand bath under flowing nitrogen. An aliquot of the sample(0.5 g) was again taken.

The sample aliquots taken during the experiment were dissolved in deionised water (1 mL) and filtered to remove any undissolved solid. The pH of the solution was then adjusted to *ca.* pH 12 using NaOH (1 M, dropwise addition) and filtered to remove any precipitate formed. |The samples were adjusted back to pH 7.5 for analysis using HCl (1 M, dropwise addition) and a *ca.* 0.5 mL portion was taken of each sample which was submitted for analysis by ^{31}P NMR spectroscopy using a D_2O capillary insert for locking purposes. NMR data is shown in Table 6.32.

6.2.15 Investigation of effects of iron (II) and iron (III) on the dry heating of sodium phosphite

Four experiments were prepared to study the effects of iron oxidation state on the production of pyrophosphite using sodium phosphite prepared using the sodium hydroxide method in 6.2.3. Experiments one and two used iron (II) chloride tetrahydrate ($FeCl_2 \cdot 4H_2O$, 0.199 g, 1 mmol) and sodium phosphite (NaH_2PO_3, 0.416 g, 4 mmol). One was dissolved in 10 mL of degassed deionised water while two was dissolved in 10 mL standard mean ocean water (SMOW) solution. Experiment three and four used iron (III) chloride ($FeCl_3$, 0.162 g, 1 mmol) and sodium phosphite (NaH_2PO_3, 0.416 g, 4 mmol) and were also dissolved in 10 mL of degassed deionised water while two was dissolved in 10 mL standard mean ocean water (SMOW) solution respectively.

Compound:	Pyrophosphate $[H_2P_2O_5^{2-}]$	Phosphite $[HPO_3^{2-}]$	Phosphate $[PO_4^{3-}]$
Conditions:		160°C, 72 hours, N_2 flow **Analysis**	
Fe²⁺			
Composition (%):	0	100	0
³¹P NMR (D_2O, 300 K, 121.49 Hz)	n/a	δ4.2 (d, $^1J_{\text{P-H}}=$ 566 Hz)	n/a
Fe³⁺			
Composition (%):	83.5	1.5	15
³¹P NMR (D_2O, 300 K, 121.49 Hz)	δ-5.1 (AA'XX', $^1J_{\text{P-H}}=$ 666 Hz, $^2J_{\text{P-P}}=$ 10 Hz, $^3J_{\text{P-H}}=$ 7 Hz)	δ3.0 (d, $^1J_{\text{P-H}}=$ 573 Hz)	δ2.0, s
Fe²⁺/SMOW			
Composition (%):	0	100	0
³¹P NMR (D_2O, 300 K, 121.49 Hz)	n/a	δ3.0 (d, $^1J_{\text{P-H}}=$ 576 Hz)	n/a
Fe³⁺/SMOW			
Composition (%):	4	96	0
³¹P NMR (D_2O, 300 K, 121.49 Hz)	δ-2.6 (AA'XX', $^1J_{\text{P-H}}=$ 667 Hz, $^2J_{\text{P-P}}=$ 10 Hz, $^3J_{\text{P-H}}=$ 7 Hz)	δ3.0 (d, $^1J_{\text{P-H}}=$ 573 Hz)	n/a

Table 6.31: Table of NMR data for ³¹P NMR spectroscopic analysis of the dry heating of calcium phosphite in the presence of ferrous iron and ferric iron to investigate the effects the different metal oxidation states have on the dry heating reactions of calcium phosphite monohydrate. The calcium phosphite was mixed with either ferrous chloride [Fe^{2+}] or ferric chloride [Fe^{3+}] in deionised water and also in SMOW. The samples were thoroughly mixed then reduced to dryness using a rotary evaporator. The samples were heated on a sand bath to 160°C under flowing N_2 for 72 hours. δ given in ppm

^{31}P NMR (D$_2$O, 300 K, 121.49 Hz)		
Compound	**Pyrophosphite [H$_2$P$_2$O$_5^{2-}$]**	**Phosphite [HPO$_3^{2-}$]**
Conditions: 160°C, 72 hours, N$_2$ flow		
Analysis		
Composition (%): 90°C	0 -	100 δ3.0 (d, $^1J_{\text{P-H}} = 577$ Hz)
Composition (%): 120°C	0 -	100 δ3.0 (d, $^1J_{\text{P-H}} = 568$ Hz)
Composition (%): 150°C	0 -	100 δ3.1 (d, $^1J_{\text{P-H}} = 571$ Hz)

Table 6.32: Table of NMR data for ^{31}P NMR spectroscopic analysis of the dry heating of phosphite in the presence of ferrous iron. The samples were dry heated on an oil bath at 90°C, 120°C and 150°C looking for the effects that each temperature has on the products obtained. The samples were thoroughly mixed then reduced to dryness using a rotary evaporator. The samples were heated on a sand bath, to the stipulated temperature, under flowing N$_2$ for 72 hours. δ given in ppm

The solutions were each stirred under flowing nitrogen for 30 minutes then each reduced to dryness on a rotary evaporator. The residues for each experiment were collected and ground in a mortar and pestle. The powder for each sample was placed in a 50 mL round bottomed flask and fitted with a gas inlet allowing a constant flow of nitrogen through the flask. The residues were then heated at 85°C for 72 hours on a sand bath.

A small portion of each sample (0.5 g) were dissolved in 1 mL deionised water and the pH of the solution was then adjusted to *ca.* pH 12 by dropwise addition of sodium hydroxide (NaOH, 2 M) then filtered to remove any precipitate formed. The sample was then adjusted to *ca.* pH 7 by dropwise addition of hydrochloric acid (HCl, 1 M). The sample was submitted for ^{31}P NMR using a capillary D$_2$O insert for locking purposes. NMR data is shown in Table 6.33.

^{31}P NMR (D$_2$O, 300 K, 121.49 Hz)		
Compound	**Pyrophosphite [H$_2$P$_2$O$_5^{2-}$]**	**Phosphite [HPO$_3^{2-}$]**
Conditions: 90°C, 72 hours, N$_2$ flow		
Analysis		
Composition (%): Fe^{3+}	0 -	100 δ3.0 (d, $^1J_{\text{P-H}} = 571$ Hz)
Composition (%): Fe^{3+}/SMOW	0 -	100 δ3.0 (d, $^1J_{\text{P-H}} = 571$ Hz)

Table 6.33: Table of NMR data for ^{31}P NMR spectroscopic analysis of the dry heating of sodium phosphite in the presence of ferric iron to investigate whether there is any aiding effect of ferric iron on the formation of pyrophosphite. The sample was heated on an oil bath to 90°C for 72 hours under flowing N$_2$. δ given in ppm

6.2.16 Reaction of sodium pyrophosphite with phosphate

Sodium pyrophosphite (Na$_2$P$_2$O$_5$, 0.869 g, 4.5 mmol) and sodium phosphate dibasic (Na$_2$HPO$_4$, 0.142 g, 1.5 mmol) were dissolved in 20 mL deionised water buffered to pH 7 with a phosphate buffer solution prepared as stated in the 58th Edition of the Handbook of Chemistry

and Physics.[?] The solution was left for 72 hours at room temperature then an aliquot (*ca.* 0.5 mL) taken for analysis by ^{31}P NMR spectroscopy using a D_2O capillary insert for locking purposes. NMR data is shown in Table 6.34.

^{31}P NMR (D_2O, 300 K, 121.49 MHz)
$Na_2H_2P_2O_5$ (0.87 g, 4.5 mmol), Na_2HPO_4 (0.14 g, 1.5 mmol), 72 hours, 25℃

	Analysis
Na_2HPO_4	phosphate (0.4, s); phosphite (δ2.7, d, $^1J_{\text{P-H}}$ = 610 Hz); hypophosphite (δ-4.8, dd, $^1J_{\text{P-H}}$ = 650 Hz, $^2J_{\text{P-P}}$ = 16 Hz), δ-7.6, d, $^3J_{\text{P-H}}$ = 16 Hz, $HP_2O_6^{3-}$); pyrophosphite (δ-5.1, AA'XX', $^1J_{\text{P-H}}$ = 667.20 Hz, $^2J_{\text{P-P}}$ = 10 Hz, $^3J_{\text{P-H}}$ = 7 Hz)

Table 6.34: Table of NMR data for the production of isohypophosphate by reaction of pyrophosphate wit phosphate in solution at room temperature. δ given in ppm.

6.2.17 Methods of detection and quantification of pyrophosphite

6.2.17.1 Raman spectroscopy

As Raman is more sensitive to non-polar molecules than polar molecules it is non-sensitive to water and can be used with no sample preparation. Due to the reliance of photon interaction with bond vibration and rotation, each molecules Raman signature will be unique meaning it would be possible to even identify a component molecule from a mixture using this technique. Raman can also be used semi-quantitatively based on intensities of peaks in the Raman spectrum providing you have reasonable calibration data and this was why this technique was selected for further investigation.

Initially it was decided to obtain Raman spectra of pure samples of the phosphorus species of interests which could be encountered during experiments and try to identify unique peaks in their fingerprints which could be sued for easy identification. Samples were analysed using a Renishaw InVia spectrometer using a 785 nm wavelength diode laser and a charge coupled detector (CCD). The samples were analysed using the 20x objective lens and were exposed to 10 acquisitions with a 10 second spot time and 100% laser power. Samples of sodium phosphite monobasic, sodium phosphite dibasic, sodium pyrophosphite and sodium pyrophosphate tetrabasic were subjected to Raman analysis and were prepared by placing a small amount on a glass microscope slide. The sample was then pressed flat using a second slide then placed in the spectrometer. The sample was then brought into focus and a wide spectrum scan was then taken using Wire 3.0 acquisition software. The Raman spectra are shown in a stacked plot in Spectrum 6.1 and the peak data is shown with tentative assignments in Table 6.35.

Sodium pyrophosphite (0.2 g, 1 mmol) and sodium phosphite (0.1 g, 1 mmol) were dissolved in SMOW (20 mL) and the pH adjusted to *ca.* 4 using HCl. Iron (II) chloride tetrahydrate (0.2 g, 1 mmol) was added and the resultant solution reduced to dryness by heating at 40℃ under flowing nitrogen. Once the sample was dry, the residue was collected and ground in a mortar and pestle. A small portion of the sample was placed onto a glass microscope slide and pressed to give a flat surface. The sample was then placed into the Raman spectrometer for analysis. The scan was taken using a 5x objective lens with the

	NaH$_2$PO$_3$		Na$_2$HPO$_3$		Na$_2$H$_2$P$_2$O$_5$		Na$_4$P$_2$O$_7$
Peak	**Assignment**	**Peak**	**Assignment**	**Peak**	**Assignment**	**Peak**	**Assignment**
955	P-OH sym str	973	P-OH sym str	1025	P-OH sym str	732	
1033	PO2 sym str	1026	PO2 sym str	1041	PO2 sym str	1029	PO2 sym str
1064	P-O sym str	1042	P-O sym str	1142	P-O-P sym str	1114	P-O-P sym str
1187		1096		1239			
2442	P-H sym str	2343	P-H sym str	2432			
		2395	P-H sym str	2452	P-H sym str		

Table 6.35: Table of peak data for Raman spectra of phosphite (monobasic [NaH$_2$PO$_3$] and dibasic [Na$_2$HPO$_3$]), pyrophosphite [Na$_2$H$_2$P$_2$O$_5$] and pyrophosphate [Na$_4$P$_2$O$_7$] using a 785 nm wavelength diode laser (10 acquisitions, 10 second exposure time and 100% laser power) and charge coupled detector (CCD).

20x objective lens, 10 acquisitions, 10 second exposure, 100% Laser power. Major peaks recorded (cm-1)

Spectrum 6.1: A stacked plot of Raman spectra obtained for phosphite (monobasic and dibasic), pyrophosphite and pyrophosphate using a 785 nm wavelength diode laser (10 acquisitions, 10 second exposure time and 100% laser power) and charge coupled detector (CCD). Data is tabulated and tentatively assigned in Table 6.35.

sample exposed to 10 acquisitions at 50% laser power with an exposure time of 1 second. The Spectrum obtained is shown in a stacked plot in Spectrum 6.2 which also contains the obtained spectra for phosphite, pyrophosphite and pyrophosphate for comparison.

6.2.18 Fluorometry

6.2.18.1 Preparation of 3,6,9,16,19,22-hexa-aza-tri-cyclo-[22.2.2.2(11,14)]-triaconta-1(26),2,8,11,13,15,22,24,27,29-decaene

Teraphthalaldehyde ($C_6H_4(CHO)_2$, 0.134 g, 1 mmol) was dissolved in acetonitrile (CH_3CN, 20 mL) in a 100 mL conical flask. Diethylenetriamine ($NH(CH_2CH_2NH_2)_2$, 0.103 g, 1 mmol) was dissolved in acetonitirile (CH_3CN, 35 mL) in a 100 mL conical flask then transferred to a 250 mL round bottomed flask. The teraphthalaldehyde solution was added dropwise with stirring to the diethyltriamine solution using a 100 mL dropping funnel over a period of 30 minutes then left to stir for 24 hours. A yellow precipitate formed which was collected by vacuum filtration using a Buchner funnel and dried overnight in a vacuum desiccator (0.12 g, 0.3 mmol, 59.6%).

A small amount taken for microanalysis, mass spectrometry and NMR analysis (^{1}H and [13]C{[1]H}). The data are shown in Chapter 2 (Table 2.5

This experiment was repeated as stated above on two further occasions but scaled up to use teraphthalaldehyde ($C_6H_4(CHO)_2$, 1.2 g, 9 mmol)dissolved in acetonitrile (CH_3CN, 150 mL) and diethylenetriamine ($NH(CH_2CH_2NH_2)_2$, 0.972 g, 9 mmol) dissolved in acetonitirile (CH_3CN, 280 mL). After washing and drying the product of each repeat the yields obtained were (1.48 g, 3.7 mmol, 81.7%) and (1.152 g, 2.86 mmol, 63.6%) respectively.
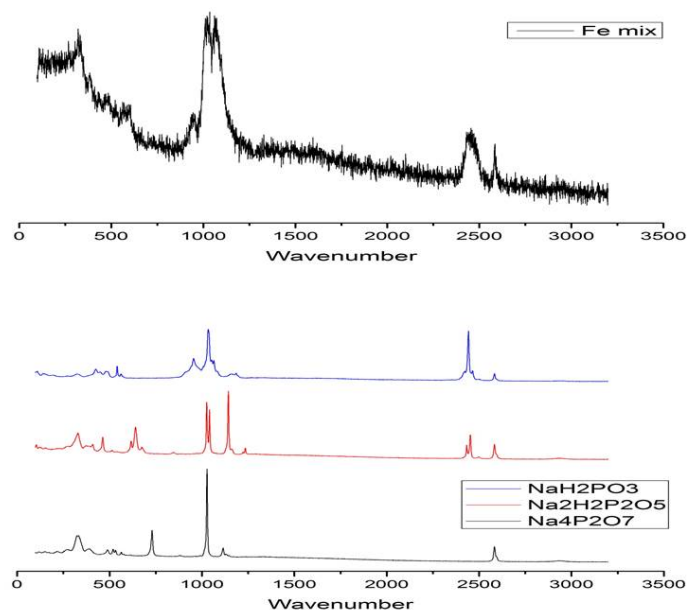
Spectrum 6.2: A composite image of Raman spectra for comparison of an iron, phosphite, pyrophosphite and SMOW mix against the Raman spectra of the individual components of the mixture to try and ascertain if Raman is a suitable technique for experimental analysis. The spectrum of the iron mix was taken using a 785 nm wavelength diode laser (10 acquisitions, 10 second exposure time and 50% laser power) and was compared to the stacked plot of Raman spectra obtained for sodium phosphite monobasic, sodium pyrophosphite and sodium pyrophosphate using a 785 nm wavelength diode laser (10 acquisitions, 10 second exposure time and 100% laser power) and charge coupled detector (CCD).

6.2.18.2   Preparation of 3,6,9,16,19,22-hexaazatricyclo[22.2.2.2(11,14)]triaconta-1(26),11,13,24,27,29-hexaene

The product from 6.2.18.1 ($C_{24}H_{30}N_6$, 0.1 g, 0.25 mmol) was dissolved in dry methanol (CH_3OH, 30 mL) and heated to 45℃. Sodium borohydride ($NaBH_4$, 0.25 g, 6.6 mmol) was added with stirring for 1 hour then allowed to cool to room temperature. The solution was reduced to dryness on a rotary evaporator. A white solid was obtained to which 1 mL deionised water and dichloromethane (CH_2Cl_2, 10 mL) were added. The organic phase was collected using a 100 mL separating funnel and then reduced to dryness on a rotary evaporator (0.084 g, 0.21mmol, 81.7%).

A small amount taken for microanalysis, mass spectrometry and NMR analysis (^{1}H and [13]C{[1]H}). The data are shown in Chapter 2 (Table 2.6.

This experiment was repeated as stated above on two further occasions but scaled up to use the product from 6.2.18.1 ($C_{24}H_{30}N_6$, 1.208 g, 3 mmol) dissolved in dry methanol (CH_3OH, 300 mL) and sodium borohydride ($NaBH_4$, 2.5 g, 66 mmol). After washing and drying the product of each repeat the yields obtained were (0.972 g, 2.37 mmol, 78.9%) and (0.864 g, 2.1 mmol, 84.5%) respectively.

6.2.18.3 Purification of 3,6,9,16,19,22-hexaazatricyclo[22.2.2.2(11,14)]triaconta-1(26),11,13,24,27,29-hexaene using hydrobromic acid

The product from 6.2.18.2 ($C_{24}H_{38}N_6$, 0.05 g, 0.12 mmol) was dissolved in a mixture of hydrobromic acid (HBr, 48%, 1 mL) and ethanol (CH_3CH_2OH, 10 mL) and the precipitate collected by vacuum filtration using a Hirsch funnel then washed with chilled methanol (CH_3OH, 10 mL) and diethyl ether ($(CH_3CH_2)_2O$, 10 mL) and allowed to dry. Acidified macrocycle ($C_{24}H_{38}N_6 \cdot 6\,HBr$, 0.1 g, 112 μmol) was dissolved in 10 mL deionised water. Sodium hydroxide (NaOH, 1 M) was added dropwise to the solution until a neutral pH (pH 7) was obtained. The solution was transferred to a 100 mL separating funnel and dichloromethane (CH_2Cl_2, 10 mL) was added. The funnel was stoppered and the solution shaken, venting by the tap occasionally to prevent gas build up. The flask was left to settle allowing the organic and aqueous phases to separate. The organic phase was then collected, filtered by gravity and reduced to dryness on a rotary evaporator. A small portion of the solid was dissolved in $CDCl_3$ and ^{1}H NMR analysis was conducted. The spectrum was indecipherable and it appears the macrocycle has decomposed.

The previous purification attempt was repeated as above but was neutralised using sodium carbonate (Na_2CO_3, 1 M), a weaker base than sodium hydroxide, which was added dropwise to the solution until a neutral pH (pH 7) was obtained. A small portion of the solid was dissolved in $CDCl_3$ and analysis by ^{1}H NMR spectroscopy was conducted. Again the spectrum was indecipherable. It seems that the macrocycle has again decomposed so due to this issue, attempts to purify macrocycle by salt method were abandoned.

6.2.18.4 Preparation of 3,6,9,16,19,22-hexa-aza-tri-cyclo-[22.2.2.2(11,14)]-triaconta-1(26),11,13,24,27,29-hexaene bi-copper(II) complex

Copper nitrate trihydrate ($Cu(NO_3)_2 \cdot 3\,H_2O$, 0.76 g, 3.15 mmol) was dissolved in methanol (CH_3OH, 50 mL)in a 100 mL conical flask. The prepared macrocycle ($C_{24}H_{38}N_6$, 0.645 g, 1.57 mmol was also dissolved in methanol (CH_3OH, 50 mL) in a 100 mL conical flask. the two solutions were mixed in a 250 round bottomed flask, fitted with a condenser and heated to reflux for 30 minutes then allowed to cool. Deep royal blue crystals precipitated during cooling and were collected by vacuum using a Buchner funnel (1.01 g, 1.95 mmol, 84.4%). Mass spectrometry and elemental microanalysis data are shown in Table 6.36

Mass spectrometry:	Expected	Obtained
$\mathbf{ESI^+}$ ($\mathbf{[(C_{24}H_{38}N_6Cu_2)^{4+}+H]^+}$)	538.7 ($[M+H]^+$)	192.1 ($[M+H]^+$)
Microanalysis:	**Expected**	**Obtained**
C	36.69	35.55
H	4.87	5.20
N	17.68	16.30

Table 6.36: Table of analytical data for the copper macrocycle showing results for the mass spectrometry analysis and elemental microanalysis.

6.2.18.5   Preparation of fluorescent indicator solution

Fluorescein ($C_{20}H_{12}O_5$, 26.58 mg, 80 μmol) was dissolved in deionised water and made up to the line in a 250 mL volumetric flask. A 25 mL portion was taken using a volumetric pipette and placed into a 250 mL volumetric flask and again made up to the line with deionised water. The copper macrocycle ($C_{24}H_{38}N_6Cu_2(NO_3)_4$, 50.28 mg, 64 μmol) was dissolved in deionised water and made up to the line in a 250 mL volumetric flask. A 0.05 M solution of HEPES (4-(2-hydroxyethyl)-1-piperazineethanesulfonic acid, $C_8H_{18}N_2O_4S$, 0.1192 g, 0.5 mmol) was dissolved in deionised water and made up to the line in a 10 mL volumetric flask. The three solutions were combined in a 1000 mL volumetric flask, the flasks rinsed with deionised water three times each then made up to the line.

6.2.18.6   Fluorometric analysis of pyrophosphate and phosphate solutions

A bulk solution of 1 mM phosphate solution was prepared using sodium phosphate dibasic dihydrate ($Na_2HPO_4 \cdot 2H_2O$, 0.0178 g, 0.1 mmol) dissolved in deionised water and made up to the line in a 100 mL volumetric flask. A bulk solution of 1 mM pyrophosphate solution was prepared using sodium pyrophosphate dibasic ($Na_2H_2P_2O_7$, 0.0222 g, 0.1 mmol) dissolved in deionised water and made up to the line in a 100 mL volumetric flask. A series of dilutions were made to the bulk solutions to make a set of standard solutions at known concentrations for analysis by fluorometry. The dilutions and concentrations of the standard solutions are shown in Table 6.37.

Fluorometry was carried out on a Perkin Elmer Lambda 900 UV/Vis/NIR spectrometer as stated. Samples were prepared for fluorometry by taking a 5 mL aliquot of each standard solution in a 25 mL conical flask and adding a 5 mL aliquot of the prepared chemosensor. The solutions mixed by swirling for 30 seconds. A *ca.* 3 mL portion of the mixed solutions was transferred to a quartz cuvette to be run in the fluorometer using deionised water as a reference. The emission intensity was recorded at 513.3 nm. The data collected is shown in Table 6.38.

6.2.18.7   Repeat of fluorometric analysis of pyrophosphate and phosphate solutions using standards prepared in the fluorescent indicator solution

A 0.1 mM standard phosphate solution and a 0.1 mM standard pyrophosphate solution was prepared using the fluorescent indicator solution, prepared as stated in 6.2.18.5 as solvent. Sodium phosphate dibasic dihydrate ($Na_2HPO_4 \cdot 2H_2O$, 0.0178 g, 0.1 mmol) and tetrasodium pyrophosphate ($Na_2H_2P_2O_7$, 0.0222 g, 0.1 mmol) were dissolved in the prepared fluorescent indicator solution in a 100 mL volumetric flask and made up to the line. A 10 mL aliquot was taken of each standard solution using a volumetric pipette and transferred to a 100 mL volumetric flask and again made up to the line with fluorescent indicator solution.

Fluorescent indicator solution (2.5 mL) was transferred into a quartz cuvette and a reading taken using deionised water as the reference. A 25 μL aliquot of the 0.1 mM phosphate solution was added to the cuvette and a further reading taken. This process was repeated

	Start Conc (M)	Vol. (L)	Vol. Added (L)	Conc. (M)	Wt. Sample (g)
Phosphate	0.001	0.1	0.0050	5.00×10^{-5}	8.90×10^{-3}
	0.001	0.1	0.0030	3.00×10^{-5}	5.34×10^{-3}
	0.001	0.1	0.0025	2.50×10^{-5}	4.45×10^{-3}
	0.001	0.1	0.0020	2.00×10^{-5}	3.56×10^{-3}
	0.001	0.1	0.0015	1.50×10^{-5}	2.67×10^{-3}
	0.001	0.1	0.0010	1.00×10^{-5}	1.78×10^{-3}
	0.001	0.1	0.0005	5.00×10^{-6}	8.90×10^{-4}
	0.001	0.1	0.0001	1.00×10^{-6}	1.78×10^{-4}
pyrophosphate	0.001	0.1	0.0050	5.00×10^{-5}	1.11×10^{-2}
	0.001	0.1	0.0030	3.00×10^{-5}	6.66×10^{-3}
	0.001	0.1	0.0025	2.50×10^{-5}	5.55×10^{-3}
	0.001	0.1	0.0020	2.00×10^{-5}	4.44×10^{-3}
	0.001	0.1	0.0015	1.50×10^{-5}	3.33×10^{-3}
	0.001	0.1	0.0010	1.00×10^{-5}	2.22×10^{-3}
	0.001	0.1	0.0005	5.00×10^{-6}	1.11×10^{-3}
	0.001	0.1	0.0001	1.00×10^{-6}	2.22×10^{-4}

Table 6.37: Table of concentrations for the prepared standards of phosphate and pyrophosphate. The standards were prepared in deionised water.

Sample	Concentration (molar)	Emission Intensity
Phosphate	5.0×10^{-05}	3.5×10^{06}
	3.00×10^{-05}	2.5×10^{06}
	2.50×10^{-05}	3.0×10^{06}
	2.00×10^{-05}	2.4×10^{06}
	1.50×10^{-05}	2.4×10^{06}
	1.00×10^{-05}	1.9×10^{06}
	5.00×10^{-06}	2.0×10^{06}
	1.00×10^{-06}	1.9×10^{06}
pyrophosphate	5.0×10^{-05}	7.3×10^{06}
	3.00×10^{-05}	3.4×10^{06}
	2.50×10^{-05}	2.6×10^{06}
	2.00×10^{-05}	2.5×10^{06}
	1.50×10^{-05}	2.3×10^{06}
	1.00×10^{-05}	2.1×10^{06}
	5.00×10^{-06}	1.8×10^{06}
	1.00×10^{-06}	1.9×10^{06}

Table 6.38: Table of initial fluorometry data for phosphate and pyrophosphate using prepared standard concentrations.

until the 3 mL volume of the cuvette was reached. The same process was repeated for the 0.1 mM pyrophosphate solution. The results are shown in Table 6.39.

6.3   Iceland Experimental Package and sampling

6.3.1   Experimental Package

The experimental package was prepared as detailed in Table 6.40. All samples were packed into 50 mL Falcon tubes and sealed as described in the table. The Falcon tubes were placed into a large test tube rack and wrapped in cling film to secure them for transportation. A full COSHH assessment was completed and affixed to the lid of the transportation container for the benefit of airport security.

6.3.2   Sampling

Water samples were collected from various hydrothermal and mud-pools and also the melt-water lake at the Kverkfjöll site. The fluids were selected to give representation to the complete range of pH and temperature encountered at the site. During investigation a pH range of between 1 and 5 was encountered with temperature ranging from 40 ℃ to *ca.* 95 ℃.

All fluid samples were collected directly from the sites in a sterile 250 mL Nalgene bottle unless otherwise stated. All fluids were added to the selected sample using a 50 mL sterile disposable syringe without filtering. A sample of the fluid was also collected for each site so that a comparison could be made with the experimental fluids.

Hydrothermal fluid (50 mL, added as described above) was added to each experiment

End Conc. of Anion (M)	Phosphate (I)	Pyrophosphate (I)
9.90×10^{-07}	3.2×10^{05}	3.4×10^{05}
1.96×10^{-06}	3.2×10^{05}	3.4×10^{05}
2.91×10^{-06}	3.2×10^{05}	3.5×10^{05}
3.85×10^{-06}	3.2×10^{05}	3.6×10^{05}
4.76×10^{-06}	3.2×10^{05}	3.7×10^{05}
5.66×10^{-06}	3.2×10^{05}	3.8×10^{05}
6.54×10^{-06}	3.2×10^{05}	3.8×10^{05}
7.41×10^{-06}	3.2×10^{05}	3.9×10^{05}
8.26×10^{-06}	3.2×10^{05}	3.9×10^{05}
9.09×10^{-06}	3.2×10^{05}	4.0×10^{05}
9.91×10^{-06}	3.2×10^{05}	4.0×10^{05}
1.07×10^{-05}	3.2×10^{05}	4.1×10^{05}
1.15×10^{-05}	3.2×10^{05}	4.2×10^{05}
1.23×10^{-05}	3.2×10^{05}	4.3×10^{05}
1.30×10^{-05}	3.2×10^{05}	4.4×10^{05}
1.38×10^{-05}	3.2×10^{05}	4.5×10^{05}
1.45×10^{-05}	3.2×10^{05}	4.6×10^{05}
1.53×10^{-05}	3.2×10^{05}	4.6×10^{05}
1.60×10^{-05}	3.3×10^{05}	4.7×10^{05}
1.67×10^{-05}	3.3×10^{05}	4.8×10^{05}

Table 6.39: Table of fluorometry data for phosphate and pyrophosphate using 25 μL micro-pipette addition method.

then resealed. The experiment was either returned to the test tube rack and allowed to cool to ambient temperature or was deployed into the original water source to maintain temperature for a period of time before collection prior to return.

After collection and prior to return, each experiment and water sample collected was placed into a Whirl-Pak bag and then packed in an upright position in a larger Ziploc bag. The samples were then packed into a box to maintain position during transport and prevent leaking.

Details of each fluid sample utilised for each experiment are shown in Table 6.41.

6.3.3 Analysis of hydrothermal experiments

The experiments were left for a period of *ca.* 3 months and were each then filtered by gravity into a sterile 50 mL Falcon tube and the pH of each fluid taken using a Jenway 350 pH meter. The ph of each water sample before and after each experiment is shown in Table 6.42.

6.3.3.1 Water Chemistry

The fluids from experiments A1 to C5 were further filtered using Pall Acrodisc 0.45 μm pore 32 mm syringe filters and diluted using deionised water to 70 mL volume. The sample was then split between two acid-washed 30 mL Nalgene sample bottles. Each sample was numbered for identification and all even-numbered samples were acidified by addition of

Iceland experimental package			
Label	# of samples	Contents	
A	8	Iron phosphide (Fe_3P, 0.25 g, 1.68 mmol)	Samples sealed 50 mL Falcon tube under nitrogen using PTFE tape to seal caps to prevent surface oxidation.
B	6	Iron phosphide (Fe_3P, 0.25 g, 1.68 mmol) and iron sulphide (feS, 0.25 g, 2.84 mmol)	Samples sealed 50 mL Falcon tube under nitrogen using PTFE tape to seal caps to prevent surface oxidation.
C	5	Sikhote Alin meteorite samples were cleaned using dilute HCl to remove surface oxidation, rinsed in deionised water then ethanol and vacuum dried.	Samples sealed 50 mL Falcon tube under nitrogen using PTFE tape to seal caps to prevent surface oxidation.
D	2	Magnesium phosphate dibasic ($MgHPO_4$, 0.1 g, 0.83 mmol)	Samples sealed 50 mL Falcon tube.
E	4	Magnesium phosphate dibasic ($MgHPO_4$, 0.1 g, 0.83 mmol) and iron sulphide (FeS, 0.1 g, 1.14 mmol)	Samples sealed 50 mL Falcon tube.
F	4	Calcium phosphite monohydrate ($Ca(H_2PO_3)_2 \cdot H_2O$, 0.1 g, 0.45 mmol) and iron sulphide (FeS, 0.1 g, 1.14 mmol)	Samples sealed 50 mL Falcon tube.
G	2	Calcium phosphite monohydrate ($Ca(H_2PO_3)_2 \cdot H_2O$, 0.1 g, 0.45 mmol)	Samples sealed 50 mL Falcon tube.
H	4	Sodium pyrophosphite ($Na_2H_2P_2O_5$, 0.1 g, 0.53 mmol)	Samples sealed 50 mL Falcon tube.
I	4	Sodium pyrophosphite ($Na_2H_2P_2O_5$, 0.24 g, 1.25 mmol) and glycine (NH_2CH_2COOH, 0.94 g, 1.25 mmol)	Samples sealed 50 mL Falcon tube.
J	2	Sodium pyrophosphate ($Na_2H_2P_2O_7$, 0.28 g, 1.25 mmol) and glycine (NH_2CH_2COOH, 0.94 g, 1.25 mmol)	Samples sealed 50 mL Falcon tube.
K	4	Potassium phosphate monobasic (KH_2PO_4, 0.17 g, 1.25 mmol) and sodium pyrophosphite ($Na_2H_2P_2O_5$, 0.24 g, 1.25 mmol)	Samples sealed 50 mL Falcon tube.
L	4	Sodium pyrophosphite ($Na_2H_2P_2O_5$, 0.24 g, 1.25 mmol) and sodium pyrophosphate ($Na_2H_2P_2O_7$, 0.28 g, 1.25 mmol)	Samples sealed 50 mL Falcon tube.
M	2	Sodium pyrophosphite ($Na_2H_2P_2O_5$, 0.05 g, 0.25 mmol) and adenosine diphosphate (ADP, $C_{10}H_{15}N_5O_{10}P_2$, 0.1 g, 0.25 mmol)	Samples sealed 50 mL Falcon tube.

Table 6.40: Table showing the contents of the experimental package prepared for Iceland. All samples were packed into a large test tube rack and wrapped in cling film to secure them for transportation.

Site Reference	pH	Temp (℃)	Samples
KHL-UCL-3	3.6	40.0	A1
KHL-BPR	4.0	79.5	A2, B1, C5
KHL-MP1	1.6	87.4	A3, B2
KHL-LP1	3.1	93.5	A4, C1
KHL-UCL-5	4.7	89.2	A5, B3, C2, E2, F2
KHL-LP3	2.5	79.2	A6, B4, C4, E3, F3
KHL-LP4	3.3	87.8	A7, B5, E4
KHL-MP3	2.7	84.7	A8, B6, F4
KHL-UCL-4	3.5	55.0	D1, E1, F1
KHL-LAG-1	5.0	21.0	H1, I1, J1, K1, L1, M1
KHL-LAG-2	5.7	20.9	H2, I2, J2, K2, L2, M2
KHL-LAG-3	5.3	11.0	H3, I3, K3, L3, M3
KHL-MEL	5.5	4.7	H4, I4, K4, L4, M4

Table 6.41: Table showing the site reference, pH and temperature of the fluids collected and used for each sample in the experimental package.

two drops of conc. nitric acid (HNO_3). The samples were then sealed under nitrogen using PTFE tape and boxed for transport to UCL for ICP-AES analysis. The ICP-AES analysis was conducted by Dr. Claire Cousins from University College London (UCL) using a Dionex Ion Chromatograph and Horoba JY Ultima 2C ICP-AES spectrometer. Analysis was conducted for iron, nickel, phosphorus and sulphur (Fe, Ni, P and S) on experimental fluid samples and also on untreated samples from the same fluid source. The water chemistry is shown in table Table 6.43.

The phosphorus content of the fluid samples was analysed by Ion chromatography by Prof. Matt Pasek at the University of South Florida, Tampa (USF) using a Perkin Elmer S-200 HPLC fitted with an IonPac AS17-C ion chromatography column. Total phosphorus was measured on the attached, in-line Perkin Elmer Elan DRC II ICP-MS. The data obtained for the total phosphorus concentrations are shown in Table 6.44.

Analysis of the phosphorus speciation was conducted by Prof. Matt Pasek at USF on a Perkin Elmer S-200 HPLC fitted with an IonPac AS17-C ion chromatography column with the total phosphorus measured on the attached, in-line Perkin Elmer Elan DRC II ICP-MS. The system was calibrated using standards for hypophosphite, phosphite and phosphate ($\times 10^{-3}$ to $\times 10^{-7}$ M), using 50μL injections, monitoring m/z= 31 with a 250 ms dwell time. The mobile phase was run at 1.5 mL/min using 3.5 mM KOH for 2 minutes then increased linearly to 35 mM concentration over 10 minutes. The concentration was then held at 35 mM for a further 10 minutes to ensure all species were eluted. As with the sample preparation for the ICP-AES analysis, the samples were diluted with ultra-pure deionised water then filtered using Millipore 0.45μm syringe filters to remove any undissolved particulates. The samples were analysed using the same injection method as the standards and the data obtained are shown in Table 6.45.

6.3.3.2 NMR Spectroscopy

labelNMRexperimental

Sample	Site	Temp (Before)	pH (Before)	Days in fluid	Temp (After)	pH (After)
A1	KHL-UCL-3	40.0	3.6	86	22.4	3.6
A2	KHL-BPR	79.5	4.0	86	22.4	5.1
A3	KHL-MP1	87.4	1.6	84	22.4	2.4
A4	KHL-LP1	93.5	3.1	84	22.4	4.7
A5	KHL-UCL-5	89.2	4.7	82	22.4	5.2
A6	KHL-LP3	79.2	2.5	81	22.4	2.7
A7	KHL-LP4	84.8	3.3	80	22.4	5.2
A8	KHL-MP3	84.7	2.7	79	22.4	2.7
B1	KHL-BPR	79.5	4.0	86	22.4	4.0
B2	KHL-MP1	87.4	1.6	84	22.4	3.7
B3	KHL-UCL-5	89.2	4.7	82	22.4	3.9
B4	KHL-LP3	79.2	2.5	82	22.4	2.8
B5	KHL-LP4	84.8	3.3	82	22.4	2.8
B6	KHL-MP3	84.7	2.7	82	22.4	2.9
C1	KHL-LP1	93.5	3.1	35	22.4	5.7
C2	KHL-UCL-5	89.2	4.7	82	22.4	8.7
C4	KHL-LP3	79.2	2.5	82	22.4	3.2
C5	KHL-BPR	79.5	4.0	82	22.4	4.9

Table 6.42: Table of temperature and pH data for samples A1-A8, B1-B6 and C1, C2, C4 and C5 (C3 was not used in the field as was kept for a controlled anaerobic corrosion experiment in natural hydrothermal fluids in the lab). It can be generally seen that the pH of the samples has increased during reaction which was expected due to hydrogen liberation.

Sample #	Sample Name	Water Source	Fe	Ni	P	S
UoL-002	Deionised water	DI	-0.07	-0.04	-0.04	0.10
UoL-004	A1	KHL-UCL-3	3.25	-0.03	0.53	110.88
UoL-006	A2	KHL-BPR	39.96	-0.04	1.01	122.92
UoL-008	A3	KHL-MP1	72.11	-0.03	2.20	300.30
UoL-010	A4	KHL-LP1	9.56	-0.04	0.53	23.80
UoL-012	A5	KHL-UCL-5	6.20	-0.04	1.20	70.14
UoL-014	A6	KHL-LP3	17.28	-0.03	0.62	0.00
UoL-016	A7	KHL-LP4	16.10	-0.04	0.77	0.00
UoL-018	A8	KHL-MP3	48.22	-0.01	2.28	377.72
UoL-020	Deionised water	DI	-0.07	-0.04	-0.05	0.20
UoL-022	B1	KHL-BPR	73.00	0.04	0.00	157.78
UoL-024	B2	KHL-MP1	71.05	-0.01	0.01	191.24
UoL-026	B3	KHL-UCL-5	33.01	-0.01	0.11	104.02
UoL-028	B4	KHL-LP3	66.70	0.03	0.18	173.32
UoL-030	B5	KHL-LP4	71.41	0.01	0.10	161.42
UoL-032	B6	KHL-MP3	67.33	-0.03	1.34	237.16
UoL-034	C1	KHL-LP1	7.82	0.02	16.78	153.48
UoL-036	C2	KHL-UCL-5	0.35	0.67	0.17	70.00
UoL-038	C4	KHL-LP3	68.01	7.52	-0.01	150.64
UoL-040	C5	KHL-BPR	11.97	1.88	0.06	90.58
UoL-042	KHL-BPR	n/a	4.11	-0.03	-0.01	141.20
UoL-044	KHL-MP1	n/a	2.23	-0.04	0.03	103.46
UoL-046	KHL-LP1	n/a	3.35	-0.04	-0.04	42.14
UoL-048	KHL-LP3	n/a	31.40	-0.04	0.08	0.00
UoL-050	KHL-LP4	n/a	1.51	-0.04	0.00	0.00
UoL-052	KHL-MP3	n/a	4.15	-0.05	0.25	0.00
UoL-054	KHL-LAG	n/a	0.00	-0.04	0.05	55.60
UoL-056	Snow melt	n/a	-0.07	-0.03	0.30	2.00
UoL-058	KHL-BPL	n/a	4.09	-0.03	0.02	121.30
UoL-060	Deionised water	DI	-0.07	-0.04	-0.02	2.30
	KHL-UCL-3	n/a	1.27	-0.02	0.53	220.55
	KHL-UCL-5	n/a	1.26	-0.01	0.54	218.64

Table 6.43: Table of water chemistry data for the hydrothermal experiments (Sample sets A, B, and C). The data gives concentrations (mg/L) detected of iron, nickel, phosphorus and sulphur by ICP-AES.

Sample #	Sample Name	Water Source	P_{UCL}	P_{USF}	Variation
UoL-002	Deionised water	DI	-0.04	0.02	0.05
UoL-004	A1	KHL-UCL-3	0.53	0.40	-0.14
UoL-006	A2	KHL-BPR	1.01	0.92	-0.09
UoL-008	A3	KHL-MP1	2.20	1.72	-0.48
UoL-010	A4	KHL-LP1	0.53	0.20	-0.33
UoL-012	A5	KHL-UCL-5	1.20	1.50	0.30
UoL-014	A6	KHL-LP3	0.62	0.47	-0.15
UoL-016	A7	KHL-LP5	0.77	0.70	-0.07
UoL-018	A8	KHL-MP3	2.28	2.00	-0.28
UoL-020	Deionised water	DI	-0.05	0.04	0.09
UoL-022	B1	KHL-BPR	0.00	0.08	0.08
UoL-024	B2	KHL-MP1	0.01	0.10	0.09
UoL-026	B3	KHL-UCL-5	0.11	0.20	0.09
UoL-028	B4	KHL-LP3	0.18	0.16	-0.02
UoL-030	B5	KHL-LP5	0.10	0.16	0.06
UoL-032	B6	KHL-MP3	1.34	1.01	-0.34
UoL-034	C1	KHL-LP1	16.78	14.30	-2.48
UoL-036	C2	KHL-UCL-5	0.17	0.06	-0.11
UoL-038	C4	KHL-LP3	-0.01	0.04	0.05
UoL-040	C5	KHL-BPR	0.06	0.07	0.02
UoL-042	KHL-BPR	n/a	-0.01	0.00	0.01
UoL-044	KHL-MP1	n/a	0.03	0.00	-0.03
UoL-046	KHL-LP1	n/a	-0.04	0.00	0.04
UoL-048	KHL-LP3	n/a	0.08	0.07	-0.01
UoL-050	KHL-LP4	n/a	0.00	0.05	0.05
UoL-052	KHL-MP3	n/a	0.25	0.00	-0.25
UoL-054	KHL-LAG	n/a	0.05	0.06	0.01
UoL-056	Snow melt	n/a	0.30	0.23	-0.07
UoL-058	KHL-BPL	n/a	0.02	0.01	-0.01
UoL-060	Deionised water	DI	-0.02	0.00	0.02

Table 6.44: Table showing the comparison of phosphorus concentration data for the fluid samples from the UCL and USF analysis. The UCL data was obtained by Dr. Claire Cousins using ICP-AES and the USF data was obtained by Prof. Matt Pasek using Ion Chromatography. The variance between the data is also recorded.

Sample	P^0	P^{3+}	P^{5+}	Total
A1	68.42	259.29	111.49	439.20
A2	23.75	309.38	105.83	438.97
A3	-	792.96	238.22	1031.18
A4	-	155.83	98.56	254.39
A5	13.99	508.59	117.89	640.47
A6	-	157.63	106.97	264.61
A7	41.03	538.68	112.04	691.75
A8	-	408.04	462.63	870.67
B1	-	76.76	115.94	192.70
B2	-	106.67	116.98	223.65
B3	17.54	78.40	32.16	128.10
B4	-	65.18	19.47	84.65
B5	-	72.81	142.99	215.79
B6	-	626.51	251.31	877.82
C1	386.46	32466.30	269.50	33122.27
C2	-	12.63	118.49	131.12
C4	-	-	-	0.00
C5	-	35.06	41.86	76.93

Table 6.45: Phosphorus speciation data from the hydrothermal experiments analysed at USF by Prof. Matt Pasek. Concentrations given are in ppb.

Analysis ^{31}P NMR spectroscopy was conducted on each sample fluid to confirm the phosphorus species present. A 10 mL aliquot of the fluid was taken and treated for iron removal using the sodium hydroxide method where the sample was adjusted to pH 12 to precipitate dissolved iron from the sample. The sample was centrifuged for 1 minute then filtered by gravity and reduced to dryness on top of a drying oven at 40°C. The residues were then dissolved in *ca.* 0.5 mL of deionised water then transferred to an 5 mm borosilicate NMR tube using a D_2O capillary insert for locking purposes. The NMR data for each sample is shown in Table 6.46.

Comparison of the percentage composition of the ^{31}P NMR spectra are shown in Table 6.47. The percentage composition was compared to the phosphorus speciation data obtained by ion chromatography shown in Table 6.45.

6.3.4 Geothermal production of pyrophosphite

Sample G1 [calcium phosphite monohydrate, $Ca(H_2PO_3)_2 \cdot H_2O$, 0.1 g, 0.45 mmol] was placed in location KHL-MP1 for dry heating. The site had a measured temperature of 92.6°C and was selected to attempt geothermal production of pyrophosphite. The sample was supported using rocks and partially submerged in the fluids. This sample was lost as it fell into the fluids.

Sample G2 [calcium phosphite monohydrate, $Ca(H_2PO_3)_2 \cdot H_2O$, 0.1 g, 0.45 mmol] was placed in location KHL-UCL-18 for dry heating. The site had a measured temperature of 94.4°C and was selected to attempt geothermal production of pyrophosphite. The sample was inserted into the geothermally heated soil and left for 72 hours. The sample was recovered and sealed for return. Upon return the sample was dissolved in *ca.* 1 mL D_2O

Sample	NMR details	Peak data
A1	^{31}**P** **NMR** (121.49 MHz, D$_2$O, 300 K)	phosphate (δ2.5, s); δ3.0, d, $^1J_{\text{P-H}}$ = 568 Hz,)
A2	^{31}**P** **NMR** (121.49 MHz, D$_2$O, 300 K)	phosphite (δ3.2, d, $^1J_{\text{P-H}}$ = 567 Hz)
A3	^{31}**P** **NMR** (121.49 MHz, D$_2$O, 300 K)	phosphite (δ3.1, d, $^1J_{\text{P-H}}$ = 571 Hz)
A4	^{31}**P** **NMR** (121.49 MHz, D$_2$O, 300 K)	phosphite (δ2.8, d, $^1J_{\text{P-H}}$ = 630 Hz)
A5	^{31}**P** **NMR** (121.49 MHz, D$_2$O, 300 K)	phosphateδ3.0, s); phosphite (δ3.2, d, $^1J_{\text{P-H}}$ = 565 Hz)
A6	^{31}**P** **NMR** (121.49 MHz, D$_2$O, 300 K)	phosphate (δ2.9, s); phosphite (δ3.2, d, $^1J_{\text{P-H}}$ = 565 Hz)
A7	^{31}**P** **NMR** (121.49 MHz, D$_2$O, 300 K)	phosphate (δ3.4, s); phosphite (δ3.3, d, $^1J_{\text{P-H}}$ = 565 Hz)
A8	^{31}**P** **NMR** (121.49 MHz, D$_2$O, 300 K)	phosphate (δ3.0, s); phosphite (δ3.2, d, $^1J_{\text{P-H}}$ = 565 Hz)
B1	^{31}**P** **NMR** (202.63 MHz, D$_2$O, 300 K)	phosphite (δ5.2, d, $^1J_{\text{P-H}}$ = 627 Hz)
B2	^{31}**P** **NMR** (202.63 MHz, D$_2$O, 300 K)	phosphate (δ2.7, s); phosphite (δ3.1, d, $^1J_{\text{P-H}}$ = 567 Hz)
B3	^{31}**P** **NMR** (202.63 MHz, D$_2$O, 300 K)	phosphite (δ2.8, d, $^1J_{\text{P-H}}$ = 629 Hz)
B4	^{31}**P** **NMR** (121.49 MHz, D$_2$O, 300 K)	phosphate (δ2.5, s); phosphite (δ3.0, d, $^1J_{\text{P-H}}$ = 578 Hz)
B5	^{31}**P** **NMR** (121.49 MHz, D$_2$O, 300 K)	phosphate (δ2.5, s); phosphite (δ3.0, d, $^1J_{\text{P-H}}$ = 578 Hz)
B6	^{31}**P** **NMR** (121.49 MHz, D$_2$O, 300 K)	phosphate (δ2.5, s); phosphite (δ3.0, d, $^1J_{\text{P-H}}$ = 578 Hz)
C1	^{31}**P** **NMR** (202.63 MHz, D$_2$O, 300 K)	phosphate (δ0.1, s); phosphite (δ2.7, d, $^1J_{\text{P-H}}$ = 629 Hz)
C2	^{31}**P** **NMR** (202.63 MHz, D$_2$O, 300 K)	phosphate (δ0.2, s); phosphite (δ2.9, d, $^1J_{\text{P-H}}$ = 629 Hz)
C4	^{31}**P** **NMR** (202.63 MHz, D$_2$O, 300 K)	phosphate (δ0.0, s); phosphite (δ2.7, d, $^1J_{\text{P-H}}$ = 628 Hz)
C5	^{31}**P** **NMR** (202.63 MHz, D$_2$O, 300 K)	phosphate (δ0.2, s); phosphite (δ2.8, d, $^1J_{\text{P-H}}$ = 628 Hz)

Table 6.46: Table of NMR data for the hydrothermal fluid samples A1 to C5. The analysis details the species entered and all calculated chemical shift and coupling constant data. δ given in ppm.

	NMR (integrated peak area)				IC (concentration in ppb)				
Sample	P^{3+}	P^{5+}	% P^{3+}	% P^{5+}	Total P	P^{3+}	P^{5+}	% P^{3+}	% P^{5+}
A1	2.02	0.25	88.99	11.01	439.20	259.29	111.49	59.04	25.38
A2	1.96	0.22	89.91	10.09	438.97	309.38	105.83	70.48	24.11
A3	1.97	0.01	99.49	0.51	1031.18	792.96	238.22	76.90	23.10
A4	2.00	0.27	88.11	11.89	254.39	155.83	98.56	61.26	38.74
A5	1.83	0.26	87.56	12.44	640.57	508.59	117.89	79.40	18.40
A6	2.17	0.29	88.21	11.79	264.61	157.63	106.97	59.57	40.43
A7	1.91	0.28	87.21	12.79	691.75	538.68	112.04	77.87	16.20
A8	1.87	0.33	85.00	15.00	870.67	408.04	462.63	46.87	53.13
B1	2.01	0.01	99.50	0.50	192.70	76.76	115.94	39.83	60.17
B2	1.95	0.08	96.06	3.94	223.65	106.67	116.98	47.70	52.30
B3	2.01	0.06	97.10	2.90	128.10	78.40	32.16	61.20	25.11
B4	1.96	0.10	95.15	4.85	84.65	65.18	19.47	77.00	23.00
B5	2.02	0.07	96.65	3.35	215.79	72.81	142.99	33.74	66.26
B6	2.00	0.13	93.90	6.10	877.82	626.51	251.31	71.37	28.63
C1	2.00	0.43	82.30	17.70	33122.27	32466.30	269.50	98.02	0.81
C2	1.96	1.19	62.22	37.78	131.12	12.63	118.49	9.63	90.37
C4	2.01	2.78	41.96	58.04	-	-	-	-	-
C5	1.99	2.30	46.39	53.61	76.93	35.06	41.86	45.57	54.41

Table 6.47: Table showing comparison of the ion chromatography data to the observed NMR data. The data shows the percentage total phosphorus of phosphate present in the samples is smaller in almost all cases to that shown in the IC data. This is thought due to the partial oxidation of the samples between the NMR analysis and the IC analysis being conducted. P^{3+} is phosphite, P^{5+} is phosphate. NMR peak areas are calculated by integration and normalised to a single phosphite peak area due to a lack of internal standard. The IC data is expressed in ppb concentration. The percentages expressed are as a percentage of total phosphorus present in each sample.

and submitted for analysis by ^{1}H and ^{31}P NMR spectroscopy. Full NMR data is shown in Table 6.48.

$Ca(H_2PO_3)_2 \cdot H_2O$ (0.1 g, 0.45 mmol), 94.4°C, aerobic	
^{1}H NMR (D$_2$O, 300 K, 500.57 MHz)	
G2	phosphite (δ6.7, d, $^1J_{P-H}$= 575 Hz); pyrophosphite (δ6.9, AA'XX', $^1J_{P-H}$= 666 Hz, $^2J_{P-P}$= 10 Hz, $^3J_{P-H}$ = 8 Hz)
^{31}P NMR (D$_2$O, 300 K, 202.63 MHz)	
G2	phosphite (δ3.7, d, $^1J_{P-H}$= 573 Hz); pyrophosphite (δ-4.4, AA'XX', $^1J_{P-H}$= 666 Hz, $^2J_{P-P}$= 10 Hz, $^3J_{P-H}$= 8 Hz)

Table 6.48: Table of NMR data for the heating of calcium phosphite by insertion in geothermally heated sand. The sand was measured at 94.4°Cand was heated under aerobic conditions for 72 hours.

6.3.4.1 Simulated geothermal production of pyrophosphite

This experiment is an attempt to simulate the experiment undertaken in 6.3.4 in a laboratory environment. Calcium phosphite monohydrate [$Ca(H_2PO_3)_2 \cdot H_2O$, 0.1 g, 0.45 mmol] was placed in a 50 mL Falcon tube and heated to *ca.* 95°C for 72 hours on a sand bath under aerobic conditions. The sample was then allowed to cool to room temperature then dissolved in *ca.* 1 mL D$_2$O and submitted for analysis by ^{1}H and ^{31}P NMR spectroscopy. Full NMR data is shown in Table 6.49.

	Ca(H$_2$PO$_3$)$_2 \cdot$ H$_2$O (0.1 g, 0.45 mmol), 95℃, aerobic
	^{1}H NMR (D$_2$O, 300 K, 500.57 MHz)
G2 sim	phosphite (δ6.7, d, $^1J_{P\text{-}H}$= 630 Hz); pyrophosphite (δ6.8, AA'XX', $^1J_{P\text{-}H}$= 672 Hz, $^2J_{P\text{-}P}$= 10 Hz, $^3J_{P\text{-}H}$= 8 Hz)
	^{31}P NMR (D$_2$O, 300 K, 202.63 MHz)
G2 sim	phosphite (δ2.6, d, $^1J_{P\text{-}H}$= 631 Hz); pyrophosphite (δ-5.5, AA'XX', $^1J_{P\text{-}H}$= 672 Hz, $^2J_{P\text{-}P}$= 10 Hz, $^3J_{P\text{-}H}$ = 8 Hz)

Table 6.49: Table of NMR data for the simulated heating of calcium phosphite by insertion in heated sand. The sand was measured at 95℃and was heated under aerobic conditions for 72 hours.

6.3.4.2 Simulated geothermal production of pyrophosphite from A sample corrosion experiments

A 30 mL aliquot of samples A1 to A5 was taken and for each sample and placed in a 100 mL conical flask. The iron was removed by adjusting to pH 12 using dropwise addition of sodium hydroxide (NaOH, 1 M) and the sample filtered to remove the precipitate. Each sample was adjusted to *ca.* pH 4 using dropwise addition of sulphuric acid (H$_2$SO$_4$, 1 M). The samples were reduced to dryness on top of a 40℃ drying oven and the residues collected and transferred to a 25 mL round bottomed flask. The flask was fitted with a gas inlet to allow a constant flow of nitrogen over the sample. The sample was heated to 90℃ on a sand bath for 72 hours then removed from the heat and allowed to cool under a flow of nitrogen. The sample was collected and ground in a mortar and pestle. An aliquot of each sample (0.5 g) was dissolved in 0.5 mL deionised water and the pH of the sample was adjusted to pH 7.5 using H$_2$SO$_4$ (0.1 M, dropwise addition). Each sample was submitted for analysis by ^{31}P NMR spectroscopy using a D$_2$O capillary insert for locking purposes. Full NMR data is shown in Table 6.50.

6.3.4.3 Simulated geothermal production of pyrophosphite using C sample corrosion experiments

A 30 mL aliquot of samples C1, C2, C4 and C5 was taken and for each sample and placed in a 100 mL conical flask. The iron was removed by adjusting to pH 12 using NaOH (1 M, dropwise addition) . Each sample was adjusted to pH 4 using H$_2$SO$_4$ (1 M, dropwise addition). The sample was then reduced to dryness on top of a 40℃ drying oven and the residues collected and transferred to a 25 mL round bottomed flask. The flask was fitted with a gas inlet to allow a constant flow of nitrogen over the sample. The sample was heated to 90℃ on a sand bath for 72 hours then removed from the heat and allowed to cool under a flow of nitrogen. The sample was collected and ground in a mortar and pestle. An aliquot (0.5 g) of the sample was dissolved in 0.5 mL deionised water and the pH of the sample was adjusted to pH 7.5 using H$_2$SO$_4$ (0.1 M, dropwise addition). The sample was submitted for analysis by^{31}P NMR spectroscopy using a D$_2$O capillary insert for locking purposes. Full NMR data is shown in Table 6.51.

90°C, 72 hours, N$_2$ flow

	^{31}P NMR (D$_2$O, 300 K, 202.63 MHz)
A1	phosphate (δ0.1, s); phosphite (δ2.7, d, $^1J_{\text{P-H}}$= 628 Hz); pyrophosphite (δ-5.0, AA'XX', $^1J_{\text{P-H}}$= 668 Hz, no other coupling constants calculated due to poor definition in the spectrum.)
A2	phosphate (δ0.6, s); phosphite (δ2.9, d, $^1J_{\text{P-H}}$= 619 Hz); pyrophosphite (δ-4.9, AA'XX', $^1J_{\text{P-H}}$= 659 Hz, no other coupling constants calculated due to poor definition in the spectrum.)
A3	phosphate (δ0.1, s); phosphite (δ2.7, d, $^1J_{\text{P-H}}$= 627 Hz); Pyrophosphite (unable to formally identify pyrophosphite though there are faintly visible peaks in the correct region of the spectrum suggesting the presence of pyrophosphite.)
A4	phosphate (δ0.6, s); phosphite (δ2.9, d, $^1J_{\text{P-H}}$= 619 Hz); pyrophosphite (δ-4.9, AA'XX', $^1J_{\text{P-H}}$ = 659 Hz, no other coupling constants calculated due to poor definition in the spectrum.)
A5	phosphate (δ1.2, s); phosphite δ3.0, d, $^1J_{\text{P-H}}$= 593 Hz); pyrophosphite (δ-5.0, AA'XX', $^1J_{\text{P-H}}$= 665 Hz, $^2J_{\text{P-P}}$= 9 Hz, $^1J_{\text{P-H}}$= 9 Hz), pyrophosphate (δ-6.1, s)

Table 6.50: Table of NMR data for the dry heated A samples. The samples were treated to remove iron prior to heating using the sodium hydroxide method. Each sample was adjusted to pH 4 prior to dehydration and heating. δ given in ppm.

^{31}**P NMR (D$_2$O, 300 K, 202.63 MHz)**	
90°C, 72 hours, N$_2$ flow	
Analysis	
C1	phosphate (δ1.8, s); phosphite (δ3.1, d, $^1J_{\text{P-H}}$= 580 Hz); pyrophosphite (δ-5.0, AA'XX', $^1J_{\text{P-H}}$= 666 Hz, $^2J_{\text{P-P}}$= 9 Hz, $^3J_{\text{P-H}}$= 8 Hz); spectrum contains P-D coupling (3.23, 2.79, 2.35) and peaks indicative of isohypophosphate and other linear tripolyphosphates.
C2	No peaks visible after several attempts to remove iron.
C4	No peaks visible after several attempts to remove iron.
C5	No peaks visible after several attempts to remove iron.

Table 6.51: Table of NMR data for the dry heated C samples. The samples were treated to remove iron prior to heating using the sodium hydroxide method. Each sample was adjusted to pH 4 prior to dehydration and heating. δ given in ppm.

6.3.4.4 Production of isohypophosphate by direct coupling or solution chemistry

Potassium phosphate monobasic (KH_2PO_4, 0.136 g, 1 mmol) and sodium pyrophosphite ($Na_2H_2P_2O_5$, 0.190 g, 1 mmol) were dissolved in 5 mL deionised water in a 25 mL conical flask and adjusted to pH 4 by dropwise addition of HCl (1M). A 0.5 mL aliquot was taken and submitted for analysis by ^{31}P NMR spectroscopy using a D_2O capillary insert for locking purposes. The sample was then submitted for further NMR analysis *ca.* every 30 minutes to observe the rate of hydrolysis of pyrophosphite compared to the rate of production of isohypophosphate in solution. Full NMR data is shown in Table 6.52.

^{31}P NMR (D_2O, 300 K, 121.49 MHz)
KH_2PO_4 (0.14 g, 1 mmol) + $Na_2H_2P_2O_5$ (0.19 g, 1 mmol), RT, aerobic

	Analysis
T= 0	phosphate (δ0.2, s, 26.21%); phosphite (δ2.7, d, $^1J_{\text{P-H}}$= 619 Hz, 4.85%); pyrophosphite (δ-5.1, AA'XX', $^1J_{\text{P-H}}$= 666 Hz, $^1J_{\text{P-P}}$= 9 Hz, $^3J_{\text{P-H}}$= 9 Hz, 68.95%)
T= 30	phosphate (δ0.2, s, 26.45%); δ2.6, d, $^1J_{\text{P-H}}$= 619 Hz, 4.48%); pyrophosphite (δ-5.1, AA'XX', $^1J_{\text{P-H}}$= 666 Hz, $^2J_{\text{P-P}}$= 9 Hz, $^3J_{\text{P-H}}$= 9 Hz, 69.42%)
T= 60	phosphate (δ2.8, s, 25.34%); phosphite (δ5.2, d, $^1J_{\text{P-H}}$= 621 Hz, 3.42%); pyrophosphite (δ-2.5, AA'XX', $^1J_{\text{P-H}}$= 667 Hz, $^2J_{\text{P-P}}$= 10 Hz, $^3J_{\text{P-H}}$= 8 Hz, 71.23%)
T= 90	phosphate (δ2.8, s, 24.52%); phosphite (δ5.2, d, $^1J_{\text{P-H}}$= 621 Hz, 4.72%); pyrophosphite (δ-2.5, AA'XX', $J_{\text{P-H}}$= 667 Hz, $^2J_{\text{P-P}}$= 10 Hz, $^3J_{\text{P-H}}$= 8 Hz, 70.75%)
T= 120	phosphate (δ0.2, s, 25.40%); phosphite (δ2.7, d, $^1J_{\text{P-H}}$= 619 Hz, 4.88%); pyrophosphite (δ-5.1, AA'XX', $^1J_{\text{P-H}}$= 666 Hz, $^2J_{\text{P-P}}$= 9 Hz, $^3J_{\text{P-H}}$= 9 Hz, 69.11%)
T= 150	phosphate (δ0.2, s, 26.19%); phosphite (δ2.7, d, $^1J_{\text{P-H}}$= 619 Hz, 3.97%); pyrophosphate (δ-5.1, AA'XX', $^1J_{\text{P-H}}$= 666 Hz, $^2J^{\text{P-P}}$= 9 Hz, $^3J_{\text{P-H}}$= 9 Hz, 69.84%)

Table 6.52: Table of NMR data for the study of production over time of isohypophosphate by reaction of pyrophosphite and phosphate in solution. The investigation hoped to identify the method of production for isohypophosphate in the Iceland samples which were dry heated to produce pyrophosphite.

6.3.4.5 pH effects on production of isohypophosphate

Two experiments were prepared using sodium phosphite (NaH_2PO_3, 0.05 g, 0.5 mmol) and sodium phosphate monobasic (NaH_2PO_4, 0.6 g, 0.5 mmol) which were dissolved in 5 mL deionised water in a 25 mL conical flask. The pH of one experiments was adjusted to pH4 using HCl (1 M, dropwise addition) and the other experiment was adjusted to pH 7 by addition of NaOH (1 M, dropwise addition). The solutions were transferred to a petri dish and dried on top of a drying oven at 40℃ oven for 72 hours. Both samples were allowed to cool to room temperature then ground in a mortar and pestle, dissolved in 1 mL D_2O and submitted for analysis by ^{31}P NMR spectroscopy. Full NMR data is shown in Table 6.53.

The pH 4 Sample was then spiked with sodium pyrophosphite ($Na_2H_2P_2O_5$) containing *ca.* 20% sodium isohypophosphate ($Na_2H_2P_2O_6$) by adding *ca.* 50 mg to the NMR tube

and shaking vigorously until the solid dissolved. The sample was resubmitted for analysis by ^{31}P NMR spectroscopy. NMR data in Table 6.53.

The pH 4 sample was then spiked with sodium pyrophosphate dibasic ($Na_2H_2P_2O_7$) by adding *ca.* 50 mg to the NMR tube and shaking vigorously until the solid was dissolved. The sample was resubmitted for analysis by ^{31}P NMR spectroscopy. NMR data in Table 6.53.

^{31}**P NMR (D$_2$O, 300 K, 202.63 MHz)**	
	40°C, 72 hours, aerobic
	Analysis
pH 4	phosphate (δ1.6, s); phosphite (δ3.1, d, $^1J_{\text{P-H}}=$ 585 Hz); weak signals in the baseline which seem indicative of isohypophosphate (δ-2.51, -5.44 and -5.67), pyrophosphite (δ-3.20 and -6.54) and pyrophosphate (δ-7.08)
pH 7	phosphate (δ0.0, s); phosphite (δ3.2, d, $^1J_{\text{P-H}}=$ 640 Hz)
$Na_3HP_2O_6$ spiked	phosphate (δ1.7, s); phosphite (δ3.1, d, $^1J_{\text{P-H}}=$ 584 Hz); pyrophosphate (δ-4.73, AA'XX', $^1J_{\text{P-H}}=$ 669 Hz, $^2J_{\text{P-P}}=$ 10 Hz, $^3J_{\text{P-H}}=$ 8 Hz); isohypophosphate (δ-3.8, dd, $^1J_{\text{P-H}}=$ 580 Hz, $^2J_{\text{P-P}}=$ 17 Hz), (δ-5.6, d, $^2J_{\text{P-P}}=$ 17 Hz); pyrophosphate (δ-6.8, s)
$Na_4H_2P_2O_7$ spiked	phosphate (δ1.1, s); phosphite (δ3.0, d, $^1J_{\text{P-H}}=$ 596 Hz); pyrophosphate (δ-4.7, AA'XX', $^1J_{\text{P-H}}=$ 669 Hz, $^2J_{\text{P-P}}=$ 10 Hz, $^3J_{\text{P-H}}=$ 8 Hz); isohypophosphate (δ-4.0, dd, $^1J_{\text{P-H}}=$ 644, $^2J_{\text{P-P}}=$ 18 Hz), (δ-5.7, d, $^2J_{\text{P-P}}=$ 18 Hz); pyrophosphate (δ-7.4, s)

Table 6.53: Table of NMR data for the pH study of the formation of isohypophosphate by slow evaporation method. The pH 4 sample was later spiked with isohypophosphate, pyrophosphite and pyrophosphate to confirm the identification of the species present in the spectrum. δ given in ppm.

6.3.4.6 Effects of SMOW on production of isohypophosphate

A series of eight experiments were set up to explore the effects of SMOW on the production of isohypophosphate. The conditions of the experiments are shown in Table 6.54.

Experiment	Content
1	NaH_2PO_3 (0.05 g, 0.5 mmol) and NaH_2PO_4 (0.06 g, 0.5 mmol), SMOW
2	NaH_2PO_4 (0.1 g, 0.83 mmol), SMOW
3	NaH_2PO_3 (0.1 g, 0.96 mmol), SMOW
4	NaH_2PO_3 (0.05 g, 0.5 mmol) and NaH_2PO_4 (0.06 g, 0.5 mmol)
5	NaH_2PO_4 (0.1 g, 0.83 mmol)
6	NaH_2PO_3 (0.1 g, 0.96 mmol)
7	NaH_2PO_3 (0.05 g, 0.5 mmol) and NaH_2PO_4 (0.06 g, 0.5 mmol), SMOW, pH 4 adjusted
8	NaH_2PO_3 (0.05 g, 0.5 mmol) and NaH_2PO_4 (0.06 g, 0.5 mmol), pH 4 adjusted

Table 6.54: Table detailing experimental setup for investigation of the effects of SMOW on the formation of isohypophosphate.

The samples were dissolved in either 5 mL SMOW solution or 5 mL deionised water in a 25 mL conical flask and samples 7 and 8 were adjusted to pH 4 using HCl (1 M, dropwise addition). The samples were transferred to a petri dish and dried on top of a drying oven at 40℃ for 72 hours. All samples were allowed to cool to room temperature then ground in a mortar and pestle, dissolved in 1 mL D_2O and submitted for ^{31}P NMR analysis. Full NMR data is shown in Table 6.55.

^{31}P NMR (D_2O, 300 K, 202.63 MHz)

	40℃, 72 hours, aerobic **Analysis**
1	phosphate (δ0.7, s); phosphite (δ2.9, d, $^1J_{P\text{-}H}$= 608 Hz); pyrophosphite (δ-4.9, AA'XX', $^1J_{P\text{-}H}$= 673 Hz, $^2J^{P\text{-}P}$= 10 Hz, $^3J_{P\text{-}H}$= 8 Hz); isohypophosphate (δ-4.1, dd, $^1J_{P\text{-}H}$= 663, $^2J_{P\text{-}P}$ = 17 Hz), (δ-6.0, d, $^2J_{P\text{-}P}$= 17 Hz); pyrophosphate (δ-6.2, s)
2	phosphate (δ1.5, s)
3	phosphite (δ3.0, d, $^1J_{P\text{-}H}$= 577 Hz); pyrophosphite (δ-4.6, AA'XX', $^1J_{P\text{-}H}$ = 673 Hz, weak spectrum so no further coupling constants can be calculated)
4	phosphate (δ0.7, s); phosphite (δ2.8, d, $^1J_{P\text{-}H}$= 604 Hz)
5	phosphate (δ2.6, s)
6	phosphite (δ3.1, d, $^1J_{P\text{-}H}$= 577 Hz)
7	phosphate (δ0.8, s); phosphite δ3.3, d, $^1J_{P\text{-}H}$ = 584 Hz); pyrophosphite (δ-4.8, AA'XX', $^1J_{P\text{-}H}$= 671 Hz, $^2J_{P\text{-}P}$= 8 Hz, $^3J_{P\text{-}H}$= 8 Hz); isohypophosphate (δ-3.8, dd, $^1J_{P\text{-}H}$= 618 Hz, $^2J_{P\text{-}P}$= 17 Hz), (δ-5.6, d, $^2J_{P\text{-}P}$ = 17 Hz)
8	phosphate (δ0.8, s); phosphate (δ2.9, d, $^1J_{P\text{-}H}$= 607 Hz); pyrophosphite (δ-4.9, AA'XX', $^1J_{P\text{-}H}$= 668 Hz, $^2J_{P\text{-}P}$= 10 Hz, $^3J_{P\text{-}H}$= 8 Hz; isohypophosphate (δ-4.4, dd, $^1J_{P\text{-}H}$= 650, $^2J_{P\text{-}P}$= 15 Hz), (δ-6.6, d, $^2J_{P\text{-}P}$= 17 Hz); pyrophosphate (δ-8.0, s)

Table 6.55: Table of NMR data for the experiment investigating the effects of SMOW on the formation of isohypophosphate. The samples were heated at 40℃ for 72 hours prior to analysis. δ given in ppm.

6.3.4.7 Temperature effects on production of isohypophosphate

Two experiments were prepared using sodium phosphite (NaH_2PO_3, 0.05 g, 0.5 mmol) and sodium phosphate monobasic (NaH_2PO_4, 0.6 g, 0.5 mmol). The experiments were prepared in 25 mL round bottom flasks. Experiment 1 was dissolved in 5 mL deionised water and experiment 2 was dissolved in 5 mL SMOW solution. The solutions were both adjusted to *ca.* pH 4 using HCl (1 M, dropwise addition). The flasks were fitted with a gas inlet which allowed a continuous flow of nitrogen over the sample and the sample was heated to 60℃ on a sand bath for 72 hours.

The samples were allowed to cool to room temperature under flowing nitrogen then collected and ground in a mortar and pestle. An aliquot of each sample (0.5 g) was taken and dissolved in 1 mL D_2O then submitted for analysis by ^{31}P NMR spectroscopy. Full NMR results are shown in Table 6.56.

^{31}P NMR (D$_2$O, 300 K, 202.63 MHz)		
60°C, 72 hours, N$_2$ flow		
Analysis		
DI water	phosphate (δ2.1, s); phosphite (δ3.1, d, $^1J_{\text{P-H}}$= 573 Hz); pyrophosphite (δ-5.0, AA'XX', $^1J_{\text{P-H}}$= 671 Hz, $^2J_{\text{P-P}}$= 10 Hz, $^3J_{\text{P-H}}$= 8 Hz)	
SMOW	phosphate (δ2.1, s); phosphite (δ3.1, d, $^1J_{\text{P-H}}$= 575 Hz); pyrophosphite (δ-5.0, AA'XX', $^1J_{\text{P-H}}$= 671 Hz, $^2J_{\text{P-P}}$= 10 Hz, $^3J_{\text{P-H}}$= 8 Hz); isohypophosphate (δ-4.0, dd, $^1J_{\text{P-H}}$= 563 Hz, $^2J_{\text{P-P}}$= 17 Hz), (δ-5.8, d, $^2J_{\text{P-P}}$= 17 Hz)	

Table 6.56: Table of NMR data for the investigation of the effect of temperature on the production of isohypophosphate. δ given in ppm.

6.3.5 Simulated anaerobic corrosion of Sample C3

labelsimC3corrosionexperimental

A sample of the Sikhote Alin meteorite (Sample C3) containing schreibersite was placed inside a 50 mL Falcon tube under an atmosphere of N$_2$. 50 mL of naturally acidic Icelandic fluid was added and the tube was then sealed with PTFE tape. The Icelandic fluid used was from site KHL-LP3 (originally recorded at pH 2.5, 79.2°C) which was reheated to its original temperature before the sample was taken to redissolve all the salts present then degassed by bubbling N$_2$ though the fluid for a period of 30 minutes prior to addition to the reaction vessel.

The Falcon tube was then suspended inside a test tube containing silicon oil and fitted with a gas inlet cap which allowed for flowing N$_2$ to be fed into the vessel to sustain a N$_2$ atmosphere. To retain the anaerobic conditions inside the vessel, all joints were greased and tied using copper wire. The test tube containing the sample was suspended in an oil bath and heated to 80°C for a period of 28 days to simulate anaerobic corrosion in natural hydrothermal fluids.

After the 28 day heating period, the sample was allowed to cool to room temperature under the N$_2$ atmosphere. The sample vessel was then transported to an anaerobic glove box where the meteorite sample was removed and dried for surface analysis and the fluids were re-sealed inside the Falcon tube and removed to a fridge at 8°C for storage while awaiting analysis.

^{31}P NMR (D$_2$O, 300 K, 300.13 MHz	
Conditions: Sikhote Alin C3, 90C, anaerobic, 28 days	
Analysis	
C3	phosphite (δ2.7, d, $^1J_{\text{P-H}}$= 628 Hz) and phosphate (0.0, s)

Table 6.57: Table of NMR data for the anaerobic corrosion of Sikhote Alin sample C3. The sample was heated in icelandic fluids for 28 days under strictly anaerobic conditions.

References

[1] S. L. Miller, H. C. Urey, and J. Oro, "Origin of organic compounds on primitive earth and in meteorites," *Journal of Molecular Evolution*, vol. 9:(1), pp. 59–72, 1976.

[2] S. L. Miller, "A production of amino acids under possible primitive earth conditions," *Science*, vol. 117, pp. 528–529, 1953.

[3] A. P. Johnson, H. J. Cleaves, J. P. Dworkin, D. P. Glavin, a. Lazcano, and J. L. Bada, "The miller volcanic spark discharge experiment," *Science*, vol. 322, p. 404, 2008.

[4] J. Rabinowitz, F. Woeller, J. Flores, and R. Krebsbac, "Electric discharge reactions in mixtures of phosphine, methane, ammonia and water," *Nature*, vol. 224, pp. 796–797, 1969.

[5] E. Fluck, "The chemistry of phosphine," *Fortschritte der Chemischen Forschung*, vol. 35, 1, pp. 1–64, 1973.

[6] J. L. Bada, "How life began on earth: a status report," *Earth. Planet. Sc.i Lett.*, vol. 226, pp. 1–15, 2004.

[7] H. J. Cleaves, J. H. Chalmers, A. Lazcano, S. L. Miller, and J. L. Bada, "Prebiotic organic synthesis in neutral planetary atmospheres," *ACS Symposium Series*, vol. 981, pp. 282–292, 2007.

[8] H. J. Cleaves, J. H. Chalmers, A. Lazcano, S. L. Miller, and J. L. Bada, "A reassessment of prebiotic organic synthesis in neutral planetary atmospheres," *Orig. Life Evol. Biosph.*, vol. 38, pp. 105–115, 2008.

[9] T. Ganti, *The Principles of Life*. Oxford University Press, 2003.

[10] Y.-F. Zhao, B. Han, J. Chen, and Y. Jiang, "Penta-coordinate phosphorus compounds and biochemistry," *Phosphorus Sulfur*, vol. 177, no. 6, pp. 1391 – 1396, 2002.

[11] N. N. Greenwood and A. Earnshaw, *Chemistry of the Elements*, ch. 12 Phosphorus, pp. 546–636. Pergamon Press, Oxford, 1993.

[12] C. R. Benitez-Nelson, "The biogeochemical cycling of phosphorus in marine systems," *Earth Science Reviews*, vol. 51, pp. 109–135, 2000.

[13] T. J. Smayda, "Harmful algal blooms: Their ecophysiology and general relevance to phytoplankton blooms in the sea," *Limnology and Oceanography*, vol. 42, pp. 1137–1153, 1997.

[14] F. Wolfe-Simon, J. S. Blum, T. R. Kulp, G. W. Gordon, S. E. Hoeft, J. Pett-Ridge, J. F. Stolz, S. M. Webb, P. K. Weber, P. C. W. Davies, A. D. Anbar, and R. S. Oremland, "A bacterium that can grow by using arsenic instead of phosphorus," *Science*, vol. 332, pp. 1163–1166, 2011.

[15] F. Wolfe-Simon, J. S. Blum, T. R. Kulp, G. W. Gordon, S. E. Hoeft, J. Pett-Ridge, J. F. Stolz, S. M. Webb, P. K. Weber, P. C. W. Davies, A. D. Anbar, and R. S. Oremland, "Response to comments on Şa bacterium that can grow using arsenic instead of phosphorusŤ," *Science*, vol. 332, p. 1149, 2011.

[16] T. J. Erb, P. Kiefer, B. Hattendorf, D. Günther, and J. A. Vorholt, "Gfaj-1 is an arsenate-resistant, phosphate-dependent organism," *Science*, vol. 337, pp. 467–470, 2012.

[17] M. L. Reaves, S. Sinha, J. D. Rabinowitz, L. Kruglyak, and R. J. Redfield, "Absence of detectable arsenate in dna from arsenate-grown gfaj-1 cells," *Science*, vol. 337, pp. 470–473, 2012.

[18] B. D. Davis, "On the importance of being ionized," *Arch. Biochem. Biophys.*, vol. 78, pp. 497–509, 1958.

[19] F. H. Westheimer, "Why nature chose phosphates," *Science*, vol. 235, no. 4793, pp. 1173–1178, 1987.

[20] T. M. Devlin, ed., *Textbook of Biochemistry: with Clinical Correlations.* John Wiley and Sons, Inc, Hoboken, NJ. USA., 1995.

[21] J. R. Knowles, "Enzyme-catalyzed phosphoryl transfer reactions," *Annual Review of Biochemistry*, vol. 49, pp. 877–919, 1980.

[22] D. L. Nelson and M. M. Cox, *Lehninger Principles of Biochemistry (Fourth Edition).* W. H. Freeman and Company, 2005.

[23] M. A. Pasek and T. P. Kee, *Origins of Life: The Primal Self-Organization*, ch. On the Origin of Phosphorylated Biomolecules, pp. 57–84. Springer Berlin Heidelberg, 2011.

[24] L. Busman, J. Lamb, G. Randall, G. Rehm, and M. Schmitt, *The nature of phosphorus in soils.* University of Minnesota Extension,, 2008.

[25] A. Keefe and S. Miller, "Are polyphosphates or phosphate esters prebiotic reagents?," *J Mol Evol.*, vol. 41:(6), pp. 693–702, 1995.

[26] G. Arrhenius, B. Gedulin, and S. Mojzsis, "Conference on chemical evolution and the origin of life," in *Chemical Evolution: Orgin of Life*, pp. 25–50, 1993.

[27] L.-K. Sha, "Whitlockite solubility in silicate melts: some insights into lunar and planetary evolution," *Geochim. Cosmochim. Acta.*, vol. 64:(18), p. 3217Ű3236, 2000.

[28] M. A. Pasek and D. S. Lauretta, "Aqueous corrosion of phosphide minerals from iron meteorites: A highly reactive source of prebiotic phosphorus on the surface of the early earth," *Astrobiology*, vol. 5, pp. 515–535, 2005.

[29] M. Pasek, T. Kee, D. Bryant, A. Pavlov, and J. Lunine, "Production of potentially prebiotic condensed phosphates by phosphorus redox chemistry," *Angewandte Chemie International Edition*, vol. 47, no. 41, pp. 7918–7920, 2008. 10.1002/anie.200802145.

[30] A. Gulick, "Phosphorus and the origin of life," *Annals of the New York Academy of Sciences*, vol. 69, pp. 309–313, 1957.

[31] F. Bronner and R. V. Worrell, *Orthopaedics: Principles of Basic and Clinical Science.* CRC Press, New York, 1999.

[32] Y. Yamagata, "Prebiotic formation of adp and atp from amp, calcium phosphates and cyanate in aqueous solution," *Orig. Life. Evol. Biosph.*, vol. 29:(5), pp. 511–520, 1999.

[33] H. Pech, A. Henry, C. S. Khachikian, T. M. Salmassi, G. Hanrahan, and K. L. Foster, "Detection of geothermal phosphite using high-performance liquid chromatography," *Environ. Sci. Technol.*, vol. 43, pp. 7671–7675, 2009.

[34] A. Redfield, "The biological control of chemical factors in the environment," *Am. Sci.*, vol. 46, pp. 205–221, 1958.

[35] E. Maciá, "The role of phosphorus in chemical evolution.," *Chem. Soc. Rev.*, vol. 34, pp. 691–701, 2005.

[36] A. Gulick, "Phosphorus as a factor in the origin of life," *American Scientist*, vol. 43, pp. 479–489, 1955.

[37] S. L. Miller and H. C. Urey, "Organic compound synthesis on the primitive earth," *Science*, vol. 130, pp. 245–251, 1959.

[38] G. Cooper, W. Onwo, and J. Cronin, "Alkyl phosphonic acids and sulphonic acids in the murchison meteorite," *Geochim. Cosmochim. Acta.*, vol. 56, pp. 4109–4115, 1992.

[39] M. A. Sephton, "Organic compounds in carbonaceous meteorites," *Natural Product Reports*, vol. 19, pp. 292–311, 2002.

[40] K. Kvenvolden, J. Lawless, K. Pering, E. Peterson, J. Floers, C. Ponnamperuma, I. R. Kaplan, and C. Moore, "Evidence for extraterrestrial amino-acids and hydrocarbons in the murchison meteorite," *Nature*, vol. 228, pp. 923–926, 1970.

[41] J. Oro, J. Gibert, H. Lichtenstein, S. Wikstrom, and D. Flory, "Amino-acids, aliphatic and aromatic hydrocarbons in the murchison meteorite," *Nature*, vol. 230, pp. 105–106, 1971.

[42] C. Ponnamperuma, "Organic compounds in the murchison meteorite," *Annals of the New York Academy of Sciences*, vol. 194, pp. 56–70, 1972.

[43] P. Schmitt-Kopplin, Z. Gabelica, R. D. Gougeon, A. Fekete, B. Kanawati, M. Harir, I. Gebefuegi, G. Eckel, and N. Hertkorn, "High molecular diversity of extraterrestrial

organic matter in murchison meteorite revealed 40 years after its fall," *Proceedings of the National Academy of Sciences*, vol. 107, pp. 2763–2768, 2010.

[44] R. de Graaf, j. Visscher, and A. Schwartz, "A plausibly prebiotic synthesis of phosphonic acids," *Nature*, vol. 378, pp. 474–477, 1995.

[45] I. Gorrell, L. Wang, A. Marks, D. Bryant, F. Bouillot, A. Goddard, D. Heard, and T. Kee, "On the origin of murchison meteorite phosphonates. implications for prebiotic chemistry," *Chem. Commun.*, vol. 15, pp. 1643–1645, 2006.

[46] O. I. Yakovlev, Y. P. Dikov, and M. V. Gerasimov, "Experimental data on the thermal reduction of phosphorus and iron and their significance for the interpretation of the impact reworking of lunar materials," *Geochem. Int.*, vol. 44, pp. 847–854, 2006.

[47] B. M. Simonson and B. P. Glass, "Spherule layers - records of an cient impacts," *Annu. Rev. Earth. PLanet. Sci.*, vol. 32, pp. 329–361, 2004.

[48] M. Grady and R. Hutchinson, *Cartalogue of Meteorites.* Cambridge University Press, Cambridge, 2000.

[49] O. Moretzki, T. Doering, V. Geist, W. Morgenroth, and M. Wendschuh, "Crystal structure of iron nickel phosphide, fe1.8ni1.2p, a schreibersite extracted from orange river meteorite," *Zeitschrift fuer Kristallographie - New Crystal Structures*, vol. 218(4), pp. 395–396, 2003.

[50] O. Moretzki, T. Doering, V. Geist, W. Morgenroth, and M. Wendschuh, "Crystal structure of iron nickel phosphide, fe1.65ni1.35p, a rhabdite extracted from morasko meteorite," *Zeitschrift fuer Kristallographie - New Crystal Structures*, vol. 218(4), pp. 393–394, 2003.

[51] O. Moretzki, T. Doering, V. Geist, W. Morgenroth, and M. Wendschuh, "Crystal structure of iron nickel phosphide, fe1.7ni1.3p, a schreibersite extracted from canyon diablo meteorite," *Zeitschrift fuer Kristallographie - New Crystal Structures*, vol. 218(4), pp. 391–391, 2003.

[52] Y. Yamagata, H. Watanabe, M. Saitoh, and T. Namba, "Volcanic production of polyphosphates and its relevance to prebiotic evolution.," *Nature*, vol. 352, pp. 516–519, 1991.

[53] P. W. A. Huebner and R. M. Milburn, "Hydrolysis of pyrophosphate to orthophosphate promoted by cobalt(iii). evidence for the role of polynuclear species," *Inorg. Chem.*, vol. 19:(5), pp. 1267–1272, 1980.

[54] P. A. Hamilton and T. P. Murrells, "Kinetics and mechanism of the reactions of ph3 with o(3p) and n(4s) atoms," *J. Chem. Soc., Faraday Trans. 2*, vol. 81, pp. 1531–1541, 1985.

[55] M. Pasek and K. Block, "Lightning-induced reduction of phosphorus oxidation state," *Nature Geoscience*, vol. 2, pp. 553–556, 2009.

[56] D. E. Bryant and T. P. Kee, "Direct evidence for the availability of reactive, water soluble phosphorus on the early earth. h-phosphinic acid from the nantan meteorite," *Chem. Commun.*, vol. 22, pp. 2344–2346, 2006.

[57] D. Glindemann, F. Eismann, A. Bergmann, P. Kuschk, and U. Stottmeister, "Phosphine by bio-corrosion of phosphide-rich iron," *Environmental Science & Pollution Research*, vol. 5: (2), pp. 71–74, 1998.

[58] K. C. Condie and A. Kröner, "When did plate tectonics begin? evidence from the geologic record," *Geological Society of America Special Papers*, vol. 440, pp. 281–294, 2008.

[59] W. H. O. WHO, "Environmental health criteria 73: Phosphine and selected metal phosphides," tech. rep., World Health Orgnization, 1988.

[60] D. Glindemann, M. Edwards, and P. Kuschk, "Phosphine gas in the upper troposphere," *Atmospheric Environment*, vol. 37, p. 2429Ǔ2433, 2003.

[61] D. Glindemann, M. Edwards, and P. Morgenstern, "Phosphine from rocks: mechanically driven phosphate reduction?," *Environ. Sci. Technol.*, vol. 39, pp. 8295–8299, 2005.

[62] D. Glindemann, M. Edwards, and O. Schrems, "Phosphine and methylphosphine production by simulated lightning Ǔ a study for the volatile phosphorus cycle and cloud formation in the earth atmosphere," *Atmospheric Environment*, vol. 38, p. 6867Ǔ6874, 2004.

[63] E. Krider, G. Dawson, and M. Uman, "Peak power and energy dissipation in a single-stroke lightning flash," *Journal of Geophysical Research*, vol. 73:(10), p. 3335, 1968.

[64] M. Uman, "Peak temperature of lightning," *J. Atmos. Terr. Phys.*, vol. 26, pp. 123–128, 1964.

[65] H. J. Christian, R. J. Blakeslee, D. J. Boccippio, W. L. Boeck, D. E. Buechler, K. T. Driscoll, S. J. Goodman, J. M. Hall, W. J. Koshak, D. M. Mach, and M. F. Stewart, "Global frequency and distribution of lightning as observed from space by the optical transient detector," *Journal of Geophysical Research*, vol. 108, p. 4005, 2003.

[66] M. A. Pasek, J. P. Dworkin, and D. S. Lauretta, "A radical pathway for organic phosphorylation during schreibersite corrosion with implications for the origin of life," *Geochim. Cosmochim. Acta.*, vol. 71, p. 1721Ǔ1736, 2007.

[67] D. E. Bryant, D. Greenfield, R. D. Walshaw, S. M. Evans, A. E. Nimmo, C. L. Smith, L. Wang, M. A. Pasek, and T. P. Kee, "Electrochemical studies of iron meteorites: phosphorus redox chemistry on the early earth," *International Journal of Astrobiology*, vol. 8:(1), p. 27Ǔ36, 2009.

[68] A. Y. Mulkidjanian, A. Y. Bychkov, D. V. Dibrova, M. Y. Galperin, and E. V. Koonin, "Origin of first cells at terrestrial, anoxic geothermal fields," *Proc. Nat. Acad. Sci.*, vol. 109, pp. 821–830, 2012.

[69] K. Zahnle, L. Schaefer, and B. Fegley, "Earth's earliest atmospheres," *Cold Spring Harb. Perspect. Biol.*, 2010.

[70] C. Hayashi, K. Nakazawa, and H. Mizuno, "Earth's melting due to the blanketing effect of the primordial dense atmosphere," *Earth. Planet. Sci. Lett.*, vol. 43:(1), pp. 22–28, 1979.

[71] J. S. Lewis and R. G. Prinn, *Planets and Their Atmospheres: Origin and Evolution.* Academic Press, Orlando, 1984.

[72] M. Ikoma and H. Genda, "Constraints on the mass of a habitable planet with water of nebular origin," *Journal of Astrophysics*, vol. 648, pp. 696–706, 2006.

[73] G. Arrhenius, B. De, and H. Alfven, *The Sea*, ch. Origin of the ocean., pp. 839–861. Wiley-Interscience, New York,, 1974.

[74] M. Lange, P. Lambert, and T. Ahrens, "Shock effects on hydrous minerals and implications for carbonaceous meteorites.," *Geochim. Cosmochim. Acta.*, vol. 49, pp. 1715–1726, 1985.

[75] J. Tyburczy, B. Frisch, and T. Ahrens, "Shock-induced volatile loss from a carbonaceous chondrite: Implications for planetary accretion.," *Earth. Planet. Sc.i Lett.*, vol. 80, pp. 201–207, 1986.

[76] Y. Abe and T. Matsui, "Early evolution of the earth: Accretion, atmosphere formation, and thermal history.," *J. Geophys. Res.*, vol. 91:(E), pp. 291–302, 1986.

[77] K. Zahnle, J. Kasting, and J. Pollack, "Evolution of a steam atmosphere during earth's accretion.," *Icarus*, vol. 74, pp. 62–97, 1988.

[78] T. Ahrens, J. OŠKeefe, and M. Lange, *Origin and Evolution of Planetary and Satellite Atmospheres.*, ch. Formation of atmospheres during accretion of the terrestrial planets., pp. 328–385. University of Arizona Press, Tuscon, 1989.

[79] L. Schaefer and B. Fegley, "Outgassing of ordinary chondritic material and some of its implications for the chemistry of asteroids, planets, and satellites.," *Icarus*, vol. 186, pp. 462–483, 2007.

[80] G. Hashimoto, Y. Abe, and S. Sugita, "The chemical composition of the early terrestrial atmosphere: Formation of a reducing atmosphere from ci-like material.," *J. Geophys. Res.*, vol. 112, 2007.

[81] L. Schaefer and B. Fegley, "Chemistry of atmospheres formed during accretion of the earth and other terrestrial planets," *Icarus*, vol. 208, pp. 438–448, 2010.

[82] H. C. Urey, "On the early chemical history of the earth and the origin of life," *Proc. Nat. Acad. Sci.*, vol. 38:(4), pp. 351–363, 1952.

[83] M. Sekiya, K. Nakazawa, and C. Hayashi, "Dissipation of the primordial terrestrial atmosphere due to irradiation of the solar euv.," *Progress of Theoretical Physics*, vol. 64:(6), pp. 1968–1985, 1980.

[84] M. Sekiya, C. Hayashi, and K. Kanazawa, "Dissipation of the primordial terrestrial atmosphere due to irradiation of the solar far-uv during t tauri stage.," *Progress of Theoretical Physics*, vol. 66:(4), pp. 1301–1316, 1981.

[85] K. Zahnle, N. Arndt, C. Cockell, A. Halliday, E. Nisbet, F. Selsis, and N. H. Sleep, "Emergence of a habitable planet," *Space Sci. Rev.*, vol. 129, pp. 35–78, 2007.

[86] W. Benz, W. L. Slattery, and A. G. W. Cameron, "The origin of the moon and the single-impact hypothesis.," *Icarus*, vol. 66, pp. 515–535, 1986.

[87] A. Cameron and W. Benz, "The origin of the moon and the single impact hypothesis.," *Icarus*, vol. 92, pp. 204–216, 1991.

[88] R. Canup and E. Asphaug, "Origin of the moon and the single impact hypothesis.," *Nature*, vol. 421, pp. 708–712, 2001.

[89] R. Canup, "Simulations of a late lunar-forming impact.," *Icarus*, vol. 168, pp. 433–456, 2004.

[90] H. Genda and Y. Abe, "Survival of a proto-atmosphere through the stage of giant impacts: The mechanical aspects.," *Icarus*, vol. 164, pp. 149–162, 2003.

[91] H. Genda and Y. Abe, "Enhanced atmospheric loss on protoplanets at the giant impact phase in the presence of oceans.," *Nature*, vol. 433, pp. 842–844, 2005.

[92] N. H. Sleep, "The hadean-archaean environment," *Cold Spring Harb. Perspect. Biol.*, 2010.

[93] M. J. Walter and R. G. Tronnes, "Early earth differentiation," *Earth. Planet. Sci. Lett.*, vol. 225, p. 253Ű269, 2004.

[94] J. Kasting, "EarthŠs early atmosphere.," *Science*, vol. 259, pp. 920–926, 1993.

[95] J. F. Kasting and D. Catling, "Evolution of a habitable planet," *Annu. Rev. Astron. Astrophys.*, vol. 41, pp. 429–463, 2003.

[96] J. F. Kasting and T. P. Ackerman, "Climatic consequences of very high-carbon dioxide levels in the earthŠs early atmosphere.," *Science*, vol. 234, pp. 1383–1385, 1986.

[97] N. H. Sleep, K. Zahnle, and P. S. Neuhoff, "Initiation of clement surface conditions on the earliest earth," *Proc. Nat. Acad. Sci.*, vol. 98:(7), pp. 3666–3672, 2001.

[98] J. Poole, "The evolution of the earthŠs atmosphere.," *Sci. Proc. Roy. Dublin. Acad.*, vol. 25, pp. 201–224, 1951.

[99] H. Holland, *Petrologic studies: a volume in honor of A.G. Buddington,*, pp. 447–447. Geological Society of America, Boulder, USA, 1962.

[100] P. Abelson, "Chemical events on the primitive earth.," *Proc. Nat. Acad. Sci.*, vol. 55, pp. 1365–1372, 1966.

[101] H. Holland, *The Chemical Evolution of the Atmosphere and Oceans.* Princeton University Press, Princeton, 1984.

[102] H. Brown, *The Atmosphere of the Earth and Planets.*, ch. Rare gases and the formation of the EarthŠs atmosphere., pp. 258–266. Univ. Chicago Press, Chicago, 1949.

[103] H. Wanke, "Constitution of terrestrial planets.," *Phil. Trans. R. Soc. A*, vol. 303, pp. 287–302, 1981.

[104] H. S. C. OŠNeill, "The origin of the moon and the early history of the earth: a chemical model. part 2. the earth.," *Geochim. Cosmochim. Acta*, vol. 55, pp. 1159–1172, 1992.

[105] B. J. Wood, M. J. Walter, and J. Wade, "Accretion of the earth and segregation of its core.," *Nature*, vol. 441, pp. 825–833, 2006.

[106] D. Frost, U. Mann, Y. Asahara, and D. Rubie, "The redox state of the mantle during and just after core formation," *Phil. Trans. R. Soc. A*, vol. 366, pp. 4315–4337, 2008.

[107] F. Tera, D. Papanastassiou, and G. Wasserburg, "Isotopic evidence for a terminal lunar cataclysm," *Earth. Planet. Sci. Lett.*, vol. 22, pp. 1–22, 1974.

[108] R. Gomes, H. F. Levison, K. Tsiganis, and A. Morbidelli, "Origin of the cataclysmic late heavy bombardment period of the terrestrial planets," *Nature*, vol. 435, pp. 466–469, 2005.

[109] A. Morbidelli, H. F. Levison, K. Tsiganis, and R. Gomes, "Chaotic capture of jupiterŠs trojan asteroids in the early solar system," *Nature*, vol. 435, pp. 462–465, 2005.

[110] K. Tsiganis, R. Gomes, A. Morbidelli, and H. Levison, "Origin of the orbital architecture of the giant planets of the solar system.," *Nature*, vol. 435, pp. 459–461, 2005.

[111] D. A. Minton and R. Malhotra, "Dynamical erosion of the asteroid belt and implications for large impacts in the inner solar system," *Icarus*, vol. 207, pp. 744–757, 2010.

[112] D. A. Minton and R. Malhotra, "Secular resonance sweeping of the main asteroid belt during planet migration," *Earth and Planetary Astrophysics*, vol. arXiv:1102.3131, 2011.

[113] E. L. Gibb, M. J. Mumma, N. D. Russo, M. A. DiSanti, and K. Magee-Sauer, "Methane in oort cloud comets," *Icarus*, vol. 165:(2), pp. 391–406, 2003.

[114] H. F. Levison and L. Donnes, *Encyclopedia of the Solar System (2nd ed.)*, ch. Comet Populations and Cometary Dynamics, p. 575Ű588. Academic Press, Boston, 2007.

[115] M. C. D. Sanctis, M. T. Capria, and A. Coradini, "Thermal evolution and differentiation of edgeworth-kuiper belt objects," *The Astronomical Journal*, vol. 121:(5), p. 2792Ű2799, 2001.

[116] K. Altwegg, H. Balsiger, and J. Geiss, "Composition of the volatile material in halley's coma from in situ measurements," *Space Sci. Rev.*, vol. 90:(1-2), pp. 3–18, 1999.

[117] P. Wiegert, D. Balam, A. Moss, C. Veillet, M. Connors, and I. Shelton, "Evidence for a color dependence in the size distribution of main-belt asteroids," *The Astronomical Journal*, vol. 133:(4), p. 1609Ű1614, 2007.

[118] W. K. Hartmann, G. Ryder, L. Dones, and D. Grinspoon, *Origin of the Earth and Moon*, ch. The Time-Dependent Intense Bombardment of the Primordial Earth/Moon System, pp. 493–512. University of Arizona Press, 2000.

[119] J. W. Valley, W. H. Peck, E. M. King, and S. A. Wilde, "A cool early earth," *Geology*, vol. 30:(4), pp. 351–354, 2002.

[120] S. A. Wilde, J. W. Valley, W. H. Peck, and C. M. Graham, "Evidence from detrital zircons for the existence of continental crust and oceans on the earth 4.4 gyr ago," *Nature*, vol. 409, pp. 175–178, 2001.

[121] B. Marty and A. Meibom, "Noble gas signature of the late heavy bombardment in the earthŠs atmosphere," *eEarth*, vol. 2, pp. 43–49, 2007.

[122] B. A. Cohen, T. D. Swindle, and D. A. Kring, "Support for the lunar cataclysm hypothesis from lunar meteorite impact melt ages," *Science*, vol. 290, pp. 1754–1756, 2000.

[123] G. Ryder, "Mass flux in the ancient earth-moon system and benign implications for the origin of life on earth," *Journal of Geophysical Research (Planets)*, vol. 107:(4), pp. 1–13, 2002.

[124] M. K. Weisberg, T. J. McCoy, and A. N. Krot, *Meteorites and the Early Solar System II*, ch. Systematics and evaluation of meteorite classification, pp. 19–52. University of Arizona Press, Tucson, AZ, USA, 2006.

[125] J. Harry Y. McSween, *Meteorites and Their Parent Planets*. Cambridge University Press, 1999.

[126] R. Hutchinson, *Meteorites - A Petrological, Chemical and Isotopic Synthesis*. Cambridge University Press, 2004.

[127] O. R. Norton, *The Cambridge Encyclopedia of Meteorites*. Cambridge University Press, Cambridge, 2002.

[128] W. Hsu, "Minor element zoning and trace element geochemistry of pallasites," *Meteorit. Planet. Sci.*, vol. 38:(8), p. 1217Ű1241, 2003.

[129] P. Buseck, "Pallasite meteorites: mineralogy, petrology, and geochemistry," *Geochim. Cosmochim. Acta.*, vol. 41:(6), pp. 711–740, 1977.

[130] T. J. McCoy and A. N. Krot, *Meteorites and the early solar system II*, ch. Systematics and Evaluation of Meteorite Classification, p. 19Ű52. University of Arizona Press, Tuscon, 2006.

[131] O. R. Norton and L. A. Chitwood, *Field Guide to Meteors and Meteorites*. Springer-Verlag, London, 2008.

[132] L. E. Orgel, "Prebiotic chemistry and the origin of the rna world," *Critical Reviews in Biochemistry and Molecular Biology*, vol. 39:(2), pp. 99–123, 2004.

[133] R. Buick, "When did oxygenic photosynthesis evolve?," *Phil. Trans. R. Soc. B*, vol. 363, pp. 2731–2743, 2008.

[134] D. C. Catling and M. W. Claire, "How earthŠs atmosphere evolved to an oxic state: a status report," *Earth. Planet. Sci. Lett.*, vol. 237, pp. 1–20, 2005.

[135] R. E. Kopp, J. L. Kirschvink, I. A. Hilburn, and C. Z. Nash, "The paleoproterozoic snowball earth: a climate disaster triggered by the evolution of oxygenic photosynthesis," *Proc. Natl. Acad. Sci.*, vol. 102, p. 11131Ű11136, 2005.

[136] H. Ohmoto, "When did the earthŠs atmosphere become oxic?," *Geochem. News*, vol. 93, pp. 26–27, 1997.

[137] R. Rye and H. D. Holland, "Paleosols and the evolution of atmospheric oxygen: a critical review," *Am. J. Sci*, vol. 298, pp. 621–672, 1998.

[138] K. Catling, D. & Zahnle, *Encyclopedia of atmospheric sciences*, ch. Evolution of atmospheric oxygen, p. 754Ű761. The Netherlands Academic Press, Amsterdam, 2002.

[139] N. Dauphas, F. Robert, and B. Marty, "The late asteroidal and cometary bombardment of earth as recorded in water deuterium to protium ratio.," *Icarus*, vol. 148, pp. 508–512, 2000.

[140] A. Morbidelli, J. Chambers, J. Lunine, J. Petit, and F. Robert, "Source regions and timescales for the delivery of water to the earth.," *Meteorit. Planet. Sci.*, vol. 35, pp. 1309–1320, 2000.

[141] F. Robert, *Meteorites and the Early Solar System II*, ch. Solar System Deuterium/Hydrogen Ratio, pp. 341–351. University of Arizona Press, Tuscon, 2006.

[142] L. Frank, J. Sigwarth, and J. Craven, "On the influx of small comets into the earthŠs atmosphere i. observations.," *Geophys. Res. Lett.*, vol. 13, pp. 303–306, 1986.

[143] D. Deming, "On the possible influence of extraterrestrial volatiles on earthŠs climate and the origin of the oceans.," *Palaeogeogr. Palaeoclim. Palaeoecol.*, vol. 146, pp. 33–51, 1999.

[144] T. Owen, *The Molecular Origins of Life*, ch. The origin of the atmosphere., pp. 13–34. Cambridge University Press. Cambridge, 1998.

[145] A. Delsemme, "The deuterium enrichment observed in recent comets is consistent with the cometary origin of seawater.," *Planet. Space Sci.*, vol. 47, pp. 125–131, 1999.

[146] N. Dauphas, "The dual origin of the terrestrial atmosphere.," *Icarus*, vol. 165, pp. 326–339, 2003.

[147] W. Rubey, "Geologic history of seawater: An attempt to state the problem.," *GSA Bull.*, vol. 62, pp. 1111–1147, 1951.

[148] K. Krauskopf and D. Bird, *Introduction to geochemistry.* McGraw-Hill, New York, NY., 1995.

[149] M. Honda, I. McDougall, D. Patterson, A. Doulgeris, and D. Clague, "Possible solar noble gas component in hawaiian basalts.," *Nature*, vol. 349, pp. 149–151, 1991.

[150] D. L. Pinti, *Lectures in Astrobiology*, ch. 3 The Origin and Evolution of the Oceans, pp. 83–112. Springer Science, New York, 2006.

[151] C. Engrand, E. Deloule, F. Robert, M. Maurette, and G. Kurat, "Extraterrestrial water in micrometeorites and cosmic spherules from antarctica: An ion microprobe study.," *Meteorit. Planet. Sci.*, vol. 34, pp. 773–786, 1999.

[152] M. Maurette, J. Duprat, C. Engrand, M. Gounelle, G. Kurat, G. Matrajt, and A. Toppani, "Accretion of neon, organics, co2, nitrogen and water from large interplanetary dust particles on the early earth.," *Planet. Space Sci.*, vol. 48, pp. 1117–1137, 2000.

[153] E. Deloule, F. Albarede, and S. Sheppard, "Hydrogen isotope heterogeneities in the mantle from ion probe analysis of amphiboles from ultramafic rocks.," *Earth. Planet. Sci. Lett.*, vol. 105, pp. 543–553, 1991.

[154] C. Lecuyer, P. Gillet, and F. Robert, "The hydrogen isotope composition of seawater and the global water cycle.," *Chem. Geol.*, vol. 145, pp. 249–261, 1998.

[155] F. Robert, *LŠenvironnement de la Terre Primitive*, ch. LŠorigine de lŠeau dans le Systeme Solaire telle quelle est enregistree par son rapport isotopique D/H., p. 79Ũ90. PressesUniversitaires deBordeaux. Bordeaux, France., 2001.

[156] G. Boato, "The isotopic composition of hydrogen and carbon in the carbonaceous chondrites.," *Geochim. Cosmochim. Acta*, vol. 6, pp. 209–220, 1954.

[157] F. Robert and S. Epstein, "The concentration and isotopic composition of hydrogen, carbon and nitrogen in the carbonaceous meteorites.," *Geochim. Cosmochim. Acta.*, vol. 46, pp. 81–95, 1982.

[158] J. Kerridge, "Carbon, hydrogen and nitrogen in carbonaceous chondrites: Abundances and isotopic compositions in bulk samples.," *Geochim. Cosmochim. Acta*, vol. 49, pp. 1707–1714, 1985.

[159] A. Drouart, B. Dubrulle, D. Gautier, and F. Robert, "Structure and transport in the solar nebula from constraints on deuterium enrichment and giant planets formation.," *Icarus*, vol. 140, pp. 59–76, 1999.

[160] N. Dauphas and B. Marty, "Inference on the nature and the mass of earthŠs late veneer from noble metals and gases.," *J. Geophys. Res.*, vol. 107:(E12), pp. 1–7, 2001.

[161] S. Kempe and E. Degens, "An early soda ocean?," *Chem. Geol.*, vol. 53, pp. 95–108, 1985.

[162] J. Walker, "Carbon dioxide on the early earth.," *Origins of Life*, vol. 16, pp. 117–127, 1985.

[163] J. Kasting, "Theoretical constraints on oxygen and carbon dioxide concentrations in the precambrian atmosphere.," *Precambrian Res.*, vol. 34, pp. 205–229, 1987.

[164] J. W. Morse and F. T. MacKenzie, "Hadean ocean carbonate geochemistry," *Aquatic Geochemistry*, vol. 4, pp. 301–319, 1998.

[165] Y. Abe, "Physical state of the very early earth.," *Lithos*, vol. 30, pp. 223–235, 1993.

[166] E. Tajika and T. Matsui, "Degassing history and carbon cycle of the earth: From an impact-induced steam atmosphere to the present atmosphere.," *Lithos*, vol. 30, pp. 267–280, 1993.

[167] P. Knauth, "Petrogenesis of chert.," *Review Mineral.*, vol. 29, pp. 233–258, 1994.

[168] L. Knauth and D. Lowe, "Oxygen isotope geochemistry of cherts from the onverwatch group (3.4 billion years), transvaal group, south africa, with implications for secular variations in the isotopic composition of cherts.," *J. Geol.*, vol. 41, pp. 209–222, 1978.

[169] K. Sugitani, "Geochemical characteristics of archean cherts and other sedimentary rocks in the pilbara block, western australia: evidence for archean seawater enriched in hydrothermally-derived iron and silica.," *Precambrian Res.*, vol. 57, pp. 21–47, 1992.

[170] W. Nijman, H. de Bruijne, and M. Valkering, "Growth fault control of early archean cherts, barite mounds and chert-barite veins, north pole dome, eastern pilbara, western australia.," *Precambrian Res.*, vol. 88, pp. 25–52, 1998.

[171] D. Pinti, K. Hashizume, and J. Matsuda, "Nitrogen and argon signatures in 3.8 to 2.8 ga metasediments: Clues on the chemical state of the archean ocean and the deep biosphere.," *Geochim. Cosmochim. Acta.*, vol. 65, pp. 2301–2315, 2001.

[172] C. de Ronde, D. Channer, K. Faure, C. J. Bray, and T. C. Spooner, "Fluid chemistry of archaean seafloor hydrothermal vents: Implications for the composition of circa 3.2 ga seawater.," *Geochim. Cosmochim. Acta.*, vol. 61, pp. 4025–4042, 1997.

[173] L. Derry and S. Jacobsen, "Thend and sr evolution of proterozoic seawater.," *Geophys. Res. Lett.*, vol. 15, pp. 397–400, 1988.

[174] M. Bickle, "Implications of melting for stabilisation of the litosphere and heat loss in the archaean.," *Earth. Planet. Sci. Lett.*, vol. 80, pp. 314–324, 1986.

[175] J. Foriel, P. Philippot, D. Banks, P. Rey, J. Cauzid, and A. Somogyi, "Composition of a 3.5 gyr shallow seawater from the north pole dome,western australia.," *Geochim. Cosmochim. Acta*, vol. 67, p. A100, 2003.

[176] R. Morris, "Genetic modelling for banded iron-formation of the hamersley group, pilbara craton, western australia.," *Precambrian Res.*, vol. 60, p. 1993, 1993.

[177] A. Isley, "Hydrothermal plumes and the delivery of iron to banded iron formation.," *J. Geol.*, vol. 103, pp. 169–185, 1995.

[178] J. Plant and A. Saunders, "The radioactive earth," *Radiation Protection Dosimetry*, vol. 68:(1/2), pp. 25–36, 1996.

[179] E. Nisbet, K. Zahnle, M. Gerasimov, J. Helbert, R. Jaumann, B. A. Hofmann, K. Benzerara, and F. Westall, "Creating habitable zones, at all scales, from planets to mud micro-habitats, on earth and on mars," *Space Sci. Rev.*, vol. 129, pp. 79–121, 2007.

[180] R. G. Strom, G. G. Schaber, and D. D. Dawson, "The global resurfacing of venus," *J. Geophys. Res.*, vol. 99:(E5), p. 10899Ű10926, 1994.

[181] L. Wilson and J. W. H. III, "Mars: Review and analysis of volcanic eruption theory and relationships to observed landforms," *Rev. Geophys.*, vol. 32:(3), pp. 221–263, 1994.

[182] M. J. Russell, "The alkaline solution to the emergence of life: Energy, entropy and early evolution," *AChem. Commun.*, vol. 55:(2), pp. i–vii, 2007.

[183] H. Ármannsson, H. Kristmannsdóttir, H. Torfason, and M. Ólafsson, "Natrual changes in unexploited high-temperature geothermal areas in iceland.," 2000.

[184] M. Ólafsson, H. Torfason, and K. Grönvold, "Surface exploration and monitoring of geothermal activity in kverkfjoll geothermal area, central iceland," 2000.

[185] W. Fyfe, "The water inventory of the earth: fluids and tectonics.," *Geol. Soc. Lond. (Special Publications)*, vol. 78, pp. 1–7, 1994.

[186] T. Tanaka, Y. Nakamura, A. Mizuike, and A. Ono, "Simultaneous determination of phosphorus, sulfur and arsenic in steel by hydride generation and gas chromatography.," *Analytical Sciences*, vol. 12, pp. 77–80, 1996.

[187] C. E. Housecroft and E. C. Constable, eds., *Chemistry: An Introduction to Organic, Inorganic and Physical Chemistry*, ch. 11 - Introduction to Spectroscopy, pp. 344–356. Prentice-Hall, 2006.

[188] "4500-p phosphorus (1999): Standard methods for the examination of water and wastewater," 1999.

[189] D. Pote and T. Daniel, *Methods of Phosphorus Analysis for Soils, Sediments, Residuals and Waters*, ch. Analyzing for Total Phosphorus and Total Dissolved Phosphorus in Water Samples, pp. 94–97. Southern Cooperative Series Bulletin No.396, 2000.

[190] J. Keggin, "Structure and formula of 12-phosphotungstic acid," *Proc. R. Soc. Lond. A*, vol. 144, pp. 75–100, 1934.

[191] L. Baker and J. Figgis, "A new fundamental type of inorganic complex: Hybrid between heteropoly and conventional coordination complexes. possibilities for geometrical isomerisms in 11-, 12-, 17-, and 18-heteropoly derivatives.," *Journal of the American Chemical Society*, vol. 92(12), pp. 3794–3797, 1970.

[192] L. Stryer, J. Berg, and J. Tymoczko, *Biochemistry*. W.H. Freeman and Company, New York, 2004.

[193] D. Voet and J. Voet, *Biochemistry*. John Wiley and Sons Inc, USA, 1995.

[194] A. Bielen, K. Willquist, J. Engman, J. van der Oost, E. van Niel, and S. Kengen, "Pyrophosphate as a central energy carrier in the hydrogen-producing extremely thermophilic caldicellulosiruptor saccharolyticus," *FEMS Microbiol. Lett.*, vol. 307(1), pp. 48–54, 2010.

[195] A. Hill and L. E. Orgel, "Trimetaphosphate-induced addition of aspartic acid to oligo(glutamic acid)s," *Helvetica Chimica Acta*, vol. 85, pp. 4244–4254, 2002.

[196] H. Baltscheffsky, L.-V. von Stedingk, H.-W. Heldt, and M. Klingenberg, "Inorganic pyrophosphate: Formation in bacterial photophosphorylation," *Science*, vol. 153, pp. 1120–1122, 1966.

[197] H. Baltscheffsky, *Origin and evolution of biological energy conversion*, ch. Energy conversion leading to the origin and early evolution of life: Did inorganic pyrophosphate precede adenosine triphosphate?, pp. 1–9. VCH Publishers Inc., New York, USA, 1996.

[198] N. G. Holm and H. Baltscheffsky, "Links between hydrothermal environments, pyrophosphate, na+, and early evolution," *Orig. Life. Evol. Biosph.*, vol. 41, pp. 483–493, 2010.

[199] M. Russell and A. Hall, "The emergence of life from iron monosulphide bubbles at a submarine hydrothermal redox and ph front.," *J. Geol. Soc. London*, vol. 154, pp. 377–402, 1997.

[200] L. Babich, A. F. Hartog, M. A. van der Horst, and R. Wever, "Continuous-flow reactor-based enzymatic synthesis of phosphorylated compounds on a large scale," *Chem. Eur. J.*, vol. 18:(21), pp. 6604–6609, 2012.

[201] L. Amat, "Sur l'existence d'un acide pyrophosporeaux," *Compt. Rend.*, vol. 106, p. 1400, 1888.

[202] D. Grant, D. S. Payne, and S. Skledar, "The pyrolysis of inorganic phosphites," *Journal of Inorganic and Nuclear Chemistry*, vol. 26, pp. 2103–2111, 1964.

[203] R. E. Mesmer and R. L. Carroll, "The kinetics and mechanism of the hydrolysis of pyrophosphite," *Journal of the American Chemical Society*, vol. 88:7, pp. 1381–1387, 1966.

[204] C. Y. Ortiz-Avila, P. J. Squattrito, M. Shieh, and A. Clearfield, "Synthesis and characterization of a new series of zinc phosphites," *Inorg. Chem.*, vol. 28, pp. 2608–2615, 1989.

[205] D. E. C. Corbridge, "The crystal structure of magnesium phosphite hexahydrate, mghpo3.6h20," *Acta Cryst.*, vol. 9, p. 991, 1956.

[206] A. Larbot, J. Durand, and P. D. L. Cot, "Structure cristalline du phosphite acide de calcium, ca(hpo3h)2 ů h2o," *Zeitschrift für anorganische und allgemeine Chemie*, vol. 508, pp. 154–158, 1984.

[207] K. E. R. Marriott, *Reduced Oxidation State Phosphorus in Prebiotic Chemistry*. PhD thesis, School of Chemistry, University of Leeds, 2012.

[208] L. Fabbrizzi, N. Marcotte, F. Stomeo, and A. Taglietti, "Pyrophosphate detection in water by fluorescence competition assays: Inducing selectivity through the coice of indicator," *Angew. Chem. Int. Ed.*, vol. 41:(20), pp. 3811–3814, 2002.

[209] D. Chen and A. Martell, "The synthesis of new binucleating polyaza macrocyclic and macrobycyclic ligands: Dioxygen affinities of the cobalt complexes," *Tetrahedron*, vol. 47:(34), pp. 6895–6902, 1991.

[210] D. Nation, A. Martell, R. Carroll, and A. Clearfield, "Host-guest interactions of inorganic phosphates with the copper(ii) complexes of the hexaaza macrocyclic ligand 3,6,9,17,20,23-hexaazatricyclo[23.3.1.111,15]triaconta-1(29),11(30),12,14,25,27-hexaene," *Inorg. Chem.*, vol. 35:(25), pp. 7246–7252, 1996.

[211] R. O. Fournier, "Geochemistry and dynamics of the yellowstone national park hydrothermal system," *US Geological Survey, Menlo Park, CA.*, 2004.

[212] S. B. Bortnikova, G. M. Gavrilenko, E. P. Bessonova, and A. S. Lapukhov, "The hydrogeochemistry of thermal springs on mutnovskii volcano, southern kamchatka," *J. Volcanology and Seismology*, vol. 3, pp. 388–404, 2009.

[213] C. R. Cousins, *An Astrobiological Study of High Latitude Martian Analogue Environments*. PhD thesis, Department of Earth Sciences, University College London, 2010.

[214] C. Cousins, I. Crawford, J. Carrivick, M. Gunn, J. Harris, T. Kee, M. Karlsson, L. Carmody, C. Cockell, B. Herschy, and K. Joy, "Glaciovolcanic hydrothermal environments in iceland and implications for their detection on mars," *J. Volcanol. Geotherm. Res*, vol. 256, pp. 61–77, 2013.

[215] H. Pech, M. G. Vazquez, J. V. Buren, L. Shi, M. M. Ivey, T. M. Salmassi, M. A. Pasek, and K. L. Foster, "Elucidating the redox cycle of environmental phosphorus using ion chromatography," *Journal of Chromatographic Science*, vol. 49, pp. 573–581, 2011.

[216] G. Wächtershäuser, "Pyrite formation, the first energy source for life: a hypothesis," *Systematic and Applied Microbiology*, vol. 10, no. 3, pp. 207 – 210, 1988.

[217] G. Wächtershäuser, "The case for the chemoautotrophic origin of life in an iron-sulfur world," *Orig. Life. Evol. Biosph.*, vol. 20(2), pp. 173–176, 1990.

[218] G. Wächtershäuser, "Evolution of the first metabolic cycles," *Proc. Nat. Acad. Sci.*, vol. 87, pp. 200–204, 1990.

[219] C. Huber and G. Wächtershäuser, "Activated acetic acid by carbon fixation on (fe,ni)s under primordial conditions," *Science*, vol. 276, pp. 245–247, 1997.

F

Appendix A

Protocols

A.1   Acid washing

Due to low concentrations of phosphorus in analysis, contaminations were removed by acid washing as follows;.

1. All glassware to be scrubbed with hot soapy water.

2. Rinse thoroughly with distilled water.

3. Leave to air dry for 24 hours.

4. Clean inside of glassware with 2M Sulphuric acid.

5. Rinse with deionised water until washings neutral.

6. Oven dry glassware for 24 hours.

7. Handle clean glassware at all times with disposable gloves.

A.2   Iron removal using sodium hydroxide

The removal of dissolved iron from solution was conducted as follows;

1. Sample treated by dropwise addition of NaOH (1M) to pH 12 and left for 1-2 minutes.

2. Sample gravity filtered to remove precipitate ($FeOH_2$).

3. Sample treated by dropwise addition of HCl (1M) to pH 4.

4. Sample tested by analysis using ^{31}P NMR spectroscopy to check clarity

5. If NMR shows poor quality, repeat steps 1 to 4.

6. If NMR still shows poor quality, add few drops Na_2S and repeat step 4.

Appendix B

Fieldwork Diary

The following details the day to day of the trip to the sampling site at Kverkfjöll on the northern edge of the Vatnajökull glacier.

Figure B.1: GPS route map from Reykjavik to Kverkfjöll at a 20 km per cm scale. (Credit: Magnus Þor Karlsson)

B.1 Day 1 - Reykjavik

Arrived in Keflavik Airport from London Gatwick mid-afternoon. A taxi was taken to transfer the group and all the equipment to the hotel. A meeting was set up with Magnus, the expedition guide, where all final travel plans were confirmed and a final equipment list was compiled and confirmed for travel onto the glacier.

B.2 Day 2 - Reykjavik

Day spent collecting the final pieces of equipment and shopping for food and supplies for the time on the glacier. A meeting was held with the Icelandic Metrological Society (IMO)

to discuss glacier conditions and the weather forecast for the time on the glacier. Access was given to the IMO warehouse for storage of equipment and food as this would serve as the departure point for the expedition the following morning.

Figure B.2: First site of the Grimsvötn IGS hut at as we approach through almost whiteout conditions. Credit: Barry Herschy

B.3 Day 3 - Reykjavik to Grimsvjötn

The expedition departed from the IMO warehouse, Reykjavik taking an easterly direction towards Grimsvjötn *via* Selfoss and Jökullheimer (Figure B.1). The route to Grimsvjötn took over 10 hours to complete driving on a mixture of tarmac and gravel roads to reach Jökullheimer, an IGS hut on the western edge of the Vatnajökull glacier. Lunch was taken at Jökullheimer, and then the journey continued on to Grimsvjötn over the glacier. The drive to the edge of the glacier was all off-road and took around one hour and including fording a fast flowing river. Driving on the glacier was slow initially due to melting snow and ice at the edge of the glacier resulting in at least one truck in our convoy of vehicles getting stuck in deep slush and having to be winched out. Further onto the glacier the weather conditions deteriorated badly with low visibility and large amounts of snowfall (Figure B.2 and Figure B.3). The remainder of the journey was undertaken in near white-out conditions which slowed progress literally to a crawl ($<$2 km/h) for the final 30 km until the Grimsvjötn hut which is situated on the eastern edge of the Grimsvjötn caldera, *ca.* 6 km from the May 2011 eruption site.

B.4 Day 4 - Grimsvjötn to Kverkfjöll

Departed from Grimsvjötn in a westerly direction towards the recent eruption site on the Grimsvjötn caldera. A brief stop to view the eruption site and to collect some samples

242

Figure B.3: The Grimsvötn IGS hut after arrival through the snow. A fresh deep covering of snow has been deposited since the recent eruption though ash and pumice deposits are still visible. Credit: Barry Herschy

Figure B.4: The Kverkfjöll IGS hut viewed from the ridge to the west. A fresh deep covering of snow has been deposited since the recent eruption. Credit: Barry Herschy

of ash then the journey continued around the south-west edge of the caldera then turning north-east towards Kverkfjöll. The journey took over 6 hours due to very difficult driving conditions because of the fresh snowfall the previous evening. After safely negotiating the route to Kverkfjöll, a final ascent of a *ca.* 1:4 gradient hill by all vehicles taking *ca.* 1 hour saw is arrive at the IGS Kverkfjöll hut (Figure B.4). Approximately 2 hours were spent preparing the site for use and unpacking equipment.
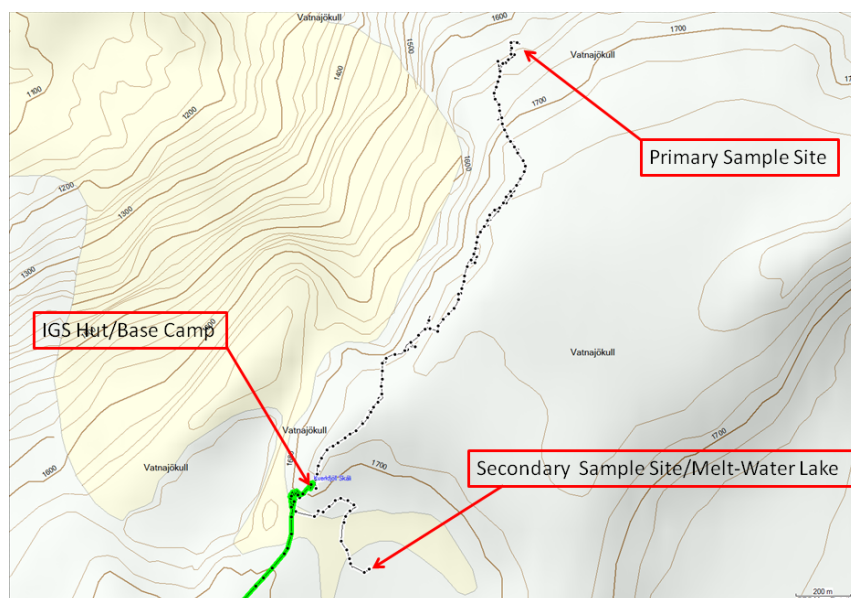

Figure B.5: GPS map of walking routes taken to primary and secondary sample sites from the Icelandic Glaciological Society (IGS) hut. (Credit: Magnus Þor Karlsson)

B.5 Day 5 - Kverkfjöll

Departing the IGS hut after breakfast, the group set off along a narrow ridge situated to the north of the hut toward the primary sampling site (Figure B.5). The weather conditions and visibility were poor and they deteriorated throughout the attempt to reach the primary sampling site. Due to concerns over safety the attempt to reach the primary site was abandoned and the group returned to the IGS hut. After lunch, a trip was organised to visit a melt-water lake situated to the south of the IGS hut. The descent was quite difficult dropping 125 m altitude during a 400 m trip through knee/thigh deep, loose packed snow.

The site next to the lake contained a large geothermally active area which was approximately 35 m wide by 20 m across and was situated to the west of the lake on an elevated plateau. The area was surrounded on all sides by snow which was gradually melting due to underlying geothermal activity and solar melting causing the area to grow in size even during the period of observation. The melt water from the snow was fed into the hydrothermal pool system by small streams and there was also a run-off stream from the hydrothermal pools off the elevated plateau into the lake *via* a small waterfall.

A quick inspection of the area showed a variety of environments for investigation which included high temperature large and small hydrothermal pools (10 - 30 cm in diameter,

visibly boiling or near boiling), bubbling mud pools (5 - 20 cm in diameter) and sulphurous fumaroles which were releasing sulphurous gasses into the environment which was identified by smell. Closer inspection of the fumaroles identified deposit of elemental sulphur on the surface. There was an area to the south of the geothermal area which was honeycombed with small fumaroles, mud and water pools. In some areas the structure had collapsed revealing a large amount of sub-surface interconnection between the features in this area. After *ca.* 5hours investigation at the lake site it was decided to head back to the IGS hut for dinner and prepare for the planned trip to the primary sampling site.

B.6   Day 6 - Kverkfjöll

The second attempt to reach the primary sampling site was abandoned due to white out conditions and high winds. Visibility was only a few feet and it was deemed too dangerous to attempt traversing the glacier. The day was spent analysing data from the previous day, also preparing and planning for the next day including potential secondary plans should the primary site not be reachable.

Figure B.6: The geothermal field photographed during the 2007 field trip by Dr. Claire Cousins that formed the basis of this fieldwork. (Credit: Dr. Claire Cousins)

B.7   Day 7 - Kverkfjöll

The expedition to the primary site departed from the IGS hut in a northerly direction along the bottom edge of the ridge previously attempted as this route was deemed safer after consulting maps. The weather was good with a light breeze and the sun shining. Thirty minutes into the walk after covering *ca.* 500 m the wind picked up, the weather closed in and visibility dropped to less than 10 m. After consultation with Magnus it was deemed safe to continue and after a further 2 hours serious hiking we reached the primary site (Figure B.6 and Figure B.7). The route was difficult to navigate as several suspected crevasses were encountered. From around half way into the trek it was agreed that a safety rope should be employed meaning that the team were tied together. Visibility was very poor and the site was barely visible. It was quickly established that the site was covered in deep snow and was completely unworkable. Safety was the major concern as the snow was covering hydrothermal pools, streams and geothermal features which could be hazardous

Figure B.7: Photographs taken of the primary hydrothermal site showing deep snow cover. This was attributed to a very cold spring in Iceland and increased snow fall through this period.

if fallen into through the snow. The site was abandoned and team returned to the IGS hut to reassess the situation and the objectives for the expedition.

The trek back to the hut took just over 3 hours employing the reverse of the route used to reach the primary site. The loss of the primary site was a serious setback and with only six days planned for working the Kverkfjöll site time was a major issue. Two days had already been lost due to weather issues and another day of very bad weather predicted attention turned to the lake site as the focus for the remainder of the expedition. It was decided that a visit to the lake site would be required to formulate a working plan for the site and that work would begin in mapping and fully working the site the following day. The visit to the lake site lasted *ca.* 4 hours and upon return, after dinner, equipment was prepared for an early start the following day.

B.8 Day 8 - Kverkfjöll

The team departed the IGS hut for the lake site after an early breakfast. The weather was overcast with a light wind and visibility was good. The day was spent mapping the geothermal area and identifying sites for sampling and deploying experiments. Approximately 7 hours spent on site collecting water samples and deploying experiments for collection. All sampled sites were mapped and photographed for completeness of records.

B.9 Day 9 - Kverkfjöll

As predicted all week the team was unable to leave the IGS hut due to extremely poor weather conditions. High winds and blizzards causing complete whiteout conditions. Even

the short trip to the toilet is a major expedition and also quite dangerous. The path that marked the route was covered over and almost invisible upon return even after a short period. The day was spent correlating collected data and drawing up rough maps of the sample area.

B.10 Day 10 - Kverkfjöll to Grimsvjötn

The group departed straight after breakfast to the lake site. The plan was to finalise all work undertaken and make it back to the IGS hut for 4 pm for departure back to Grimsvjötn for departure off the glacier. All deployed samples were collected and a final check of sample sites and measurements were completed. Upon return to the IGS hut all samples were packed according to transportation requirements and loaded into the truck for the journey back to Reykjavic. Departing from Kverkfjöll, the convoy follows the tracks of the IGS guide and Hut Keeper Vilhjalmur Kjartansson who drove over from Grimsvötn to assist with the return to Reykjavik. The trip to Grimsvjötn took *ca.* 3 hours driving over the obviously melting snow on the surface of the glacier. The melting snow had strange statue-like structures and large valley like areas due to insulation of the snow from the sun due to the ash fall from the Grimsvötn eruption. After what had been a very long week on the glacier an early night was in order ready for the trip off the glacier back to Reykjavik in the morning.

B.11 Day 11 - Grimsvjötn to Reykjavik

The group depart after breakfast heading east towards Jökullheimer. The melting of the surface snow made progress slow, often encountering slush and running water *ca.* 40 cm deep, melt features in the snow as previously described meaning the route had to be picked carefully through these features. Descending off the glacier, the group encounter a rapidly flowing melt-water river which had to be forded. This had to be approached carefully and was attempted one vehicle at a time to make sure crossing was possible and safe. After fording the river the drive continued to Jökullheimer where there was a brief stop before continuing on to Reykjavik *via* Selfoss.

The group spent two further nights in Reykjavik before flying back to London Gatwick on the 21st June 2011.